

MICROCOPY RESOLUTION TEST CHART  
NATIONAL BUREAU OF STANDARDS-1963-A

UNLIMITED

BR 56499

①

# ERA

TECHNOLOGY

R&D in electrical and electronic engineering  
Energy supply, utilisation and conservation  
Product design and prototype construction  
Materials, systems and component testing  
Market research and technology transfer

A133 361

LOW SIDELobe ANTENNA STUDY

FINAL REPORT

PART I LITERATURE SURVEY AND REVIEW

P R FOSTER and A W RUDGE

DTIC FILE COPY

DTIC  
OCT 07 1983  
S  
A  
E



**ERA Technology Ltd**

Cleeve Road, Leatherhead, Surrey KT22 7SA. England  
Telephone: Leatherhead (0372) 374151 Telex: 264045

**ERA**  
**TECHNOLOGY**

**TITLE PAGE/COVER:**

**BR 56799**

**UNLIMITED**

**Serial No.**

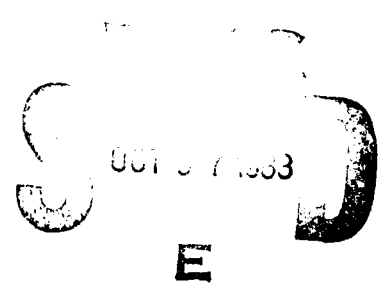
**LOW SIDELobe ANTENNA STUDY  
FOSTER and RUDGE**

**LOW SIDELobe ANTENNA STUDY**

**FINAL REPORT**

**PART I LITERATURE SURVEY AND REVIEW**

**P R FOSTER and A W RUDGE**

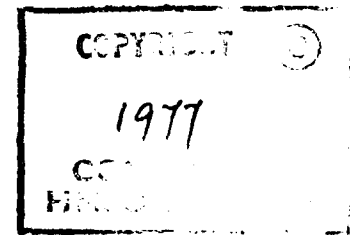


**R F TECHNOLOGY CENTRE**

**ELECTRICAL RESEARCH ASSOCIATION**

**LEATHERHEAD, SURREY.**

**OCTOBER 1977**



**Prepared for**

**PROCUREMENT EXECUTIVE, MINISTRY OF DEFENCE**

**Contract No. K/LR21b/1120**

**UNLIMITED**

ABSTRACT

This report is concerned with a study of the sidelobe performance of a broad range of antenna types. The survey is based almost entirely upon data available in the open literature, although in reviewing this material, the authors have tempered the information in the light of their own experience, and that of their colleagues, in this field. The emphasis of the review has been directed toward establishing the level of sidelobe suppression which can be achieved with antennas of differing types and dimensions; and towards determining to what extent these levels represent fundamental limitations with respect to sidelobe performance. Efforts have also been made to identify the principal parameters governing the sidelobe performance for any given antenna type.

The main conclusion of this survey and review is that sidelobe suppression to lower levels than that commonly achieved with existing antennas is, in many cases, both theoretically and practically feasible. The rather indifferent sidelobe performance of many existing antennas is considered to be a result of insufficient emphasis being given to this aspect of the system electrical performance. This has often led to an acceptance of levels of sidelobe radiation which, in view of the existing jamming threat, must now be considered as totally unrealistic.

Accession For

ITIC 6711  
DEC 1967  
U.S. AIR FORCE

*Letter on file*

0718  
COPY  
INCOMPLETE

**A**

CONTENTS

	<u>Page No.</u>
ACKNOWLEDGEMENTS	5
LIST OF FIGURES	6
1 INTRODUCTION	9
2 SIMPLIFIED THEORETICAL PREDICTIONS OF SIDELOBE PERFORMANCE	12
2.1 Linear Aperture Distributions	12
2.2 Sidelobe Levels and Directivity	19
2.3 Circular Aperture Distributions	19
2.4 Conclusion	27
3 LOW GAIN ANTENNAS	39
3.1 Horn Antennas	39
3.2 Dielectric Antennas	53
3.3 Broadband Antennas	59
3.4 Conclusions: Low Gain Antennas	64
4 MEDIUM GAIN ANTENNAS	73
4.1 Corner Reflectors	73
4.2 Backfire Antennas	74
4.3 Hoghorn Antennas	75
5 HIGH GAIN ANTENNAS	86
5.1 The Axisymmetric Parabolic Reflector	86
5.2 Asymmetric (Offset) Parabolic Reflectors	147
5.3 Non-parabolic and Partially Parabolic Reflectors	162
5.4 Lens Antennas	169
5.5 Array Antennas	176
6 MULTIPLE-BEAM ANTENNAS	200
7 TRACKING <sup>1</sup> ANTENNAS	203
8 RADOMES	206
9 BRIEF COMMENTS ON ANTENNA TEST RANGES	208
10 CONCLUSIONS	210
11 LIST OF REFERENCES	214
12 GLOSSARY	237
DOCUMENT CONTROL SHEET	239

ACKNOWLEDGEMENTS

The authors gratefully acknowledge the assistance of their colleagues at the RF Technology Centre and the considerable contribution of Mr R Garnham and Dr G N Taylor in the preparation of this report.

---

LIST OF FIGURES

- FIG: 2.1-1 Radiation pattern of a uniform line-source
- FIG: 2.1-2 Radiation pattern envelopes for uniform line-sources
- FIG: 2.1-3 Half-power beamwidth for line-sources with different illuminations
- FIG: 2.1-4 Half-power beamwidth for line-sources with different illuminations
- FIG: 2.2-1 Gain of a line-source for Dolph-Chebyshev illuminations
- FIG: 2.2-2 Gain of a line-source for Taylor illuminations
- FIG: 2.3-1 Radiation pattern of a uniform circular aperture
- FIG: 2.3-2 Radiation patterns of circular aperture with parabola-on-a-pedestal distributions
- FIG: 2.3-3 Sidelobes for parabola-on-a-pedestal distributions
- FIG: 2.3-4 Aperture efficiency for parabola-on-a-pedestal distributions
- FIG: 2.3-5 Three distributions giving -25 dB first sidelobes
- FIG: 2.3-6 Beamwidth of a circular aperture for several illuminations
- FIG: 2.3-7 Loss due to random phase errors
- FIG: 2.3-8 Radiation pattern when random phase errors are present
- FIG: 2.3-9 Sidelobe levels when random phase errors are present
- FIG: 2.3-10 Far-out sidelobes when random phase errors are present
- FIG: 3.1-1 Cross-polarised radiation from rectangular and circular fundamental-mode horns
- FIG: 3.1-2 Multi-mode horn characteristics - circular aperture
- FIG: 3.1-3 Multimode horn characteristics - square aperture
- FIG: 3.1-4 Twin-wire horn
- FIG: 3.1-5 Gain for a narrow-angle corrugated horn
- FIG: 3.1-6 Radiation pattern of a narrow-angle corrugated horn
- FIG: 3.2-1 Radiation pattern of an ideal polyrod
- FIG: 4.1-1 Corner reflector geometry
- FIG: 4.1-2 Backlobe radiation from a corner reflector
- FIG: 4.2-1 Backfire antenna geometry
- FIG: 4.3-1 Geometry of two types of hoghorn
- FIG: 4.3-2 Radiation pattern of a hoghorn
- FIG: 4.3-3 Blinders on a hoghorn
- FIG: 4.3-4 Radiation patterns of a modified hoghorn
- FIG: 4.3-5 Sidelobe envelope for a Casshorn of 30 wavelengths aperture

LIST OF FIGURES (CONTD)

- FIG: 5.1-1 32 $\lambda$  Cassegrain reflector radiation pattern
- FIG: 5.1-2 Radiation pattern of reflector with compensated feed
- FIG: 5.1-3 Comparison of predicted and experimental radiation patterns for reflectors - 40  $\lambda$  aperture - horn feed
- FIG: 5.1-4 Comparison of predicted and experimental radiation patterns for reflectors - 10  $\lambda$  aperture - dipole feed
- FIG: 5.1-5 Comparison of predicted and experimental radiation patterns for reflectors - 10  $\lambda$  aperture - horn feed
- FIG: 5.1-6 Reflector efficiency and spillover
- FIG: 5.1-7 Extraneous effects in a Cassegrain reflector
- FIG: 5.1-8 Effects of an edge shield on radiation patterns
- FIG: 5.1-9 Strut scattering
- FIG: 5.1-10 Dwingeloo 25 m radio telescope - radiation pattern
- FIG: 5.1-11 Sidelobe envelope of a 394 $\lambda$  Cassegrain
- FIG: 5.1-12 Cross-polarised field from a sub-reflector
- FIG: 5.1-13 Radiation pattern of Goonhilly II - near-in
- FIG: 5.1-14 Radiation pattern of Goonhilly II - far-out
- FIG: 5.1-15 Edge taper vs sidelobe level
- FIG: 5.1-16 Space loss
- FIG: 5.1-17 Generalised feed radiation pattern
- FIG: 5.1-18 Feed diameter vs edge taper
- FIG: 5.1-19 Backlobe for a reflector
- FIG: 5.1-20 Blockage for a reflector
- FIG: 5.1-21 RMS phase errors
- FIG: 5.1-22 Lateral feedshift effects in a reflector
- FIG: 5.1-23 Axial feedshift effects in a reflector
- FIG: 5.1-24 Mesh losses
- FIG: 5.2-1 Offset reflector geometry
- FIG: 5.2-2 Open Cassegrain geometry
- FIG: 5.2-3 Doubly offset reflector
- FIG: 5.2-4 Space attenuation for offset reflectors
- FIG: 5.2-5 Sidelobe level for offset reflectors
- FIG: 5.2-6 The effect of edge taper in offset reflectors
- FIG: 5.2-7 Peak cross-polarisation on offset reflectors
- FIG: 5.2-8 Offset reflector radiation patterns
- FIG: 5.3-1 Spherical reflector geometry
- FIG: 5.3-2 Limits on spherical reflector diameter

LIST OF FIGURES (CONTD)

- FIG: 5.3-3 Torus reflector
- FIG: 5.4-1 Lens antenna
- FIG: 5.5-1 Directivity for a linear array with sidelobe level
- FIG: 5.5-2 Directivity for a hexagonal array with sidelobe level
- FIG: 5.5-3 Grating lobe suppression
- FIG: 5.5-4 Maximum element area
- FIG: 5.5-5 Vestigial grating lobes
- FIG: 5.5-6 Sidelobe degradation for positional errors - square array
- FIG: 5.5-7 Sidelobe degradation for positional errors - linear array
- FIG: 5.5-8 Gain degradation in an array with positional errors
- FIG: 5.5-9 Array radiation patterns for a 10 element array at 50 GHz
- FIG: 5.5-10 Constrained feed network
- FIG: 5.5-11 Optical feed network
- FIG: 8.1 Effect of radome on the radiation pattern of a  $160 \lambda$  aperture reflector
- FIG: 8.2 Effect of radome on the radiation pattern of a  $80 \lambda$  aperture lens
- FIG: 9.1 Rayleigh distance vs antenna aperture

## 1 INTRODUCTION

This literature survey is concerned with the sidelobe performance of a wide range of antenna types. The fundamental questions toward which this survey is directed are:

- (i) What level of sidelobe suppression has been, and can be, achieved with antennas of differing types and dimensions?
- (ii) To what extent do these levels represent fundamental limits with respect to sidelobe performance?
- (iii) What are the principal parameters governing the sidelobe performance for any given antenna type?

Although a survey of this type cannot answer these questions directly, it is hoped that the information presented here will help to provide useful insight into the antenna types considered and thereby aid the reader in making intelligent judgments and estimations with regard to low-sidelobe antenna performance.

Sidelobe levels are quantified here in relation to the peak co-polarised forward gain of the antenna. Cross-polarisation is treated as another form of unwanted radiation and, where this exceeds the levels of the co-polarised field levels, is considered as the dominant sidelobe level. The spatial sphere surrounding the antenna is crudely divided into three general regions. These are referred to here, in terms of the magnitude of the angles subtended from the antenna boresight, as 'near-in', 'far-out' and 'back-lobe' regions. A more precise definition of these regions would be desirable but unfortunately the major part of the data available from the literature does not permit a finer distinction to be made.

This literature survey has considered a broad range of antenna types without specific restrictions on frequency, bandwidth, polarisation or gain, although very small antennas have not been considered if, like the half-wave dipole, they produce essentially toroidal radiation-patterns.

Since the sidelobe performance of an antenna is, in general, not independent of the other major parameters of the device, details of these

parameters, wherever possible, have been included in the data presented. The interaction between sidelobe suppression and the other important aspects of antenna performance is given due attention.

With the rapid growth of radar and communications applications, the need for good sidelobe suppression has become increasingly important from the point of view of reducing mutual unintentional interference on the one hand, and avoiding deliberate interference, or jamming, on the other. In most radar applications good sidelobe suppression is generally desirable to minimise clutter effects and unintentional interference. However, with the rapid development of jamming techniques and devices in recent times, sidelobe suppression has become a critical feature with regard to the ultimate performance of the radar in a hostile environment. Dax<sup>1</sup> has expressed the opinion that for long range radars to avoid jamming, the level of all antenna sidelobes must be suppressed to better than -40 dB and desirably to better than -60 dB.

In terrestrial communication systems, the need to suppress sidelobe levels has been apparent for a number of years<sup>2,3</sup>. The proliferation of microwave communication links, for example, has led to quite severe specifications being imposed, particularly for the far-out and backlobe regions.

For certain other applications, such as spacecraft antennas, the near-in sidelobes are generally considered to be more important than those occurring at the wider angles. However, the design of these antennas is more often dominated by the need to achieve high antenna efficiencies, to enable maximum gain coverage to be provided within the limits imposed by a given volumetric and mass constraint on the space vehicle. At the earth terminals of space-communication systems, sidelobe performance has tended in the past to be considered as a secondary parameter to the antenna gain and the optimisation of the Figure of Merit (i.e., gain to noise temperature ratio). However, the rapid increase in the number of Earth Stations, and the increasing utilisation of the geostationary orbit, has led to an increased concern for improved sidelobe suppression, to avoid interference effects.

To provide some insight into the fundamental factors governing the sidelobe performance of aperture antennas, Chapter 2 of this report reviews

some techniques which provide simplified theoretical predictions for these antenna types. The techniques are commonly applied to such devices as reflector antennas, horn antennas and antenna arrays. Although the results can be very informative, they cannot be used as reliable predictions of the actual performance which will be achieved with a practical antenna. Many factors act to modify the simplified theoretical predictions and these are referred to in Chapter 2 and the following text.

In Chapter 3, low-gain antennas are considered. The critical and practical radiation characteristics are given, as well as tables of expected parameters. Each subsection, e.g. on horns, dielectric antennas and broadband antennas, is complete in itself containing all tables and diagrams within each section. References, numbered separately for each subsection, are collected together at the end of the report in Chapter 11.

The chapter on medium gain antennas (Chapter 4) considers corner reflectors, backfire antennas and hoghorns, though large horns and small reflectors could be included. Medium gain is taken to be 15-25 dB of forward gain.

Chapter 5 contains details of high gain antennas, reflectors, lenses and arrays. By far the largest amount of information is available on the first type and this is indicated by the amount of space devoted to it. Each subsection contains a discussion of theories together with experimental verification, details of practical antennas and, where possible, a set of graphs and tables to assist the designer. Each subsection again contains its own reference list, though all are collected together in Section 11.

Chapters 6,7,8 and 9 cover the topics of multiple-beam antennas, tracking antennas, radomes and antenna test ranges very briefly. Chapter 10 is an extended summary of the report and its conclusions.

## 2 SIMPLIFIED THEORETICAL PREDICTIONS OF SIDELOBE PERFORMANCE

An ideal aperture distribution might be considered to be one which provided maximum forward gain with zero sidelobes. Unfortunately, for any given radiating aperture, the maximum forward gain corresponds to uniform illumination across the aperture; this condition corresponds to a relatively poor sidelobe response (-13.2 dB for a linear aperture, -17.7 dB for circular). Various mathematical expressions suitable for use as illumination functions have been devised and their characteristics will be considered in the following pages. The results are somewhat unrealistic since the possibility of achieving these distributions will not be considered here, nor will the effects of a 'real' antenna be studied in this chapter. Such factors as the finite size of an array element (which results in a stepwise approximation in amplitude and phase to the wanted illumination) and the spillover and blockage in a reflector antenna are but a few of the realities which will be considered in later chapters. However, the relationship between the illumination distribution across an aperture and the sidelobe performance is an important one which merits some attention, and the accuracy to which a desired aperture illumination must be held in order not to degrade performance serves as a useful guide to tolerances. Only linear and circular distributions are dealt with here. Rectangular distributions are briefly dealt with by Elliot<sup>1</sup> and their general performance can be inferred by a superposition of the linear aperture results. Other aperture shapes, such as elliptical, have not been treated as thoroughly in the literature. However, their general behaviour can also be inferred from the data presented below.

### 2.1 Linear Aperture Distributions

#### 2.1.1 Uniform illuminations

Hansen<sup>1</sup> discusses the uniformly illuminated linear (i.e., one dimensional) source along the x-axis from  $x = -\frac{L}{2}$  to  $x = +\frac{L}{2}$ .

The radiation pattern of such a source is

$$F(u) \propto L \frac{\sin \pi u}{\pi u} \quad (1)$$

where

$$u = \frac{L \sin \theta}{\lambda}$$

and  $\theta$  is the angle off boresight,  $\lambda$  is the free space wavelength. Table 2.1.1 gives details of this radiation pattern (Fig.2.1-1).

Table 2.1.1

Radiation characteristics of a uniformly illuminated line source

Half power beam width	=	$2 \arcsin \left( 1.39 \frac{\lambda}{\pi} L \right)$
	=	$0.885 \frac{\lambda}{L}$ radians for $L > 10 \lambda$
Sidelobe level (dB)		
	1st	-13.2
	2nd	-17.8
	3rd	-20.6
	4th	-22
Aperture efficiency (with no allowance for spillover, blockage, etc.)		100%

For  $L > 10 \lambda$  the sidelobes decay as  $L^{-2}$  in power for a set value of  $\theta$ . This indicates that the far-out sidelobes of a large antenna will be lower than those of a small aperture, but the  $n$ th sidelobe from boresight will always have the same value. Figure 2.1-2 shows the sidelobe envelope for  $L = 10 \lambda$  and  $100 \lambda$ .

### 2.1.2 Cosine distributions

1. The family of illuminations given by  $\cos^n \left( \frac{p}{2} \right)$  where  $p = \frac{2 \pi x}{L}$  and the distribution runs from  $x = -\frac{L}{2}$  to  $x = +\frac{L}{2}$ , is important. It has reduced efficiency because the illumination always reduces to zero at the ends of the aperture, i.e. at  $x = \pm \frac{L}{2}$ . The radiation pattern  $F(u)$ , where  $u = \frac{L \sin \theta}{\lambda}$  and  $\theta$  is the angle off boresight can be obtained in closed form (see Table 2.1.2).

Table 2.1.2

Cosine-power illuminations

n	F(u)	1st sidelobe (dB)	Voltage sidelobe decay as	Beamwidth (radians)	G/Go
0	$\frac{\sin \pi u}{\pi u}$	-13	$u^{-1}$	$0.88 \frac{\lambda}{L}$	1.00
1	$\frac{\cos \pi u}{1-4u^2}$	-23	$u^{-2}$	$1.2 \frac{\lambda}{L}$	0.81
2	$\frac{\sin \pi u}{\pi u(1-u^2)}$	-32	$u^{-3}$	$1.45 \frac{\lambda}{L}$	0.67
3	$\frac{\cos \pi u}{(1-4u^2)\left(1-\frac{4u^2}{9}\right)}$	-40	$u^{-4}$	$1.66 \frac{\lambda}{L}$	0.58

The power sidelobe envelope for far-out sidelobes decays as  $u^{-2(n+1)}$  so that even for  $n = 1$ , far-out sidelobes are much reduced.  $G/Go$  is the directivity (forward gain) relative to that of a uniformly illuminated line source of length.

2. Another useful family is that of the cosine-on-a-pedestal. The radiation pattern is the sum of the radiation patterns for a cosine distribution and a uniform aperture (Table 2.1.3).

Table 2.1.3

Cosine-on-a-pedestal - Radiation characteristics

Aperture edge illumination (dB)	1st sidelobe level	Beamwidth (radians)	G/Go
10	-20	$1.06 \lambda/L$	0.90
15	-22	$1.13 \lambda/L$	0.84
$\infty$ (cosine alone)	-23	$1.20 \lambda/L$	0.81

The far-out sidelobes for edge tapers below 15 dB are dominated by the effect of the pedestal and fall off slowly (as  $u^{-2}$  in power).

Although the cosine-on-a-pedestal distribution is widely used to approximate practical aperture distributions, it can be seen that the dependence of the

first sidelobe level on the aperture edge illumination is very weak. In practical reflector antennas this is certainly not the case. This example illustrates the importance of the illumination taper function itself (as opposed to the value of the aperture edge illumination) in forming the sidelobes. This case also illustrates the need for accurate modelling of the illumination taper across an antenna aperture if sidelobe level predictions are to be meaningful and simplified techniques must be used with great caution when low side-lobe performance is sought.

Figure 2.1-3 shows the variation of beamwidth against sidelobe level for a cosine squared illumination on a pedestal<sup>2</sup>. The sidelobe patterns of the two parts of the illumination are out of phase and tend to cancel. The cusppoint corresponds to the pedestal height at which the sidelobes cancel exactly.

### 2.1.3 Gaussian distributions

These are little used because to be useful, the edge taper should be zero, in which case the Fourier transform of the illumination function (the radiation pattern) is also gaussian but the aperture is infinite. This has low directivity though good sidelobe performance. For a truncated gaussian, the calculations are complex and there is no advantage over more easily managed distributions such as a cosine plus pedestal.

The envelope of voltage sidelobes will be dominated by the presence of the pedestal and will therefore decay as the  $\sin \pi u / \pi u$  function.

### 2.1.4 Two-parameter family

Bickmore and Spellmire<sup>3</sup> originated a family of two parameter illumination functions. The resultant radiation pattern is:

$$F(u) \propto J_\nu \left[ \pi (u^2 - C^2)^{\frac{1}{2}} \right] / \left[ \pi (u^2 - C^2)^{\frac{1}{2}} \right]^\nu \quad (2)$$

were  $\nu$  and  $C$  are the parameters. In this  $C$  controls the near-in sidelobe level while  $\nu$  controls the envelope decay. Hansen<sup>1</sup> shows that for sidelobe levels lower than -25 dB the sidelobe level is insensitive to  $\nu$  and dependent only on  $C$ . The real interest in this family is when  $\nu = \frac{1}{2}$  when  $F(u)$  reduces to a modified  $\frac{\sin \pi u}{\pi u}$ , and  $\nu = -\frac{1}{2}$  when the Taylor distribution is achieved.

2.1.5 Taylor line source

This has the advantage of providing a narrow beamwidth and low sidelobe levels<sup>1,4</sup>. The radiation pattern consists of a number of equal near-in sidelobes out to a value of  $n$ , beyond which the sidelobes decay as  $\frac{\sin \pi u}{\pi u}$ . The illumination functions have two parameters which control the near-in sidelobe value and the value of  $n$ . (The Dolph-Chebyshev illuminations are a variant of the Taylor distribution in which  $n$  is pushed beyond the visible range so that all sidelobes are equal).

Figure 2.1-4 shows the half power beamwidth in radians as a function of sidelobe level in dB for a Dolph distribution (the most extreme case). Tables of parameters for less extreme cases are given in Ref.1.

2.1.6 Modified  $\sin \pi u/\pi u$

In this (for which the Bickmore-Spellmire parameter  $v = \frac{1}{2}$ ) the Taylor illumination function fixes the value of the first sidelobe and thereafter the sidelobe envelope is  $\frac{\sin \pi u}{\pi u}$ . The beamwidth  $\times \frac{L}{\lambda}$  radians as a function of sidelobe level in dB is shown in Fig.2.1-4.

Intermediate forms of the Taylor function will lie between these two curves.

Table 2.1.4 gives details of the behaviour of this aperture illumination function. Note that when the first sidelobe level has been chosen, all other parameters are fixed.

Table 2.1.4

Modified  $\sin \pi u/\pi u$  distribution  
(sometimes called a one-parameter distribution)

First sidelobe level	$\frac{\text{Beamwidth} \times L}{\lambda}$	G/Go	Edge taper (dB)
-13.2	0.88	1.0	0
-15	0.90	0.993	2.5
-20	1.0	0.933	9.2
-25	1.10	0.863	15.3
-30	1.19	0.801	21.1
-35	1.28	0.751	26.8
-40	1.38	0.709	32.4

2.1.7 Comparison

A line source generally implies an array of some form and therefore the aperture illumination will not be predetermined to the same degree as, for instance, the illuminations over a reflector fed by a primary feed horn will be. In theory, any illumination distribution can be imposed. The only constraint is the accuracy with which the desired illumination can be generated.

Since we are primarily interested in sidelobe levels of better than -30 dB, some distributions can be discarded at once, for instance, uniform, cosine and cosine on a pedestal. Tables 2.1.5 and 2.1.6 give details of possible distributions for sidelobe suppressions of 30 and 40 dB.

Table 2.1.5

Distributions to achieve -30 dB near-in sidelobe levels

Distribution	G/Go	$\frac{\theta_o L}{\lambda}$	Edge taper (dB)	Sidelobe decay
Cosine squared (gives -32 dB)	0.67	1.45	$\infty$	$u^{-3}$
Modified $\frac{\sin \pi u}{\pi u}$	0.80	1.19	21.1	$u^{-1}$
Dolph	*	1.05		no decay

\* a function of  $\frac{L}{\lambda}$

Clearly the Dolph distribution, though giving the narrowest beam, is unsatisfactory as the sidelobes are -30 dB everywhere. The modified  $\frac{\sin \pi u}{\pi u}$  has the advantage of a narrow beam and higher gain (0.77 dB) but the far-out sidelobes do not decrease so rapidly as the cosine squared distribution.

Table 2.1.6

Distributions to achieve -40 dB near-in sidelobe levels

Distribution	G/Go	$\frac{\theta_o L}{\lambda}$	Edge taper (dB)	Sidelobe decay
Cosine cubed	0.58	1.66	$\infty$	$u^{-4}$
Modified $\frac{\sin \pi u}{\pi u}$	0.709	1.38	32.4	$u^{-1}$
Dolph	*	1.2		no decay

\* a function of  $\frac{L}{\lambda}$

Again the Dolph has no sidelobe decay, and the modified  $\frac{\sin \pi u}{\pi u}$  has the advantage of higher gain while the cosine cubed has a faster far-out sidelobe decay. For lower sidelobe levels still, the Dolph might be acceptable, though there is the problem of achieving and maintaining the desired currents on the aperture.

An interesting extension of this work is that by Elliot<sup>6</sup> where he has provided an illumination function based on Taylor's work<sup>4</sup> to depress the sidelobe level on one side only. This is useful for low altitude radars to reduce ground clutter. Experimental work with a slot array verified these techniques. There is, however, a main beam offset caused by the skewed phase distribution required to give the desired patterns. This also affected the difference pattern in a monopulse configuration. The null was offset more than the main beam.

Table 2.1.7 shows the directivity for various sidelobe levels. It is also noteworthy that Elliot claims that the tolerances necessary to maintain these asymmetrical sidelobe suppressions correspond to those necessary to maintain the average sidelobe level rather than the lower level of the two specified. Elliot<sup>6</sup> has extended this work to reducing the sidelobes in selected angular ranges which is useful for 'blocking out' regions which give rise to interference.

Table 2.1.7

Directivity of a linear aperture for unequal sidelobe levels

Sidelobe level	G/Go	Sidelobe level	G/Go
-15/-15	0.99	-20/-20	0.965
-15/-25	0.95	-20/-30	0.915
-15/-30	0.90	-20/-35	0.89
-15/-40	0.88	-20/-40	0.87

The required amplitude and phase distribution contain much fine structure so that large arrays have to be used or, alternatively, the elements must be excited so as to give rise to the nulls of the radiation pattern in the correct position. This last is illustrated with the theoretical pattern for a 15 element array of  $0.475 \lambda$  spacing in which the sidelobes on one side are constant at -25 dB and the first on the other is -45 dB. The envelope rises from this value to -15 dB. The use of such an antenna seems very limited.

## 2.2 Sidelobe Levels and Directivity

The directivity of an antenna can be defined as the ratio of maximum power per unit solid angle radiated by the antenna to the power per unit solid angle obtained from an isotropic radiator radiating the same total power.

Consider a large array with a Dolph distribution which will give a fixed sidelobe ratio everywhere outside the main beam. If the array length,  $L$ , is increased, the main beam will be narrowed but the sidelobe level remains unchanged. In the limit the total power in the sidelobes will dominate, which is another way of saying that the directivity decreases. For line sources with uniform illumination, this does not occur, since the radiation pattern 'closes up' as  $L$  increases and the new sidelobes which appear in the visible region are smaller than those already present. This is also true of a cosine-on-a-pedestal distribution. This defect afflicts Taylor distributions to a lesser degree (but not modified  $\frac{\sin \pi u}{\pi u}$  distributions).

Figures 2.2-1 and 2.2-2 show this for a Dolph array (the most sensitive) and a Taylor source with one quarter of the sidelobes equal. (Various sidelobe levels are shown in each case). For low sidelobe levels the limitations in directivity are correspondingly reduced.

These limitations are only valid for distributions where there are some equal sidelobes in the radiation pattern or where the envelope decays more slowly than  $\frac{\sin \pi u}{\pi u}$ .

## 2.3 Circular Aperture Distributions

### 2.3.1 Uniform illumination

This gives a radiation pattern  $F(u)$ , described by

$$F(u) \propto J_1(\pi u) / \pi u \quad (3)$$

where  $u = \frac{2a \sin \theta}{\lambda}$ ,  $a$  = radius of circular aperture and  $\theta$  = angle off boresight. The pattern is identical on all planes. The half-power beamwidth is  $\frac{1.02 \lambda}{2a}$  radians and the first few sidelobes (Fig.2.3-1) are -17.6, -24, -28 and -31.1 dB.

2.3.2  $A + B \left(1 - (r/a)^2\right)^n$  distribution

This distribution (sometimes called parabola-on-a-pedestal) has been extensively studied since feed illuminations for reflectors approximate closely to this<sup>1,2</sup>. The radiation pattern can be obtained in closed form as:

$$F(u) = \frac{\pi^2 r}{2} \left[ A \Lambda_1(\pi u) + \frac{B \Lambda_{n+1}(\pi u)}{(n+1)} \right] \quad (4)$$

$A + B = 1$  and  $\Lambda_n(x) = n! \frac{J_n(x)}{\left(\frac{x}{2}\right)^n}$ ;  $r$  is the radius variable.

Table 2.3.1 gives parameters for various values of  $\frac{A}{B}$ ,  $n$ .

Table 2.3.1  
Circular distribution of  $A + B \left(1 - \left(\frac{r}{a}\right)^2\right)^n$  where  $(A + B) = 1$

n	A/B = 0				A/B = 0.25				A/B = 0.5			
	Edge taper = ∞				Edge taper = 14 dB				Edge taper = 9.5 dB			
	0	1	2	3	0	1	2	3	0	1	2	3
First side-lobe (-dB)	17.60	24.70	30.70	36.10	-	23.70	32.30	32.30	-	22.00	26.50	30.80
Beam-width $\times \frac{2a}{\lambda}$	1.02	1.27	1.47	1.65	-	1.17	1.23	1.25	-	1.13	1.16	1.16
G/Go*	1.00	0.75	0.55	0.45	-	0.87	0.81	0.79	-	0.92	0.88	0.87

\*Go is  $4\pi^2 a^2 / \lambda^2$  for the uniformly illuminated circular aperture

Clearly a distribution with a pedestal is more effective. Taking the case with approximately 30 dB sidelobes, the illumination with  $\frac{A}{B} = 0.5$  is narrower in beamwidth and more efficient than distributions chosen from the other two values of  $\frac{A}{B}$ .

Sciambi<sup>3</sup> provides complete sets of curves for the parabola-on-a-pedestal. As an example,  $n = 2.5$  and  $A$  varying from 0 to 1 is reproduced in Fig.2.3-2. The numbers on the lines of maxima are the sidelobe levels (relative to

the main peak) for those parameters of  $n$  and  $A$ . Notice the low sidelobe values in the region of  $A = 0.1$ . This is due to the cancellation of the two radiation patterns due to two distributions, one uniform of amplitude  $A$ , the other tapered as  $B \left(1 - \left(\frac{r}{a}\right)^{2n}\right)$ . For other values of  $n$ , this 'break-point' occurs as listed in Table 2.3.2.

Table 2.3.2

Values of  $n$  and  $A$  for the 'break-point' in sidelobes

$n$	$A$
1.5	0.1
2.0	0.1
2.5	0.1
3.0	0.25
4.0	0.3

That for  $n = 1.5$  is not clearly marked.

Inspection of Fig.2.3-3 (which shows the worst sidelobe level as a function of  $A$  and  $n$ ) shows that in the region of lowest sidelobes, the radiation pattern is extremely sensitive to change in taper. For example, with  $n = 2.5$ , a change of edge taper from 20 dB to 17 dB will degrade the sidelobes by 15 dB, because the low sidelobes are achieved by a cancellation method.

The aperture efficiency is shown in Fig.2.3-4 as a function of  $A$  and  $n$  and is given relative to a uniformly illuminated circular aperture. Naturally, high values of  $A$  are best, but for good sidelobe performance,  $A$  should be in the range of 0.1-0.3.  $n = 2.5$  gives a good approximation to a Taylor distribution (see Fig.2.3-5).

### 2.3.3 Circular Taylor distribution

These have been thoroughly tabulated<sup>4,5</sup>. The two parameters,  $n$ ,  $\eta$ , serve the same function as for a line source distribution.  $n$  determines the number of equal sidelobes and  $\eta$  the near-in (constant) sidelobe level. The beamwidth is dependent on both  $\eta$  and  $n$ . For large  $n$ , the illuminations are peaked at the edge of the aperture. Although this may be possible for a large array of small elements, it is unrealistic for a reflector. For small  $n$  (say less than 5), the distributions are monotonic. Table 2.3.3

gives beamwidths for several values of  $n$  and sidelobe level and compares those with values from a suitable  $\left(A + B \left(1 - \frac{r^2}{a^2}\right)^n\right)$  distribution.

Table 2.3.3

Beamwidths for a circular aperture with a Taylor distribution

Taylor			$A + B \left(1 - \frac{r^2}{a^2}\right)^n$			
Sidelobe (dB)	n	Beamwidth (radians)	Sidelobe (dB)	Taper (dB)	n	Beamwidth (radians)
-25	4	1.13	-24.7	-∞	1	1.27
			-23.7	-15.0	1	1.17
			-26.5	-9.5	2	1.16
-30	4	1.20	-32.3	-15.0	2	1.23
			-30.8	-9.5	3	1.16
-35	5	1.25	-36.1		3	1.65
-40	5	1.31	-40.9		4	1.81

For sidelobes below -35 dB, the Taylor distribution has a narrower beam. For levels between -25 and -35 dB, there is little to choose between the distributions and indeed the aperture illuminations look very alike (Fig.2.3-5).

Note that the beamwidth for the Taylor distribution is not very sensitive to changes in the design sidelobe level.

Figure 2.3-6 shows beamwidth  $\times \frac{2a}{\lambda}$  (radians) against sidelobe level for various distributions.

2.3.4 One-parameter circular distribution

Recently, Hansen<sup>6</sup> has discussed a circular distribution which is the counterpart of the modified  $\frac{\sin \pi u}{\pi u}$  distribution for a line source. The radiation pattern has a far out sidelobe structure similar to  $\frac{J_1(\pi u)}{\pi u}$ , decaying from the first sidelobe whose value is determined by the single parameter. Table 2.3.4 gives the properties for this distribution which is:

$$g\left(\frac{\pi r}{a}\right) = I_0 \left[ H \pi \sqrt{1 - \frac{r^2}{a^2}} \right] \tag{5}$$

$I_0$  is a modified Bessel function.

The parameter, H, uniquely determines the first sidelobe level which can be expressed as:

$$17.57 + 20 \log_{10} \left[ \frac{2I_1(\pi H)}{\pi H} \right] \text{ dB} \quad (6)$$

Table 2.3.4

One-parameter circular distribution

1st sidelobe (dB)	Edge taper (dB)	Beamwidth $\times 2a/\lambda$	G/Go*
-17.57	0	1.0000	1.0000
-20.00	-4.49	1.0483	0.9786
-25.00	-12.35	1.1408	0.8711
-30.00	-19.29	1.2252	0.7595
-35.00	-25.78	1.3025	0.6683
-40.00	-31.98	1.3741	0.5964
-45.00	-38.00	1.4407	0.5390
-50.00	-43.89	1.5038	0.4923

(See Fig.2.3-6) \*Go is the forward gain of a uniformly illuminated circular aperture.

2.3.5 Comparison of circular distributions

The one-parameter function is only marginally worse than a Taylor distribution down to sidelobe levels of -45 dB. At -20 to -30 dB level, there is very little difference between all three distributions (see Tables 2.3.1, 2.3.3, 2.3.4) which explains the popularity of the  $A + B \left( 1 - \left( \frac{r}{a} \right)^2 \right)^n$  distribution since it is easy to handle. The optimum Taylor distribution is most suited to an array for n equal sidelobes where n is large since it is peaked at the edges. This does depend on the desired sidelobe suppression. For instance, the distribution becomes non-monotonic for  $n \geq 6$  and sidelobes of -25 dB but for levels of -35 dB, the distribution is non-monotonic for  $n > 10$ .

2.3.6 Asymmetric distributions

All the distributions considered above have circular symmetries and constant phase across the aperture. Elliot<sup>7</sup> has modified the circular Taylor distribution to treat an antenna whose desired radiation pattern has much lower sidelobes in one quadrant. A non-uniform asymmetric phase front is

required. This type of distribution can only be adequately represented by a large diameter array.

### 2.3.7 Non-constant phase fronts

Some studies have been carried out<sup>8,9</sup> on the effects of changing the phase front symmetrically across a circular aperture. The sidelobes are not reduced but the nulls are filled in if the phase taper is small. As the taper is increased, the pattern loses any trace of sidelobe structure, but the value of the altered pattern in the sidelobe region is higher than the original value. Examinations of the radiation patterns of Burns et al<sup>9</sup> shows that the quoted sidelobes are correct but that large 'shoulders' are clearly visible nearer to the boresight, corresponding to 1st, 2nd etc. sidelobes. The phase distributions do not affect the gain or beamwidth much.

### 2.3.8 Accuracy of distribution fit: amplitude

Figure 2.3-5 shows three different aperture distributions which result in 1st sidelobes of -25 dB and beamwidths  $\approx 1.13/(2a/\lambda)$ . It indicates a range of amplitudes through which the illumination function is permitted to vary and that the illumination could be inaccurate by  $\pm 0.75$  dB at the edge without much resultant error in the radiation pattern (either  $\pm 1$  dB in sidelobe or  $\pm 0.01$  in beamwidth). However,  $\pm 0.25$  dB is needed around a normalised radius of 0.5. The accuracy of fit required increases as the design sidelobe level decreases and an examination of Hansen<sup>5</sup> shows that an edge error of  $\pm 1.5$  dB for a distribution giving 35 dB will produce an error of  $\pm 2.5$  dB in sidelobe level.

The one parameter circular distribution<sup>6</sup> seems less sensitive. The edge taper changes from 32 dB to 38 dB as the design sidelobe level changes from 40 to 45 dB.

We conclude that the accuracy of fit of the amplitude distribution is not crucial to the achievement of low sidelobes, but the required accuracy does increase as lower levels of sidelobes are designed for, as for instance, in special cases of the distribution  $A + B\left(1 - \left(\frac{r}{a}\right)^2\right)^n$ , near the cancellation point.

### 2.3.9 Accuracy of distribution fit: phase

The distributions discussed so far have had constant phase across the aperture though it has been shown that using symmetric phase distributions

to remove sidelobes, causes null infilling and does not actually reduce the value of the radiation pattern in the sidelobe region (Section 2.3.7). Other forms of phase distribution which may occur have other effects.

- (i) Linear - this shifts the radiation pattern to a new main beam position.
- (ii) Quadratic - this is symmetric and of the type discussed above and is equivalent to a defocusing.
- (iii) Cubic - since this is asymmetric a pattern squint occurs, with an associated beam deformation; a 'coma lobe' is formed on one side of the beam.
- (iv) Periodic errors which may occur in a phased array, cause grating lobes.

Each of these error types has a different importance according to the antenna type considered and will be discussed as appropriate under each separate antenna heading.

#### 2.3.10 Random errors

The work which has been carried out on random phase front errors is equally applicable to all antenna types though the method by which they are caused will be very different. Ruze<sup>10</sup> has treated the topic in great detail and Vu<sup>11</sup> has extended Ruze's work to cover circular apertures with non-uniform illumination and larger correlation intervals. In a circular aperture, diameter  $D$ , a random phase error is defined as having rms value  $\sigma$  radians over a correlation interval,  $C$  (defined as 'the distance on average where the errors become independent'). Because this type of treatment is statistical, accurate predictions of the peak sidelobe levels in specified regions cannot be made. This theory should, however, correctly predict the loss of forward gain. The 'average' radiation pattern is usually interpreted as the average of patterns taken in all planes through the antenna boresight axis but this is only true for an axisymmetric illumination. Vu's work covered large values of  $C/D$  which are important, particularly for reflectors, where loading and the method by which the surface is attached to the backing structure may produce phase errors with large values of  $C$ .

Vu claims that the gain degradation is not much affected by the type of illumination used and that adequate values may be found by considering a uniformly illuminated aperture (Fig.2.3-7). Losses of 2 dB are sustained for rms phase errors  $\sigma = 0.6$  radians ( $\sim 0.1 \lambda$ ).

Such phase errors cause unacceptable sidelobe degradation and although the sidelobe level behaviour is affected by the aperture illumination, the pattern always breaks up (null infilling, increases in sidelobe level) with increasing  $\sigma$ .

Figure 2.3-8 gives some typical examples with a cosine squared (circular aperture) illumination and Fig.2.3-9 gives other values of sidelobe level with  $\sigma$  for various illuminations; with increasing  $\sigma$ , the sidelobe level is degraded into a wide angular response which resembles the response of a single small aperture of size  $C$ . Figure 2.3-9 shows that for a 3 dB rise in sidelobe level, the permissible phase error varies with sidelobe level and correlation interval and  $\sigma$  may be  $0.05 \lambda$  for a cosine squared distribution (32 dB goes to 29 dB) but can be  $0.10 \lambda$  for a  $\left(1 - \left(\frac{r}{a}\right)^2\right)$  distribution (25 dB degrading to 22 dB).

A much more important aspect is the wide angle behaviour. If the phase errors were sinusoidal, then the aperture would behave like a grating and far-out grating lobes would appear, which correspond to the periodicity of the sinusoidal error. This treatment has been applied by Dragone and Hogg<sup>12</sup> to an aperture with a 10 dB tapered illumination. Fig.2.3-10 shows the envelope of radiation pattern with various phase errors.

The errors are peak to peak phase errors and the rms error can be assumed to be one-third of this for a Gaussian distribution. Dragone and Hogg take as their criteria that the far-out pattern envelope must not be more than 3 dB higher than the zero error pattern which limits the peak to peak phase error to  $0.05 \lambda$ . This is an rms error of  $0.017 \lambda$  which is much more stringent than for the near-in sidelobes.

This work is unfortunately all theoretical and there does not appear to be any direct substantiating experimental work.

As far as reflectors are concerned, the far-out sidelobes are more seriously affected by other effects (spillover, edge diffraction and the aperture blocking effects when present). Another type of statistical treatment is available for phased arrays which will be dealt with in that

## 2.4 Conclusion

The data presented here provides some insight into the relationships between the illumination tapers in aperture antennas and the resultant sidelobe suppression. The effects of tolerances in introducing small perturbations of the amplitude and phase of the wavefront in the aperture plane has also been considered.

From this data, it is clear that for good sidelobe suppression it is necessary to consider the complete illumination taper across the aperture and not merely the value of the aperture edge illumination. Although these simplified scalar distributions can be used to study the importance of generating and maintaining the correct illumination characteristics of aperture antennas, they must be interpreted with some caution in attempting to predict the performance, or optimise the design, of a practical low-sidelobe antenna. For low sidelobe reflector antennas, the actual illumination taper produced is a function of the primary-feed characteristics and the reflector geometry. In view of the sensitivity of the sidelobe performance to the illumination characteristics, there is little point in assuming a particular aperture illumination function which may not be realisable by a practical feed and reflector configuration. In addition, the sidelobe performance of any reflector antenna will be strongly influenced by spillover and aperture-blockage effects, and for axis-symmetric antenna systems this will be a dominant factor in defining the sidelobe radiation characteristics. For offset reflector systems, the blockage effects can be avoided but the nature of the aperture illumination taper still cannot be independently specified without due consideration of the primary-feed and reflector characteristics. This is not to infer, however, that offset reflector systems cannot produce low sidelobe characteristics.

For antenna arrays the nature of the desired aperture illumination can be specified more freely and in this sense the simplified theoretical analysis can be applied more directly. However, the cumulative effects of tolerance errors and spurious radiation from the non-continuous elements making up the array aperture (which is assumed to be continuous here) will play a dominant role in defining the overall antenna performance.

For aperture antennas of the microwave horn variety, the practicality of the simplified analysis is limited by the difficulties of achieving the desired illumination taper in the aperture of the horn. Hence, although certain illumination functions can be approximated in practice these usually fall into a fairly limited class of distributions.

Finally it is worth noting that 'good' sidelobe performance does not necessarily demand that sidelobes be reduced to the same low level at all points in space. Such a requirement is very demanding with regard to the mechanical tolerances of the system and may be unnecessary in many applications. The meaning and implications of 'good' sidelobe performance should be considered carefully in each application. A general over-specification of sidelobe requirements can lead to inferior performance with regard to the sidelobe-related aspects of the antenna as well as reducing gain or other performance parameters.

For example, in some cases it may be a worthwhile trade-off to accept a somewhat higher level of near-in sidelobes providing the sidelobe envelope exhibits a rapid fall-off with angle from the antenna boresight. When the antenna aperture dimensions are limited, this trade-off may also be preferable in that the broadening of the base of the main beam (which occurs as a result of strong illumination tapers) may be more harmful than the higher near-in sidelobes which the taper is intended to reduce. In other cases the sidelobes in one sector may be more critical than others. In such cases overall performance and cost advantages may be gained by relaxing the sidelobe specifications in the less critical regions.

Thus, in general, it is desirable not to specify sidelobe performance by means of a single number, but rather to provide some form of performance envelope, towards which the antenna design should be directed.

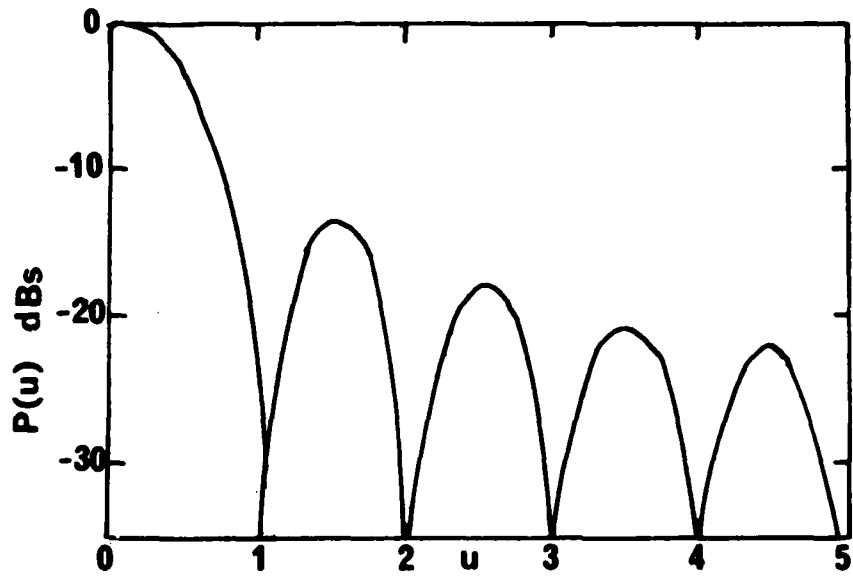


Fig.2.1-1 : The radiation pattern,  $P(u)$ , of a uniform line source of length  $L$ .  $u = L \sin \theta/\lambda$ .

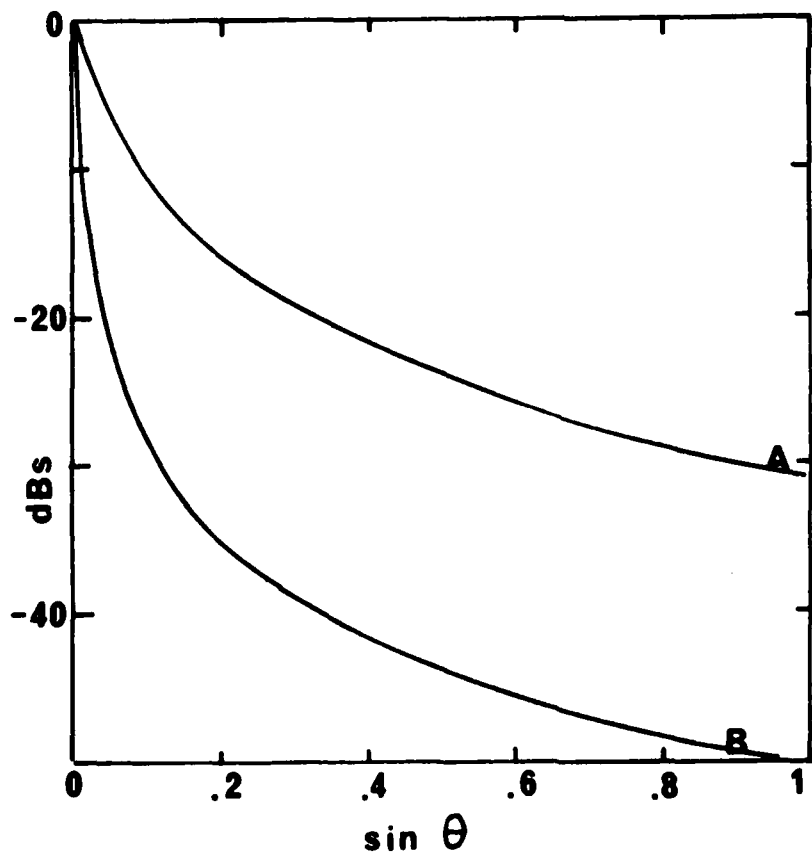


Fig: 2.1-2 The envelope of the radiation pattern of a uniform line source as a function of  $\sin \theta$  where  $\theta$  is the angle off bore-sight. A is for a line of length 10 wavelengths, B one of 100.

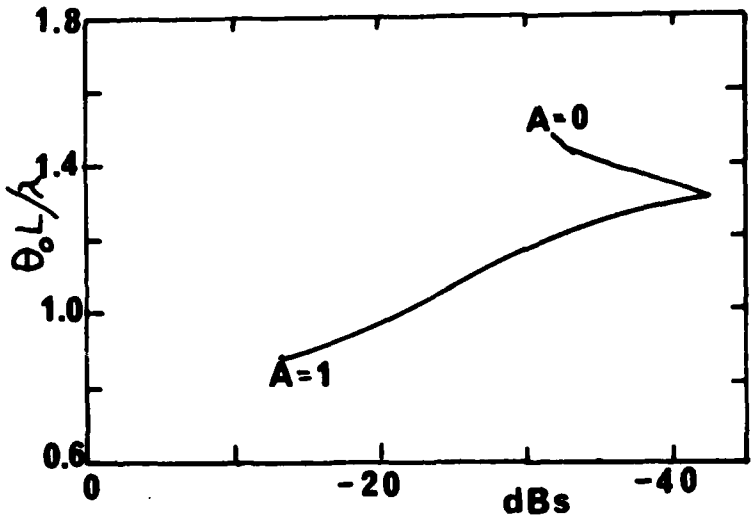


Fig.2.1-3:  $\theta_0 L / \lambda$  where  $\theta_0$  is the half-power beamwidth in radians and  $L$  the aperture length, as a function of the level of the first sidelobe for a line source of illumination function  $A + B \cos^2(x/2)$  :  $A + B = 1$  where  $x$  is the normalised aperture parameter.

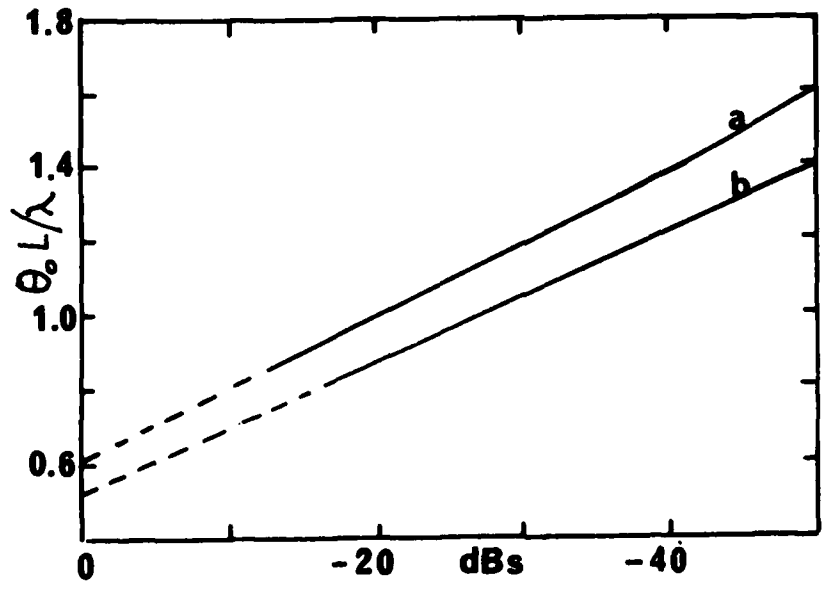


Fig.2.1-4:  $\theta_0 L / \lambda$  as a function of the first sidelobe level for a line source (a) with modified  $\sin \pi u / \pi u$  illumination (b) with Dolph-Chebyshev illumination.

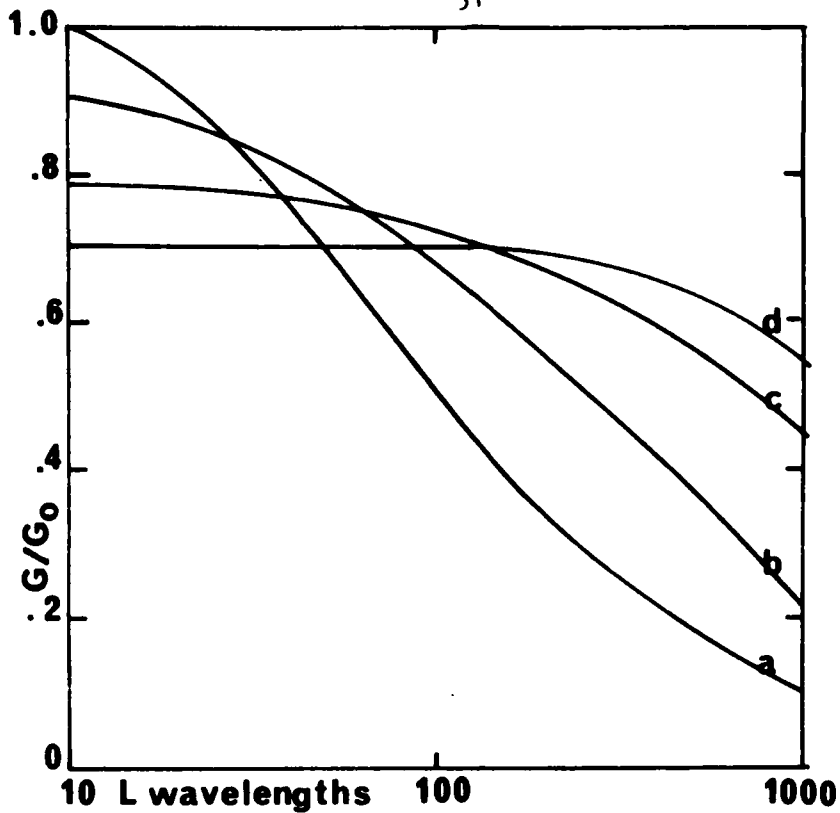


Fig.2.2-1: Gain,  $G/G_0$ , normalised to that of a uniform line source as a function of line length for a Dolph-Chebyshev distribution giving sidelobes of (a)-20 dB, (b)-25 dB, (c)-30 dB, (d)-35 dB.

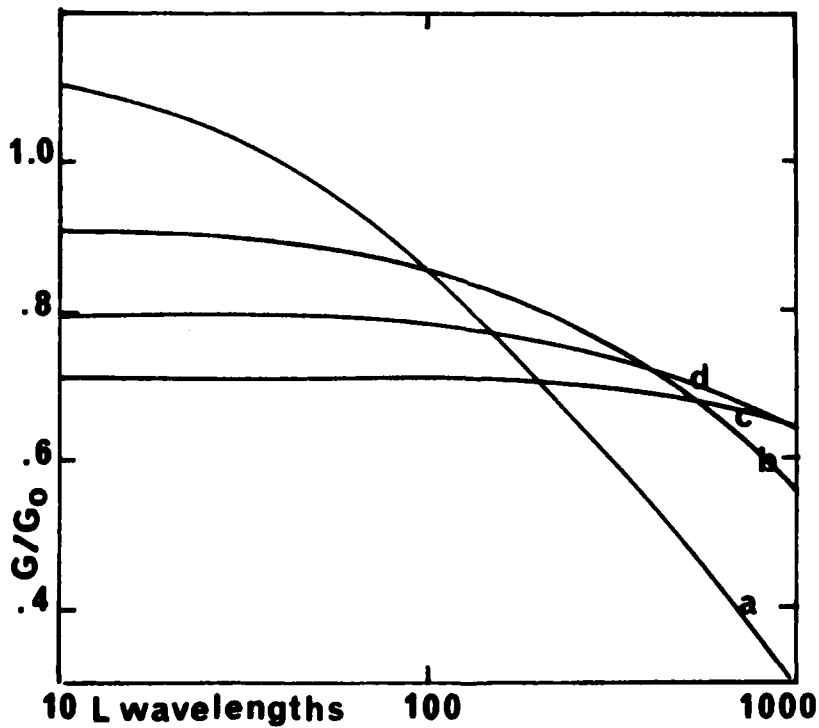


Fig.2.2-2: Gain,  $G/G_0$ , normalised to that of a uniform line source as a function of line length for a Taylor distribution giving sidelobes of (a)-20 dB, (b)-25 dB, (c)-30 dB, (d)-35 dB. ( $n = m/4$  for the Taylor function). (Hansen R C: Gain Limitations of Large Antennas. Trans. IEEE on Ant. and Prop. AP-8, p.490).

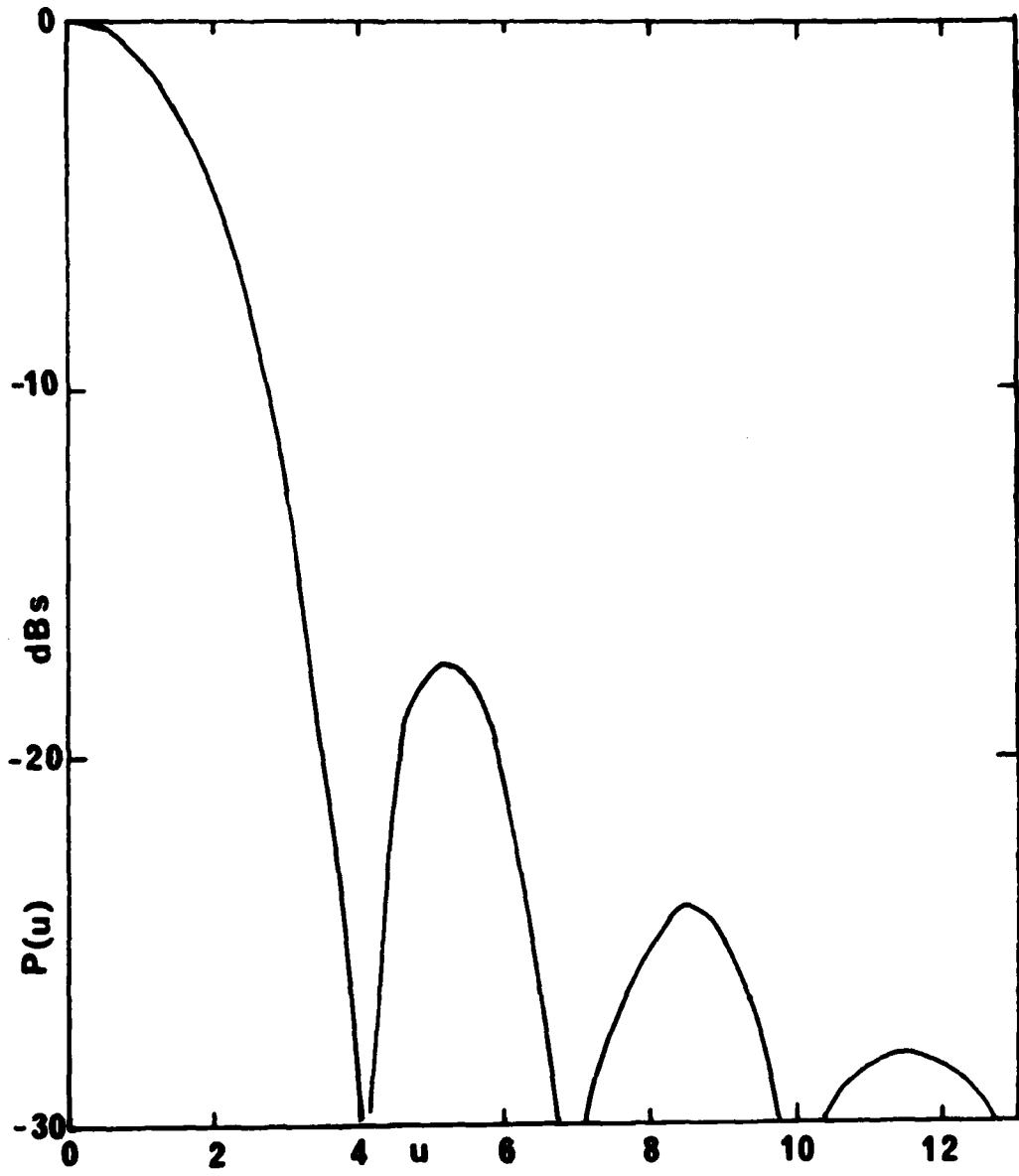


Fig.2.3-1: The radiation pattern,  $P(u)$ , for a uniform circular aperture, radius  $a$ .  $u = 2\pi a \sin \theta/\lambda$ .  $\theta$  is the angle off-axis.

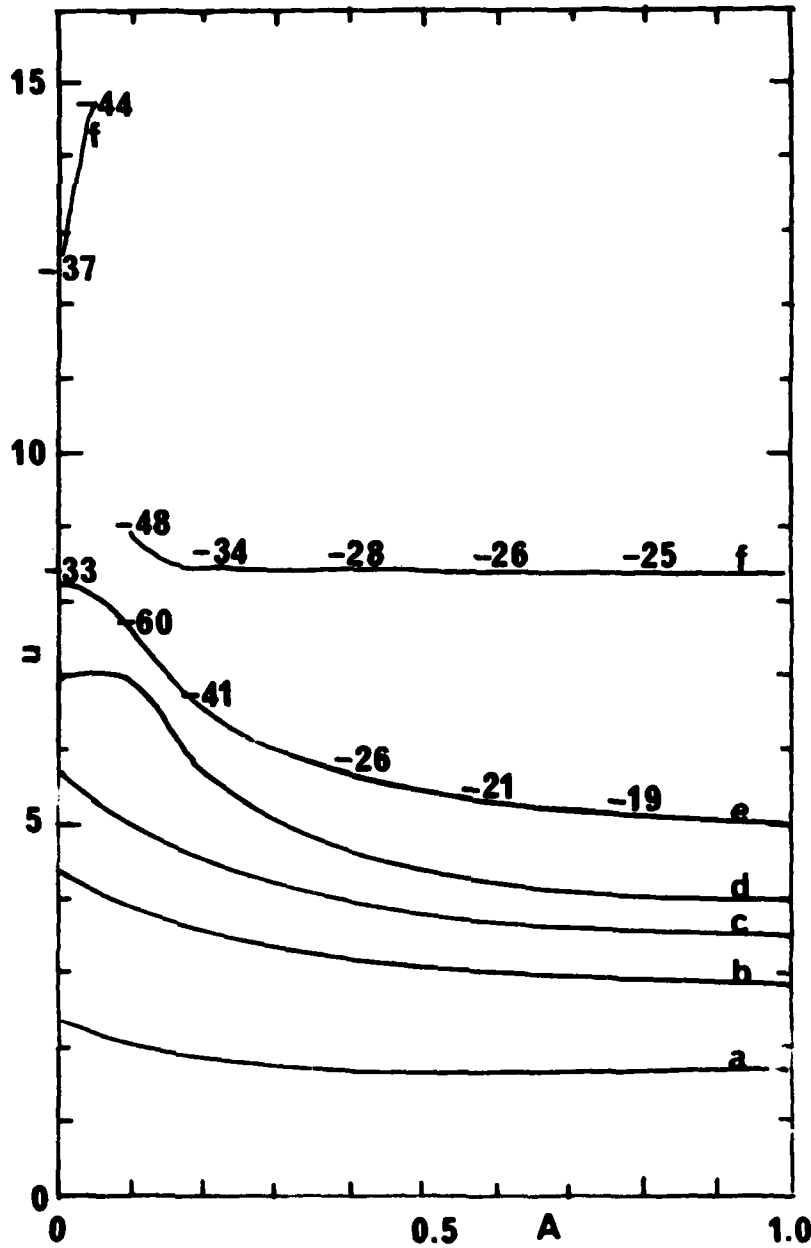


Fig.2.3-2: The variation of the radiation pattern from a circular aperture radius  $a$ , with an illumination of the form  $A + B(1 - (r/a)^2)^n$ :  $A + B = 1$ ,  $n = 2.5$ . The variable is  $A$  and contours of various pattern levels against  $u = 2\pi \sin \theta / \lambda$  are shown.

- |                            |                      |                                 |
|----------------------------|----------------------|---------------------------------|
| (a) -3 dB                  | } level on main beam | (e) position of first sidelobe  |
| (b) -10 dB                 |                      | (f) position of second sidelobe |
| (c) -20 dB                 |                      |                                 |
| (d) position of first null |                      |                                 |

Numbers on (e) and (f) are dB down on main beam.

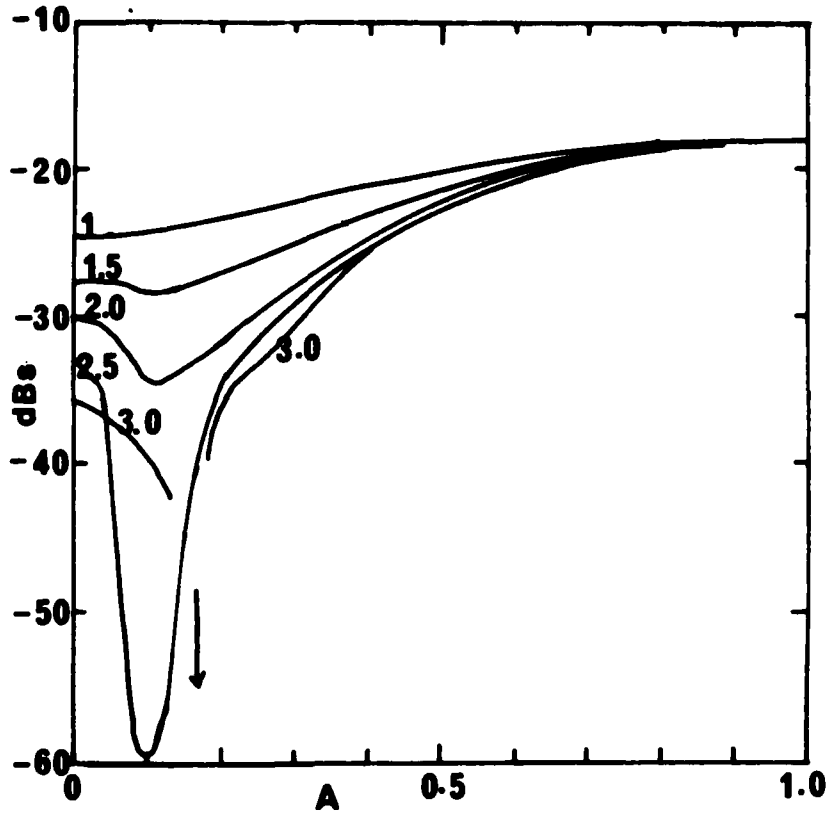


Fig.2.3-3: Worst sidelobe level in dB as a function of A where  $A + B(1 - (r/a)^2)^n$  is the illumination function. 5 values of n are shown.

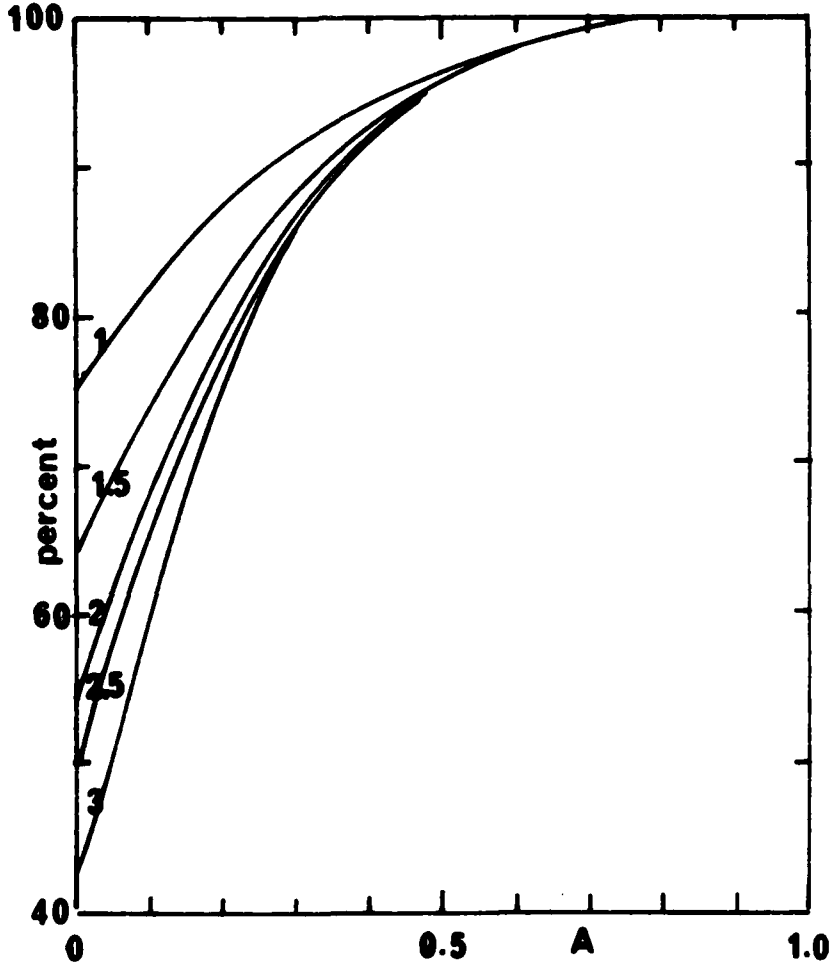


Fig.2.3-4: Aperture efficiency (per cent) as a function of A where the illumination on a circular aperture, radius a, is  $A + B(1 - (r/a)^2)^n$ ;  $A + B = 1$ . 5 values of n are shown.

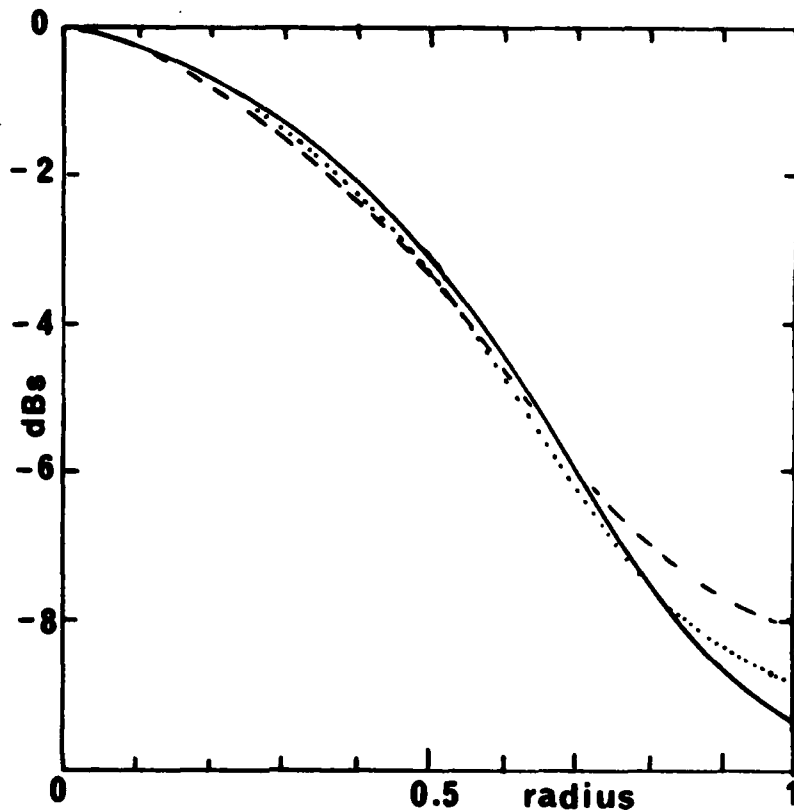


Fig.2.3-5: Illumination function (dB) across a circular aperture of normalised radius for three distributions each giving -25 dB first sidelobes. Solid curve, parabola-on-a-pedestal,  $A/B = 0.5$ ,  $n = 2$ .  
 Dashed curve -25 dB Taylor  $n = 3$ .  
 Dotted curve Parabola-on-a-pedestal,  $n = 2.5$ ,  $A/B = 0.575$ .

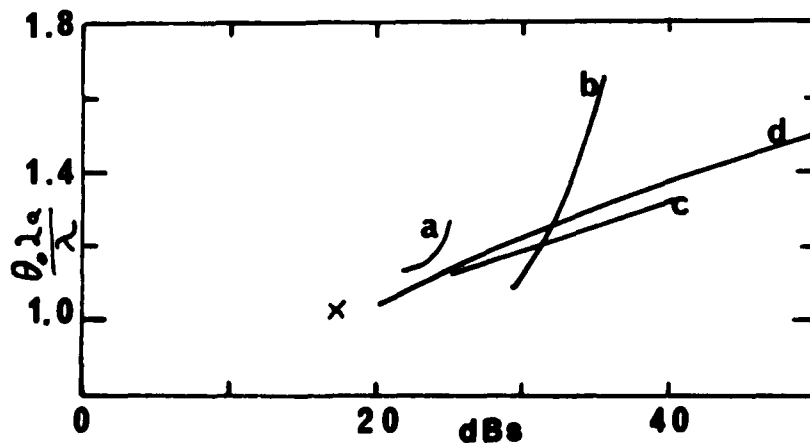


Fig.2.3-6:  $\theta_0 2a/\lambda$  vs first sidelobe level (dB) for a circular aperture radius  $a$ .  $\theta_0$  is the half-power beamwidth in radians. Illumination functions are:  
 (a)  $A + B (1 - (r/a)^2)$  (c) Taylor  
 (b)  $A + B (1 - (r/a)^2)^3$  (d) modified one-parameter-Hansen  
 The cross indicates a uniform distribution.

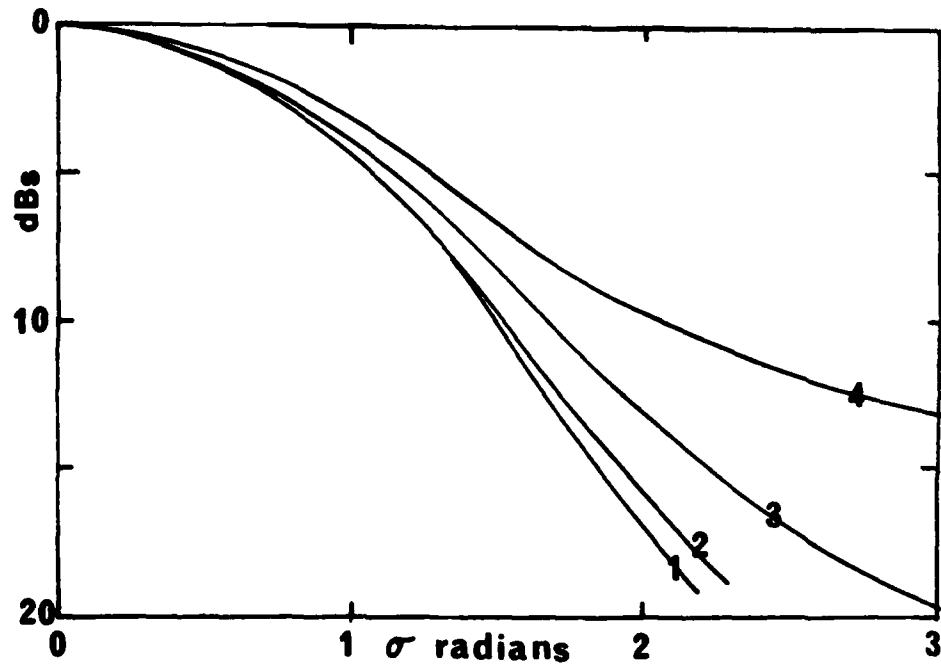


Fig.2.3-7: Gain loss in dB as a function of the rms phase error,  $\sigma$  in radians, for a circular aperture of diameter  $D$ . Correlation distances,  $C$ , are (1)  $D/50$ , (2)  $D/12.5$ , (3)  $D/8$ , (4)  $D/4$ .

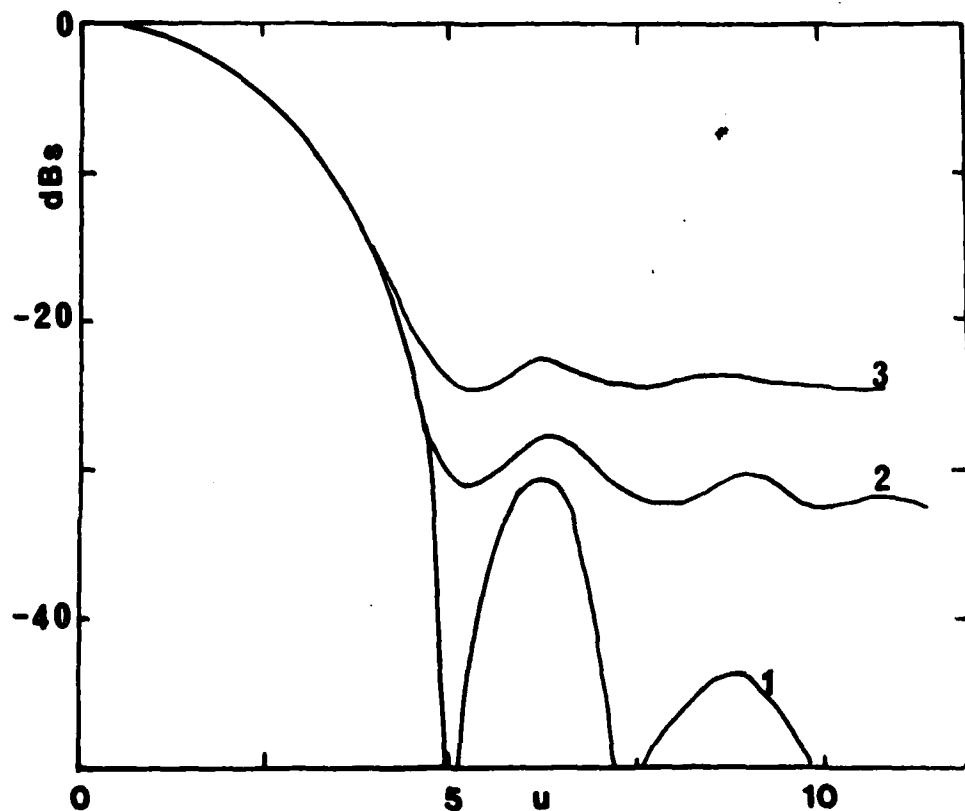


Fig.2.3-8: Radiation pattern for a circular aperture diameter,  $D$ , with a cosine squared illumination.  $u = \pi \sin \theta D/\lambda$  where  $\theta$  is the angle off axis.

- 1. No error. 2.  $\sigma = \lambda/16$ ,  $C = D/24$ .
- 3.  $\sigma = \lambda/8$ ,  $C = D/24$

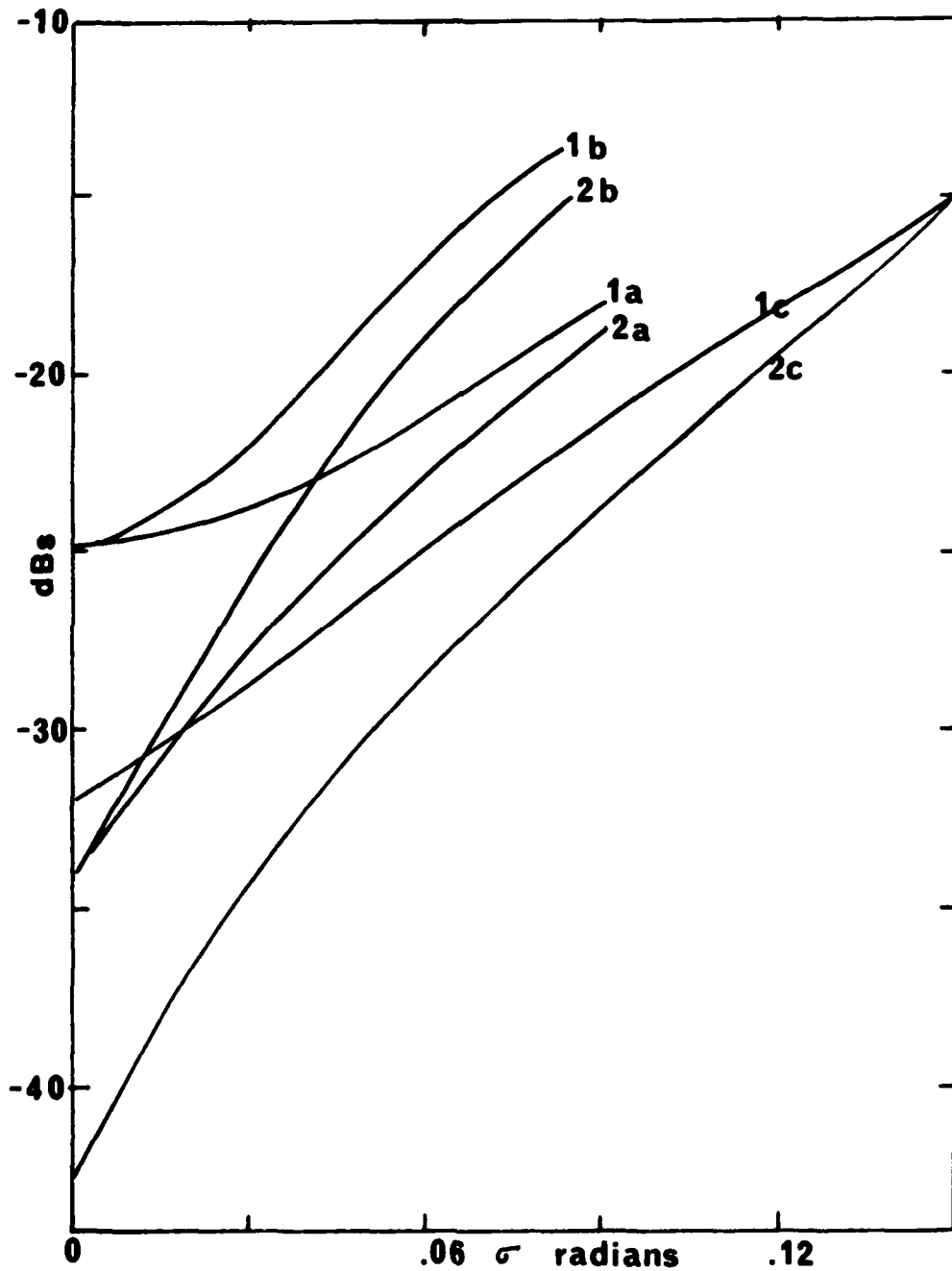


Fig.2.3-9: First and second sidelobe levels for a circular aperture, diameter  $2a$  (curves labelled as 1 and 2) as a function of the rms phase error,  $\sigma$  in radians.

- (a) illumination  $1 - (r/a)^2$ ,  $C/D = 0.05$
- (b) illumination  $1 - (r/a)^2$ ,  $C/D = 0.1$
- (c) cosine squared illumination  $C/D = 0.04$

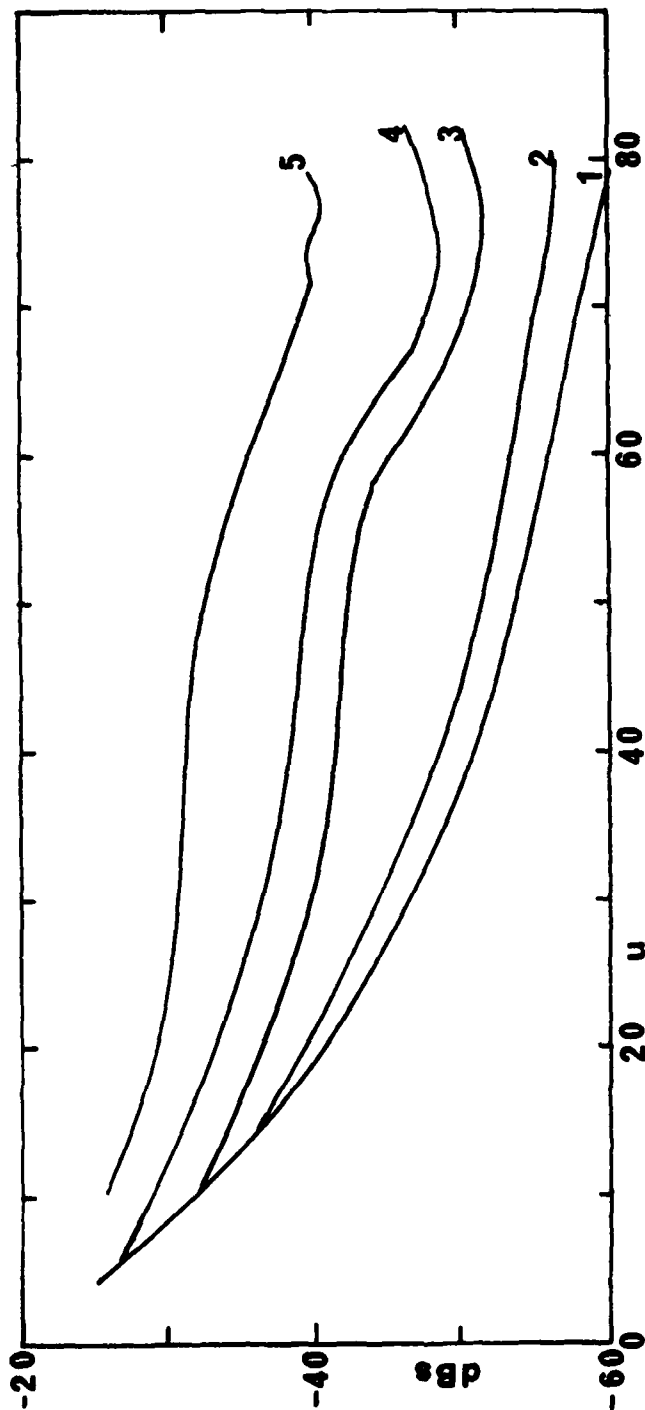


Fig.2.3-10: Sidelobe envelope of a circular aperture with a 16 dB taper.

- 1. No error
  - 2. 0.048 peak to peak error
  - 3. 0.1 peak to peak error
  - 4. 0.155 peak to peak error
  - 5. 0.31 peak to peak error
- } wavelengths

Ordinate is  $u = 2\pi a \sin \theta/\lambda$ .

### 3 LOW GAIN ANTENNAS

#### 3.1 Horn Antennas

##### 3.1.1 Smooth-walled fundamental-mode waveguide horns

###### (i) Rectangular pyramidal horns

This has been thoroughly covered in the literature. Silver<sup>1</sup> gives formulae for the radiation pattern of rectangular waveguide horns and many examples with varying parameters. The rectangular aperture horn obtained by flaring from standard rectangular waveguide has unequal beamwidths in the E and H plane. Empirical formulae for the 10 dB beamwidths of a rectangular aperture, B x A flared from rectangular waveguide are:

$$\text{E plane } \theta_{10} = 88 \lambda/B \text{ degrees for } 2/3 < B/\lambda < 2.5 \quad (7a)$$

$$\text{H plane } \theta_{10} = 31 + 79\lambda/A \text{ degrees for } 5/4 < A/\lambda < 3 \quad (7b)$$

For a pyramidal horn of square aperture, the ratio of H plane to E plane half power beamwidth is ~1.35.

These values are for 'optimum' horns (i.e., those which have minimum length without gain degradation) and a symmetric phase error is permitted across the aperture. Providing the symmetric phase error is small, the sidelobes in the H plane are good, with the first sidelobe below -25 dB, due to the horn's tapered distribution in that plane. The sidelobes in the E plane are poor since the illumination in this plane is essentially uniform. The first sidelobe is -13 dB which is degraded still further in the 'optimum' horn by the aperture phase error.

The backlobe levels have been investigated by Yu et al<sup>2</sup> using an edge diffraction technique. Their results agree well with measured rectangular horns and confirm that backlobe performance is poor when good forward gain is required. Values range from -25 to -35 dB, though for practical horns, suppression to 25-27 dB would be more likely.<sup>3</sup>

The efficiency of a large 'optimum' rectangular horn varies according to the phase error across the aperture and Thourel<sup>4</sup> quotes several measured values which centre around 60%. (Values of 60-70% seem likely).

The maximum flare angle decreases with increasing aperture in order to keep the symmetric phase error constant. Symmetric phase errors with magnitudes of more than  $\pi$  will cause pattern breakup. For large apertures, some method of minimising of the horn length is desirable to prevent the antenna becoming unwieldy. If the phase error could be corrected, a shorter horn could be used. This may be achieved by use of a phase-correcting lens<sup>5</sup> which, in addition to providing a flat phase-front, also tapers the amplitude. This improves side- and backlobe performance particularly in the E plane. Sidelobes better than -30 dB have been obtained in an H-plane sectoral horn. One of the major problems is matching the lens which otherwise reflects a large proportion of the incident radiation. Various matching techniques can be found in the literature, a surface layer of a different dielectric constant, a grooved matching layer etc. (see Section 5.4). Although these enable good electrical performance to be obtained, they have the disadvantage of decreasing the bandwidth to 10 to 20%. Such horns are, of course, more expensive to manufacture and perfect impedance matching for one linear polarisation only can be achieved.

However, the reduction in the horn mass may compensate for these factors (though the method is hardly suitable for large aperture horns where the mass of the lens will offset the mass savings in the horn and other solutions such as the hog horn are more suitable - Section 4.3). As an example, an H plane horn of aperture 18 wavelengths would have a maximum flare angle of  $14^\circ$  (an axial length from apex to aperture of 69 wavelengths). A horn of this aperture when lens corrected could have a flare angle of  $60^\circ$ , giving a length of 14.7 wavelengths.

The cross-polarisation is likely to be that of an optimum horn of the same aperture. The cross-polarisation is a function of the aperture dimensions and improves as the size increases. Rudge and Shirazi<sup>6</sup> give measured values of -20 dB and -30 dB for two small flare-angle horns of dimensions,  $0.92 \times 1.11$  and  $1.75 \times 2.22$  wavelengths respectively. A theoretical model based upon the tangential electric fields in the horn aperture plane and termed the 'E field model' appears to provide good prediction of performance<sup>17</sup>. The values quoted are peak values measured in the far-field diagonal planes of the horns. (Fig. 3.1-1a).

(ii) Cylindrical waveguide (or conical) horns

For a smooth walled fundamental-mode conical horn for linear polarisation where  $\frac{2a}{\lambda} > 1.33$  and 'a' is the radius of the horn aperture, we find

$$\text{E plane half power beamwidth} = 60 \lambda/2a \text{ degrees} \quad (8a)$$

$$\text{H plane half power beamwidth} = 70 \lambda/2a \text{ degrees} \quad (8b)$$

The first E plane sidelobe occurs at  $90 \lambda/2a$  and is about -10 to -15 dB due to the relatively uniform aperture illumination in this plane and the symmetric phase error of an 'optimum' flared horn<sup>9</sup>. The second sidelobe is about -20 dB which is of the same order as the first H-plane sidelobe. The backlobe is again in the range -25 to -35 dB but can be improved by using a circular flange or ground plane. An improvement from -24 dB to -30 dB has been quoted<sup>10</sup>. Silver<sup>1</sup> gives the efficiency of a perfect horn as 75-80% which would fall to lower levels in an 'optimum' horn.

Figure 3.1-1b shows the measured levels reached by the peak cross-polarisation in the diagonal plane of the radiation pattern<sup>16</sup>. Recent work<sup>18</sup> by Adatia has successfully predicted this performance by using the E field model. The null is due to cancellation between the field curvature effect at large diameters and the dipole effect which dominates at small diameters. Unlike rectangular aperture horns, the cross-polarisation performance of conical smooth-walled horns is poor for large apertures, with peak cross-polarised lobes in the diagonal planes (relative to the polarisation vector) of the order of -18 to -20 dB.

Various methods have been applied to improve the performance of these horns. For instance, the addition of a lens at the horn aperture to correct the phase error would enable a shorter horn to be used for larger apertures. This can improve the sidelobes by 12 dB as well as giving mass savings<sup>5,11</sup>. Another method of improving performance of a very small horn lies in adding a peripheral choke to the aperture<sup>12</sup>. In this design, the overall horn diameter, including the choke, is of the order of 1 wavelength and the aperture diameter approximately 0.78 wavelengths. The E and H plane patterns are identical down to levels of -15 dB (where the beamwidth is  $60^\circ$ ) and the cross-polarisation peak is less than -30 dB. Efficiency is 75 to 85% (Ref.12). There are no sidelobes and no information is given on backlobe performance, but it should be reasonably good

since one function of the peripheral choke is to suppress the edge currents which contribute to the back radiation.

This method has been extended to several annular chokes on small aperture horns<sup>13,14</sup>. The backlobe which at -13 dB is poor for small horns can be improved to -40 dB by using these chokes. The bandwidth can be large (20%) but the penalty paid is that the original aperture diameter is increased from  $0.86 \lambda$  to  $1.94 \lambda$ . An efficiency of 95% is claimed but this is not clearly defined and cannot be an aperture efficiency. In the feed described by Cowan<sup>12</sup>, (see above) the increase in diameter is  $0.78$  to  $1 \lambda$ , but the bandwidth over which the cross-polarisation radiation from the feed is low, is rather narrow, i.e., typically 5%. Note that this particular treatment is aimed primarily at improved co-polar radiation pattern symmetry and cross-polarisation suppression and is only applicable to horns with apertures small in terms of wavelengths.

Epis<sup>15</sup> has described a third method where radial pins are placed every  $15^\circ$  round the outside of the circular aperture. This has no effect on the H plane illumination which is zero at the edge, but effectively reduces the E plane aperture which increases the beamwidth. This method has the advantage that the same technique works for two orthogonal linear polarisations. The bandwidth is 40%, VSWR < 1.25 and beamwidth equality in E and H planes was obtained to -8 dB. However, this method does widen the physical aperture of the horn and it is unlikely that the method could be applied successfully to horns of larger aperture than the  $1.5 \lambda$  used here.

### 3.1.2 Multimode smooth-walled horns

The sidelobe suppression which is achievable with smooth-walled fundamental-mode waveguide horns is limited by the essentially uniform field distribution which is set up in the E plane of the horn aperture. As we have discussed, this can be modified by adding a peripheral structure around the aperture of small horns, but these techniques have little or no effect when the horn diameter is increased. The illumination taper in the aperture plane of a waveguide horn antenna can be modified by controlled overmoding techniques and some of these will now be discussed.

(i) The diagonal horn antenna

Love<sup>1</sup> has constructed a horn whose radiation pattern is almost circularly symmetric and has low sidelobes in all planes (-23 dB). The horn is a 'diagonal horn' where the electric field lies along a diagonal of a square aperture. This is achieved by transforming from standard  $TE_{10}$  guide to  $TE_{11}$  in circular guide from which another transition is made to a square section oriented at  $45^\circ$  to the original rectangular axes.

This horn provides equal E and H plane patterns with first and second sidelobes at -32 and -42 dB respectively. Theoretically, the sidelobes in the  $45^\circ$  plane should be -19 dB. In practice, these occurred at -26 dB which Love attributes to the amplitude tapering effect of a lens inserted to correct errors in the aperture phase. The half power beamwidth is  $58.5 \lambda/D^\circ$  where D is the side dimension of the square aperture. This should be compared with  $51 \lambda/D^\circ$  for the E plane of a fundamental mode horn. The aperture efficiency was in the range 60 to 70%.

The major defect of this horn is the high level of cross-polarisation present on the  $45^\circ$  plane. The peak level is -16 dB at an angle of  $60 \lambda/D^\circ$ . There is no cross-polarisation above the -40 dB level in the principal planes. The other defect is the horn length. The transitions are of fixed length regardless of the final aperture dimensions. This will make a low-gain horn rather longer than is normally desirable. In addition, the theory does not work well for small horns with values of  $D/\lambda$  approaching unity. The models built and tested were all in the region  $D = 10 \lambda$  giving a main beam which is rather narrow to be used as a reflector feed (for example, half power beamwidths of 5.5 and  $8.5^\circ$  for the two models), except for Cassegrain reflectors with large effective F/D ratios.

(ii) The Potter or dual mode horn

A much superior horn with good axisymmetric radiation characteristics and relatively low sidelobe levels is described by Potter<sup>2</sup>. This is a conical horn in which both  $TE_{11}$  and  $TM_{11}$  modes propagate. The higher order mode is excited by an axisymmetric step in diameter just outside the throat region. The length of the  $TM_{11}$  mode generating and phasing section and the distance to the horn aperture act to narrow the bandwidth for an axisymmetric radiation pattern to about 5% since the modes must radiate from the aperture with the correct relative phase and the mode

velocities are different within the device. Note that the impedance bandwidth of these devices is essentially similar to the fundamental-mode conical horn.

Over this relatively narrow bandwidth the sidelobes of the Potter horn can be suppressed to below the -30 dB level in all planes. At the band edges there is a tendency for 'shoulders' to occur on the main beam of the radiation pattern at levels of the order of -25 dB. For linear polarisation, the peak cross-polarised lobes radiated by the Potter horn occur on the diagonal plane and can be suppressed to the -33 dB level for a well designed horn<sup>3</sup>.

The backlobe of this antenna is due to edge diffraction. However, since the two modes are out of phase and tapered to the edge, a low value of -50 to -60 dB can be achieved. Potter states that equalising the E and H plane beamwidths of the conical horn always results in minimising the backlobe radiation.

A further modification by Bailey<sup>4</sup> has produced a somewhat shorter horn by putting all the phasing and mode conversion into the horn section. The patterns in E and H planes are identical down to the -10 dB level over a 6% band and the VSWR is less than 1.1 over a 20% band while the axial ratio was less than 1.2 dB from 1375 to 1550 MHz. Sidelobes are less than -30 dB in all planes.

### (iii) Rectangular overmoded horns

A rectangular aperture horn of this type has been described by Han and Wickert<sup>5</sup>. Besides having a step in waveguide dimensions to excite TE/TM<sub>12</sub> and TE/TM<sub>21</sub> modes, two separate flared sections are employed. This is because higher modes are generated at flare changes, whose amplitude is proportional to the change in flare and the change in flare angle should be restricted to 5°. An experimental horn was tested at X band which gave a good circularly polarised pattern with an elliptical contour. The sidelobes were less than -28 dB and the axial ratio was less than 1 dB (i.e., peak cross-polarised levels of less than -24 dB).

There is no information on efficiency, backlobe or VSWR which is stated to be good. Nor is there any information on bandwidth which is likely to be narrow.

It is worth noting that this type of rectangular multimode horn could act as a feed for an elliptical reflector though in the referenced case it was designed for direct use on a spacecraft and therefore had a beam to half power of  $15.2^\circ \times 8.8^\circ$ . No structural dimensions are given in the literature.

Another multi-flared pyramidal horn is described by Cohn<sup>6</sup> who aimed at converting some  $TE_{10}$  to  $TE_{12}$  and  $TM_{12}$  as above. Cohn took precautions against exciting higher modes such as  $TE_{14}$  by using successive small flare angle changes instead of abrupt steps. Due to this procedure, the differential phase shift between the point of mode-excitation and the aperture is decreased. The standing wave ratio was less than 1.02 and the E and H plane patterns were closely equal down to -15 dB over the frequency range 3.7 to 4.2 GHz. Sidelobes were -22 dB in E plane at 3.7 GHz, otherwise were less than -28 dB. At 4 GHz the aperture was  $7.45 \lambda$  and the length  $52.49 \lambda$ .

Another version<sup>7</sup> is quoted as having an aperture efficiency of  $75 \pm 3\%$  over the range 9.5 to 10.5 GHz. The backlobe performance is not specified but is probably better than -40 dB.

(iv) Dielectrically loaded overmoded horns

Satoh<sup>8</sup> has conducted a thorough study of useful modes and the power required in each to give the most axisymmetric radiation patterns from both circular and rectangular aperture horns. Fig.3.1-2 shows, for a circular aperture, the ratio of E plane to H plane half power beamwidth, the first (E plane) sidelobe and the maximum cross-polarisation as a function of the percentage of power in  $TM_{11}$  (he assumes  $TE_{11}$  and  $TM_{11}$  to be the only modes present). The best results were obtained when the power in  $TM_{11}$  was about 11%. 10 to 17% would give acceptable performance.

Figure 3.1-3 shows the same functions for a square horn. Satoh took modes  $TE_{10}$  and  $TE_{12}/TM_{12}$  to be present. Each of the additional modes produces cross-polarisation but the fields are opposite so there is some chance of cancellation.

The optimum ratio of powers is claimed to be:

$$TE_{10} : TE_{12} : TM_{12} = 82 : 4 : 14 \quad (9)$$

The halfpower beamwidth in the  $45^\circ$  plane was 2% different from the E and H plane beamwidths when those were equal.

Satoh then generated these modes by inserting dielectric rings part way down the flare of a conical smooth walled waveguide horn. For this conical horn, the cross-polarisation was lowered from -16 dB to -40 dB over a 3% band and -28 dB over 13% band. Sidelobes were lower than -35 dB. The pattern in E, H and  $45^\circ$  planes were identical down to the -25 dB level. In this horn the dimensions were such that higher-order modes could be generated and grooves were cut in the horn walls to suppress them.

Similar results were obtained by Satoh<sup>8</sup> for a square horn, performance was good, though the cross-polarisation was poorer (for inexplicable reasons). See Tables 3.1.1, 3.1.2 for comparative data. (Section 3.1.4).

(v) Twin-wire horn

Ajioka and Harry<sup>9</sup> describe another type of low sidelobe conical horn. In this multi-mode horn the  $TM_{11}$  mode is generated by a version of a TEM mode structure (see Fig.3.1-4). The dominant mode ( $TE_{11}$ ) propagates through the horn throat and a fraction of the power is coupled to the TEM rod structure. This fraction is controlled by the stub height, and can be 15 to 20%.

The  $TM_{11}$  mode is launched at the end of the stubs and both modes propagate to the mouth of the horn. The length L controls the relative phases of the modes and the phasing can be correct over a 20% bandwidth. The behaviour of the radiation pattern is much like that of the Potter horn; there are two disadvantages. The first is that the structure is fragile. Clearly any vibration which alters the rod position will produce incorrect moding. Also the horn is very long. The aperture diameter discussed in this paper is  $2.31 \lambda$  and the overall length is 18 wavelengths (at 9 GHz).

By way of comparison, a dual mode horn of the Potter type described by Shirazi<sup>3</sup> for 30 GHz operation has an aperture diameter of  $2.8 \lambda$  and an overall length of  $6.61 \lambda$ . These dimensions can be decreased still further employing the techniques of Bailey<sup>4</sup>.

### 3.1.3 Corrugated hybrid-mode horns

It has already been shown that by the addition of higher order modes or by the addition of peripheral chokes to a circular aperture, significant improvements can be made in the axisymmetry of the radiation patterns obtained from such structures, with additional benefits in improved side-lobe and cross-polar lobe suppression. These effects can also be achieved by use of cylindrical horns with circular corrugations within the flare itself.

In the Potter horn  $TE_{11}$  and  $TM_{11}$  modes have to be present in the correct ratio at the aperture. Because of the differing phase velocities of these modes in the horn, the bandwidth is limited. A corrugated horn can be designed such that both modes propagate with equal phase velocities, thereby combining to form a single hybrid mode ( $HE_{11}$ ). Since the  $TE_{11}$  and  $TM_{11}$  modes can be made to be essentially degenerate in this structure, bandwidths of up to 50% are feasible.

#### (i) Large flare-angle horns (Scalar-horns)

Simmons and Kay<sup>1</sup> measured circularly symmetric patterns for various horns with included flare angles between  $80^\circ$  and  $140^\circ$  and found sidelobes to be less than -30 dB. For these large flare-angle horns, the half power beamwidths have been found to be less frequency dependent than would be anticipated from consideration of a fixed diameter circular aperture. The -10 dB beamwidth of the scalar feed has been found to be about 0.75 of the flare-angle.

Examples of patterns for an included angle of  $60^\circ$  are shown by Clarricoats and Saha<sup>2</sup> who found the E and H plane radiation patterns equal down to levels of -35 dB which occurred at angles of  $\pm 50^\circ$  from boresight. The maximum sidelobe is stated to be -45 dB and there is an implication that the back-lobe may be less than this, but the wording is vague.

Clarricoats and Saha in another paper<sup>3</sup> have attempted to shorten the length of the horn by using a correcting lens. This widens the main beam of the radiation pattern. Since the angle of flare is now large, up to  $120^\circ$ , the backlobe is poor at 30-40 dB and the efficiency must be decreased. In another publication Cahill et al<sup>4</sup> define the efficiency of a similar horn plus lens arrangement as 70% which seems high - the first sidelobe

A similar arrangement tested by Smith<sup>5</sup> had a first sidelobe at -30 dB, the backlobe better than -40 dB and the aperture efficiency had the more plausible value of 55%.

Only the effect of the flare angle has been mentioned so far. Jansen et al<sup>6</sup> have measured the radiation pattern of horns with an included flare-angle of  $120^\circ$  and with two slant heights of 1.31 and 6.36 wavelengths. The widths to 10 dB were practically identical but the larger feed had a flat-topped radiation pattern and a much sharper fall-off than the small version. The larger feed is more suitable as a reflector feed where spillover will be minimized. In both cases the H and E plane radiation pattern were alike. Under these conditions it is clearly not possible to discuss such parameters as aperture efficiency though the upper limit on efficiency is stated to be 69%.

Although no dimensions are given in the literature, the rectangular horn described by Frank<sup>8</sup> which uses triangular shaped corrugations must be a wide angle horn. This horn had a gain of 11 to 12 dB over the band 7.5 to 18 GHz and the beamwidths (E and H plane) remained within the range  $42^\circ \pm 5^\circ$ . Sidelobes are less than -20 dB up to 12 GHz but deteriorate at higher frequencies.

(ii) Narrow flare-angle corrugated horns

As a consequence of their useful qualities as high-performance dual-polarised feeds for reflector antennas, the theory of these horns has been the subject of considerable investigations. The reader is referred to the papers collected in Ref.7 for details. The design and optimisation of the corrugations has been of particular interest. Mentzer and Peters<sup>9</sup> suggest that the density and shape of the corrugations should be varied along the horn taper to obtain minimum transmission loss and VSWR. The dimensions of the horn (included flare-angle usually less than  $60^\circ$ ) are chosen according to the rules for fundamental mode horns.

Narasimhan<sup>10</sup> gives details of design for horns of an included flare-angle less than  $60^\circ$  (see Fig.3.1-5). Coleman et al<sup>11</sup> gives the full pattern of a corrugated circular horn (Fig.3.1-6) which shows the low backlobe obtainable with the corrugated horn. E and H plane patterns are essentially identical. This is a Q-band example of gain 23.2 dB.

Clarricoats and Saha<sup>2</sup> have provided a comprehensive analysis, and state that the efficiency of a corrugated feed horn of small included angle is 65 - 70%.

Considerably less information on sidelobe level is available for a rectangular corrugated feed horn. The first sidelobe level of one such horn<sup>12</sup> varied between -20 and -34 dB over the band 8-11 GHz. Cross-polarisation had a maximum value of -28 dB on axis but the peak values which might be expected to occur in the diagonal planes were not reported. Gain was 0.6 to 2.0 dB lower than an ordinary rectangular horn, i.e., 87 to 63% of the efficiency of a gain-optimised rectangular horn. Considerable difficulties were encountered in the design of the horn, as a result of undesired higher order modes. This may account for the low efficiency and high cross-polarisation levels reported.

Bahret and Peters<sup>13</sup> have also discussed a square corrugated horn of small flare-angle ( $15.2^\circ$ ) into which they have introduced higher order modes. At 10.6 GHz the aperture is 6 wavelengths and there is no evidence of sidelobes or backlobes above -55 dB. However, at the nearby frequency of 9.5 GHz, the sidelobes were extremely high. This narrow bandwidth must be attributed to the use of higher order modes which have to be correctly phased in the radiating aperture to give the designed radiation characteristics.

#### 3.1.4 Horn antennas: Summary

The prediction of the co-polarised radiation from most forms of waveguide horn can be achieved with reasonable accuracy in the main beam area by means of well established techniques. The cross-polarised fields in this region can also be predicted with acceptable accuracy using techniques based upon an approximate knowledge of the tangential electric field in the aperture-plane of the horn (i.e., the E field method). The prediction of the overall sidelobe performance from low-gain horns is less satisfactory although the E field method can usually provide adequate predictions of the first sidelobe levels providing the tangential electric field assumed for the horn aperture is reasonably accurate, and due allowance is made for any spherical phase error introduced by the flaring of the horn. Accurate knowledge of the wide-angle radiation from low-medium gain horn antennas must still be obtained from experimental data.

In practice, significant deviations between predicted and measured side-lobe performance may result from unwanted overmoding in the horn structure, or tolerance effects. For small horns the immediate vicinity of the antenna must be considered as a part of the radiating structure and as such, can significantly modify the overall radiation.

Good sidelobe suppression can be achieved with horn antennas, particularly if the field distribution in the aperture of the horn can be made to taper smoothly to a low value at the aperture edge. Choked and dual-mode (Potter) conical horns can provide these characteristics over narrow bandwidths (i.e. 5%) and the more massive (and more expensive) cylindrical corrugated (hybrid-mode) horns can produce similar performance over bandwidths of up to 50%. Achieving pattern symmetry in these devices, which is a common design goal when the antennas are used as high-performance reflector-antenna feeds, also appears to optimise the cross-polar and sidelobe and backlobe suppression.

For rectangular horn geometries a similar pattern emerges although the development of high-performance rectangular corrugated horns lags considerably on their cylindrical counterparts. The analysis of rectangular corrugated devices is somewhat more complex than the cylindrical types and, in practice, considerable difficulties are encountered in avoiding the generation of unwanted higher-order modes in these antennas. Present levels of achievement in these devices are generally inferior to those of cylindrical corrugated horns in most aspects of their performance. However, in certain applications, the rectangular geometry will be essential and this may outweigh any other considerations.

In Table 3.1.1, typical performance characteristics of most of the useful horn types are summarised. This data is based upon measured performance data obtained from the literature survey.

Table 3.1.2 provides dimensions for specific gain values for various horn types which are commonly applied. This data is obtained from the references in Sections 3.1.1 to 3.1.3.

Dividing the horns into three general types, Table 3.1.3 shows an attempt to provide a very simple categorisation of their performance. This table is useful only for the most general comparison since the selection of a horn for any specific application will be heavily influenced by a range of weighting factors which have not been included here.

Table 3.1.1

Characteristics of horn antennas

Antenna type	Sidelobes (dB)		Back-lobe (dB)	Cross-polarisation		Bandwidth (%)	Eff. (%)
	E plane	H plane		Peak (dB)	Plane of maximum		
1 Optimum-gain* rect.	-10 to -13	<-26	-25	-20 to -45*1	45°	30	60-70
1a Plus lens	-30	<-30	<-35	*2	45°	10	60
2 Optimum-gain* circular	-10	-27	-25	-20 to -30*3	45°	40	60
2a Plus lens	<-22	<-30	<-35	*2	45°	10	60
3 Choked horn (D<1.2λ)	<-50	<-50	-40	-32	45°	5	75
4 Potter horn	<-30	<-30	-50	<-33	H	5	60
5 Diagonal horns	-32*4	<-40	<-40	-16	45°	?	65
6 Scalar (wide angle)	<-30	<-30	-50	-30 to -40	on axis	50	65
6a Plus lens	-27	<-30	-50	<-40	on axis	15	55
7 Narrow angle circular corrugated horn	< 50	< 50	< 80	-40 to -50*5	on axis	40	65
8 Corrugated rect. horn	-30	<-30	-50	-15 to -30	on axis	30	50

\* Defined as the shortest possible horn with gain degradations <0.2 dB.

\*1 Performance improves with increasing aperture.

\*2 As the optimum fundamental horn, unless the lens is zoned in which case it deteriorates. Zoning is necessary for mass purposes (say an aperture in a large dielectric lens of more than 15 wavelengths).

\*3 For 1.33 wavelength aperture. Performance improves as diameter decreases to an optimum diameter of 1.14 wavelength.

\*4 -26 dB in the 45° plane.

Table 3.1.2

Examples of measured performance of horns

Gain (dB)	Dimensions			HPBW (degrees)		Sidelobes (dB)		Back-lobe (dB)	Maximum cross-polarisation	Band-width (%)	Antenna type
	D/λ	L/λ	L/λ	E	H	E	H				
22 15.5	5.2 2.0	9.5 2.6		12 30	18 35	-10 -10	-27 -27	-25 -25	-18 -19	40 40	Smooth walled conical horn. D is diameter.
- -	D <sub>1</sub> /λ 1.0 1.94	D <sub>2</sub> /λ 0.7 0.86	L/λ	60 70	60 70	<-50 <-40	<-50 <-40	<-40 <-40	<-32 <-30	3 20	Choked horn. D <sub>1</sub> total diameter. D <sub>2</sub> diameter without choke.
22.1 15.5	a/λ 6.07 2.62	b/λ 4.5 1.8	L/λ 9.055 1.765	11.7 35	11.7 35	-11 -11	-25 -25	-25 -25	<-35 <-35	40 40	Smooth walled rectangular horn. Aperture a x b.
22.1 15.5	D/λ 4.45 1.68	L/λ 9+X 1.8+X		13.0 35.0	13.0 35.0	-32 -32	<-32 <-32	-40 -40	-16 -16	5 5	Diagonal horn. Side D X = transition length.
17	D/λ 2.8	L/λ 6.61		24	24	<-30	<-30	<-50	-27	5	Potter horn. Diameter D. Length L.
22.35	8.2	12.8		19	19	<-34	<-35	-57	<-28	5?	Corrugated horn. Square aperture Side D.
19	3.4	3.5		21.7	21.7	<-40	<-40	<-40	<-30	40?	Circular corrugated horn. Diameter D.

L is the axial length.

Table 3.1.3  
Comparative ratings for 3 horn types

Type	Fundamental mode	Multi-mode	Corrugated
Minimum outer dimensions	1	1	2
Minimum length	1	2	3
Minimum mass	1	2	3
Best sidelobe suppression	3	2	1
Best backlobe suppression	3	2	1
Best cross-polarisation suppression	3	2	1
Largest operational bandwidth	1	3	2

1 is best, 3 is worst

### 3.2 Dielectric Antennas

#### 3.2.1 Dielectric rods

A dielectric cylinder may support a guided wave and this property can be used in the construction of antennas. The phase velocity is a function of the rod diameter  $d$  and the dielectric constant,  $\epsilon_r$  (see Ref.1). If the cylinder is terminated, the end will radiate in the same way as an open waveguide does. There are, however, important differences.

The manner in which the travelling wave is bound to the rod (usually most of the power flows outside the rod) is dependent on the phase velocity. The nearer the phase velocity to free space velocity, the thinner the rod and the less the wave is bound and the larger the final effective aperture. The illumination in a transverse plane across the end of the rod will be near Gaussian and the resultant radiation pattern, whose beamwidth decreases with the rod diameter, has no sidelobes and is perfectly smooth (Fig.3.2-1). The usual mode is a dipole mode,  $HE_{11}$  which is the lowest propagating mode (linear polarisation). Provided the initial diameter is not too large, no higher modes will be generated.

This is the ideal case. In practice there are several complicating factors. The antenna is usually fed from waveguide. Waveguide has a lower limit on its diameter and the final diameter of the dielectric rod is much less

than this so a taper must be introduced to reach the final required diameter. Clearly, if the dielectric constant is high, say greater than 5, precautions have to be taken to avoid higher order modes being generated which will radiate as soon as the rod becomes too thin to bind them effectively. Also, some symmetric modes have an end fire null and thus any energy in such modes will radiate into the sidelobe region.

If the dielectric-rod taper is too severe, radiation will occur along the rod and interfere spatially with that originating from the end of the rod. Methods are available<sup>2</sup> for choosing a suitable taper to minimise this effect. Equally, the immediate surroundings of the antenna must be kept free of conducting obstacles, which might affect the fields along the rod.

The antenna feed point (often called the 'launcher') is another source of interference. It is difficult to launch a wave on to a rod with 100% efficiency. 80% from a waveguide would be accounted fair and 90% good. The difficulty lies in matching the fields on the rod to those on the guide. (The larger the launcher diameter the easier this operation tends to be). The excess radiation is radiated directly from the launcher and gives a wide radiation pattern which will interfere with the wanted pattern since the phase centres are separated by the length of the rod.

If there is no radiation from the launcher or the taper, then the rod may be terminated as soon as the desired diameter is reached. However, it is essential that the radiation from the rod and launcher be correctly phased in the forward direction in order to maximise the gain. This governs the length of rod at the final diameter beyond the end of the taper. The phase velocity for a small diameter rod approaches that of free space; thus the differential phase shift between rod and launcher increases slowly and high gain antennas are long and slender. This gives a practical upper limit to the gain of around 20 dB for structural reasons. The guided wave to be properly held to the rod must have the rod straight to certain limits of bend and roughness<sup>3</sup>. These limits become more stringent as the gain increases.

The characteristics of the break down of proper binding without overmoding is radiation from along the final straight section which interferes with the main beam causing high sidelobes and a loss of forward gain.

There is a lower limit to gain which is given by the maximum useful value of the relative phase velocity  $\frac{\lambda_0}{\lambda}$  at  $-1.2$  ( $\lambda_g$  is the wavelength of the

guided wave). For this value, the forward gain is a little greater than a quarter-wave monopole over a ground plane.

The final radiation pattern is the sum of these various patterns. With good design, only the launcher pattern and the rod pattern itself will remain. (The launcher pattern can be matched to the surface wave field precisely by a long tapered horn. However, such a horn is so large that the physical advantages of the polyrod antenna are lost<sup>4</sup>).

The result of the interference of these two patterns is that sidelobes are high for a low-gain antenna and decrease as the forward gain increases, also as the launcher efficiency increases (Table 3.2.1).

Table 3.2.1

First sidelobes for polyrods of various gains

Halfpower beamwidth (degrees)	16	20	30
Gain (dB)	17	15	10
	<u>First sidelobe (E plane)</u>		
launcher efficiency $\eta = 85\%$	-12.6	-10	-6
95%	-15	-14	-14

At the angle where the two sources of radiation are in phase again, the primary rod pattern is down by -16 to -18 dB on the peak. This can never be improved since the basic rod pattern has a wide skirt. The aperture efficiency is typically 30-40% and is obtained from the measured gain and directivity.

From these figures, it is clear that the backlobe radiation from the dielectric-rod antenna will be poor, since both sources of radiation contribute and the backlobe levels of open waveguide are generally high. Values of -10 to -15 dB are normal. This backlobe radiation can be suppressed to levels of the order of -30 dB by suppressing the launcher backlobe with chokes. However, this procedure does tend to narrow the bandwidth to 15% from the more usual 30% (Ref.5).

Since the E and H plane patterns are equal and it is easy to launch two linear orthogonal polarisations, the polyrod has been widely used as a

reflector feed<sup>6,7</sup>. In a typical example, a 9.2 wavelength teflon tube fed from standard waveguide and a 1.625 wavelength feed-cone had equal half power beamwidths of  $34^\circ$  at 6.4 GHz. The first sidelobe was -17 dB. (Ref.7).

Small polystyrene cylinders<sup>6</sup> have been used of length 0.4 and 0.6 wavelengths. These had equal E and H plane HPBWs at  $75^\circ$  and  $60^\circ$  respectively. Sidelobes were -22 dB in the E plane and the backlobe was -25 dB. The cross-polarisation was -25 dB in the  $45^\circ$  plane. By adding a small ring slot near the end of the waveguide launcher, compensating radiation cancelled the backlobe and it was reduced to less than -40 dB over a 15% bandwidth. These antennas exhibited the usual low coupling values of less than 20 dB for spacings greater than 0.6 wavelengths.

Preliminary attempts<sup>8</sup> have been made to make polyrods to mate with MILIC (Microwave Image Line Integrated Circuit) transmission line. Two materials used at 15 GHz had dielectric constants of 2.25 and 9.8 respectively. Gains of 14 to 16 dB were obtained with sidelobes around -15 to -17 dB. A maximum gain of 16.2 dB at 15 GHz was measured although the antenna should have had a gain of 18 dB. This low gain was attributed to dimensional sensitivity and launching losses but it is also possible that the dielectric-rod tapers were injudiciously chosen. Antennas with gains of less than 14 dB functioned as expected.

Several attempts have been made to use three-dimensional dielectric shapes to improve performance of an open ended waveguide, particularly with respect to cross-polarisation and backlobe. A series of papers by Crosswell et al (see, for example, Ref.9) deals with the use of small spheres of plexiglass (with a dielectric constant of 2.57 and a loss tangent of 0.0065). The original open-ended circular waveguide had a backlobe of -20 dB and cross-polarisation of -30 dB on axis. The dielectric spheres provided 2 dB more gain but had a deleterious effect on the backlobe and sidelobes. However, coupling between closely spaced antennas was reduced. This was essentially a cut-and-try experiment. Lighthart and Hollander<sup>10</sup> computed the effect of a shaped dielectric mounted on an open-ended waveguide, treating it as a type of lens in which the surfaces should be optimised. They measured the pattern of a sphere and an optimised pear-shaped object with a dielectric constant  $\epsilon_r = 2.53$ . The sphere had the usual properties of narrow beamwidth and

bad sidelobes. The sidelobe envelope lies at approximately -20 dB in the angular range  $\pm 30^\circ$  to  $\pm 180^\circ$  which must result in poor efficiency. The pear-shaped dielectric antenna was more satisfactory though the far-out sidelobe envelope is still poor at around -25 dB. The authors point out that the main beam bears a close relationship to the pattern of a corrugated horn (see Table 3.2.2). This antenna could be used in a confined space but the spillover efficiency would be poor since one would expect the corrugated horn to have near-in sidelobes less than -30 dB and a backlobe of better than -50 dB.

Table 3.2.2

Dimensions of a dielectric antenna and a corrugated horn of the same beamwidth at 11.81 GHz (all in mm)

Dielectric antenna		Corrugated horn	
Length	88.9	Length	174.1
Maximum diameter	76.9	Maximum diameter	121.3

Halfpower beamwidth is  $20^\circ$  in E and H planes for both antennas.

### 3.2.2 Dielectric horns and Dielguide

In the past few years, considerable attention has been given to dielectric horns, cones or pyramids, hollow and solid, because they have good cross-polarisation properties and are smaller in diameter than the corresponding conical horn though usually longer by a factor of as much as 50% (Ref.11). The sidelobes from these devices, however, are always poor; -15 dB in the E plane, -20 dB in the H plane are typical first sidelobe values. Backlobes can be kept below -30 dB usually because of the presence of a launching feed horn. Gains of up to 24 dB can be achieved with operational bandwidths of 30% (Refs.12,13).

The most important version of these antennas is the Dielguide<sup>14</sup>. In this antenna a dielectric cone is extended along the principal axis of a parabolic or Cassegrainian reflector system. The material used by Bartlett and Moseley<sup>14</sup> to form the Dielguide antenna had a dielectric constant between 1.08 and 1.15 with a loss tangent of  $4 \times 10^{-4}$ . These antennas provide a relatively high-efficiency illumination of the reflector. Patterns for a Cassegrain Dielguide feed were flat topped with sidelobes

less than -32 dB in E, H and  $45^\circ$  planes. The pattern was virtually symmetric so that the cross-polarisation was very low.

One additional advantage is that the Dieguide will act as a support for the feed horn launcher and supporting struts etc. are not required. This will reduce blockage with subsequent improvements in gain and sidelobe performance for the secondary radiation pattern.

However, the Dieguide feed is not without problems; in particular:

- The presence of higher order modes which will lead to enhanced sidelobes and cross-polarisation.
- An inability to handle large powers in transmission.
- Increased susceptibility to the effects of rain falling on the Dieguide cone.

### 3.2.3 Synopsis of dielectric antennas

Dielectric rods and horns are suitable for locations where the available cross-sectional area is limited because their maximum diameter is much less than that of the equivalent waveguide horn. Their cross-polarisation characteristics can in principle be adequate for many applications but their sidelobe performance is not good and cannot be improved for fundamental physical reasons. With careful design, i.e., slots etc. the backlobe may be reduced to levels of the order of -40 dB. The gain of a dielectric rod is restricted to 20 dB by structural considerations. A dielectric horn could achieve gain values of the order of 26 dB.

Dieguides are a particularly useful form of dielectric horn which is used in a near field condition as a feed for a parabolic reflector. In this configuration the poor sidelobe performance tends to be unimportant. It cannot however be used in a multiple beam antenna. Table 3.2.3 gives typical achievable performance figures.

Polyrods have been used at 60 GHz though their performance in this case was poor due to dimensional inaccuracy. The lower frequency limit is set by the mass of the antenna. It is probably about 1 GHz. Powers up to 20 kW CW have been reported with antennas of this type although a forced-air cooling system was necessary.

Table 3.2.3

Performance possible with a dielectric antenna

	Aperture Efficiency %	Gain range (dB)	Sidelobes		Backlobe (dB)	Bandwidth %
			(dB) (E plane)	(dB) H plane		
Dielectric rod	30-40	5-20	-16	-20	-35	20
Dielectric horn	40	10-26	-15	-26	-40	30

### 3.3 Broadband Antennas

#### 3.3.1 Helices

The standard single wire helix<sup>1</sup> over a ground plane has a bandwidth of 1.7 : 1 with a sidelobe suppression of better than -13 dB. End fire gains are between 10 and 23 dB according to axial length (between 0.7 and 10 wavelengths) and the antenna operates in circular polarisation, the hand depending on the direction of winding. The helix circumference must be between 0.75 and 1.25 wavelengths for end fire radiation. The backlobe can be troublesome and values of -12 to -18 dB are common, even with a ground plane of 2 or 3 wavelengths ( $\lambda$ ) diameter. If this could be as large as 10  $\lambda$ , the backlobe would be reduced but the size of the antenna would be large compared to the forward gain. The backlobe of an array of several helices over a common ground plane can be reduced to below -30 dB (Ref.2). For helices the axial ratio between 3 dB points is  $(2n + 1)/2n$  where  $n$  is the number of turns in the helix. Frequencies between 100 MHz and 35 GHz can be used<sup>3</sup>.

The quadrifilar helix<sup>4</sup> has four counterwound tape helices, equally spaced circumferentially round a cylinder and fed with signals of equal amplitude but relative phases of 0°, 90°, 180° and 270°. It will operate over a 6 : 1 band. Sidelobes are reported to be typically in the range -10 to -15 dB.

The Counterwound Quadrifilar Helix<sup>4</sup> responds to linear polarisation. Bandwidth is 4 : 1 for sidelobes better than -10 dB. The cross-polarisation level varies between -11 and -30 dB over the band but is reported as being mostly better than -22 dB.

The backlobes of quadrifilar elements are reported as being virtually uncontrollable even with a ground plane. Values vary between -6 and -20 dB for circular, and -14 and -30 dB for linear polarisation elements. Over most of the operational band, values are better than -15 dB but narrowing the antenna bandwidth will not improve the mean level.

On the whole, these elements will not provide low sidelobe performance though their radiation performance appears to be very predictable<sup>1,4</sup>.

Table 3.3.1

Helix performance characteristics

	Helix	Quad helix	Counterwound quad helix
Gain range (dB)	0-23	10-23	10-23
Sidelobes (dB)	<-15	-10 to -15	-10 to -15
Backlobe (dB)	-12 to -18	-6 to -20	-14 to -30
Polarisation	Circular	Circular	Linear
Axial ratio (dB)	1.2	<1.8	-
Cross-polarisation (dB)	-	-	<-22
VSWR	<2	<2	<2
Bandwidth	1.7 : 1	6 : 1	6 : 1
Frequency range (GHz)	0.02 to 40	0.02 to 10	0.02 to 10
Dimensions	Length: 0.7 to 10 $\lambda$ 1 wavelength in circum- ference	As helix	As helix

### 3.3.2 Conical-spiral antennas

These antennas can be considered to lie between helices and planar spiral antennas and are essentially frequency-independent antennas, i.e., the gain and performance should be nearly constant over a wide bandwidth.

The cone surface has an included angle of less than 45°. Larger angles degrade the impedance match. The cone base must be at least 3/8 of a wavelength in diameter at the lowest frequency. The radiation patterns are circularly polarised to 40° off boresight. The actual value of the half power beamwidth varies between 70° and 180° and is dependent on the pitch angle of the winding.

**Table 3.3.2**  
Data for conical spiral

Gain	5 dB
Sidelobes	none
Backlobe	<-15 dB
Polarisation	circular
Axial ratio	<1.2
VSWR	<1.5
Bandwidth	20:1
Frequency range	0.1 to 10 GHz
Dimensions	$\lambda_1/3$ diameter at base of cone. $\lambda_1$ = longest wavelength included angle $<45^\circ$
Efficiency* (%)	75-85

**3.3.3 Cavity backed spiral antennas**

A planar spiral antenna is a bidirectional antenna. To make it unidirectional, a cavity is used to back the radiator, which may be cylindrical (2.5 : 1 bandwidth) or conical (5 : 1 bandwidth). As might be anticipated, the use of a cavity does give better backlobe performance.<sup>1,2</sup>

**Table 3.3.3**  
Data for cavity backed spiral antennas

Gain (dB)	4-6
Sidelobes	none
Backlobe (dB)	<-25
Polarisation	CP
Axial ratio	<1.2
VSWR	<2
Frequency range	0.1-10 GHz
Bandwidth	3 : 1
Dimensions	$\lambda_1/3$ diameter where $\lambda_1$ is the largest wavelength
Efficiency (%)	90

\* Obtained from the measured gain and directivity.

### 3.3.4 Log periodic dipole antennas

This class of antenna provides linear polarisation; in its basic form the bandwidth and gain depend on the length of the antenna and the number of resonant elements. Forward gains of 7-12 dB can be achieved, though a high gain LPDA tends to be structurally unwieldy. Backlobes are approximately -17 dB for a high gain antenna but can be -10 dB for low gain versions. Arrays of LPDAs have better backlobes and sidelobes are not usually present since the half power beamwidth is at best  $50^\circ$ . When sidelobes do occur, they are of the order of -10 dB. LPDAs can be deployed orthogonally in space and excited in phase quadrature to provide circular polarisation.

Table 3.3.4

Data on LPDAs

Gain (dB)	7-12
Sidelobes (dB)	none or -10
Backlobes (dB)	-10 to -17
Polarisation	linear
Bandwidth	20 : 1
Frequency range (GHz)	0.01-10
VSWR	<1.6
Efficiency (%)	65

For all these frequency-independent antennas the sidelobe and backlobe performance is poor. This is not surprising since the element is small in wavelengths and there are no parameters which can be used to adjust the aperture illumination.

### 3.3.5 Ridged horns

Ridged waveguide is known to have a broader bandwidth than normal rectangular waveguide. This theory has been extended to flared waveguide, i.e., horns with ridges and these function as broad-band horns.

King et al<sup>1</sup> describe one which has four tapered ridges, one in the centre of each horn wall. The isolation of two orthogonal linear polarisations was better than 18.5 dB and the VSWR <2 over the band 2 to 12 GHz. The E and H planes were equal and the gain varied between 8 and 24 dB monotonically. There is no backlobe information regarding this antenna but there are occasional E plane sidelobes at the higher frequencies which rise to -9 dB (Hplane -16 dB) at 12 GHz. This is a constant aperture horn rather than a frequency independent antenna such as an LPDA (which provides constant gain over its operational bandwidth). Kerr<sup>2</sup> has discussed a constant gain ridged horn with two opposed ridges (linear polarisation only). For this antenna the gain between 1 and 12 GHz varied by only a few decibels ( $12 \pm 1$  dB). The radiation patterns show the occasional sidelobe of -10 dB and the backlobe was around -10 dB though this was said to be due to the poor range used for measurements. However, the size of the horn was small in that it comprised an 138.2 mm square aperture and an overall length of 186.1 mm for a gain of 12 dB.

These horns do have wider bandwidths than is common in conventional waveguide horns but the radiation performance characteristics leave a great deal to be desired. Whether it would be possible to have, say, a 3 : 1 bandwidth and improve the sidelobe performance, is not clear.

Table 3.3.5

Ridged horn data

Gain range (dB)	10-20 dB
Sidelobes (dB)	-10 to -15
Backlobe (dB)	-10 to -15
Polarisation	linear or circular
VSWR	<2
Bandwidth	10 : 1
Frequency range (GHz)	0.1 to 30

### 3.4 Conclusions: Low Gain Antennas

With low gain antennas, the degree of control which can be exercised over the antenna aperture illumination characteristics tends to be limited because the aperture is relatively small in terms of wavelengths. Only in the case of certain waveguide horns such as the multi-mode and corrugated types, can the illumination be tapered to improve sidelobe performance significantly. However, in these cases the sidelobe and backlobe performance of the horn can be optimised to suppress these spurious radiations to reasonably low levels. Fortunately, for cylindrical horns, the parameter optimisation which leads to maximum radiation-pattern symmetry and minimum cross-polarised radiation also appears to coincide with the conditions necessary to achieve maximum sidelobe and backlobe suppression.

With most wideband and frequency-independent antenna types the control of sidelobe radiation appears to be extremely limited and the available parameters are generally optimised with the broad-band characteristics of the antenna in mind. Little work appears to have been reported on the trade-off between radiation performance and bandwidth for these antennas.

Dielectric antenna types are rarely inherently low sidelobe devices, since increased difficulties exist in exerting total control of fields which may be only lightly bound to an open structure.

The choice of antenna type to be deployed for a given application will always be dependent upon a number of factors. However, if minimum spurious radiation were the only factor of concern, it appears clear that horn antennas, and particularly cylindrical or conical versions producing axisymmetric field distributions, would be an obvious choice.

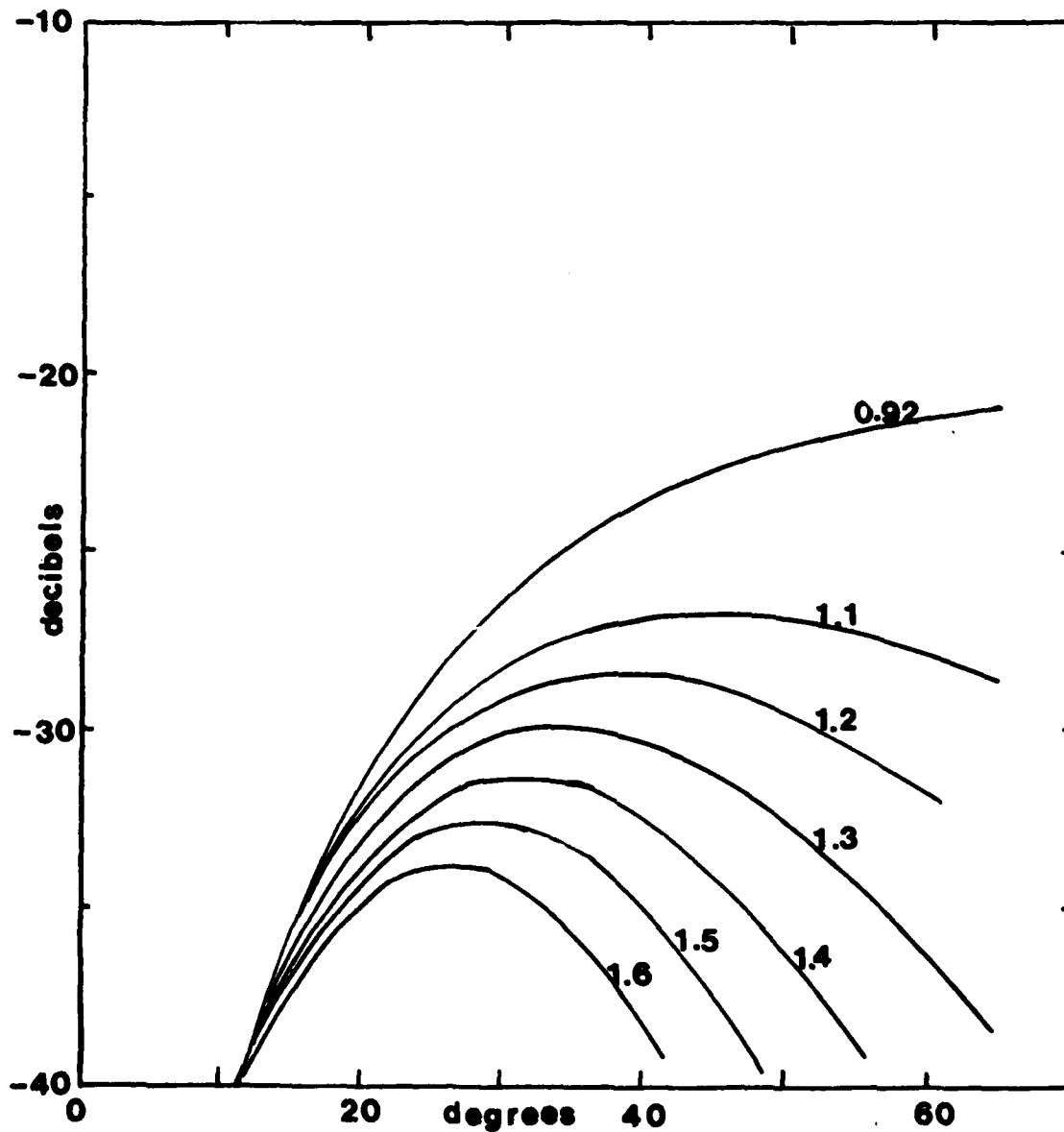


Fig.3.1-1a: Cross-polar radiation field from a fundamental mode rectangular aperture smooth walled horn. Aperture dimensions  $a/\lambda$ (E plane)  $\times$   $\rho a/\lambda$ (H plane). For the values of  $a/\lambda$  shown  $\rho = 1.36$  except for  $a/\lambda = 0.92$  where  $\rho = 1.2$ . Half the radiation pattern in the  $45^\circ$  plane is shown.

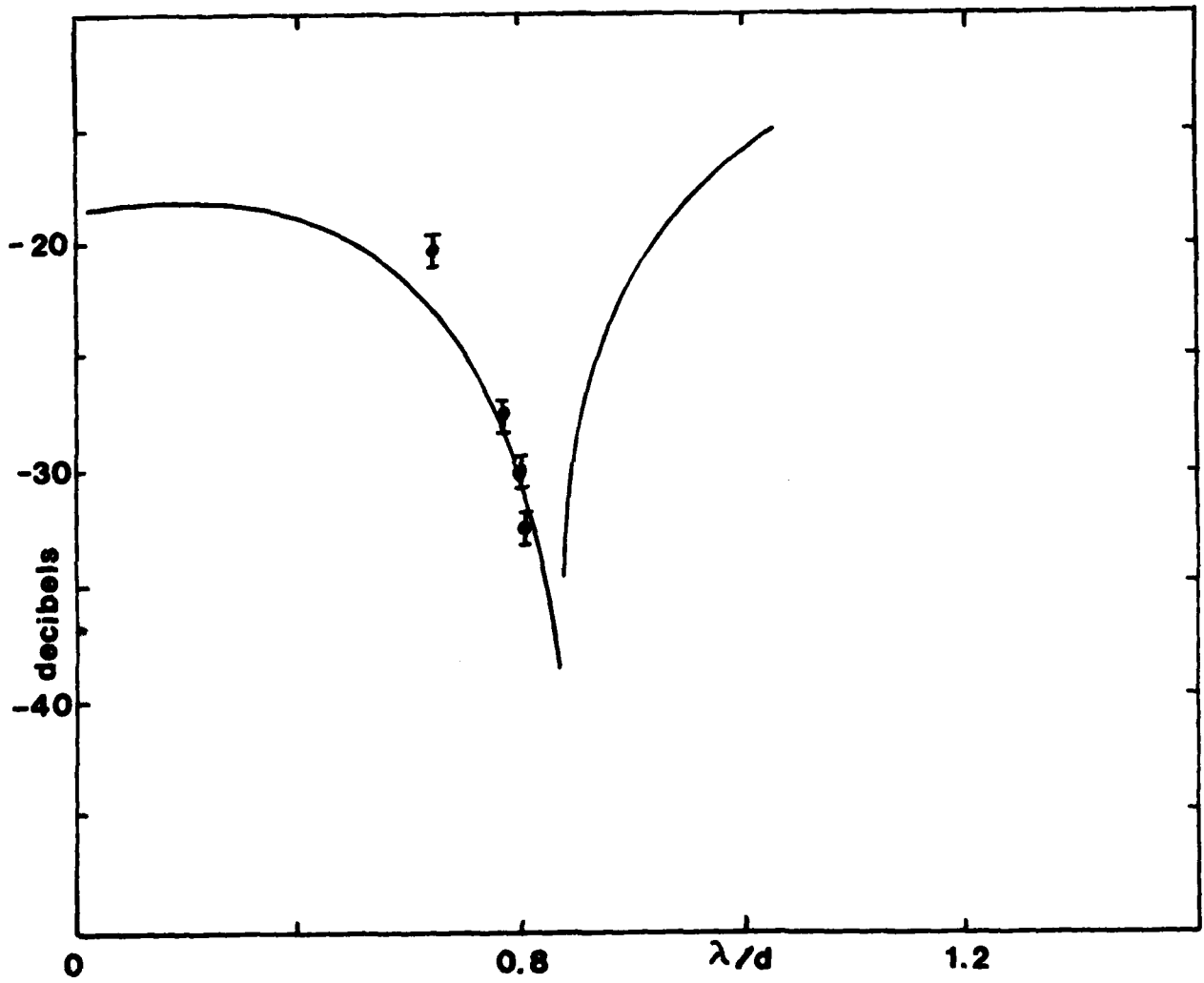


Fig.3.1-1b: Variations in the peak cross-polar radiation from fundamental mode conical horns of aperture diameter,  $d$ , as predicted by the E field model.  $\phi$  are measured data.

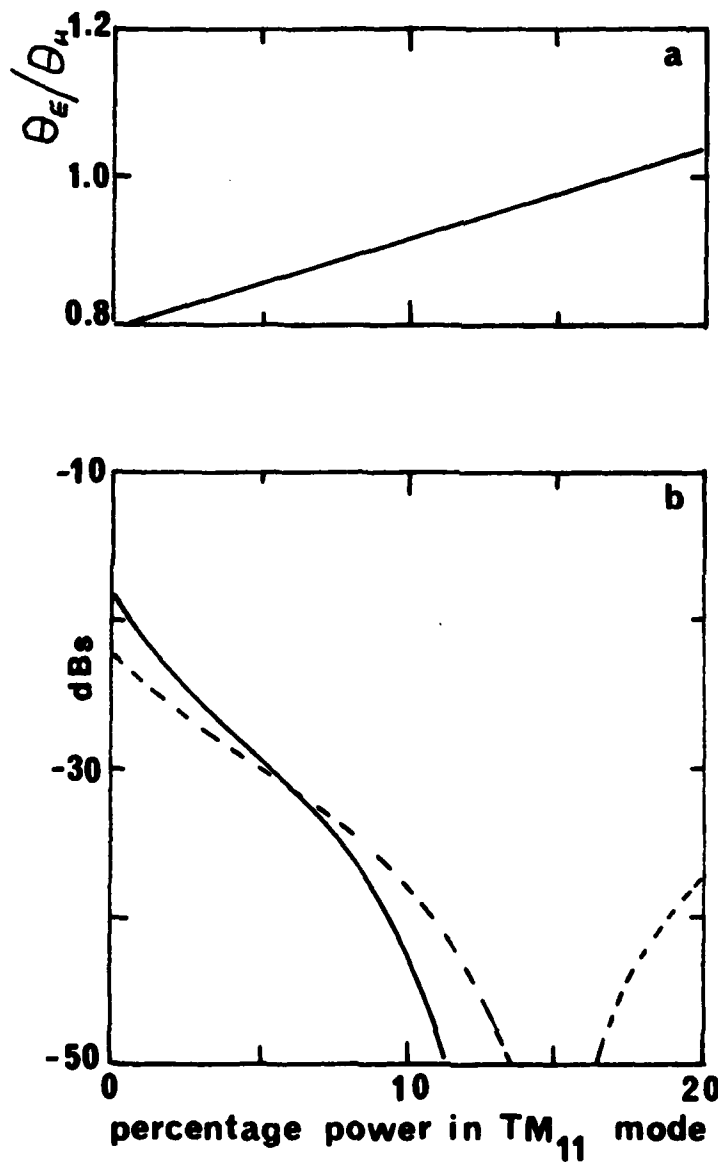


Fig.3.1-2: The effect of varying the percentage of  $TM_{11}$  mode power present in a conical multi-mode horn of aperture 4.06 wavelengths.

- (a) Ratio of E plane to H plane half-power beamwidth
- (b) Solid curve; first sidelobe in the E plane; dashed curve; peak cross-polarisation within the -3 dB beamwidth.

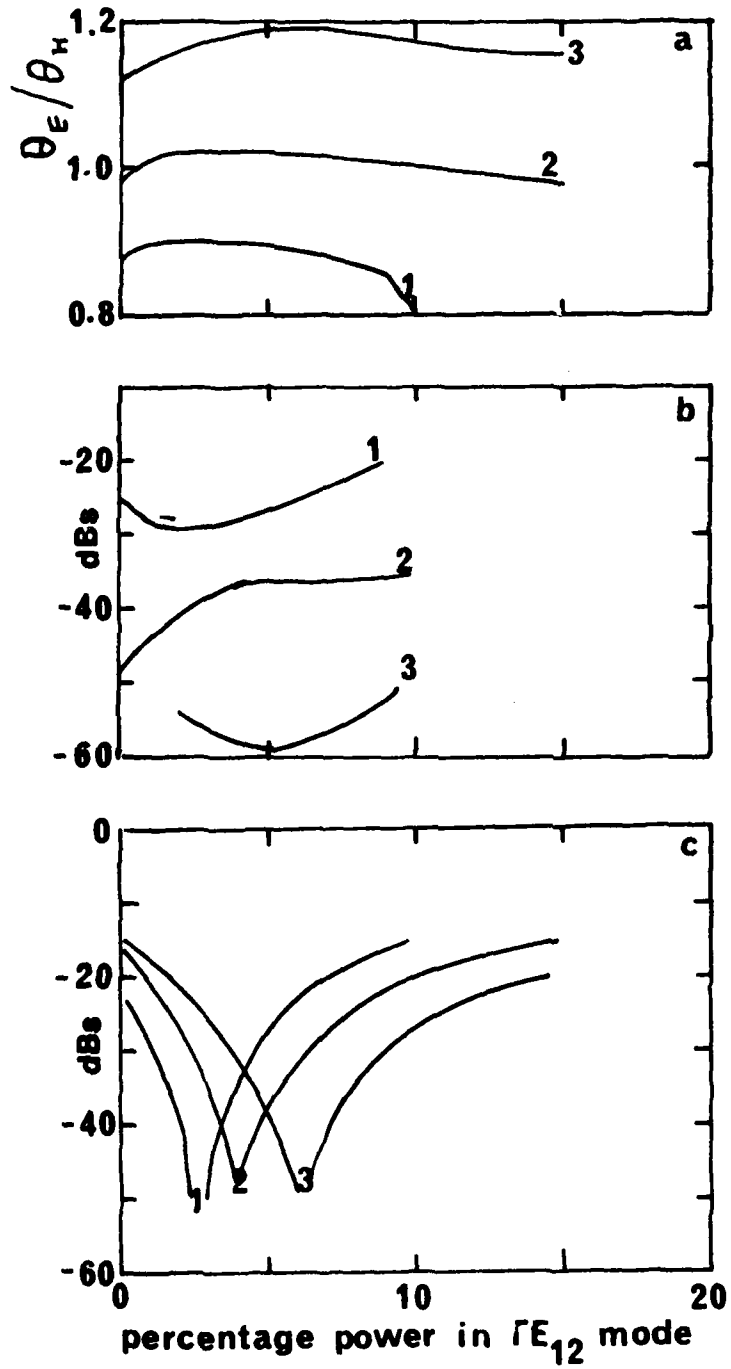


Fig.3.1-3: The effect of varying powers in the modes TE<sub>10</sub>, TE<sub>12</sub>, TM<sub>12</sub> for a multi-mode square horn of side 4.06 wavelengths.  
(a) Ratio of E plane to H plane half-power beamwidth  
(b) First sidelobe in the E plane  
(c) Peak cross-polarisation  
1, 2 and 3 are 90, 80 and 70 per cent power in the TE<sub>10</sub> mode respectively.

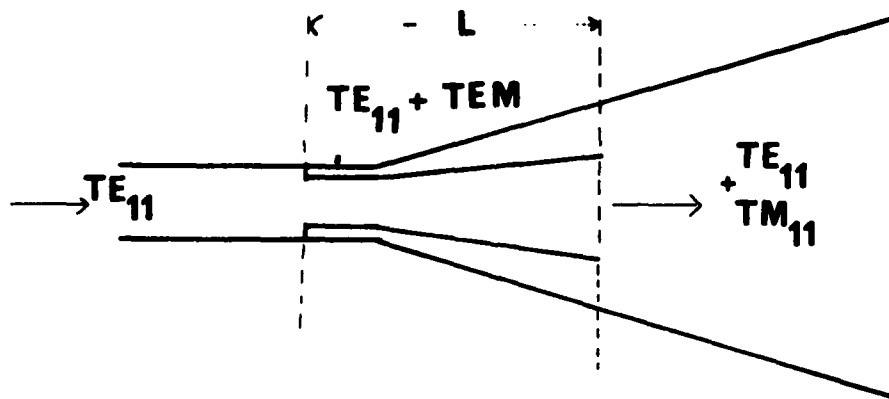


Fig.3.1-4: Twin-wire horn

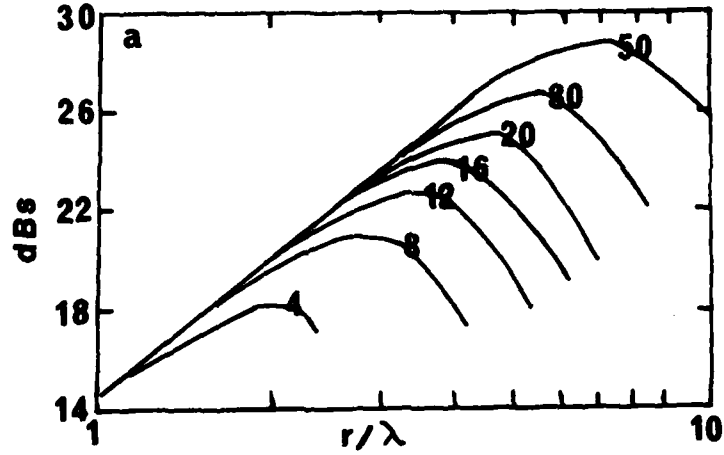


Fig.3.1-5a: Gain (dB) vs aperture radius,  $r/\lambda$ , for various axial lengths in wavelengths for a narrow angle corrugated horn.

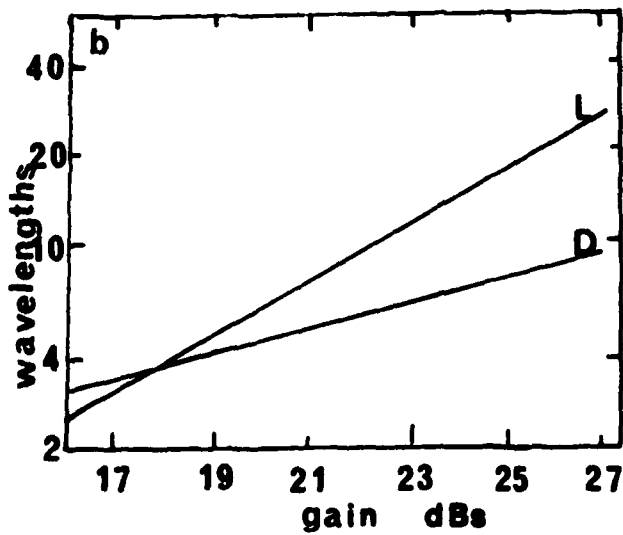


Fig.3.1-5b: Length, L, and diameter, D, in wavelengths vs gain for a narrow-angle corrugated horn of optimum dimensions.

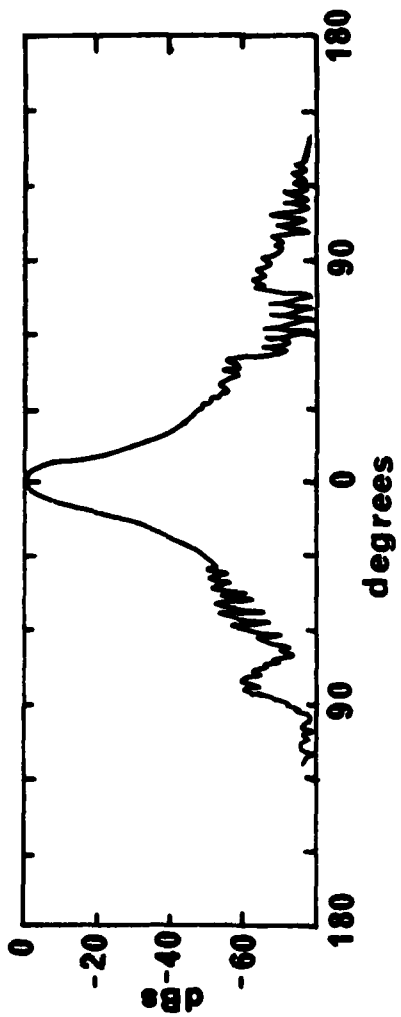


Fig.3.1-6: Radiation pattern of a corrugated horn of gain, 23.2 dB. E and H plane are identical.

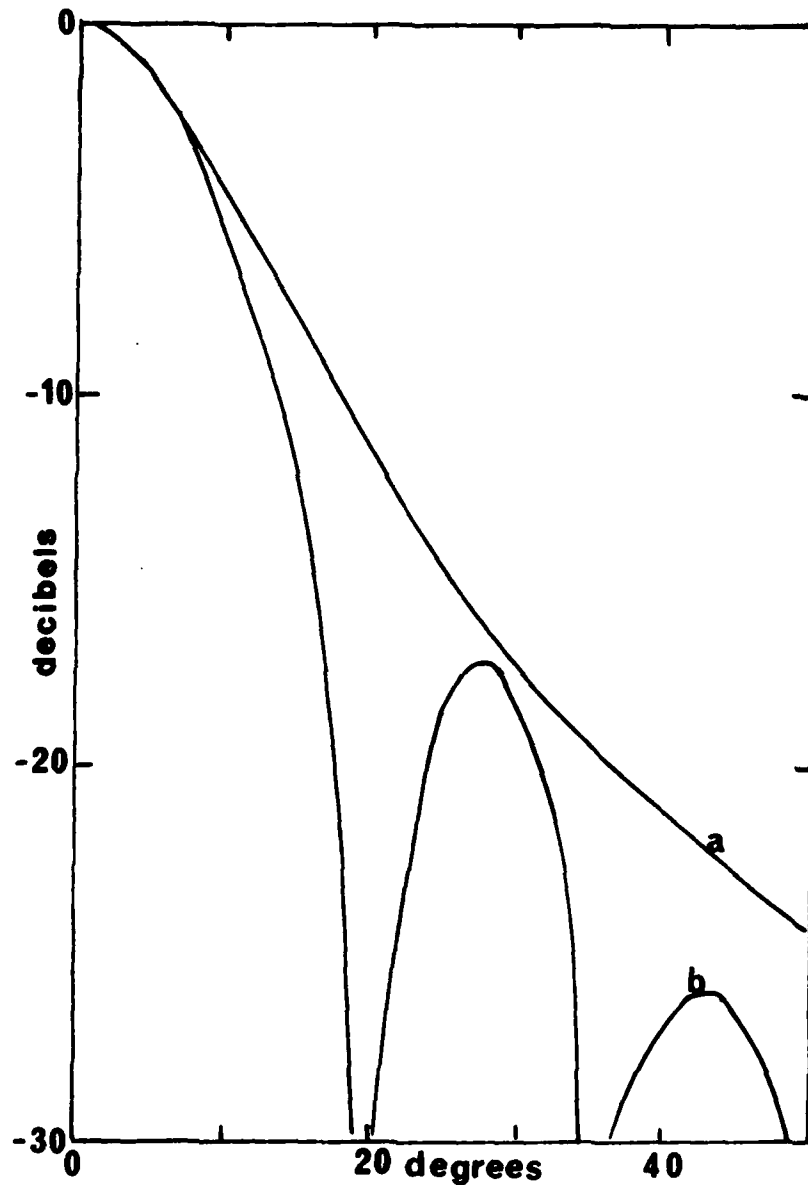


Fig.3.2-1: Radiation patterns of:  
(a) An ideal polyrod.  
(b) A uniform circular aperture of the same half-power beamwidth.

#### 4 MEDIUM GAIN ANTENNAS

These antennas may have gains in the range 15-30 dB. They are all amenable to control of their aperture illuminations to give improved sidelobe and backlobe performance.

##### 4.1 Corner Reflectors

These antennas (Fig.4.1-1) consist of two reflecting sheets forming a corner of angle  $\theta$ . The width is  $W$  and the slant length,  $L$ . They are driven by at least one feed element, usually a dipole which is symmetrically placed at a distance,  $s$ , from the apex line. Cottony and Wilson<sup>1,2</sup> investigated the E and H plane radiation patterns of antennas, at 2000 MHz, with  $1 < \frac{W}{\lambda} < 10$  and  $0.5 < \frac{L}{\lambda} < 5$ .  $\theta$  and  $s$  were varied at each setting to give maximum gain though the aperture efficiency was always poor at 30 to 40%. The forward directivity increased from 5 to 18 dB as  $L$  and  $W$  increased. Since infinite extension in  $\frac{L}{\lambda}$  does not affect the aperture illumination, this parameter can be limited to two wavelengths. The E and H plane beamwidths change very little beyond this value of  $L$ .

For these optimised configurations, the H plane sidelobes were generally below -30 dB while the E plane values were below -20 dB. The mean level of the backlobe radiation in the range  $-140^\circ$  to  $180^\circ$  to  $+140^\circ$  is shown in Fig.4.1-2.

Cottony and Wilson were interested in an antenna design having very low sidelobes and tested a corner reflector fed by a collinear array of 10 half-wave dipoles,  $0.8 \lambda$  apart, with a Chebyshev amplitude distribution. This array was parallel to the dimension  $W$ ;  $L$  was two wavelengths and  $W$ , 10. All sidelobes and backlobes were less than -40 dB and the authors suggest that -50 dB is feasible. In order to reduce the backlobe still further, Wilson and Cottony placed chokes round the reflector edge. No significant change in the radiation pattern was observed even when the choke was filled with absorber. Closing the ends of the reflector with metal plates caused deterioration in the backlobe suppression.

Table 4.1.1 gives some typical performance figures.

Table 4.1.1

Corner reflector characteristics

	Single element	Collinear array
Gain range (dB)	5-18	As required
Sidelobes (dB)	<-20	<-40
Backlobe (dB)	<-40	<-40
Polarisation	linear	linear
VSWR	<1.5	<1.5
Bandwidth (%)	20	5*
Frequency range (GHz)	0.1 to 10	0.1 to 10
Efficiency (%)	<40	<40

\*determined by the array.

4.2 Backfire Antennas

This antenna type was developed from a surface wave antenna which was terminated in a plane reflector, to provide enhanced gain in the backfire direction. The length of the surface wave section made this a cumbersome antenna and Ehrenspeck<sup>1</sup> replaced the surface wave section with a small reflecting disc half a wavelength from the main reflector, with a dipole, or similar small driven element, near the midpoint between the two reflectors (see Fig.4.2-1).

A variety of these antennas has been developed, ranging from a sleeve dipole in a small cavity<sup>2</sup> of gain 10 dB, to the short backfire antenna (SBF) with several feed elements giving gains up to 25 dB (Refs.1,3). The sidelobes and backlobes can be reduced by adjusting the height of the rim which affects the aperture illumination. This parameter is normally used to maximise the forward gain and aperture efficiencies of 70-90% have been achieved. Quoted sidelobe levels (of experimental models) are around -20 dB and backlobes -20 to -30 dB. Improvements might be achieved if the rim height was adjusted for minimum sidelobe radiation rather than maximum aperture efficiency. The cross-polarisation is that of the feed element but this topic is not dealt with in detail.

A version which is more suitable for frequencies above 3 GHz has been described by Large<sup>5</sup>. An open ended waveguide is used as the driven

element at 9 GHz. This has the advantage of high power operation, low transmission loss and better bandwidth. With the feed halfway between the two reflectors (spacing  $0.6 \lambda$ ), a gain of 13.5 dB was obtained from a two wavelength diameter antenna. E and H plane beamwidths were equal and E plane sidelobes were -16 dB while H plane were better than -30 dB. This is not as good as the dipole-fed antenna. A further version used a trough-shaped aperture in place of the circular cavity. This aperture was fed by a sectoral horn. The E plane sidelobes were at best -12 dB.

Theory on the SBF antenna and its variants is lacking; the quoted results (Table 4.2.1 below) are experimental and have been obtained from various workers<sup>3,4,5</sup>. A good review is provided by Hristov and Kumar<sup>6</sup>.

Table 4.2.1

Data on the short backfire antenna

Gain range (dB)	10-18 <sup>*1</sup>
Bandwidth	2 : 1 <sup>*2</sup>
Frequency range (GHz)	0.1 to 10
Dimensions	A cylinder 1.5 to 2.5 $\lambda$ in diameter x 0.5 $\lambda$ high
Sidelobes (dB)	<-20
Backlobe (dB)	<-30
Polarisation	As feed element
Cross-polarisation	Not confirmed
VSWR	<1.8

\*1 Gains up to 25 dB can be achieved if a larger cavity is used with an array of feeds.

\*2 Gains are reduced by as much as 6 dB for octave bandwidths.

#### 4.3 Hoghorn Antennas

An antenna<sup>1</sup> which has particularly good sidelobe performance in the far-out and backlobe region is the 'hoghorn' which comprises a conical horn section coupled with an offset section of a paraboloid reflector (Fig.4.3-1). The edges of the conical horn are normally extended to meet the reflector.

A simplified hoghorn<sup>2</sup> using a corrugated horn (Fig.3.1-6 shows the radiation of the horn alone gain 23.2 dB) with an offset paraboloidal section provided a final gain of 40 dB. The half-power beamwidth was  $1.7^\circ$ . Sidelobes were present out to  $180^\circ$  at the -75 to -80 dB level but included a major peak of -50 dB at  $60^\circ$  from boresight on one side. This is due to spillover from the conical horn section which does not intercept the hoghorn reflector. When the hoghorn aperture was shrouded and the shroud lined with absorber, this high sidelobe disappeared and beyond  $\pm 30^\circ$  from boresight all sidelobes were less than -78 dB. The beamwidth was unchanged but the gain had decreased by 0.2 dB due presumably to losses in the absorber. The near-in sidelobes were reduced slightly though beyond  $\pm 10^\circ$  they were already less than -40 dB. This antenna gives some indication of the excellent wide angle sidelobe performance to be obtained from antennas of the hoghorn type.

The cross-polarisation performance of these antennas tends to be rather poor, however, as a consequence of the offset reflector surface. For the hoghorn configuration, an offset parabolic surface with large offset angle is implied and peak cross-polar levels of the order of -20 to -30 dB can be expected.

Hogorns have been thoroughly studied, theoretically and experimentally by the Bell Telephone Laboratories. The original version<sup>3</sup> had -15 dB first sidelobes and the radiation pattern was down to -30 dB by  $\pm 10^\circ$ . The half power beamwidth was  $1^\circ$  at 2.39 GHz with an aperture efficiency of 76%. There was a prominent spillover lobe of -30 dB at  $70^\circ$  from boresight. Some improvements<sup>4</sup> resulted in the pattern of Fig.4.3-2. The original defects were:

- A plateau between  $30^\circ$  to  $60^\circ$  at -50 dB but only in vertical polarisation. This was traced to 18 bolts which fastened on the weather cover and projected into the pyramidal part of the antenna just below the aperture. By modifying the fastening so that there were no periodic projections inside, the sidelobe level was reduced below -60 dB.
- A spillover lobe of -30 dB at  $70^\circ$  to  $80^\circ$  from boresight in horizontal polarisation. The window edge of fibreglass acted as a slit radiator. After it was covered over with conducting tape, the lobe reduced to -50 dB. Blinders were tried first but merely spread the lobe over a wider angle.

There remained a lobe at  $90^\circ$  at a level of  $\approx 50$  dB. This was reduced to  $-58$  dB by attaching a half blinder to the opposing sides of the antenna aperture (Fig.4.3-3). The angle of this blinder and its size and length are critical to the suppression of the sidelobe. The general level of sidelobes between  $10^\circ$  and  $30^\circ$  is still higher than theoretical by 10 to 15 dB and this is regarded as unsatisfactory by Bell Telephone Laboratories.

One of the disadvantages of blinders is that they do not have a wide-band correction effect. The half-blinder described above operated successfully at 4 and 6 GHz, but modern frequency allocations require that the antenna operates at 11 GHz as well. Siller<sup>6</sup> considered the effects of using an array of small edge blinders (see Fig.4.3-3). This gives a large number of parameters for adjustment and the spillover lobe was successfully reduced to below  $-70$  dB in all three frequency bands. The backlobe was less than  $-80$  dB. Full details of the procedure for adjusting the parameters are given in Siller's paper<sup>6,9</sup>.

This detail has been included to show the care that is necessary to achieve sidelobe suppressions of this order. It should be noted that the papers cited span the years 1961 to 1975, showing how much effort has been invested.

Similarly good sidelobe performance was obtained by Afifi<sup>7</sup> who increased the hohorn reflector focal length to infinity by using a flat reflector and fed this with a plane wave from the near field of a paraboloid. This, he claimed, should reduce the backlobe from  $-50$  dB to  $-\infty$ . In practice, backlobes of  $-60$  dB were measured (Fig.4.3-4). The sidelobes were improved by using 'forming cylinders which were covered with absorber'.

A more compact version of the hohorn is the little used 'Cass-horn'<sup>8</sup>, where the feed horn of the original hohorn is replaced by a hyperboloid sub-reflector and feed horn as shown (Fig.4.3-1). The sidelobes are low and the backlobe less than  $-60$  dB (Fig.4.3-5). This antenna had an aperture of 30 wavelengths at 11 GHz. The gain was 36.3 dB giving an aperture efficiency of 50%. This seems lower than possible.

To summarise, the sidelobe levels outside the near-in region and backlobe levels of hoghorns can be reduced by careful designs to very low levels. The efficiency can be as high as 76% although this may not be realisable with a very low sidelobe design. The main drawback is that it is cumbersome and requires a special, large, pedestal, though the Cass-horn version is less bulky. It should, however, be recognised that a great deal of work has been expended on achieving these low sidelobes and possibly similar performance could be obtained from other antenna types if the same amount of care and attention was applied.

Table 4.3

Data on hoghorn

Gain range (dB)	20-40
Bandwidth	as feed
Frequency range (GHz)	1-60
Sidelobes near-in (dB)	Dependent on the illumination -15 to possibly -35
far-out (dB)	<-50
backlobe (dB)	<-70
Peak cross-polarisation (dB)	<-27*
VSWR	<1.1
Efficiency (%)	75 for 15 dB first sidelobe <50 for 35 dB first sidelobe

\* Measured for Andover hoghorn. This will depend on the feed type and new multi-mode feeding techniques might suppress this to lower levels<sup>10</sup>. These techniques are discussed further in Section 5.2 on offset parabolic reflector antennas.

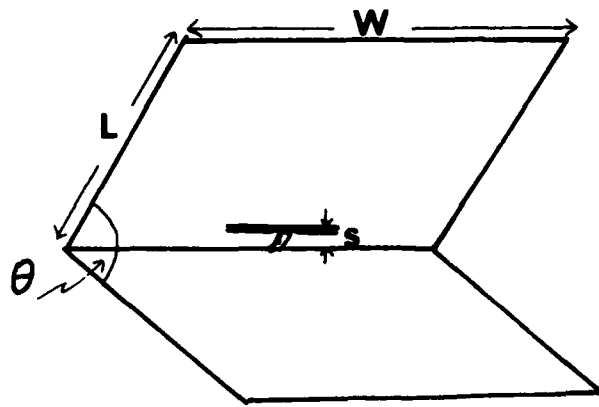


Fig.4.1-1: Schematic representation of a corner reflector antenna.

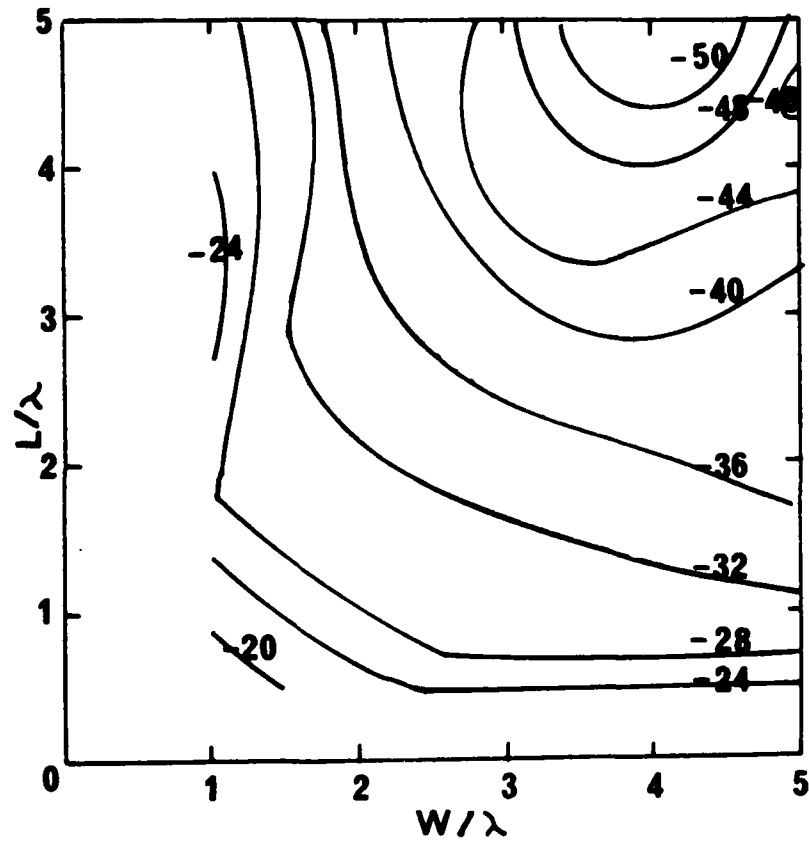


Fig.4.1-2: Contours of constant backlobe radiation (in dB) for a corner reflector as a function of the dimensions  $W$  and  $L$  in wavelengths.

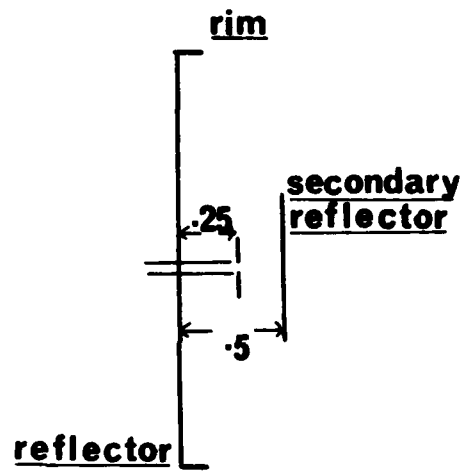


Fig.4.2-1: Schematic representation of a backfire antenna. Dimensions are in wavelengths.

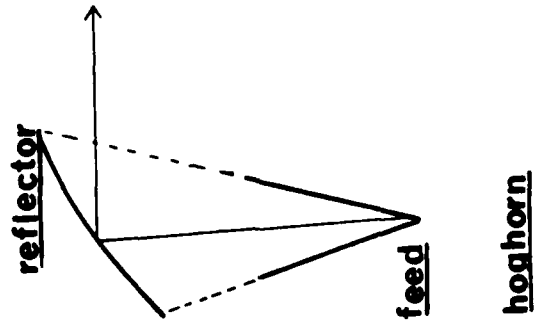
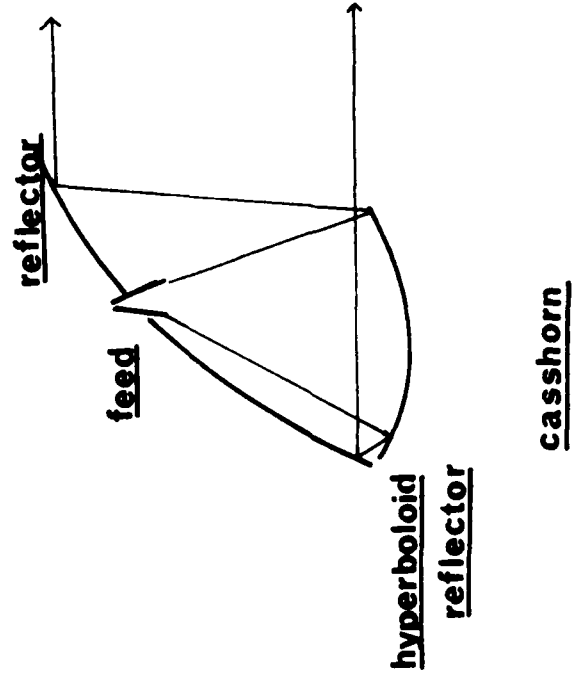


Fig.4.3-1: Geometry of two types of hoghorn.

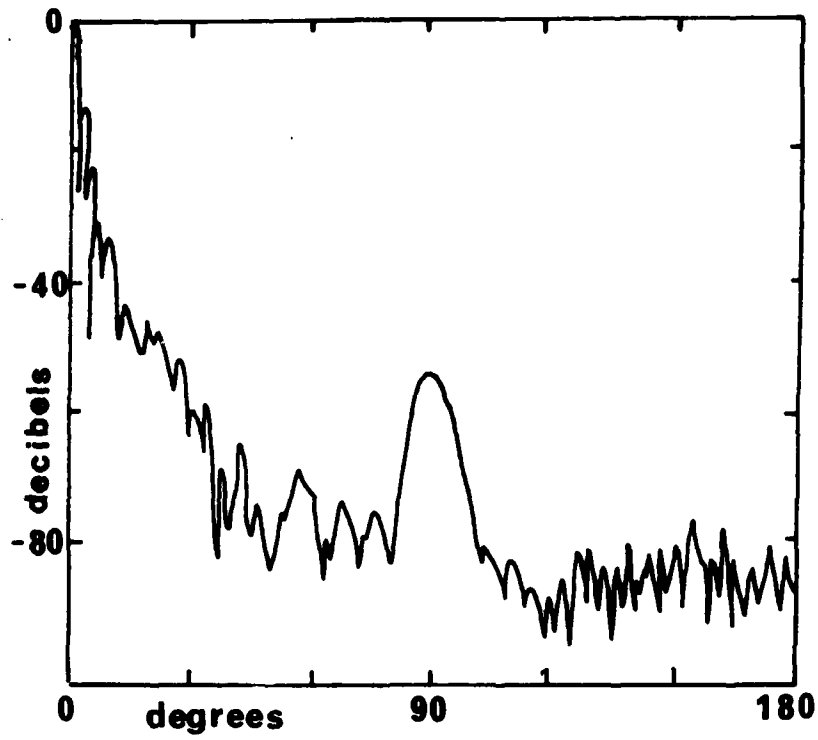


Fig.4.3-2: Hoghorn radiation pattern at 3.74 GHz (horizontal polarisation).

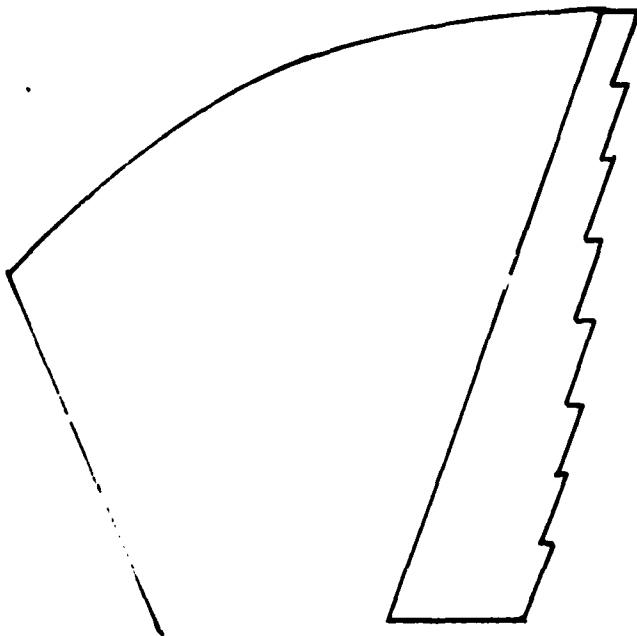


Fig.4.3-3: Arrangement of edge blinders for a hoghorn (Siller).

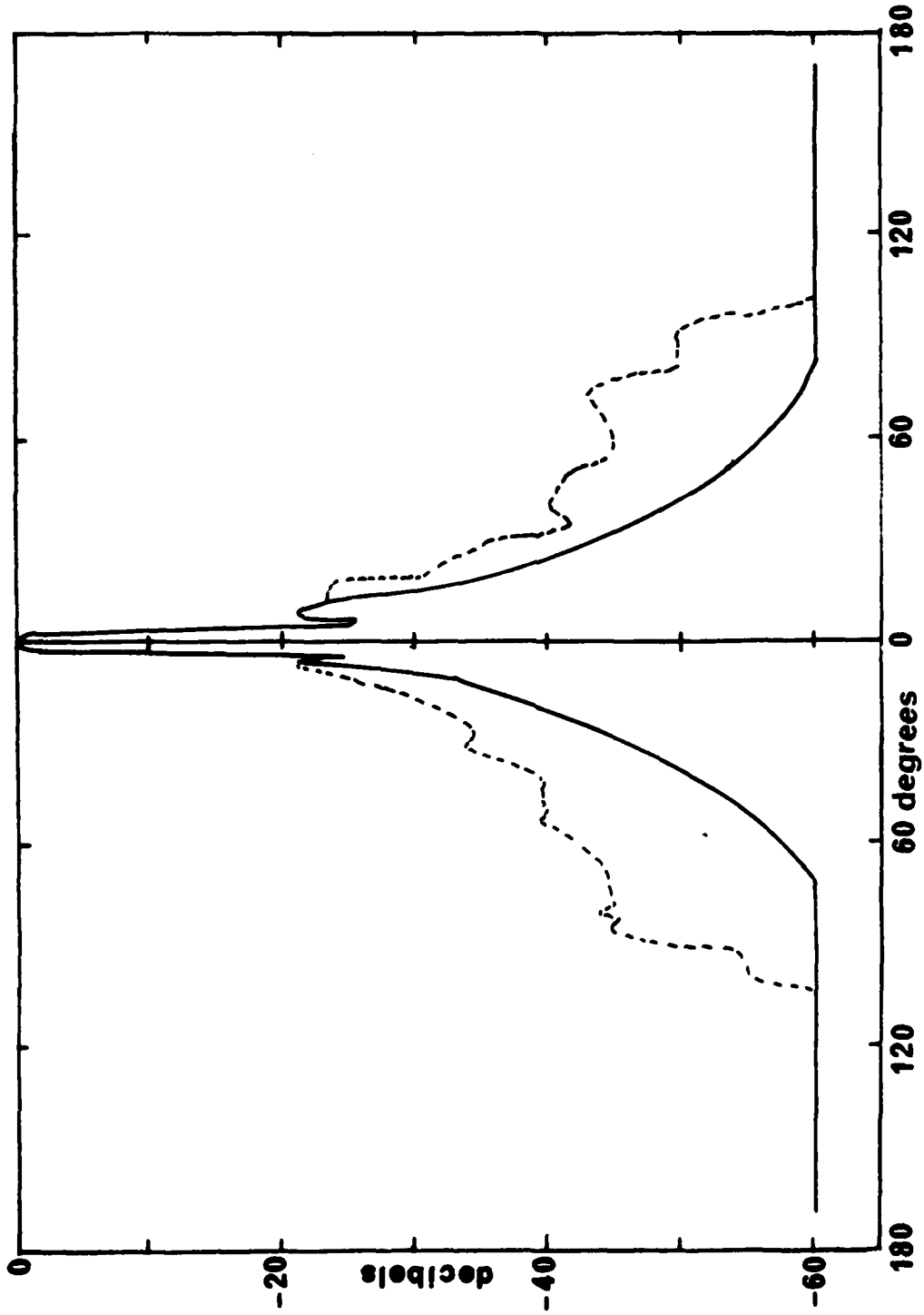


Fig.4.3-4: Radiation patterns for a plane reflector fed from the near-field of a paraboloid. Antenna aperture 36 wavelengths.  
Dashed curve - No precautions  
Solid curve - Forming cylinder lined with absorber and placed between the two reflectors.

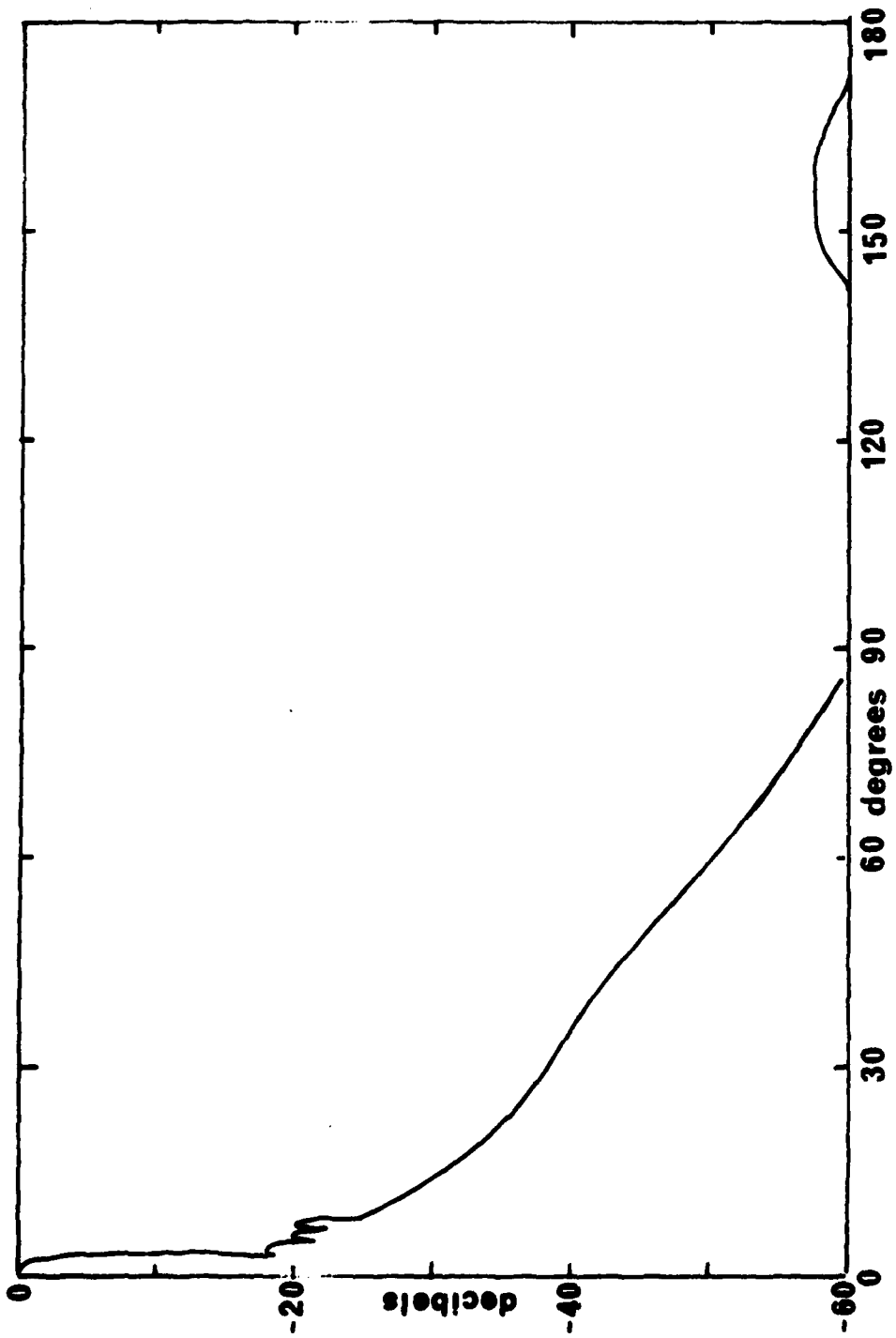


Fig.4.3-5: Sidelobe envelope for a Casshorn of aperture 30 wavelengths at 11 GHz.

## 5 HIGH GAIN ANTENNAS

High gain is achieved by the use of an antenna whose aperture dimensions are large in terms of wavelengths. The aperture illumination is much more amenable to adjustment and there is generally more scope for suppression of sidelobe and backlobe radiation with these antennas than for the types previously discussed.

The radiation patterns resulting from specific aperture illumination functions were discussed in Chapter 2. The following sections consider various antenna types with a view to discovering what aperture illuminations may be achieved in practice and what additional factors must be taken into account.

Each major section contains a sub-section on theory plus comparison with relevant results in order to confirm the general viability and quality of the theoretical predictions. A following sub-section presents some measured results, arranged where possible in tabular form and a last sub-section provides tables and a graphical presentation of backlobe/sidelobe parametric dependence.

### 5.1 The Axisymmetric Parabolic Reflector

Of the many forms of antenna which can be designed to provide high-gain performance, the parabolic reflector antenna and its variants are the most popular. This preference for the parabolic reflector is soundly based on a cost-effective criterion and is unlikely to be radically changed in the next decade. However, as a consequence of the increasingly demanding performance specifications which are emerging, it appears that improvements and refinements in the design of these antennas must be forthcoming if they are to maintain their dominance in applications where sidelobe suppression is critical. To place such improvements and refinements in perspective, we will first consider the radiation performance of some typical reflector antennas and the correlation between the sidelobe suppression realised in practice, and that predicted by various techniques including the simplified scalar theory described in Chapter 2.

The axisymmetric parabolic reflector in either its front-fed or Cassegrain form is the most commonly utilised configuration for antenna systems and the sidelobe characteristics of this class of radiator will be considered initially.

### 5.1.1 Sidelobe prediction using simple aperture-distribution theory

In Chapter 2, a simple scalar aperture-distribution theory was adopted to illustrate the relationships between a given illumination taper in the aperture plane of an antenna and the radiated sidelobes. However, for axisymmetric reflector antennas, the design of a primary-feed antenna to provide a specific aperture illumination will not be sufficient to ensure that the radiated sidelobe levels comply with the scalar predictions. This fact is demonstrated in Fig.5.1-1. The figure shows the radiation-pattern of a 32 wavelength diameter Cassegrain antenna with its aperture illumination tapered to approximately -8 dB at the reflector rim. The dashed line in the figure denotes the envelope of the sidelobes to be expected from an ideal uniformly illuminated circular aperture, which should (according to the simple scalar theory) produce a higher level of sidelobe radiation than the tapered illumination case. In this case it is the large blockage of the aperture introduced by the sub-reflector which is a principal source of the sidelobe degradation. There are other factors, however, which will be considered in due course.

The electric field distribution in the aperture plane of an unblocked front-fed paraboloid is dependent upon the primary-feed radiation characteristics and the geometrical parameters of the reflector itself. This distribution can often be modelled quite accurately by a function of the form:

$$A + B \left( 1 - \left( \frac{r}{a} \right)^2 \right)^n \quad (10)$$

where A, B and n are selected constants and r is the distance along a radial line from the centre of the antenna aperture of radius a. However, since low sidelobe levels are very sensitive to the aperture illumination function, it is first necessary to accurately fix the parameters A, B and n, which demands an accurate knowledge of the aperture field distribution. The fact that any practical axisymmetric reflector system will suffer from blockage, and that the effects of blockage will dominate the sidelobe characteristics of the antenna, tends to make a discussion of precise illumination tapers purely academic. Typically the effect of blockage will result in peak sidelobes in the range -25 to -30 dB (depending upon geometry) even when the illumination taper set up by the primary-feed indicates much lower levels.

It is certainly conceivable that one might employ a multiple-element primary-feed to generate a high-efficiency illumination taper in the aperture-plane of a reflector. The array feed element described by Rudge and Withers<sup>2</sup> or the multi-ring coaxial feed due to Koch<sup>3</sup> are possible candidates, for example. However, to achieve very low sidelobe performance the feed would also have to compensate for the fields scattered from the struts and the blockage itself, and this seems far less feasible.

Figure 5.1-2 shows the radiation pattern of a  $60 \lambda$  diameter reflector ( $F/D = 0.36$ ) illuminated by the Koch feed. The efficiency of the antenna is claimed to be 78% which is high, but the near-in sidelobe performance is indifferent, as one might expect from a high-efficiency design.

In Cassegrain antennas the aperture-illumination taper can be adjusted by shaping the main and sub-reflectors<sup>4,5</sup>. Again this can be employed to improve the aperture efficiency of the antenna but, in view of the blockage effects, it seems unlikely that it can provide the basis for low sidelobe designs. Nevertheless it must be noted that the possibility of optimising the shaped Cassegrain antenna for maximum sidelobe suppression has not received attention in the literature.

The simplified scalar theory described in Chapter 2 can be improved by putting to zero the aperture illumination in those regions of the aperture plane which are effectively 'shadowed' by the primary-feed hardware (or the sub-reflector) and the associated supporting struts. This scalar diffraction technique will provide some indication of the effect of blockage in the near-in sidelobe region, but it does not overcome the problem of defining the actual aperture-plane illumination taper set up by the primary feed. Although this technique can be used to obtain some indication of the sidelobe performance with typical reflector antennas, it provides no insight into the interaction of the primary-feed and reflector parameters, and thus cannot be employed as a design aid or in a parameter-optimisation role. Finally, the scalar theory provides no indication of the antenna cross-polarisation characteristics.

#### 5.1.2 More accurate techniques for the prediction of sidelobe radiation

The limitations of the simple aperture-distribution techniques in providing accurate predictions of reflector antenna sidelobe performance are

such that they are totally inadequate when low-sidelobe or highly optimised antenna designs are of interest. In a practical axisymmetric reflector antenna, all of the following factors must be modelled when accurate prediction of sidelobe performance is of concern.

- (i) The vector diffraction pattern arising from the reflection of the primary-feed fields from the reflector surface.
- (ii) Blockage and electromagnetic scattering due to the primary-feed hardware (or sub-reflector) and its supporting struts.
- (iii) Primary-feed spillover radiation (i.e., that which is not incident upon the reflector surface).
- (iv) Imperfections in the reflector surface profile.
- (v) Misalignment of the primary feed or sub-reflector.
- (vi) Backlobe radiation.

(i) The vector diffraction field arising from the reflector

With the blockage effects included, the vector diffraction field dominates in the near-in sidelobe region. The reflector diffraction can be predicted with good accuracy employing physical-optics techniques, providing the radiation fields from the primary-feed antenna can be adequately modelled. For reflectors having diameters greater than 20 wavelengths, either the vector aperture-field or surface current techniques are adequate in the near-in sidelobe region. For smaller diameter reflectors the surface-current method is to be preferred<sup>6,31</sup> and can be usefully applied to reflectors with diameters exceeding about 10 wavelengths.

In the aperture-field technique the vector electric field reflected from the parabolic surface is determined as a function of the primary-feed radiation fields by applying the physical-optics approximation. This vector field is then projected into the reflector aperture-plane to define the tangential electric field in this plane. The surface current technique is also physical-optics based, and in this case the reflector surface currents are determined as a function of the magnetic field component radiated by the primary feed. The tangential aperture-field method

results in somewhat simpler mathematical expressions and is therefore more convenient to use in the near-in sidelobe region of large reflectors (i.e. diameters greater than about 20 wavelengths). At wide angles, however, the additional approximation involved in projecting the reflected field into the aperture-plane becomes more significant and the surface-current technique is more reliable. Figure 5.1-3 shows an example of predicted and measured data using the tangential aperture field method.

Employing the surface current method, the current distribution over the reflector can be estimated using the physical-optics approximation. For reflectors having diameters of at least 10 wavelengths, this gives good predictions of the reflector-diffracted fields within angles of about  $\pm 30^\circ$  from boresight. The surface-current technique can be used to predict the diffracted field accurately in the far-out sidelobe region, although in this region other effects, such as scattering from feed struts and spillover, may play a dominant role in defining the sidelobe levels. The method fails in the shadow region because currents on the back of the reflector are neglected. For small reflectors, with aperture diameters less than 10 wavelengths or reflectors having high edge illuminations, an 'edge-correction' current can be introduced to improve the physical-optics approximation<sup>8,43</sup>. Over the illuminated surface of the reflector, the physical-optics component will normally dominate the overall current distribution up to about one wavelength from the reflector edge. In the non-illuminated region of the reflector, where the physical-optics current is zero, only the edge-correction component will exist. Hence for these cases the correction affects only the predicted rearward radiation. For smaller diameter reflectors the edge correction may be more significant in the forward half-plane, particularly when the edge illumination is strong.

For reflector antennas with surface-current distributions which do not exhibit an essential axisymmetry, the computation of wide-angle sidelobes can become a very costly operation in terms of computational effort, since a pair of two-dimensional numerical integrations are necessary at each field point.

For sidelobe predictions outside of the main-beam area, techniques based upon the Geometric Theory of Diffraction (GTD) can be usefully employed<sup>7,11</sup>. GTD<sup>9</sup>, which is essentially a combination of ray-optics and diffraction coefficients, also provides accurate predictions of the sidelobe radiation in the shadow region. However, in general the method demands careful application. Since GTD fails in the region of the antenna boresight, a combination of vector aperture field theory for this region, and GTD for the far-out sidelobes and backlobe region, is well suited for large reflector antennas<sup>11</sup>. In the far-out sidelobe region, the agreement between GTD and surface-current methods is generally good<sup>12</sup>. Figure 5.1-4 shows measured and computed E plane patterns for a paraboloid with a short dipole feed. The H plane agreement is equally good. Discrepancies in the backlobe were attributed to poor feeding arrangements at the back of the reflector. Comparison of predictions and measurements for a 10 wavelength paraboloid with  $F/D = 0.43$  fed by a horn feed showed better agreement in the backlobe region<sup>9,10</sup>. This result is shown in Fig.5.1-5.

With Cassegrain antennas the parabolic and hyperbolic reflector profiles may also be modified to provide improved efficiency<sup>5</sup>. These techniques generally result in antennas with relatively high near-in sidelobe levels, as a direct consequence of the near uniformity of the field distribution in the main reflector aperture-plane. The mathematical modelling of these shaped surfaces involves no additional fundamental difficulties, however, and the techniques referred to above can be applied as before.

(ii) Blockage and strut and sub-reflector scattering effects

Central blockage due to the presence of the primary feed or sub-reflector is commonly modelled using shadow-diffraction techniques<sup>6</sup>, in which currents or fields lying in the shadow of the blocking hardware are put to zero. The shadow is assumed to be that when the antenna is illuminated normally from the boresight direction. However, Rusch and Sorensen<sup>22</sup> have shown that essentially similar predictions are obtained if the blocking shadow is projected on to the reflector surface from the angle corresponding to each field point. Providing the central blockage region is large relative to the wavelength, these techniques provide quite accurate predictions of the effect on the antenna gain and the near-in sidelobes. For blockage regions with dimensions on the order of one wavelength or less, it becomes necessary to give the central blockage an 'effective area' which is somewhat larger than the projected shadow.

The blockage effects arising from the supporting struts can also be treated approximately by shadow-diffraction techniques. However, there are scattering effects which modify the cross-polarised radiation and far-out sidelobes which are not adequately modelled by shadow-diffraction. Rusch and Sorensen<sup>22</sup> have attempted to model the strut effects mathematically by determining an approximate current distribution on the assumed metallic struts. Their techniques, although approximate, do appear to offer improvements over shadow-diffraction methods. For example, one result of interest which emerged from their theoretical study was that, in terms of scattering effects, struts with rectangular cross-sections are less desirable than struts with circular cross-sections. This result has yet to be confirmed experimentally, but it does suggest that strut geometries may warrant more careful attention if low sidelobe performance is of concern.

(iii) Primary-feed spillover radiation

The accurate prediction of the radiation field from a reflector antenna, and particularly the sidelobe and cross-polar radiation, is very dependent upon the accuracy with which the incident primary-feed radiation fields can be defined<sup>30</sup>. Accurate mathematical models for the vector radiation from the primary feed antennas must be available, or suitable measured data, if the overall sidelobe prediction is to be meaningful. The spillover radiation from the primary feed antenna itself can make a significant direct contribution to the sidelobes of the overall antenna. This effect can be particularly strong when the parabolic reflector is not large. Peters has provided an approximate formula for the direct spillover level ( $S_p$ ) from either front-fed or Cassegrain paraboloid as follows<sup>45</sup>:

$$S_p = G_F - G - T + 6 \text{ dB} \quad (11)$$

where  $G_F$  is the primary feed gain,  $G$  is the antenna gain,  $T$  is the reflector edge illumination taper and all parameters are expressed as decibels. Fig.5.1-6 shows spillover and aperture efficiency as calculated for various illumination functions by Afifi<sup>12</sup>.

With Cassegrain antenna configurations the prediction problem can be compounded by the fact that the primary feed antenna may be located in the

near-field of the sub-reflector. The geometry in this case is also more complex, as illustrated by Fig.5.1-7. In this case direct spillover occurs between the angles  $\beta_H$  and  $\beta_R$  and reflected spillover between  $\alpha_H$  and  $\alpha_p$ . For angles beyond the shadow boundary at  $\theta = \beta_H$  all of the diffracted fields may contribute to sidelobe radiation. To illustrate the complexity of accurate predictions it is worth noting that for this case the diffracted field components include the following<sup>14</sup>:

From the rim of the paraboloid:

- direct illumination by the feed
- reflected fields from the hyperboloid
- diffracted fields from the hyperboloid rim
- diffracted fields from the opposite edge of the paraboloid

From the hyperboloid sub-reflector:

- direct illumination from the feed
- fields from the feed twice reflected
- fields diffracted from the opposite edge of the hyperboloid

In all cases reported in the literature, a complete mathematical model for the antenna scattering has not been considered feasible, and in general, attempts have been made to isolate the dominant effects in specific regions of the antenna radiation field. The paper by Menzer and Peters is an example of this approach<sup>14</sup>.

It is also worth noting that for good sidelobe performance with reflector antennas with diameters which are not very large, the near-in and far-out sidelobe performance of the primary feed itself must be given attention. This aspect of reflector antenna design, either front-feed or Cassegrain, appears to have received relatively little attention in the past.

#### (iv) Imperfections in the reflector surface profile

Reflector profile errors can be treated as an equivalent phase-error distribution in the reflector aperture-plane fields (or surface currents) providing that the magnitude of the errors does not exceed about one wavelength<sup>47</sup>. The general effects of phase-errors have been discussed in Chapter 2 of this report. For accurate predictions with larger profile deformations, it becomes necessary to perturb the unit vector in

the mathematical expressions defining the parabolic surface. However, even relatively small profile-errors can produce a significant degradation in gain and sidelobe performance and thus for high-performance antennas the phase-error approach is generally adequate.

It is worth noting that it can be shown that phase-errors cannot generate additional cross-polarised fields, although they can cause existing cross-polarised radiation (i.e., from the primary feed) to be redistributed in space<sup>47</sup>. This result implies that the effects of small-magnitude deformations in the reflector are a reduction of the antenna gain and deterioration in the co-polar sidelobe suppression, providing the cross-polarised radiation from the antenna was small prior to the deformation. The general effect of profile errors is thus the removal of energy from the main-beam of the antenna and the redistribution of this energy into the sidelobe region. If the reflector profile-error has a strong periodic content in its spatial distribution, then the displaced energy may be redirected into a lobe or series of lobes in the antenna far-field. For good peak sidelobe suppression, periodically distributed errors are even less desirable than randomly distributed errors of the same magnitude.

(v) Misalignments of the primary feed or sub-reflector

Small primary-feed misalignments can be treated mathematically on the basis of a movement in the phase-centre of the feed<sup>29,31</sup>. This phase-only technique cannot be applied to large feed misalignments, and in these cases more exact vector co-ordinate transformation techniques must be applied<sup>48</sup>. There are no fundamental difficulties in performing the co-ordinate transformations numerically but considerable computational effort can be saved if the phase-only technique is adopted for feed offsets of not more than a few wavelengths.

The principal effects of feed and sub-reflector misalignments on sidelobe performance can be understood in terms of the defocusing and comatic phase-error effects discussed in Chapter 2. These effects will not be discussed further here.

(vi) Backlobe radiation

The inaccuracy of the physical-optics-based techniques in predicting the backlobe radiation from reflector antennas has been commented on above. GTD methods can be usefully applied in this region and the edge-correction current technique may also be helpful. Knop<sup>13</sup> has developed an

approximate formula which appears to provide meaningful results, with an accuracy of about 1 dB (at -40 dB levels). This formula can be expressed as a front to back ratio given by:

$$G + T + K - G_F \text{ dB} \quad (12)$$

where  $G$  is the reflector gain,  $T$  is the reflector illumination taper,  $G_F$  is the primary-feed gain and all parameters are expressed in decibels. For a reflector of focal length  $F$  and diameter  $D$  the constant  $K$  is given by:

$$K = 20 \text{ Log}_{10} \left( \frac{\sqrt{1 + 16(F/D)^2}}{4F/D} \right) \quad (13)$$

Knop provided a considerable quantity of experimental data to support his formula<sup>13</sup>.

To summarise, mathematical models, generally in the form of computer programs, can be developed with capabilities of accommodating all of the effects referred to above. Using these techniques, the sidelobe performance of an axisymmetric reflector antenna, with moderate sidelobe suppression, can be predicted with reasonable accuracy. However, for very low sidelobe performance the accuracy required to predict the radiated fields becomes more difficult to achieve. The modelling of the reflector itself is not a major constraint but the relatively crude strut and blockage modelling methods are likely to be a limiting factor in this respect.

#### 5.1.2 Factors influencing the sidelobe performance of axisymmetric reflector antennas

##### (i) Blockage effects and backlobe radiation

Physical-optics techniques, employing either the aperture-field or current distribution methods are extensively employed in work reported in the literature. The accuracy of the technique and its limitations for wider angle sidelobe-radiation predictions have been discussed in the previous section. Employing combinations of physical-optics and GTD, improved predictions for reflector antenna radiation have been achieved, for example by Ratnasiri and his co-workers<sup>11</sup> for a 20 wavelength reflector with  $F/D = 0.3$  at Xband. They successfully predicted the radiation-

patterns measured by Afifi<sup>12</sup> down to -50 dB levels. Afifi was particularly concerned with the spillover radiation from the primary-feed which occurs just forward of the shadow boundary. The characteristic shape of this spillover is a wide lobe with a sloping cut-off toward the shadow region (e.g., see the radiation characteristics between  $40^\circ$  and  $100^\circ$  in Fig.5.1-4). This lobe can be reduced by reducing the edge illumination and, if a steeper illumination taper can be contrived, the reduction in spillover need not involve a loss of antenna efficiency.

Mentzer and Peters<sup>14</sup> have used a combination of physical-optics and GTD methods to analyse the radiation from Cassegrainian antennas. However, consideration of strut scattering effects which would influence the radiation-patterns in the angular range  $30^\circ$ - $70^\circ$  off boresight was discarded as being too difficult. For the far-out sidelobe region, GTD was employed, while in the region close to the rear axial caustic of the main reflector, the equivalent current technique was applied. Although specimen computed patterns are shown for a small reflector of diameter 20 wavelengths, no measured data is provided for this case. Some general observations can be made, based upon these results. With regard to sidelobe performance, blockage effects are clearly dominant and the small Cassegrain configuration offers poor sidelobe suppression. Back-lobe performance is also poor as a consequence of the small diameter and relatively efficient illumination characteristics. Cassegrain reflectors are more typically employed for applications demanding radiating apertures of 50 wavelengths or more, where the blockage effects are reduced.

For large paraboloids with diameters exceeding 100 wavelengths, spillover and backlobe radiation can be suppressed below -50 dB by good design practice. For smaller antennas, additional techniques such as edge shields, edge-castellations or diffraction screens will be necessary to achieve these levels<sup>17-21</sup>. Edge shields or castellations can be usefully employed to suppress wide-angle and backlobe radiation even on the larger reflector antennas. Figure 5.1-8 shows the effect on the sidelobe envelope of a 135 wavelength front-fed paraboloid when edge-shields are added. The principal improvement occurs in the angular range  $100^\circ$ - $180^\circ$  from boresight. There is no significant effect on the radiation within  $70^\circ$  of boresight.

AD-A133 361

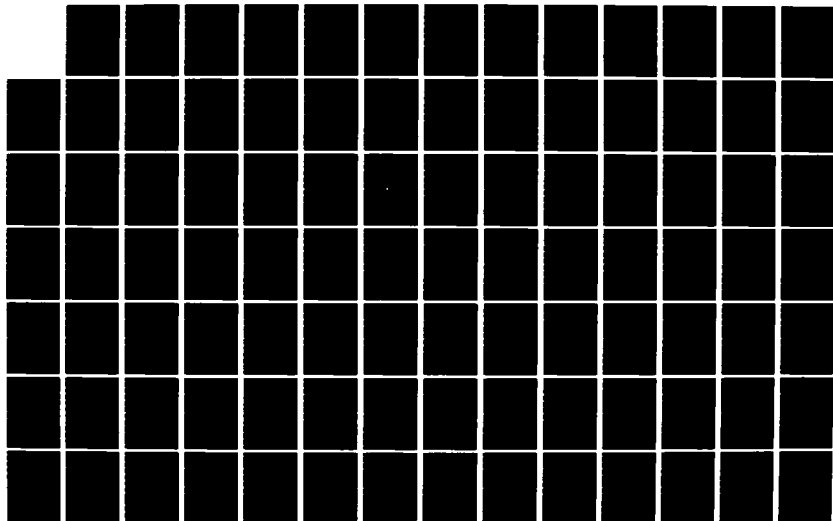
LOW SIDELobe ANTENNA STUDY PART 1 LITERATURE SURVEY AND  
REVIEW(U) ELECTRICAL RESEARCH ASSOCIATION LEATHERHEAD  
(ENGLAND) P R FOSTER ET AL. OCT 77 ERA-RFTC-190476/1  
DRIC-BR-56799

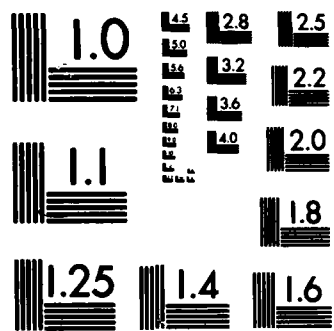
2/3

UNCLASSIFIED

F/G 9/5

NL





MICROCOPY RESOLUTION TEST CHART  
NATIONAL BUREAU OF STANDARDS-1963-A

James<sup>7</sup> has devoted considerable attention to the analysis of castellated edges for parabolic reflectors. He found only few edge geometries amenable to mathematical treatment and, on the whole, agreement with measured data was not good. Castellations 0.35 wavelengths deep on the rim of a reflector having a diameter of 10 wavelengths, reduce the backlobe by 6 dB. One point that James makes is that the peak cross-polarised radiation in the shadow region may increase by up to 10 dB due to the presence of the castellations.

The castellations, like blinders for hoghorns (see Section 4.3), are frequency sensitive. A 12 ft castellated reflector<sup>16</sup> had the backlobe reduced by 7 dB over an 11% band without loss of forward gain. According to Lewin<sup>17</sup>, the theoretical improvement which can be realised by means of rim castellation is 50 dB, but this is a spot-frequency value. When mechanical and structural constraints permit, edge shields or tunnel-shields lined with absorber offer a better and more broad band solution<sup>18,19</sup>. Yokoi and Fukumoro<sup>44</sup> give full details of the use of absorber at the rim of a reflector. For several designs, the sidelobes in the spillover region and the back region were reduced by 10 dB. There appeared to be no reduction in forward gain.

Aperture blocking effects are commonly treated in the literature by means of the shadow-diffraction techniques described in the previous section. For the centrally-located blockage where the blocking object is much larger than a wavelength, the effect on the total radiation pattern is essentially obtained by subtracting the voltage radiation pattern of the obstacle aperture from that of the total aperture. This assumes that the illumination of the full aperture is uniform over the central obstacle which is likely to be accurate to a few per cent if the ratio of the blocking diameter,  $D_s$  to the reflector,  $D_0$ , is less than 0.2. For such cases the pattern of the obstacle is  $D_0/D_s$  times the width of the final radiation pattern and is a slowly decreasing function over the first few sidelobes of the final pattern. Since the phases of these sidelobes alternate, the final pattern has the first, third and subsequent odd-numbered sidelobe levels enhanced while the even numbered sidelobes are depressed (see Fig.5.1-20a). This sidelobe effect is accompanied by a loss of forward gain (see Fig.5.1-20b).

To obtain more accurate information on the effect of central blockage, the diffraction round the edge of the obstacle must be accounted for.

This is rarely treated in predictions of reflector antenna performance.

Rusch and Sorensen<sup>22</sup> have treated the case of blockage in a Cassegrain reflector and compared three different methods:

1. Aperture field shadow-diffraction.
2. Surface current shadow-diffraction where the shadow is fixed, i.e., the shadow is that seen along the reflector axis.
3. Surface current shadow-diffraction where the shadow is moving and is the geometrical shadow for any given distant field point.

A comparison of the radiation patterns of the blockage obstacle shows that all methods are in good agreement in the near-in sidelobe region. The forward gain degradation is also predicted accurately, but for the far-out sidelobe regions the use of GTD is to be preferred.

Clearly the blockage should be kept to a minimum.  $D_S/D_0$  should be less than 0.1 and preferably less than 0.05 for a low sidelobe design. The sub-reflector diffraction effects increase sharply as  $D_S$  is decreased and values of less than 3-4 wavelengths should not be used. The lower limit for a Cassegrain main reflector diameter is loosely said to be 50-80 wavelengths which is really derived from this blockage information. For a prime focus system and moderate  $F/D$  ( $<0.8$ ) the diameter of a typical primary-feed is of the order of 2 wavelengths and for  $F/D = 0.3$ , about one wavelength. This does imply that for very small reflectors the  $F/D$  should not be large if sidelobe suppression is of concern.

Support struts are also a source of shadow-diffraction and the treatment of this problem has an extensive literature. Unfortunately, the scattering which arises from strut blockage has yet to be quantified adequately. If the strut diameter is several wavelengths, the problem may be treated by shadow-diffraction techniques with reasonable accuracy in the near-in sidelobe region. Maanders<sup>15</sup> provides tables of near-in sidelobe levels for a reflector diameter of 330 wavelengths with a central sub-reflector ( $D_S/D_0 = 0.1$ ) supported by four struts of various widths. The worst results are for the largest struts of 5 wavelengths width where the gain is reduced by 0.82 dB and the first sidelobe increased from -24.3 to -18.8 dB. The third sidelobe is increased from -38.3 to -25.3 dB.

For small struts, the shadow-diffraction method becomes increasingly inaccurate. Rusch and Sorensen<sup>22</sup> computed the radiation pattern of a reflector by treating the strut currents as though they were flowing on an infinite cylindrical structure (with the same cross-section as the physical struts) immersed in an infinite plane wave with the same polarisation and direction of incidence as the local geometrical ray emerging from the aperture. Computations with various strut widths, angles relative to the boresight axis, and disposition relative to the incoming polarisation are presented but the work is not accompanied by any experimental verification. Nor do the results go beyond the first 6 or 7 sidelobes, whereas a major interest here is in the far-out range of angles around  $60^{\circ}$ - $100^{\circ}$  off axis.

The far-out sidelobe effects of struts have been investigated by considering the field scattered from the strut as similar to that from a phased line source<sup>24</sup>, which maximises on a conical surface (see Fig.5.1-9). The local maxima are given by:

$$\cos \left[ \phi_{\max} - \phi_0 \right] = \tan \left( \frac{\theta_{\max}}{2} \right) \tan \alpha \quad (14)$$

where  $\alpha$  is the strut angle to the vertical,  $\phi_0$  is the plane in which the strut lies<sup>22</sup>. Typical patterns then are interlocking circles which pass through the boresight axis. For instance, the far-out pattern of the Dwingeloo 25 m radio telescope ( $F/D = 0.48$ ) is shown in Fig.5.1-10\*. This antenna<sup>23</sup> had a taper of 16.6 dB in the E plane and 13.7 dB in the H plane. The basic features of the radiation pattern are the spillover ring which is -52 dB at  $120^{\circ}$  from the boresight which is 6 dB above the surrounding level, and the obvious features of 3 interlocking rings at 50-55 dB down which are due to the tripod support (each strut being one wavelength wide). This level is about 6 dB higher than the local level. For Cassegrain reflectors the actual levels of spurious far-out radiation have been more carefully examined by Kreutel<sup>24</sup> who calculates the sidelobe envelope. Comparisons with measured antennas show remarkable agreement (Fig.5.1-11). One point of interest is that the level relative to isotropic remains virtually unchanged when the reflector gain is increased by 12 dB. The levels in Fig.5.1-11 are therefore only acceptable for large antennas, i.e., with diameters greater than about  $90 \lambda$  if far-out levels of <-50 dB are required.

\* The frequency is 1.415 GHz

An investigation of blockage in radomes<sup>25</sup> which considers the radome support structure as a set of scattering cylinders of various cross-sections may be relevant to the problem of strut blockage. The authors conclude that rounding off corners or using a triangular cross-section improves performance, but it is not clear whether this is really due to the shape or to the reduced area of cross-section. Further experimental investigation of the effect due to solid metal support struts in a Cassegrainian antenna<sup>26</sup> shows that, with a dimension less than one wavelength, using the geometrically shadowed area is inadequate. In general this treatment will be sufficient to indicate performance at angles close to boresight, but the major effect is to produce rings or radial ridges of enhanced sidelobes. For examples see Table 5.1.5 and Fig.5.1-10. Changing the depth of the support strut had little effect.

In summary, the literature on blocking effects shows some general tendencies. It is impossible to quantify the effect of strut blockage without knowledge of the precise geometry to be used and access to an appropriate computer program. Most published work has been carried out with design near-in sidelobes of around -25 dB which is not low enough for our purposes. Comparison with the effects of central blockage indicates that the problem will be much more serious at low sidelobe levels. Strut blockage effects certainly demand further attention if low sidelobe performance is to be sought from front-fed antennas. Each strut will produce a circular ridge of sidelobes in the far-out region as well as degrading near-in sidelobes and the forward gain but the larger the reflector diameter,  $D_o$ , the smaller the far-out sidelobes. Cross-polarisation will also be produced in certain circumstances, particularly when circular polarisation is employed.

Central blockage either by a feed or a sub-reflector generally tends to affect only the forward gain and near-in sidelobes. For blockage diameters of more than a few wavelengths, the aperture field shadow-diffraction method is usually adequate.

For prime-focus reflectors, the feed diameter will not be large and for moderate size reflectors (i.e., diameters greater than 25 wavelengths), the central blockage will be small although not negligible for low sidelobe purposes. Small F/D ratios are to be preferred because the reflector curvature improves sidelobe suppression at wide angles and a smaller

primary-feed is implied. However, the sidelobes in all regions will be dominated by the struts, and peak sidelobe values of the order of -25 to -30 dB are unlikely to be bettered for a reflector of 25 wavelengths diameter.

In Cassegrain antennas, because the sub-reflector must be large with respect of wavelength, the main reflector diameter must also be large; usually a minimum of 50 wavelengths is desirable. Near-in sidelobes and forward gain will be degraded by the presence of the sub-reflector and far-out sidelobes raised to at least -50 dB at angles around  $70^\circ$  off axis. With the main reflector diameter larger than 50 wavelengths this level decreases. On the whole, the radiation patterns of Cassegrain antennas are more affected by the sub-reflector than by the struts though these may produce significant cross-polarisation degradation.

In order to check blockage effects experimentally, measurement of one plane of the radiation pattern is not sufficient. At least four ( $0^\circ$  and  $45^\circ$  in both planes of polarisation) are required for a quadripod and possibly more for a tripod.

(ii) Imperfections in the reflector profile

The modelling of reflector profile errors as effective phase-errors was discussed in Section 5.1.2 and the effect of such phase-errors in a circular aperture was treated in Chapter 2. Further details are provided in Section 5.1.4 (Fig.5.1-21).

(iii) Systematic phase and amplitude errors in the reflector aperture field distribution

Modern multi-mode and corrugated horn feeds have well-defined phase centres. For obvious reasons the phase centres of E and H plane radiation should be coincident if astigmatic effects are to be avoided. Rusch<sup>27</sup> has considered the phase ripple across the aperture of a Cassegrain antenna caused by diffraction at the sub-reflector and concludes that this has a negligible effect on forward gain. However, Wood<sup>5</sup> has shown that it had an adverse effect on near-in sidelobes.

Lateral displacement of the primary-feed<sup>28,29</sup> gives rise to a beam shift, a gain loss and a degradation of sidelobes because the aperture illumination becomes asymmetric in amplitude and phase. The near-in sidelobe

degradation is much more marked than the gain loss (Fig.5.1-22) and the degradation is more marked for a low sidelobe design. To decrease the sensitivity of the system to lateral shift, a long F/D is to be preferred and the use of a Cassegrain configuration is particularly helpful here as very large effective F/D values can be achieved.

An axial primary feed displacement<sup>28,29</sup> produces a symmetrical phase error across the aperture. This results in null infilling and enhanced sidelobes but the pattern is still symmetric. Again a large F/D reflector is less sensitive to small axial displacements of the primary feed.

#### (iv) Cross-polarisation

It is generally accepted that the contribution made by the parabolic reflector itself to the overall cross-polarised radiation is of little practical significance in the majority of applications, providing only that the diameter of the reflector is large relative to the operating wavelength. For small diameter reflectors the cross-polar contribution of the reflector can be computed using the physical-optics surface current technique. The largest cross-polarised contribution which can be attributed to the reflector curvature, occurs at small F/D ratios. For example, a large parabolic reflector with  $F/D = 0.25$  and a 12 dB illumination taper will generate a peak cross-polarised lobe at a level of approximately 45 dB below the peak of the main co-polar beam and this level will rapidly reduce as the F/D ratio is increased<sup>30</sup>.

The principal sources of cross-polarised radiation from front-fed axisymmetric reflector antennas have been identified as firstly the primary feed radiation and secondly the struts supporting the primary feed hardware. The F/D ratio of the reflector plays a significant role only in terms of the specification it imposes upon the polarisation purity of the primary feed radiation. The use of a smaller F/D ratio implies that the primary feed must retain its low cross-polarisation characteristics over a wider range of spatial angles. For this reason there has been a tendency to favour large F/D ratio configurations when good cross-polarisation performance is of prime importance. However, primary feeds can be, and have been, designed with good polarisation properties over wide angles, and thus small F/D reflectors can be employed in low cross-polarisation applications.

For linearly polarised axisymmetric parabolic reflectors the peak cross-polar radiation normally occurs in the diagonal planes (relative to the plane of polarisation). The peak value normally occurs at an angle corresponding to the -12 to -20 dB level of the main co-polar beam. For circularly polarised antennas the location of the peak is difficult to predict, since it is strongly affected by the struts.

Although no detailed experimental work has yet been reported in the literature, it seems probable from initial theoretical studies that the effect of small profile errors in the reflector surface will not result in a serious deterioration of the antenna cross-polarised performance<sup>27</sup>. Rudge and Shirazi<sup>31</sup> have reported that the peak cross-polarised lobes of both axisymmetric and asymmetric reflectors are not sensitive to small phase-error effects introduced by offsetting the primary feed from the reflector focus. Other forms of phase-error distribution have been briefly examined and it appears that, in the presence of phase-errors, the degradation of the antenna co-polarised sidelobe levels is likely to exceed any significant cross-polar sidelobe effects<sup>47</sup>.

In Ref.31, the following approximate guide to the sources of cross-polarised radiation has been proposed for reflectors with diameters greater than 20 wavelengths, fed by prime-focus primary feeds producing edge illumination tapers of -10 dB or greater (Table 5.1-1A).

Table 5.1-1A

Cross-polarised lobe levels	Probable source
-10 to -35 dB	Primary feed radiation
-30 to -45 dB	Primary feed and/or aperture blockage
Below -45 dB	Primary feed and/or aperture blockage and/or higher order reflector effects

Rusch and Sorensen<sup>22</sup> have developed a theoretical model for strut blockage and have predicted results which suggest that the feed-supporting struts may generate a somewhat higher level of cross-polarisation than that indicated in Table 5.1-1A. In the worst case shown in Ref.30 a peak cross-polar level of -28 dB is predicted for a  $27.5\lambda$  diameter paraboloid, with  $F/D = 0.5$

fed by a circularly-polarised primary feed. The reflector is blocked by a small disc of diameter  $0.076 D$ , with a quadripod arrangement of four rectangular struts. The result is somewhat surprising in that for the same configuration with four equivalent cylindrical struts (diameter  $0.274 \lambda$ ) a peak cross-polar level of approximately  $-34$  dB is predicted. No experimental data is available to confirm these predictions but this rather unexpected strong dependence upon the strut cross-section could have important implications and certainly warrants further investigation. However, a feed support strut will only generate cross-polarisation on boresight if it is not aligned parallel or perpendicular to the incident electric field. If the struts are so aligned, or if they are aligned symmetrically (i.e., an equiangular tripod), there will also be no final boresight cross-polarisation.

From Ref.31, measured cross-polar/co-polar isolations are defined in terms of the ratio of cross-polar to co-polar field at a specified level of the co-polar beam. Table 5.1.1B shows some values obtained with a  $38 \lambda$  diameter paraboloid with  $F/D = 0.4$ , fed by a rectangular waveguide horn producing a 19 dB illumination taper. The peak cross-polar levels were measured as  $-23$  dB (in the diagonal planes) and were largely attributed to the primary feed radiation. This conclusion was supported by theoretical predictions and measurements performed on the radiation field of the feed-horn. An improvement in the figures quoted of between 8 and 10 dB could be anticipated employing a low cross-polarisation type feed.

Table 5.1.1B

Cross-polar/co-polar isolation data (measured)

Co-polar beam level (dB)	Isolation ratio (dB)
-3	23.5
-6	20.0
-10	13.0

In Ref.32 a reflector antenna is described with a relatively large degree of aperture blockage (i.e., central disc of diameter  $1 \lambda$  on a  $15 \lambda$  diameter reflector). The peak contribution to the cross-polarised field due to this blockage, including supporting struts, was deduced as approximately  $-40$  dB. Since in general we are concerned here with reflectors

having smaller blocking ratios, it might be concluded that the overall blockage effects will be somewhat less than -40 dB.

The cross-polar response of the axisymmetric Cassegrainian antenna is a function of both the primary-feed type and the geometrical parameters of the sub-reflector. With electrically small hyperbolic sub-reflectors, the diffraction effects can produce significant cross-polarised radiation which is not evident in a front-fed configuration. Figure 5.1-12 illustrates the cross-polarised scattered-field radiated from a  $19 \lambda$  diameter hyperbolic sub-reflector illuminated by an ideal (i.e., cross-polarisation free) primary-feed producing a 9 dB illumination taper on the sub-reflector. The peak cross-polarised component occurs at a level of -35 dB with respect to the boresight value of the co-polarised field. An interesting feature of the scattered field from the sub-reflector is the close proximity of the first cross-polarised lobe to the axis of rotation. Any small misalignment in the axis of the sub-reflector, relative to that of the main reflector will therefore result in a cross-polarised component along the boresight axis of the overall antenna. To avoid this effect, stringent specifications must be imposed upon the alignment tolerances of the two reflectors.

The -35 dB cross-polarisation level shown for the hyperbolic sub-reflector could be improved by either increasing the sub-reflector diameter or by employing an 'ideal' feed for the hyperboloid. Koffman<sup>33</sup> has shown that a cross-polarisation-free field can be obtained from the hyperboloid by introducing a small eccentricity in the radiation characteristics of the primary-feed. This general result could also be achieved by performing a diffraction optimisation of both the main and sub-reflector surfaces.

(v) Mesh losses

It is the custom at lower frequencies to use a metal mesh surface instead of a continuous reflector. The mesh spacing will affect the transmission loss which will affect the forward gain and the backlobe since some feed radiation will be transmitted. Figure 5.1-24 shows this effect<sup>34</sup>. The effect on the backlobe can be calculated approximately as:

$$\text{Back to front ratio} = -\left(G_O + T_M - G_F\right) \text{ dB} \quad (15)$$

where  $G_O$  is the main reflector gain,  $T_M$ , the mesh transmission and  $G_F$  the

feed gain. This will be negligible compared with the diffracted back-lobe if  $T_M$  is much less than  $T$ , the aperture taper. However, if edge shields are used in order to avoid the diffracted backlobe, then back-lobe levels will be around -70 dB and  $T_M$  must be kept low. In practice, this is not likely to be less than 30 dB because of the forward loss which would be implied.

### 5.1.3 Some specific examples of paraboloid reflector performance

Individual sources of performance degradation were discussed in the last section. In this section, specific published examples are discussed. Table 5.1.2 gives data for a variety of reflectors.

Pratt and Claydon<sup>41</sup> calculate the sidelobes expected from a 90 ft Cassegrain earth station at 4 and 6 GHz. The sub-reflector profile was shaped to give nearly uniform illumination over the main reflector when the sub-reflector has an edge taper of -13.5 dB (Ref.38). The main reflector shape was slightly altered from a paraboloid to remove phase errors. This is therefore a shaped dual-reflector system. The following sources of degradation were allowed for:

- diffraction pattern of the main reflector.
- blockage by the sub-reflector. Aperture field subtraction was used.
- blockage by struts, same method as for sub-reflector.
- effect of profile errors of 0.04 in rms; Vu's theory<sup>42</sup> was used.

As each correction was added, agreement with the measured radiation patterns improved. Figure 5.1-13 shows the final near-in patterns both measured and computed, including all the above corrections. Figure 5.1-14 shows the measured radiation pattern over a wider angular range. Between  $6^\circ$  and  $8^\circ$  off boresight, the sidelobes dropped to below -40 dB. One of the reasons for making no predictions over a very wide angular range is the extreme difficulty of measuring low levels of power in a large reflector system. In particular, spurious site reflections are difficult to detect and remove.

Similar patterns are shown by Ravenscroft and Knox<sup>36</sup> for Goonhilly I, though these are not accompanied by any predictions. The sidelobe level

is below -60 dB for angles beyond  $20^\circ$  and below -50 dB beyond  $5^\circ$ . The antenna was intended for use at an elevation angle of only  $5^\circ$ , so that there was great interest in reducing the sidelobes which would otherwise cause an increase in the system noise temperature. The reflector was front fed, and the specific surface tolerances implied considerable mechanical problems. In order to maintain the required performance, a surface accuracy of  $\pm 0.025$  in (0.063 cm) over 99% of the reflector surface was implied. This was considered uneconomic for an antenna of 25 m diameter so the reflector was assembled from accurately profiled panels 4 ft square. The smooth profile gives low levels of wide angle radiation; scattering due to panel misalignment occurs near boresight.

The twist Cassegrain reflector<sup>37</sup> eliminates sub-reflector blockage effects by the use of linear polarisation which is twisted in the main reflector by  $90^\circ$ . The small blockage due to the presence of the feed horn remains however. The sub-reflector is a perfect reflector for parallel polarisation and gives good transmission for orthogonal polarisation. It is to a large degree 'invisible' but in practice some scattering is likely to occur due to the imperfections in the twist reflector components. The principal advantage can be seen in Table 5.1.2 where a Cassegrain twist reflector of diameter 22.9 wavelengths has good far-out sidelobe and cross-polarisation characteristics.

It is difficult to draw any conclusions from the literature on the achieved rms surface errors (Table 5.1.2) except that, if the diameter is small (less than 5 m) achieving surface errors of  $\frac{\lambda}{200}$  is feasible. This limit on the diameter is quite arbitrary as the limit is probably a function of cost rather than present-day limits of manufacturing techniques.

Table 5.1.2  
Characteristics achieved by operational axisymmetric reflectors

Antenna	Type	Basic frequency F/D	Frequency (GHz)	Taper (dB)	First side-lobe (dB)	Sidelobe performance		Back-lobe (dB)	Cross-Pol. (dB)	VSWR	Diameter D/λ	Efficiency %	rms		Ref.
						10°-45°	70°-120°						surface (mm)	error (λ)	
Mojave	Axisymmetric Cassegrain	0.40	4.2	11.8	-20						172	50	0.76	λ/100	1
Rosman II	Front-fed axisymmetric	0.423	4.1	6	-16						364	50	1.02	λ/72	1
130 ft Cassegrain <sup>1</sup>	Cassegrain	0.40	2.1	8	-18						61	52	0.81	λ/176	1
130 ft, Satcom	Cassegrain	0.40	4	14	-16						122	40	0.81	λ/92	1
114 ft Cassegrain <sup>1</sup>	Cassegrain	0.469	2.3	9	-17						32	50	-	-	1
Lincoln Lab.	Prime focus	0.440	35		-24					<1.3	1000	53	0.03	λ/200	35
Goonhilly I 85 ft	Prime focus		4.16	11	-26	-50	-60	-70			354	56	0.3	λ/240	36
Twist Cassegrain	Cassegrain		10		-28	<-30	<-45	<-50	<-38		22.9	60	-	-	37
Goonhilly II	Dual shaped reflector	0.344	4		-16	<-50		-60E	AR=0.5 due to feed	<1.15	45.4	65	1.016	λ/74	38
Texas Univ. 16 ft	Prime focus	0.8E	35	10	-23						574	59	0.076	λ/112	39
Dwingeloo 25 m	Prime focus	0.48	70.9	10	-18						1148	52	0.076	λ/56	23
Cassegrain	Beam waveguide feed		4		-14.5	<-35		<-70E	AR=1.24	<1.13	427	73	-	-	40
Cassegrain	Shaped		4	Uni-form		<-55	-65	-70			394	60E	-	-	24
RCA	Cassegrain	0.3	4/6	7	-19	<-25	<-26*	-44	-39		135	70	0.25	λ/200	45

\*A spillover lobe at 96° from boresight. E = estimated.

#### 5.1.4 Graphical data and comments on some factors affecting axisymmetric reflector sidelobe performance

##### Aperture illumination

Figure 5.1-15 shows the first sidelobe levels predicted for a parabola-on-a-pedestal distribution, calculated by Hansen<sup>4</sup> in the absence of blocking effects. The optimum values of  $n$  and the pedestal have been chosen for each value of the sidelobe level. Since blocking effects will dominate the first sidelobe levels for axisymmetric antennas, this curve cannot be used for accurate design predictions for low sidelobe applications. In addition, the accuracy of the assumed distribution in representing the actual aperture fields of a parabolic reflector antenna is not sufficient to provide any more than an indication of the general trends involved.

In Fig.5.1-16 the space-attenuation introduced by the variation in path-lengths from the focus to points on the parabolic reflector is given in decibels. In Fig.5.1-17 the generalised radiation characteristics of two primary feed types are shown. The normalised parameter 'u' is given by  $\pi d \sin \theta^* / \lambda$  where  $d$  is the diameter of the primary feed and  $\theta^*$  is the semi-angle subtended by the rim of the reflector. A value of  $20 \log_{10} \left( \frac{1 + \cos \theta^*}{2} \right)$  must be added to the taper value obtained from the graph to determine the relative level of the feed radiation in the direction of the reflector rim.

For total illumination tapers of less than 10 dB, the values obtained from Figs.5.1-16 and 5.1-17 can be employed in conjunction with Fig.5.1-15 to determine approximately the first diffraction sidelobes levels in the absence of blocking. It must be noted, however, that this process becomes increasingly unreliable as the illumination taper is increased. The near-in diffraction sidelobes are dependent upon the shape of the illumination function and not merely the edge value. This factor becomes increasingly important as the illumination taper is increased. The approximate dimensions of the primary feed aperture necessary to feed reflectors of various F/D ratios is illustrated in Fig.5.1-18. (The hybrid mode feed of Fig.5.1-17 has been assumed).

##### Backlobe radiation

Some estimation of the backlobe radiation which can be anticipated from a paraboloidal reflector antenna, without rim shields or castellations, can be obtained by use of Table 5.1.3, Fig.5.1-19 and the approximate formula for backlobe radiation:

$$\text{Front to back ratio} = G + T + K - G_F \text{ dB} \quad (16)$$

where  $G$  is the reflector gain,  $T$  is the edge taper,  $K$  is a factor dependent on  $F/D$  and  $G_F$  is the feed gain.

It can be seen from Fig.5.1-19b that the antenna efficiency is a relatively unimportant parameter in this calculation for most practical cases, and thus relatively crude estimations of the antenna overall efficiency will still allow an approximate value to be obtained for the backlobe radiation level.

Table 5.1.3

Feed gain as a function of  $F/D$

First sidelobe level (dB)		-30	-40
Reflector edge taper (dB)		11	18
$F/D = 1$	$G_F$ (dB) =	9.7	11.8
0.75	=	8.4	8.5
0.5	=	5.0	8.7

$G$ , the gain of the reflector, is given in Fig.5.1-19b for two values of aperture efficiency.

From this may be calculated the minimum reflector diameter in wavelengths (efficiency = 60%) which will give a specified backlobe performance at any given  $F/D$  (see Table 5.1.4 for values corresponding to a backlobe of -50 dB).

Table 5.1.4

Diameters of axisymmetric reflector antennas providing a backlobe of -50 dB

Parameter	Case 1	Case 2
Reflector illumination taper (dB)	11	18
Minimum $\frac{D_0}{\lambda}$ for $F/D = 0.5$	94	54
= 0.75	94	54
= 1.0	134	75
First diffraction sidelobe level in the absence of blocking (dB)	-30	-40

### Spillover lobe

This may be calculated from:

$$G + T - G_F - 6 \quad \text{dB} \quad (17)$$

Data for the backlobe calculations can be used.

### Choice of primary-feed horn

The choice of primary-feed horn for any specific application is likely to be dominated by the overall requirements of the antenna system. In this sense there is no clear-cut 'optimum' feed configuration for all applications. For good overall sidelobe suppression, however, it is desirable that the wide-angle radiation of the primary feed itself be well-suppressed. This requirement becomes more important in applications where the diameter of the main reflector is not large (in terms of wavelengths), but can still be relevant for very large antennas when very low sidelobe radiation levels are specified. In this respect, the waveguide-horn feed has definite advantages, particularly those types which provide good axisymmetrical radiation characteristics with low far-out radiation levels. The cylindrical corrugated horn, the dual-mode horn and the choked conical horn are examples of such primary feed antennas. These antennas can also be designed to provide a variety of illumination tapers with a wide range of reflector F/D ratios.

In designing a low sidelobe antenna based upon an axisymmetric paraboloid configuration, there is little point in attempting to achieve very severe illumination tapers, since the blockage effects will govern the near-in sidelobe level. For an optimum design, the trade off between the antenna gain and the sidelobe performance is best performed by use of a suitable computer program which includes blocking effects. In most cases it will be found that illumination tapers of more than 18 dB provide worse efficiency with no near-in sidelobe improvement. In many cases the optimum value of illumination taper may be much closer to 10 dB.

The case for more severe illumination tapers could be made when good backlobe performance is mandatory. The antenna backlobe performance is a function of the edge excitation and the diameter of the paraboloid. For example, Table 5.1.4 shows the minimum reflector diameter in wavelengths

which will provide a backlobe of -50 dB with the two edge illuminations shown. A constant antenna efficiency of 60% has been assumed in this tabulation which will not be correct in view of the variation in illumination tapers and F/D ratios indicated. In fact, the Case 1 Antennas will provide higher efficiencies than their Case 2 counterparts. However, in terms of the backlobe radiation level the variation in antenna efficiency, which is unlikely to exceed  $\pm 1$  dB, can be neglected in the comparison.

After blocking effects are accounted for, the two cases shown in Table 5.1.4 are likely to provide similar values of near-in sidelobe levels. The far-out sidelobe levels will be dependent upon the reflector F/D ratio, the primary-feed sidelobe envelope and the nature of the blocking. The backlobe radiation will be better for the lower efficiency (18 dB taper) Case 2 examples, but this order of performance could be obtained from the more efficient Case 1 antennas by use of a rim shield or by rim castellations.

#### Central blockage

To provide some guidance to the effects of central blockage upon the near-in sidelobe performance of an axisymmetric reflector, Fig.5.1-18 shows the approximate blockage diameter of primary-feed horns required to feed reflectors with various F/D ratios. In Fig.5.1-20a the level of the first sidelobes are indicated as a function of the blockage ratio  $D_S/D_O$ , where  $D_S$  is the diameter of the blockage region and  $D_O$  the main reflector diameter. Four parabola-on-a-pedestal illumination distributions are shown, ranging from zero taper (i.e. uniform illumination) to an 18 dB taper, which would generate diffraction sidelobes at the -40 dB level in the absence of blocking. Note that strut blockage will modify these results and is not accounted for here. Figure 5.1-20b shows the approximate loss in forward gain arising from three parabola-on-a-pedestal distributions. In Fig.5.1-20c the loss of gain resulting from the blockage is expressed in terms of its effect on the aperture efficiency,  $\eta_A$ .

The effects of strut blockage can only be estimated when the strut disposition is known. The difficulty of predicting strut blocking and scattering effects has been commented on previously in this report. Gain reduction and, to some extent, near-in sidelobe effects can be calculated with reasonable accuracy by use of shadow diffraction techniques, but wide-angle strut scattering is more difficult to deal with. The data shown in Table 5.1.5 may be helpful in providing some indication of the general

Table 5.1,5

Details of far-out scattered radiation due to struts (taken from Ref.26)

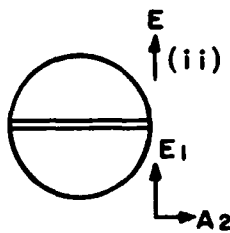
Primary reflector diameter 84 wavelengths at 9.2 GHz

$F/D = 0.25$  half power beamwidth is approximately  $0.9^\circ$

$w$  = strut width in aperture plane

$d$  = depth of strut

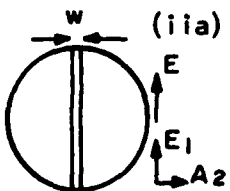
(i) Sub-reflector only - supported by piano wires which are assumed to have no effect on the radiation pattern. The radiation pattern is below  $-40$  dB outside of a radius of  $10^\circ$ .



(ii) Spars in the aperture (i.e. in the aperture plane). One diametric spar placed perpendicular to the incident polarisation.

$w = 0.77 \lambda \quad d = 2 \lambda$

Result: A long ridge in elevation worse than  $-40$  dB out to  $\pm 40^\circ$ .

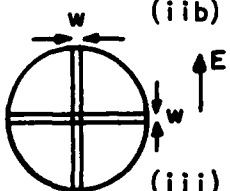


(iia) One diametric spar parallel to incident polarisation.

$d = 2 \lambda$

Result: Long ridge  $-40$  dB out to  $\pm 54^\circ$  in azimuth for

$w = 0.286, 0.5, 1 \lambda$



(iib) Two crossed spars

$w = 0.38 \lambda \quad d = 1.53 \lambda$

Result: Crossed ridges plus 3 concentric circles at radii  $20^\circ, 30^\circ, 40^\circ$ . All worse than  $-40$  dB.

(iii) Spars inside aperture i.e. apex beyond aperture plane; feet internal to edge. 4 spars, i.e., Quadripod

$w = 0.38 \lambda \quad d = 1.53 \lambda$

(measured at right angles to spar).

Result: Widespread degradation: Pattern is worse than  $-40$  dB within a circle of radius  $25^\circ$ .

(iv) Spars outside the aperture, i.e., feet on edge of reflector apex beyond aperture plane

$w = 0.38 \lambda \quad d = 1.153$

Result: Crossed ridges of radiation worse than  $-40$  dB. These ridges all bifurcated.

(v) Diagonal spars produce diagonal ridges.

(vi) Tripods produce circles crossing on boresight.

RMS phase errors

The graphs of gain loss (Fig.5.1-21a) and sidelobe degradation (Fig.5.1-21b) are for rms phase error in the aperture field. The curves are obtained

with the assumption of random phase errors with a small correlation interval. The translation of this into surface tolerances can be performed by dividing by 2 if the F/D ratio is large. If F/D is less than 0.8, then a correction factor P must be applied. In Fig.5.1-21c the correction factor P is given as a function of F/D for an illumination of the cosine form. The true mean square phase error is given by  $P \times 4\pi \delta/\lambda$  where  $\delta$  is the rms surface error.

### Feed lateral displacements

To determine the sensitivity of the antenna sidelobe performance to small misalignments of the primary feed, data has been provided to illustrate the effect of small lateral feed-shifts. This data is derived from scalar theory and is approximate. However it does serve to provide some indication of the general trends.

In order to provide some general curves, the sidelobe degradation and forward gain loss are plotted as a function of:

$$X = n \frac{\left(\frac{D}{F}\right)^2}{1 + 0.02\left(\frac{D}{F}\right)^2} \quad (18)$$

where n is the number of half power beamwidths scanned off axis. This can be re-arranged to give:

$$X = \frac{F}{D} nQ = \frac{B}{A} \cdot \frac{d}{\lambda} \cdot Q \quad (19)$$

where

$$Q = \frac{\left(\frac{D}{F}\right)}{\left[\left(\frac{F}{D}\right)^2 + 0.02\right]} \quad (20)$$

B is the beam deviation factor and A is the beamwidth factor, i.e., the ratio of the half power beamwidth for the chosen aperture distribution to that with uniform illumination.  $\frac{d}{\lambda}$  is the lateral shift in wavelengths.

Figure 5.1-22a shows Q as a function of F/D. Figure 5.1-22b shows B as a function of F/D. Table 5.1.6 tabulates A and Fig.5.1-22c and Fig.5.1-22d give the sidelobe degradation and loss in forward gain.

Table 5.1.6

For an antenna radiation pattern having the form of a modified  $J_1(u)/u$  function (which is close to that resulting from a parabola-on-a-pedestal distribution)

Design near-in peak sidelobe level	A
-17.85 dB (uniform)	1
-20	1.0483
-25	1.1408
-30	1.2252
-35	1.3025
-40	1.3741

Figure 5.1-22e shows the coma lobe degradation as a function of F/D for two lateral shifts,  $0.5 \lambda$  and  $0.25 \lambda$ . The illumination is  $(1 - (\frac{r}{a})^2)^2$  which provides a zero field at the reflector edge and a first sidelobe of -30 dB. However, the diagram shows clearly that higher F/D ratios are much less sensitive to lateral feed displacements. Note that the gain loss is very small at these levels (Fig.5.1-22d).

Feed axial displacements

The effect of axial displacements of the primary-feed, in an axisymmetric reflector system, is essentially to defocus the far-field radiation pattern of the antenna at infinity. This defocusing will result in a loss of antenna gain. With regard to sidelobe performance, axial defocusing will result in an increase in the near-in sidelobe levels, but small defocusing will not significantly impair the wide-angle radiation for most systems. In Fig.5.1-23a the gain loss ( $\delta G$ ) due to an axial feed shift from the focus of  $\delta$  wavelengths is shown as a function F/D for two aperture-illumination distributions.

The sidelobe levels, as a function of the axial shift  $\delta$  are shown in Fig.5.1-23b. Three values of F/D ratio are shown with a parabola-on-a-pedestal illumination distribution giving a -10 dB taper. This illumination would provide a -22 dB first sidelobe level in the absence of blocking.

Again it must be emphasised that these curves are approximate and should only be interpreted in terms of general trends rather than specific values.

### Cross polarisation

Cross-polarised field components arising from the curvature of axisymmetric parabolic reflectors are themselves very low, i.e., less than -45 dB and the most important effects are those due to the cross-polarised radiation from the primary-feed and aperture blockage by the feed and support struts. The choice of feed is governed by the reflector F/D. However, primary-feed antennas which provide good cross-polarised feed suppression can be designed for both small and large F/D ratios. For the linear polarisation, the peak cross-polarised radiation from both the primary-feed and the overall antenna will normally occur in the diagonal planes (relative to the polarisation vector) and will usually occur at angles corresponding (approximately) to the -12 to -20 dB contour of the main co-polarised beam. The primary-feed contribution to this radiation can be suppressed to below -40 dB with good design practice. However, it must be emphasised that the suppression which can be achieved may be dependent upon other constraints imposed by the design. A small linearly-polarised rectangular horn, operating in its fundamental-mode, and designed to feed a paraboloid of small F/D ratio (i.e., F/D less than 0.5) can produce a peak cross-polar field in the diagonal plane of the overall antenna far-field, which is of the order of -20 dB. The rectangular horn cross-polarisation reduces as the horn dimensions increase, hence the feed is more suitable for larger F/D ratios in this respect. The cross-polar suppression of conical fundamental-mode horns, however, tends to improve with decreasing diameter. This is not the time or place to enter into a detailed discussion of primary-feed design. Let it suffice to say that, in principle, feeds with good cross-polar properties can be designed for both small and large F/D reflectors, within the limitations set by the other aspects of the antenna design.

With circularly-polarised antennas, the primary-feed cross-polar radiation is distributed in all planes and a 'diagonal plane' has no meaning for this case. The more uniform distribution of the cross-polarised energy for this case tends to reduce the peak levels by averaging the energy over all planes. Strut blockage and scattering effects are particularly difficult to avoid in this case, since no optimum orientation of the struts, relative to the polarisation vector, is evident.

For Cassegrainian configurations, diffraction from the sub-reflector will be an additional source of cross-polarised radiation. These effects can be minimised with good design practice. In general terms, small sub-reflectors (in terms of wavelengths) are undesirable in this respect.

#### Mesh transmission losses

These may be important for low frequency reflectors where mesh surfaces are commonly used, since the backlobe may be dominated by the spurious feed radiation transmitted through the reflector. The front to back ratio will be:

$$G - G_F + T \quad \text{dB} \quad (21)$$

where  $G$  is the gain of the main reflector,  $G_F$  is the feed gain and  $T$  is the transmission loss. Figure 5.1-24 shows  $T$ , and the associated loss on reflection,  $R$ , as a function of the wire spacing in wavelengths.

#### 5.1.5 Axisymmetric reflectors: Conclusions

The principal limitations on the sidelobe performance of axisymmetric reflector antennas arise as a consequence of aperture blocking and scattering effects. When all other, less fundamental, factors are allowed for, aperture blocking is largely responsible for the increase in near-in sidelobe levels above those predicted by simple aperture illumination techniques. Scattering from primary-feeds and their supporting struts are major contributors to the wider angle spurious radiation from the antenna. The minimisation of blocking, by use of very thin struts, for example, and the optimisation of the blocking geometry could lead to significant reductions in the sidelobe levels commonly realised with practical antennas. However, the presence of some level of blockage is an inherent *feature of all axisymmetric reflector configurations* and this will always serve to limit the sidelobe-suppression potential of this class of antennas.

Axisymmetric antennas of the twist reflector Cassegrain type do offer the means of avoiding sub-reflector and strut blockage, although a small central blockage and scatter from the primary-feed hardware itself will remain. These antennas offer, in theory, the lowest sidelobe performance available for axisymmetric systems but there is a severe limitation, in

that twist reflector designs are limited to one hand of linear polarisation. In addition, considerable attention must be given to the construction of the twist reflectors if additional scattering effects are not to be introduced by these components.

In Table 5.1.7 below, the projected performance of two axisymmetric antennas is shown. It is assumed that low near-in sidelobes are an objective and thus the antennas have been given a relatively large illumination taper. The tabulation has then attempted to identify the contributions to the overall sidelobe and backlobe radiation. It must be emphasised that, although the comparison made is between a small diameter prime-focus reflector and a larger diameter Cassegrain, the results are not intended to illustrate that the Cassegrainian is superior to the prime-focus configuration. The differences between the two sets of results principally reflect the differences in diameter, although some aspects of the Cassegrain performance are advantageous. It must also be noted that these results are projected, and although some supporting evidence for the prime-focus antenna could be inferred from results obtained from somewhat larger reflectors (i.e., 40 wavelengths diameter rather than 10 wavelengths) there is no known supporting evidence for the Cassegrain result. It appears that most of the Cassegrain antennas which have been reported in the literature were designed for high antenna efficiencies rather than low sidelobe performance.

Table 5.1.7

Projected sidelobe levels of axisymmetric reflectors intended for low sidelobe performance

	Aperture diameter = $10 \lambda$	
	$10 \lambda$	$100 \lambda$
Antenna type	Prime focus	Cassegrain
F/D	0.4	>1.0
Feed type	Choked horn	Corrugated horn
Illumination taper (dB)	-18	-18
Aperture efficiency (%)	60	60
Theoretical gain for the above efficiency (dB)	25.8	45.8
Half-power beamwidth (degrees)	8.1	0.81
Backlobe (dB)	-33	-46
First diffraction sidelobe (dB) (in the absence of blocking)	-40	-40
Degradation in first sidelobe (dB) due to		
(a) a lateral feedshift of $0.25 \lambda$	-36	No effect
(b) an axial feedshift of $0.25 \lambda$	-39	No effect
(c) to central blockage (strut dependent)	-25 to -32	-34
(d) of $\lambda/64$ rms surface-errors	-37	-37
Strut blockage effect on far-out sidelobes (dB)	-40	-50
Peak cross-polarisation (dB)	-35	-35
Estimated final level of first sidelobe (dB)*	-22.5 to -28.5	-32
Level of direct spillover past reflector	-27	-40

\*for frequencies below 30 GHz.

Total losses for both antenna types amount to about 1 dB.

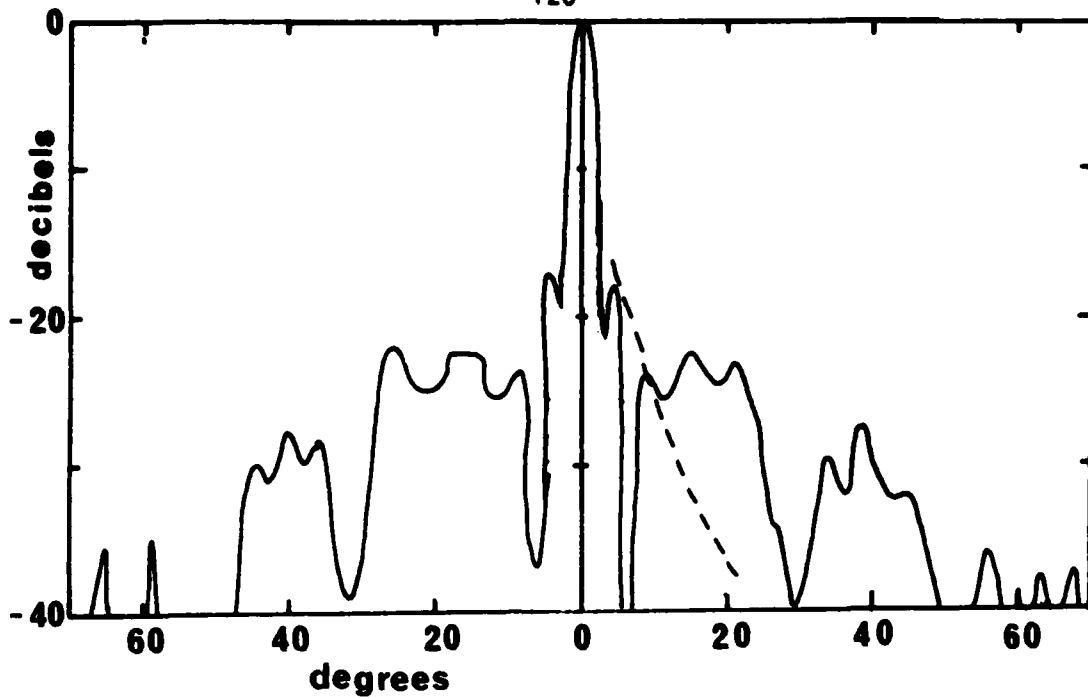


Fig.5.1-1: Radiation pattern of a 32 wavelength Cassegrain at 2.27 GHz. Illumination taper is -8 dB. Dashed line is the envelope of the sidelobes for an ideal circular aperture with the same half-power beamwidth.

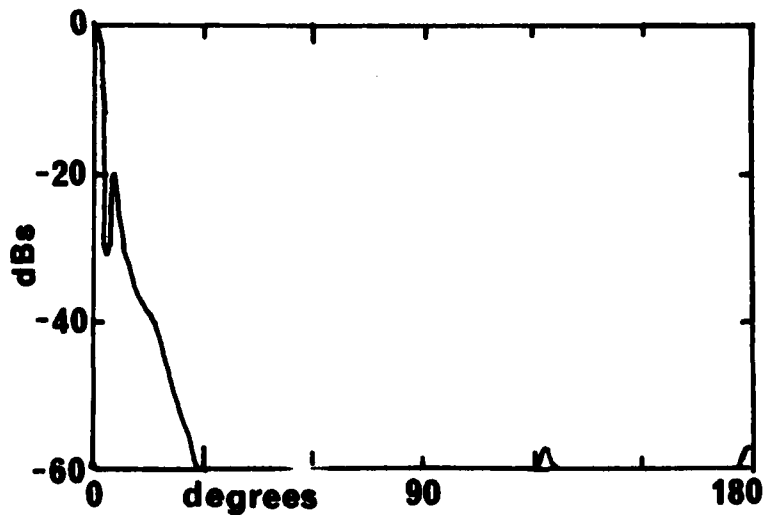


Fig.5.1-2: Radiation pattern of a 60 wavelength axisymmetric reflector with a multi-ring coaxial feed at the prime focus.

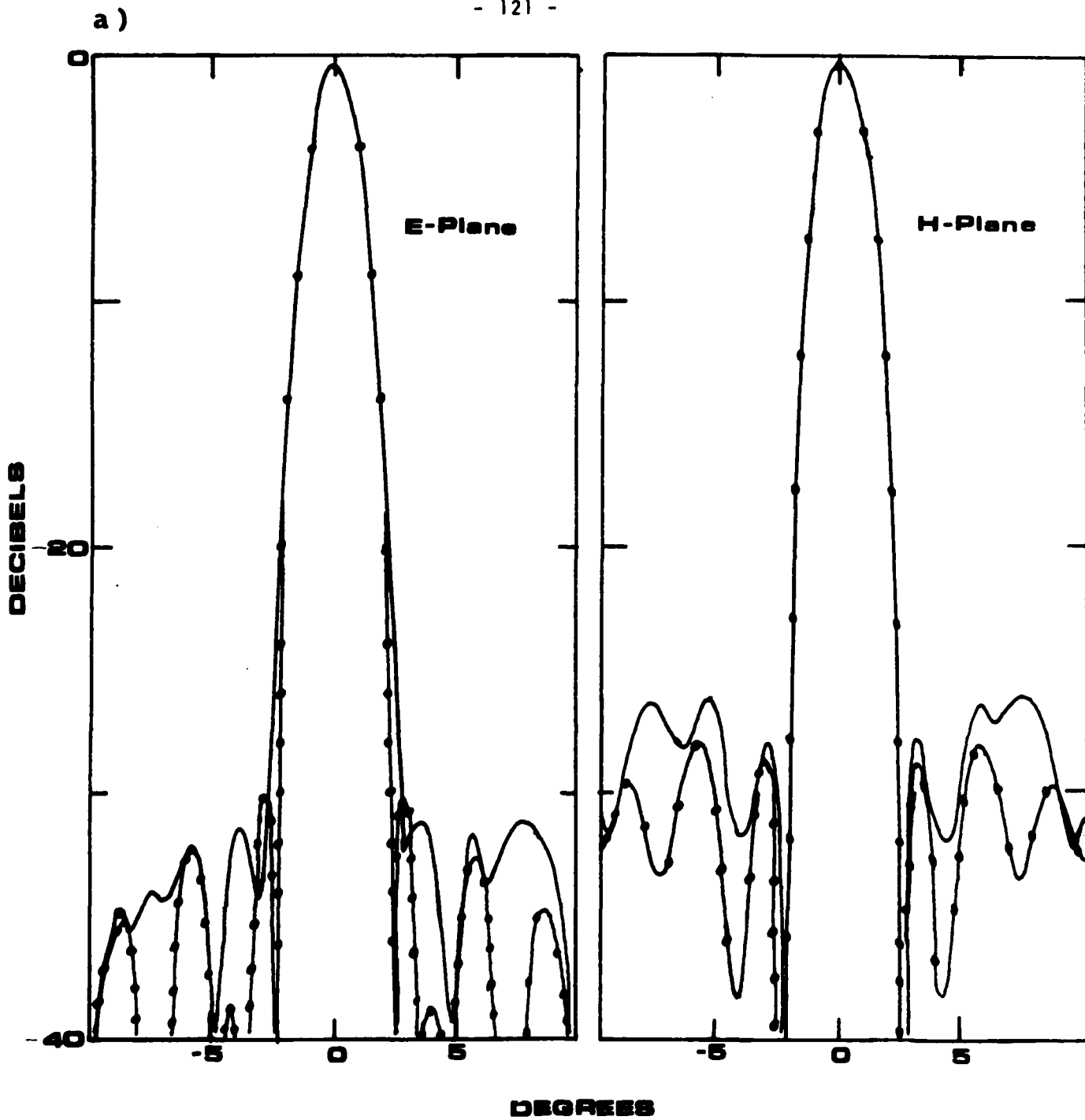


Fig.5.1-3a: Radiation patterns of a 40 wavelength axisymmetric reflector at 30 GHz with a single strut supporting the feed. The feed is a rectangular smooth-walled waveguide horn giving -19 dB edge illumination.

Measured ——— predicted —●— by tangential aperture field method.

(a) Co-polar radiation patterns.

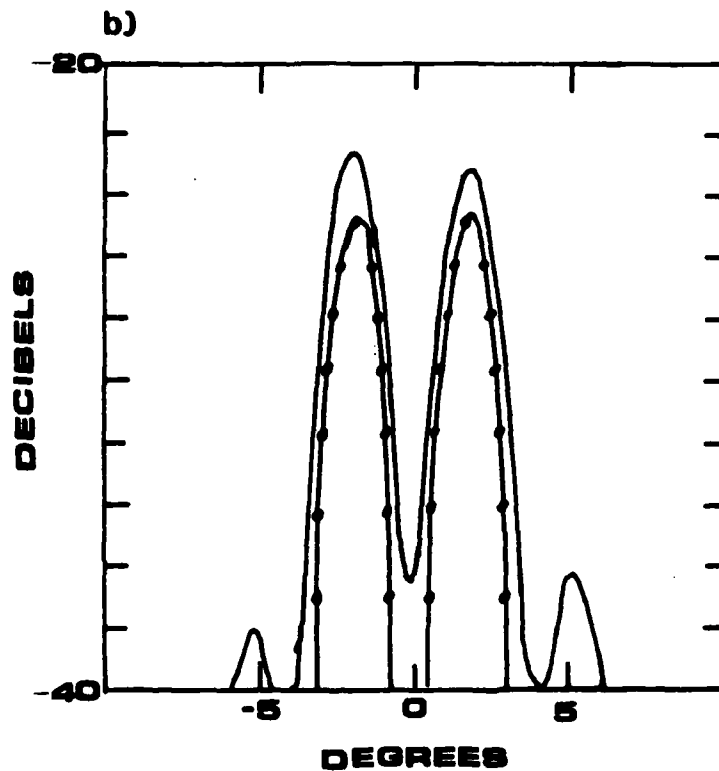


Fig.5.1-3b: Radiation patterns of a 40 wavelength axisymmetric reflector at 30 GHz with a single strut supporting the feed. The feed is a rectangular smooth-walled waveguide horn giving -19 dB edge illumination.

Measured ——— predicted ———○——— by tangential aperture field method.

(b) Cross-polar radiation patterns in the diagonal plane.

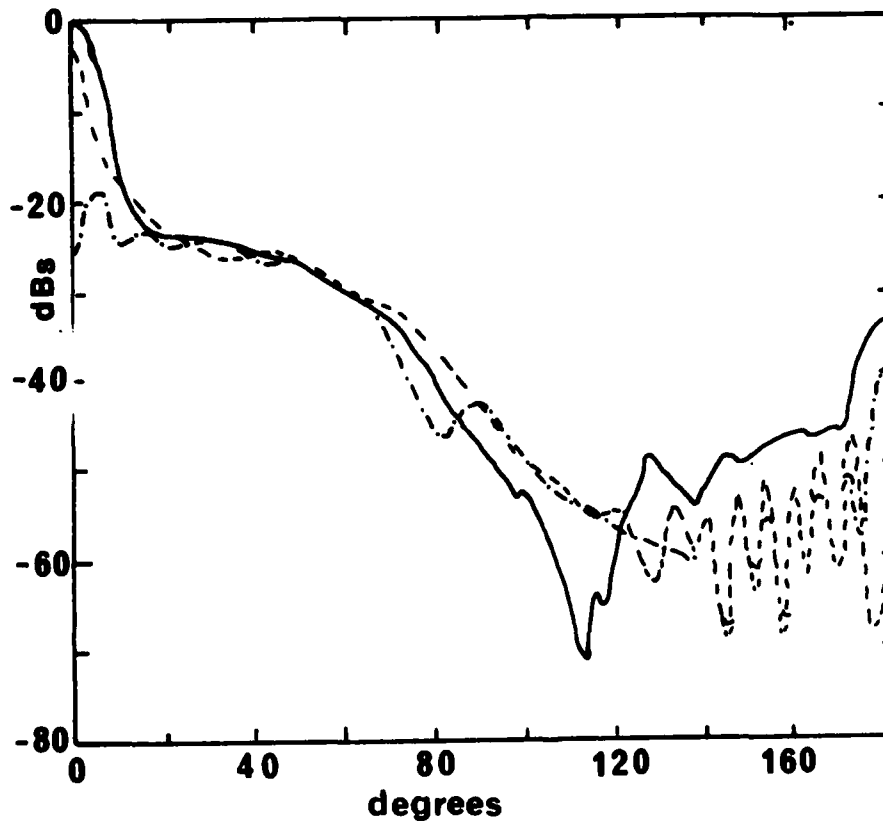


Fig.5.1-4: Comparison of E plane radiation patterns for a 10 wavelength reflector with a dipole at the prime focus. (Ref.10).

———— Physical Optics    --- Measured    -.- Equivalent Current

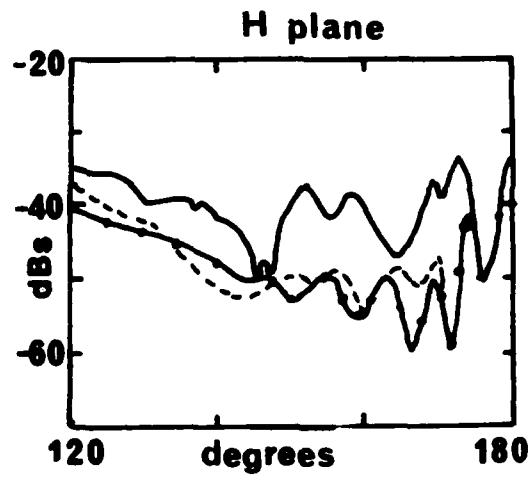
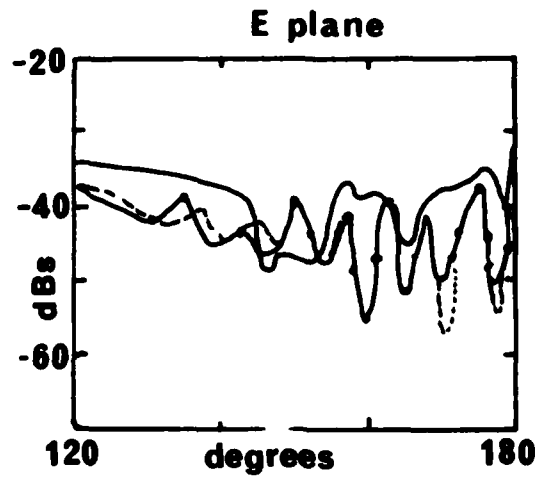


Fig.5.1-5: Comparison of E and H plane shadow radiation patterns for a 10 wavelength reflector with a horn feed at the prime focus.

———— Physical Optics    —○— Measured    --- Edge  
Diffraction

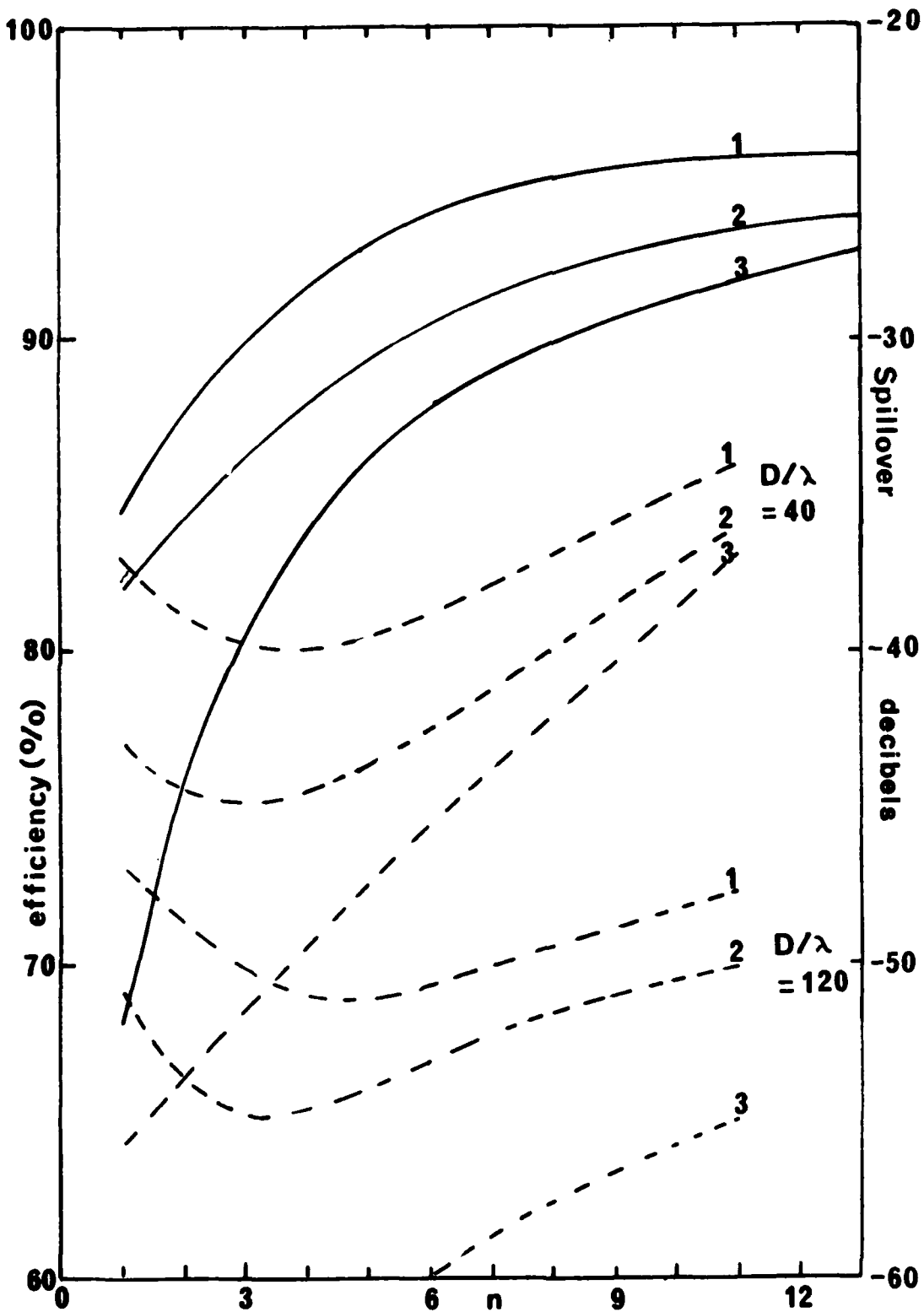


Fig.5.1-6: Aperture efficiency (solid curves) and spillover lobe (dashed curves) for a reflector with aperture illumination  $1 - A(r/a)^n$ . The variable is  $n$ . Three values of  $A$  are shown (1) 0.7; (2) 0.85; (3) 1.0. The spillover lobe is shown for two different aperture diameters,  $D/\lambda$ .

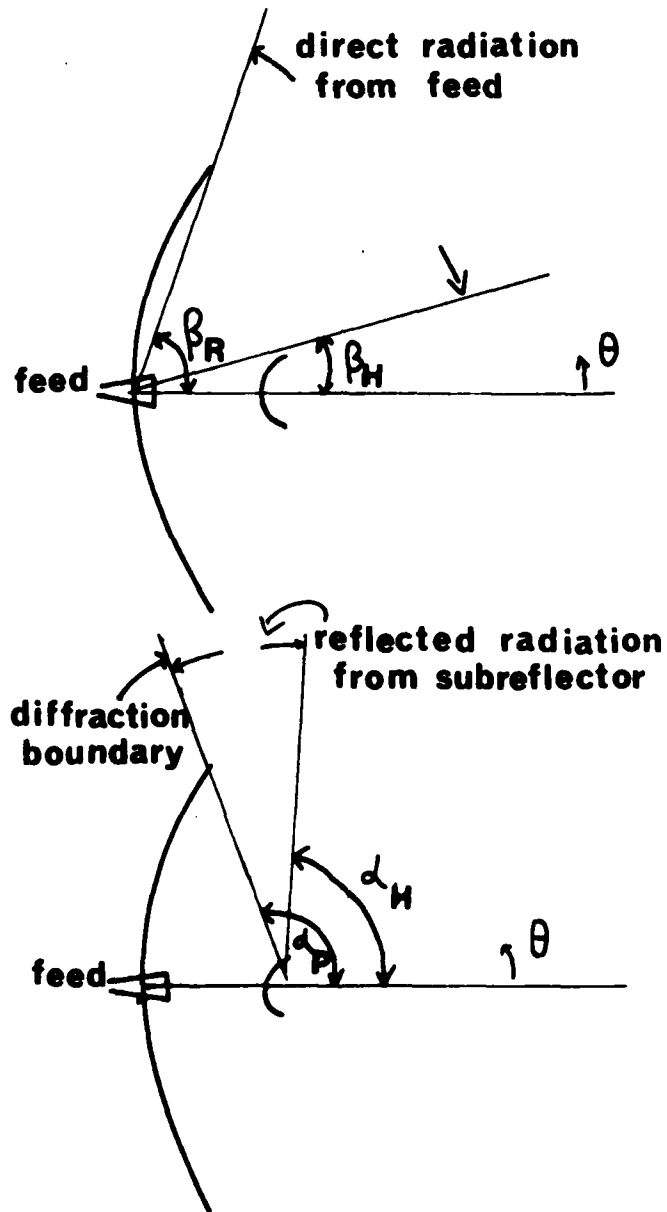


Fig.5.1-7: Sources of extraneous radiation in a Cassegrain reflector.

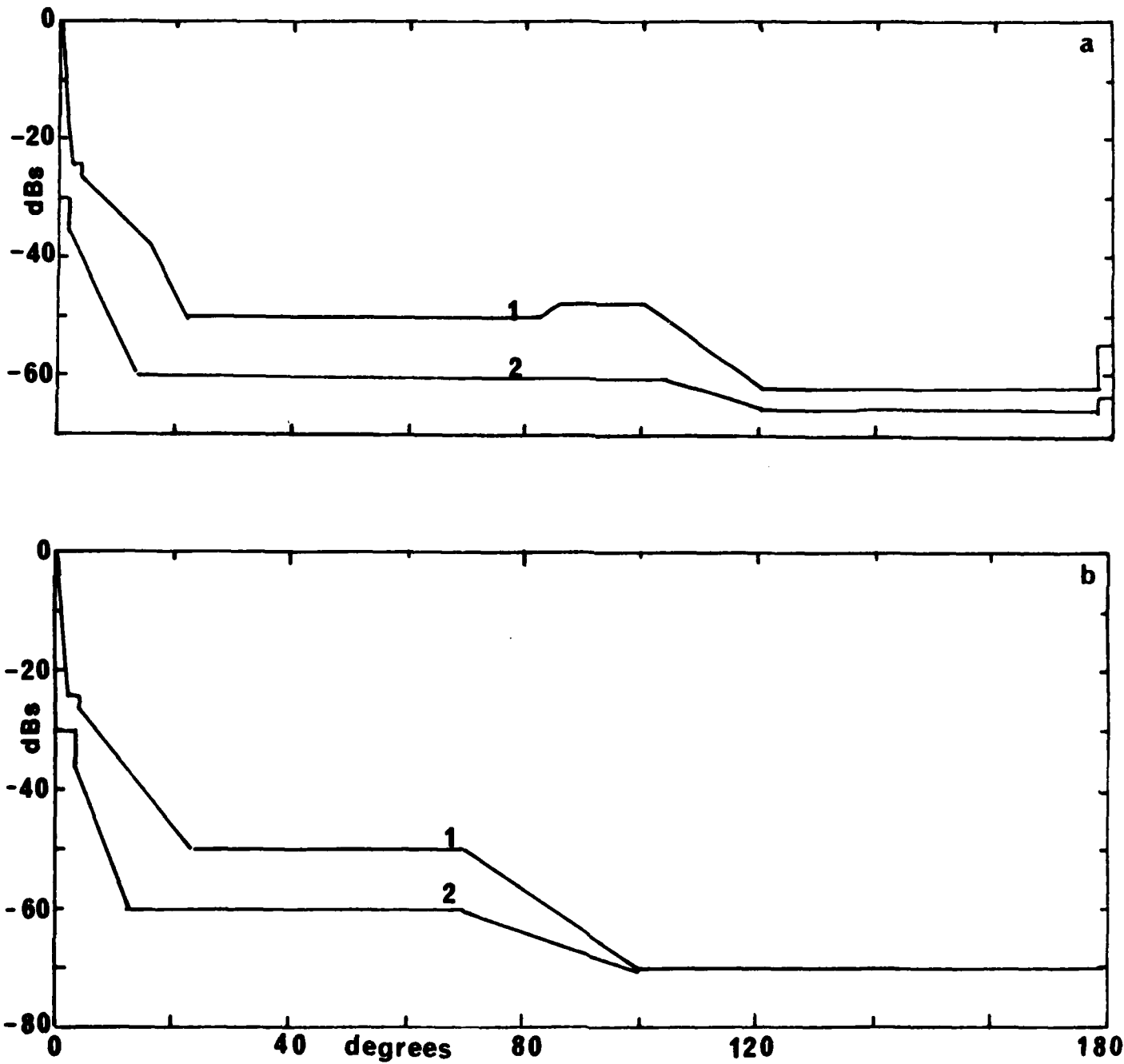


Fig.5.1-8a: Radiation patterns of a 12 ft diameter prime-focus reflector in the range 10.7 to 11.7 GHz. 1 is principal polarisation. 2 is cross-polarisation.

b: The same with a rim shield.

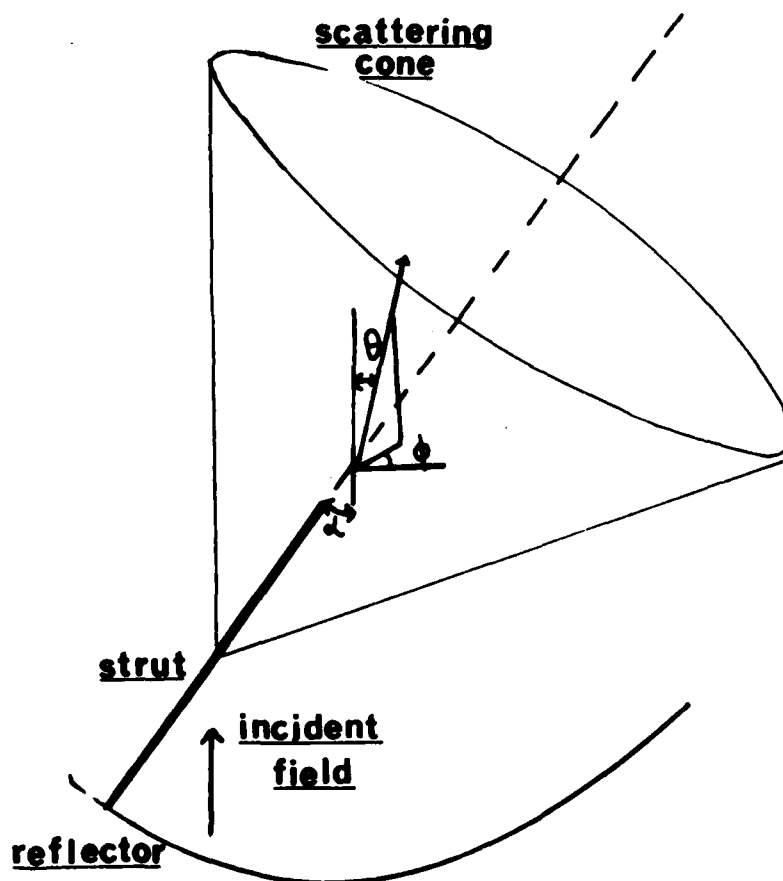


Fig.5.1-9: Scattering by a strut.

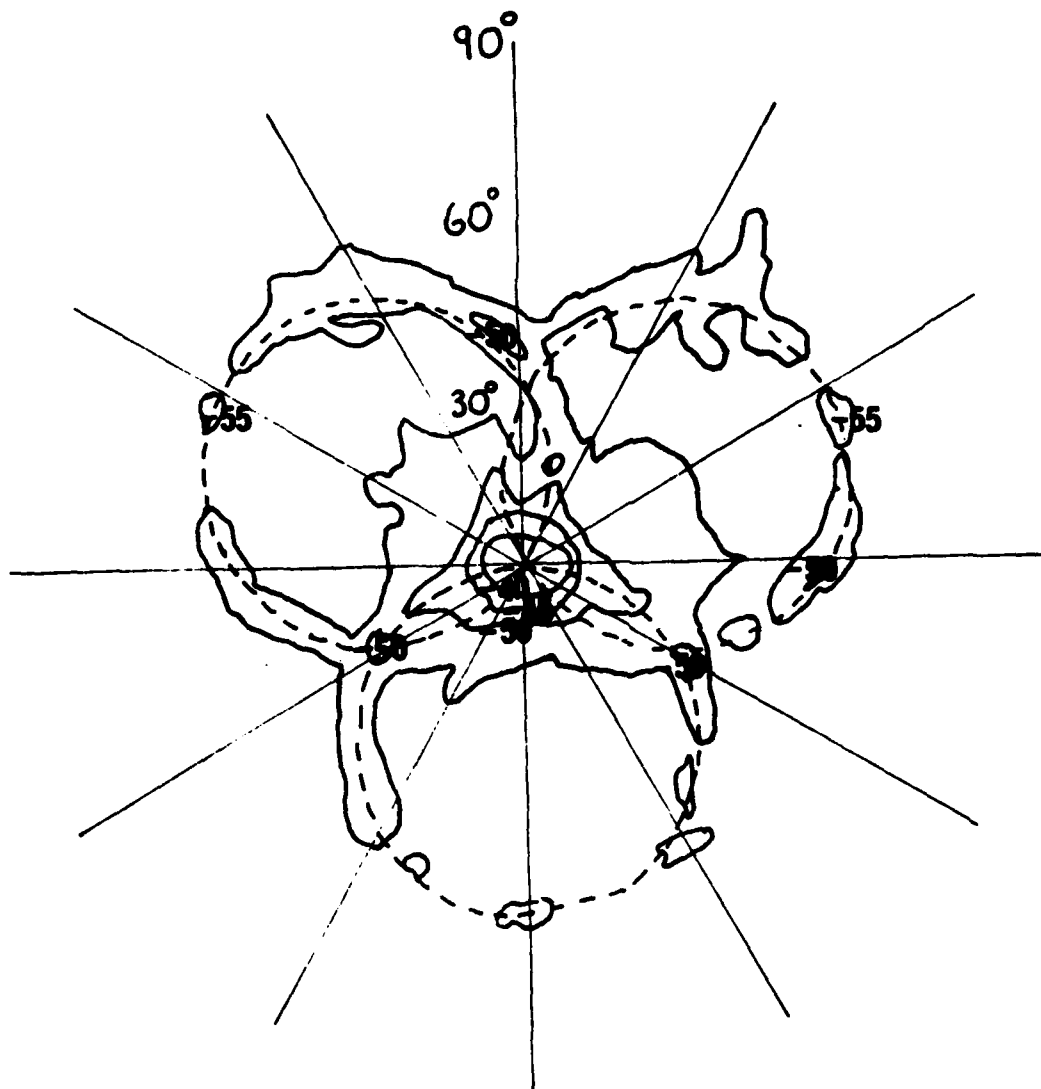


Fig. 5.1-10: Radiation pattern plot for the Dwingeloo 25 m radio-telescope at 1.415 GHz. The dashed circles show the expected positions for strut blockage sidelobes. Contours are in dB. Those not marked are -60 dB.

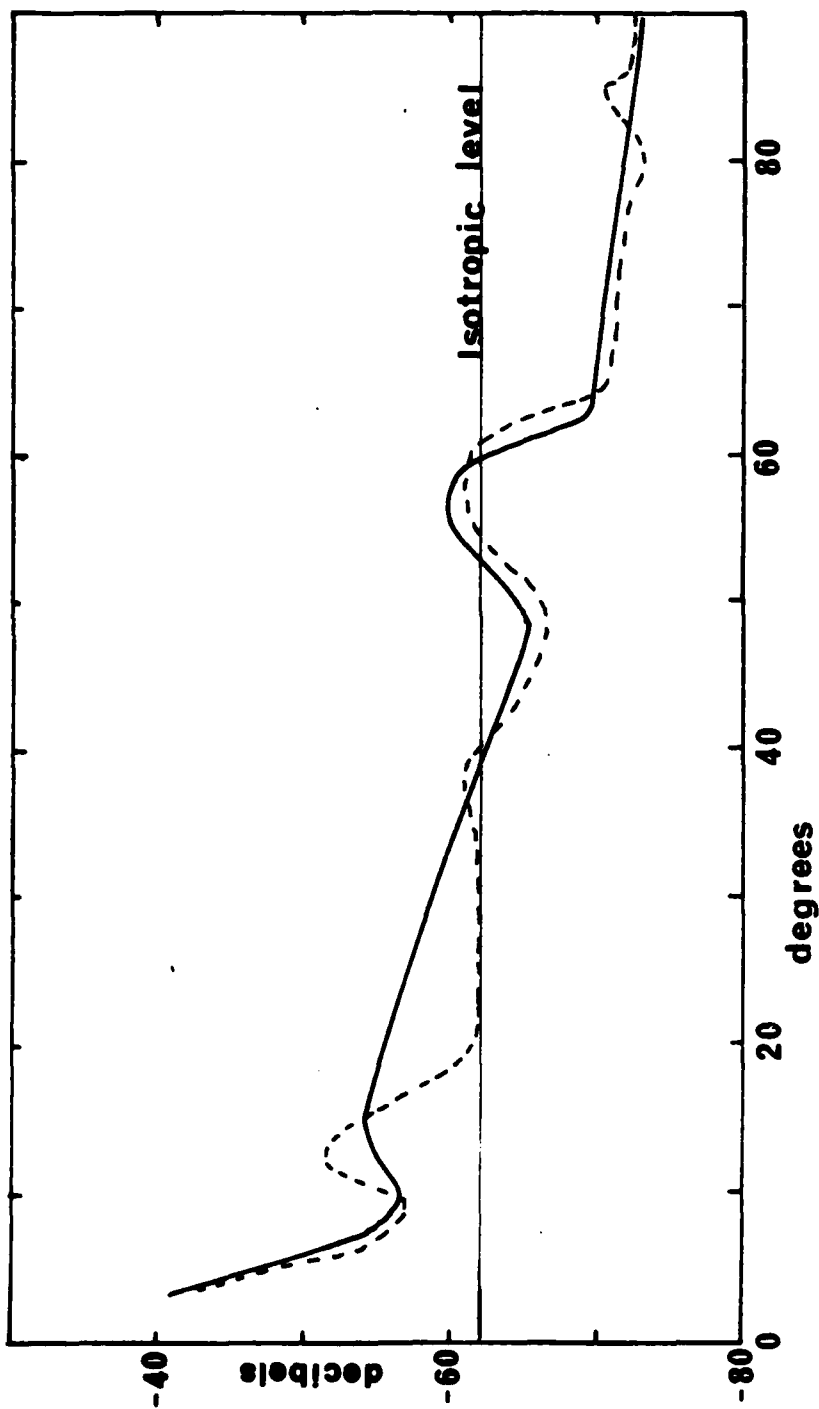


Fig. 5.1-11: Calculated (solid) and measured (dashed curve) radiation pattern envelope for a 394 wavelength diameter Cassegrain. Sub-reflector diameter is 39.4 wavelengths; four struts at an angle of 54 degrees.

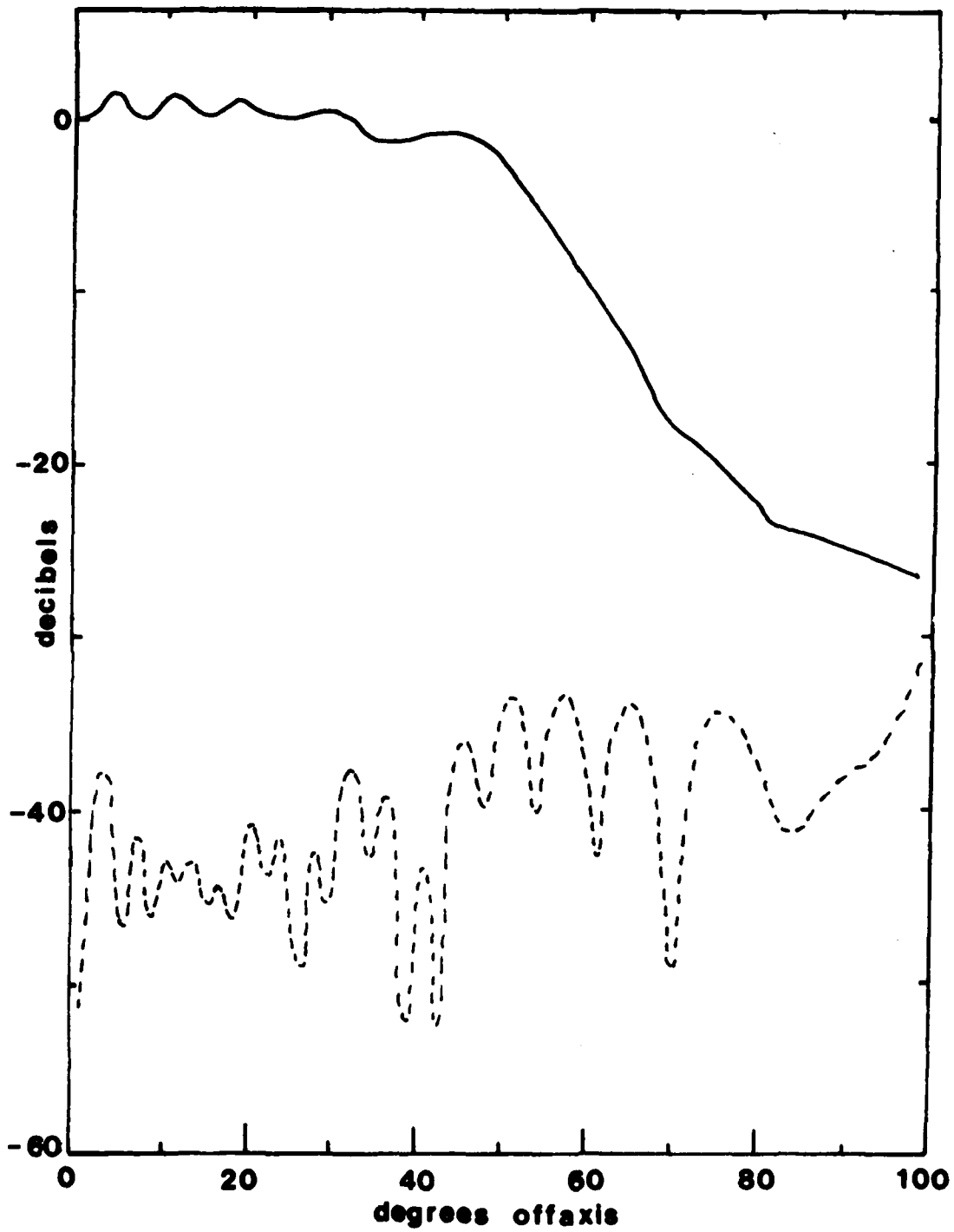


Fig.5.1-12: The cross-polarised scattered field from a 16 wavelength hyperbolic sub-reflector illuminated by a Huygens type source. Dashed line is cross-polar. Full line co-polar.

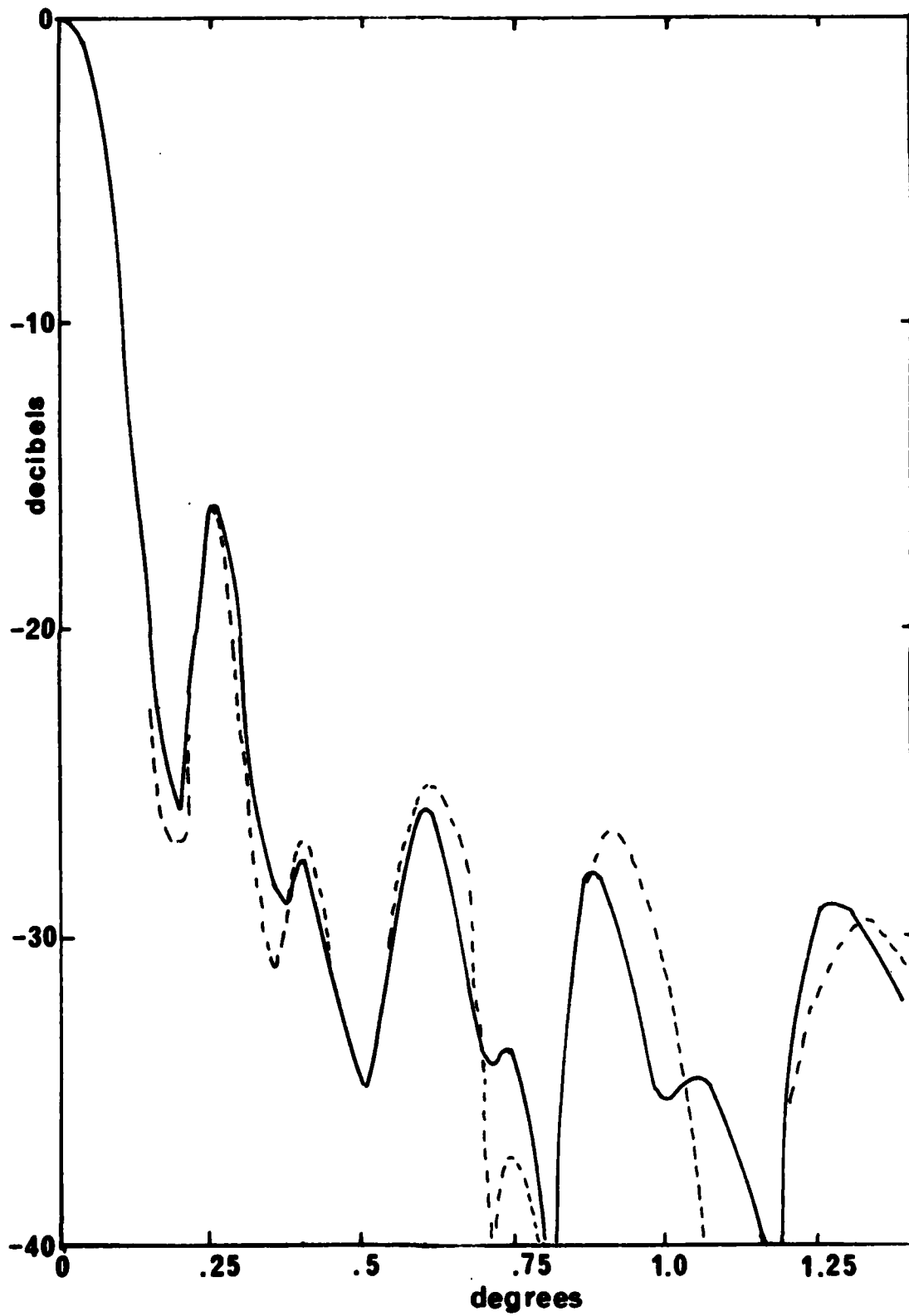


Fig.5.1-13: Goonhilly II: radiation patterns at 3.95 GHz.  
Solid - measured                      Dashed - predicted

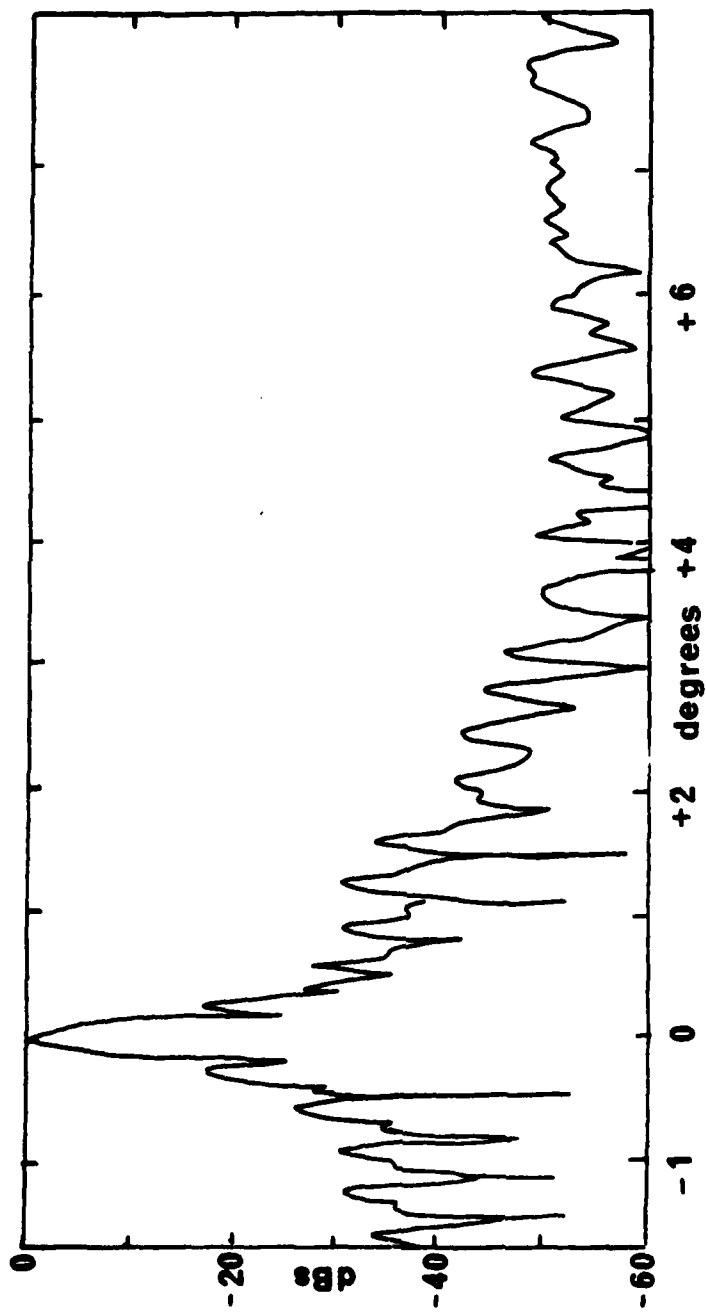


FIG. 5.1-14: Goonhilly II: measured radiation pattern.

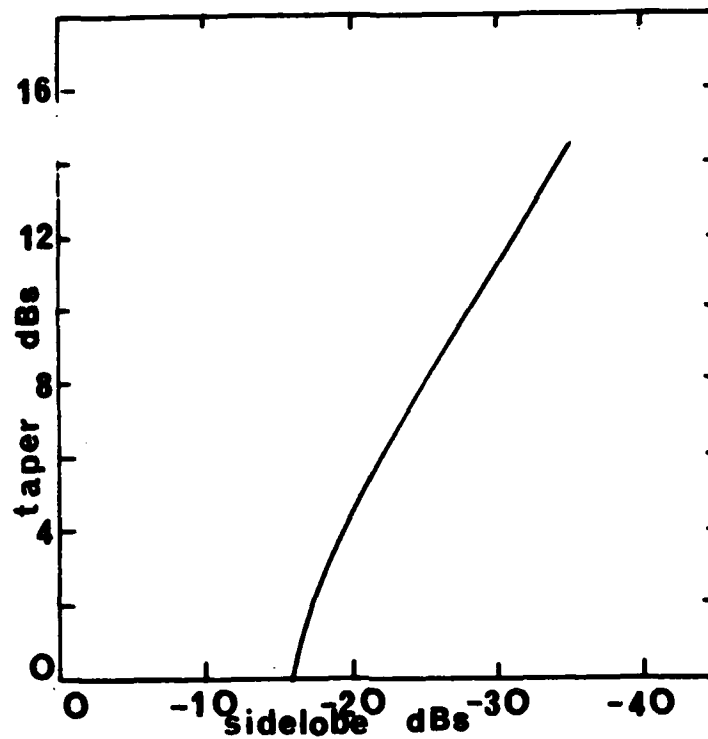


Fig.5.1-15: Aperture edge taper (dB) vs sidelobe level (dB) for an optimum parabola-on-a-pedestal illumination without blocking effects.

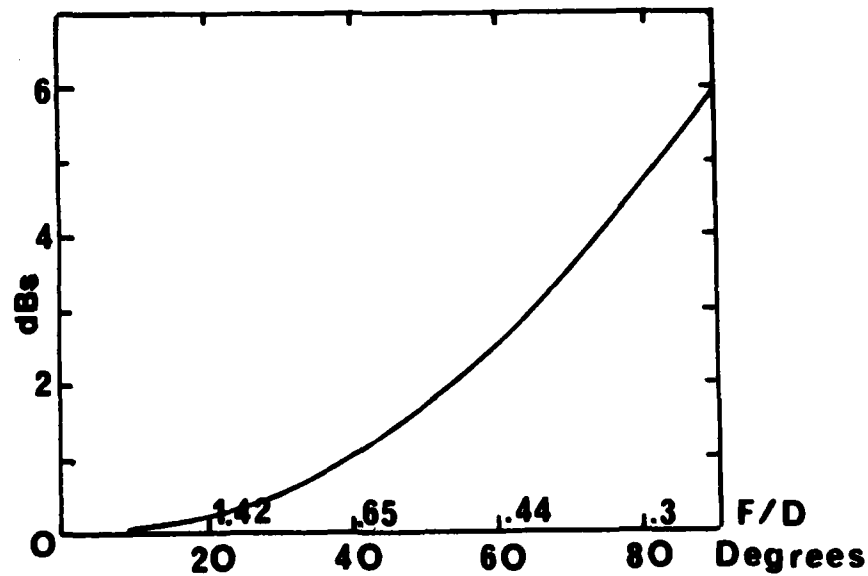


Fig.5.1-16: Space loss (dB) in a reflector vs  $\theta$ , degrees. The semi-angle subtended by the reflector at the focus. Equivalent F/D ratio is also shown.

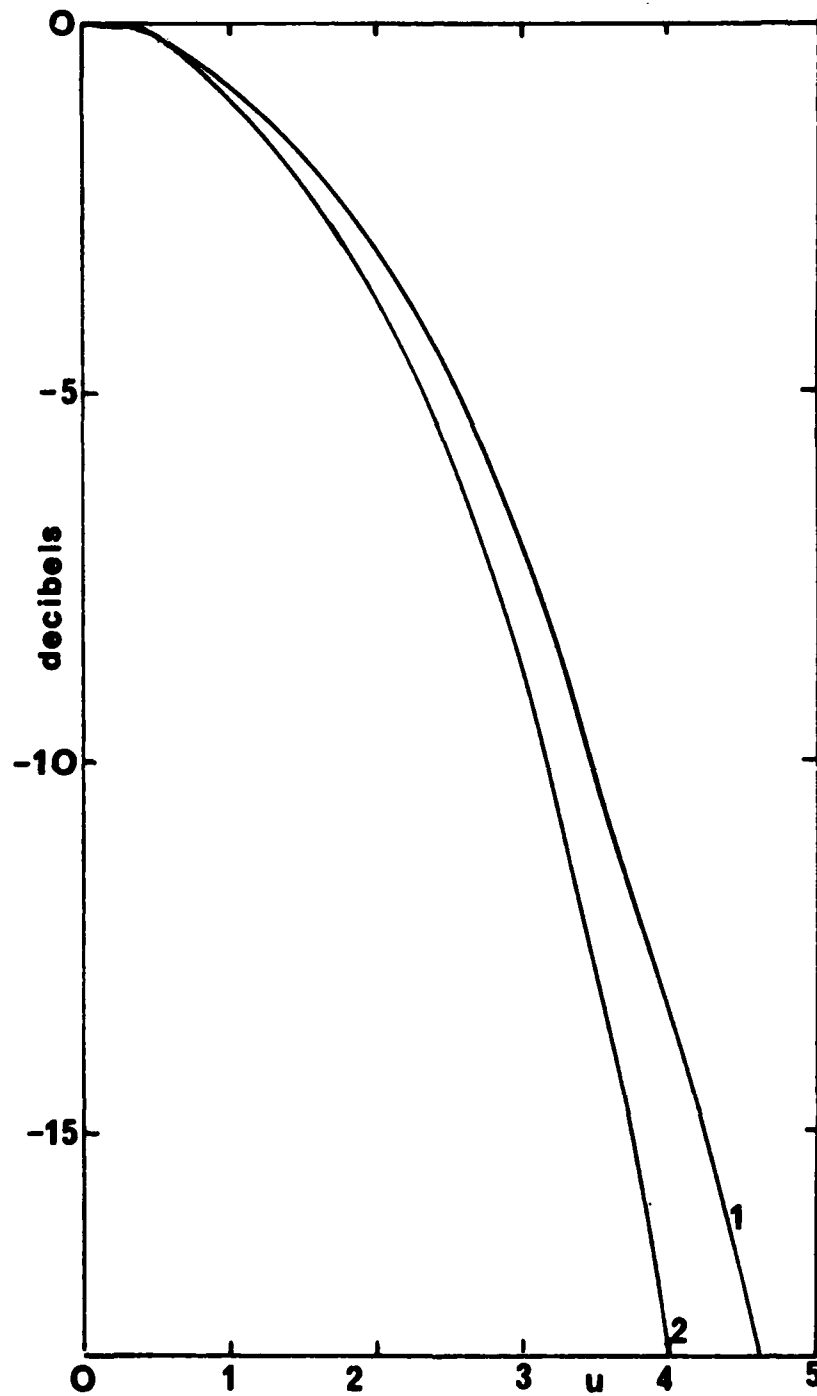


Fig. 5.1-17: Generalised feed radiation.  $u = \pi \sin \theta^+ d/\lambda$ , where  $d$  is the aperture diameter,  
1. A hybrid mode or dual mode horn  
2. Fundamental mode conical horn in circular polarisation

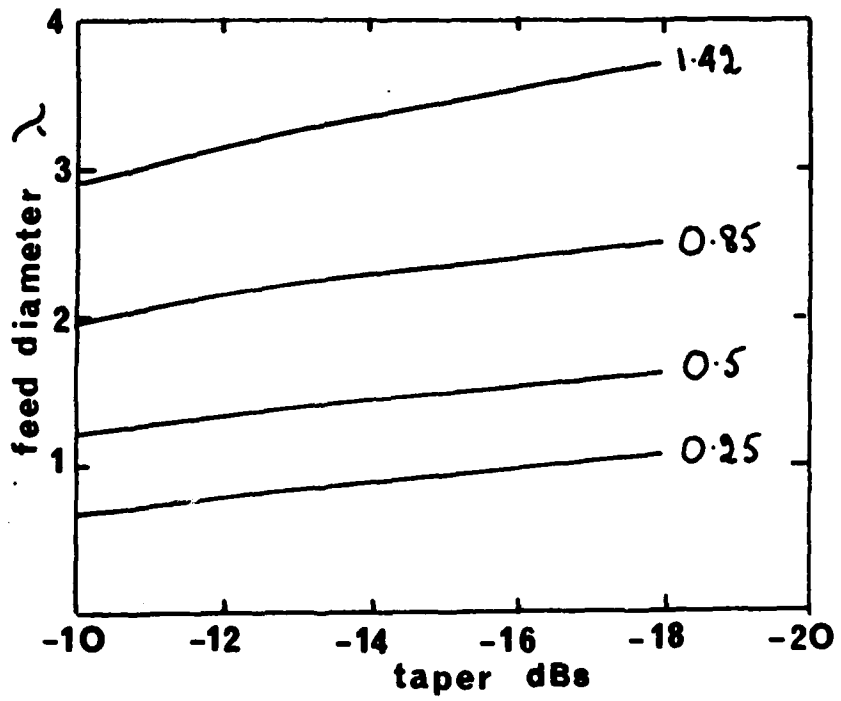


Fig.5.1-18: Feed diameter in wavelengths as a function of edge taper due to the feed for four values of F/D (hybrid mode feed of Fig.5.1-17).

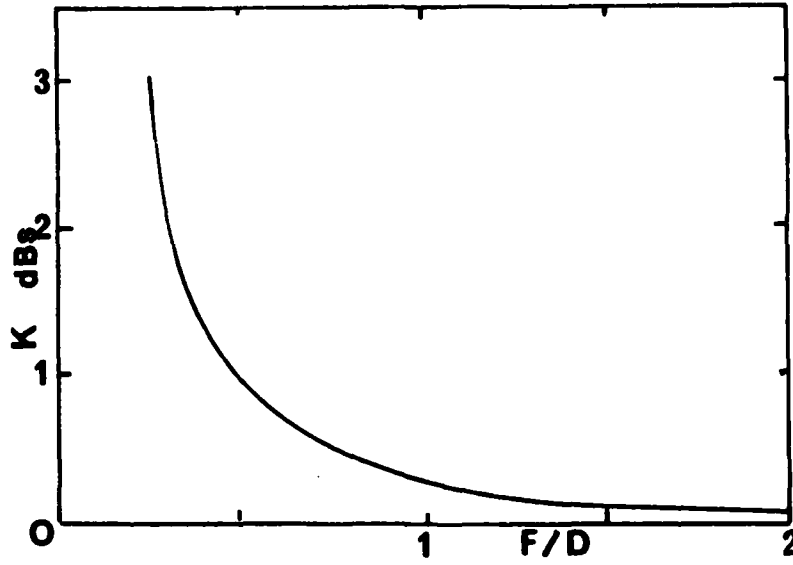


Fig.5.1-19a: Backlobe parameter,  $K$ , in dBs against  $F/D$  ratio.

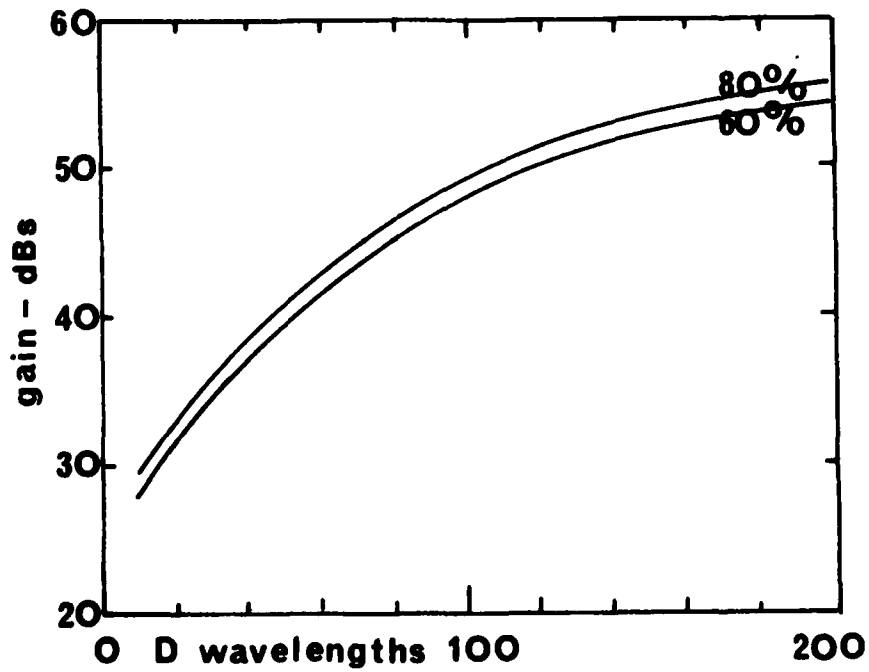


Fig.5.1-19b: Gain (dB) for a reflector of diameter,  $D$ , wavelengths for 80 and 60 per cent efficiency.

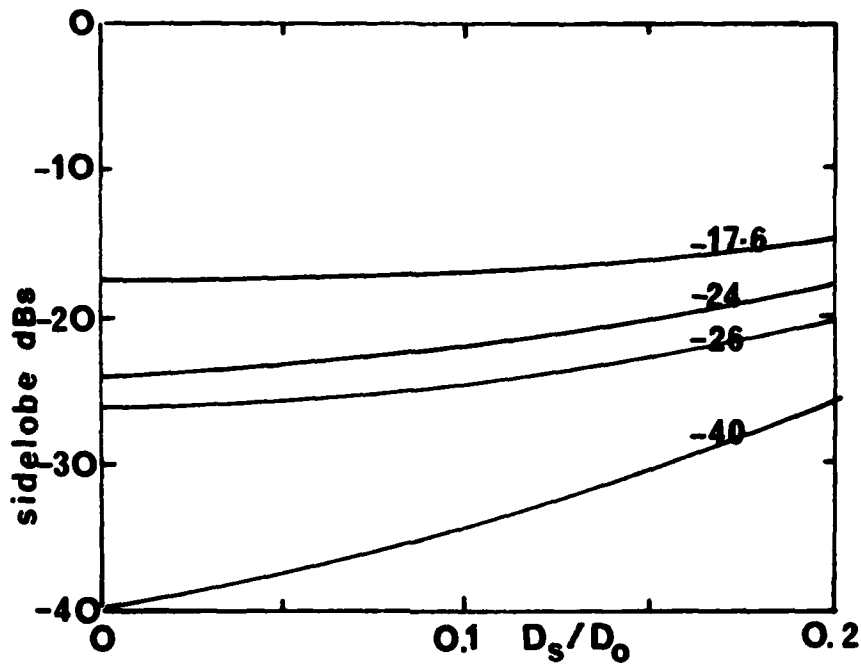


Fig.5.1-20a: Change in first sidelobe level (dB) with blockage ratio ( $D_s/D_o$ ) for a parabola-on-a-pedestal illumination giving first sidelobes of -17.6, -24, -26 and -40 dB (unblocked). ( $D_s$  is blockage diameter,  $D_o$  the reflector diameter).

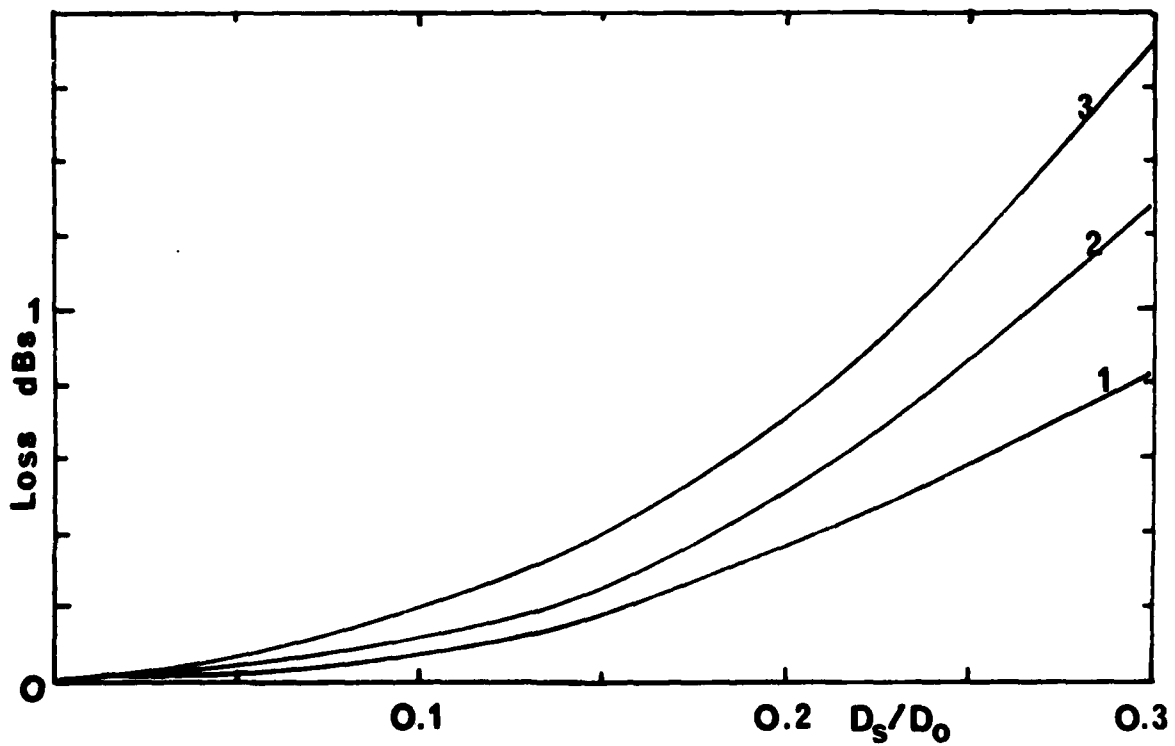


Fig.5.1-20b: Loss in forward gain (dB) for first sidelobe values (unblocked) of:  
(1) -17.6 dB, (2) -22 dB, (3) -25 dB.

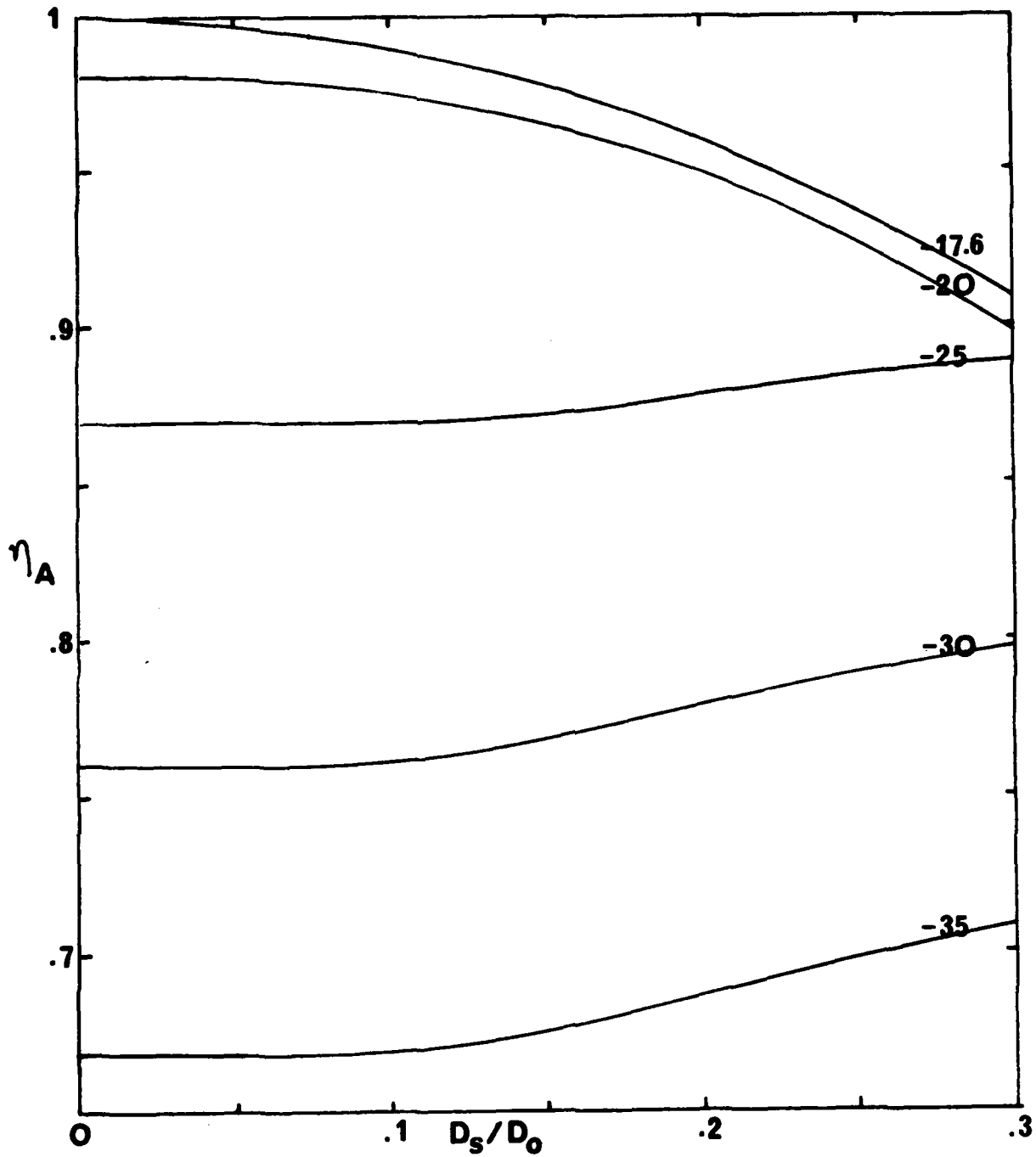


Fig.5.1-20c: Variation in aperture efficiency,  $\eta_A$ , with  $D_s/D_0$  for several sidelobe levels (illumination is modified one-parameter circular). (Hansen Ref.4).

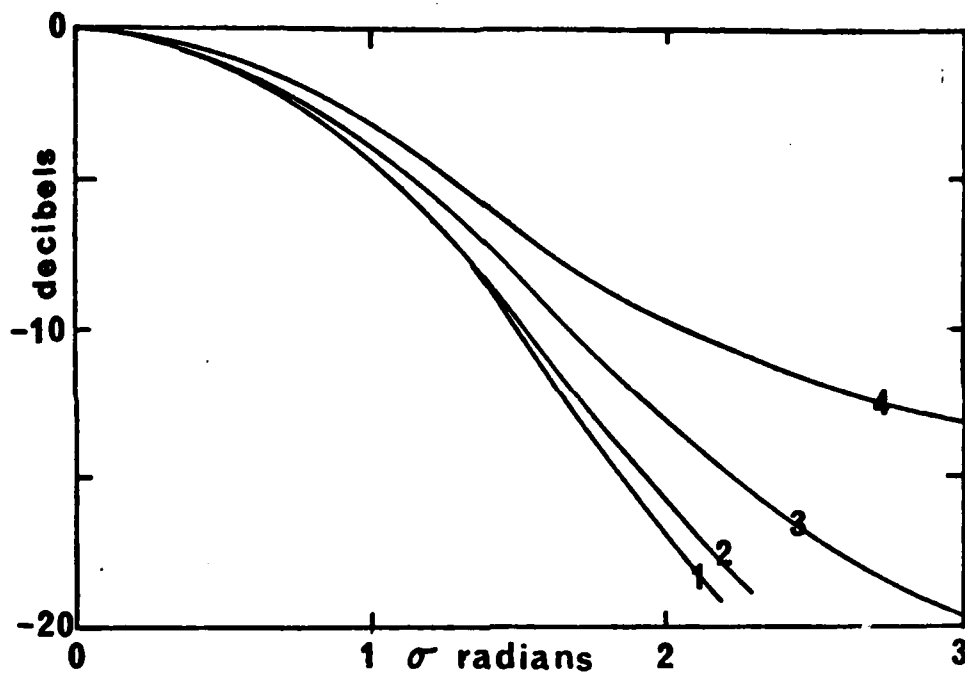


Fig.5.1-21a: The gain loss (dB) vs rms phase errors, for four correlation intervals: (1) D/50, (2) D/12.5, (3) D/8, (4) D/4.

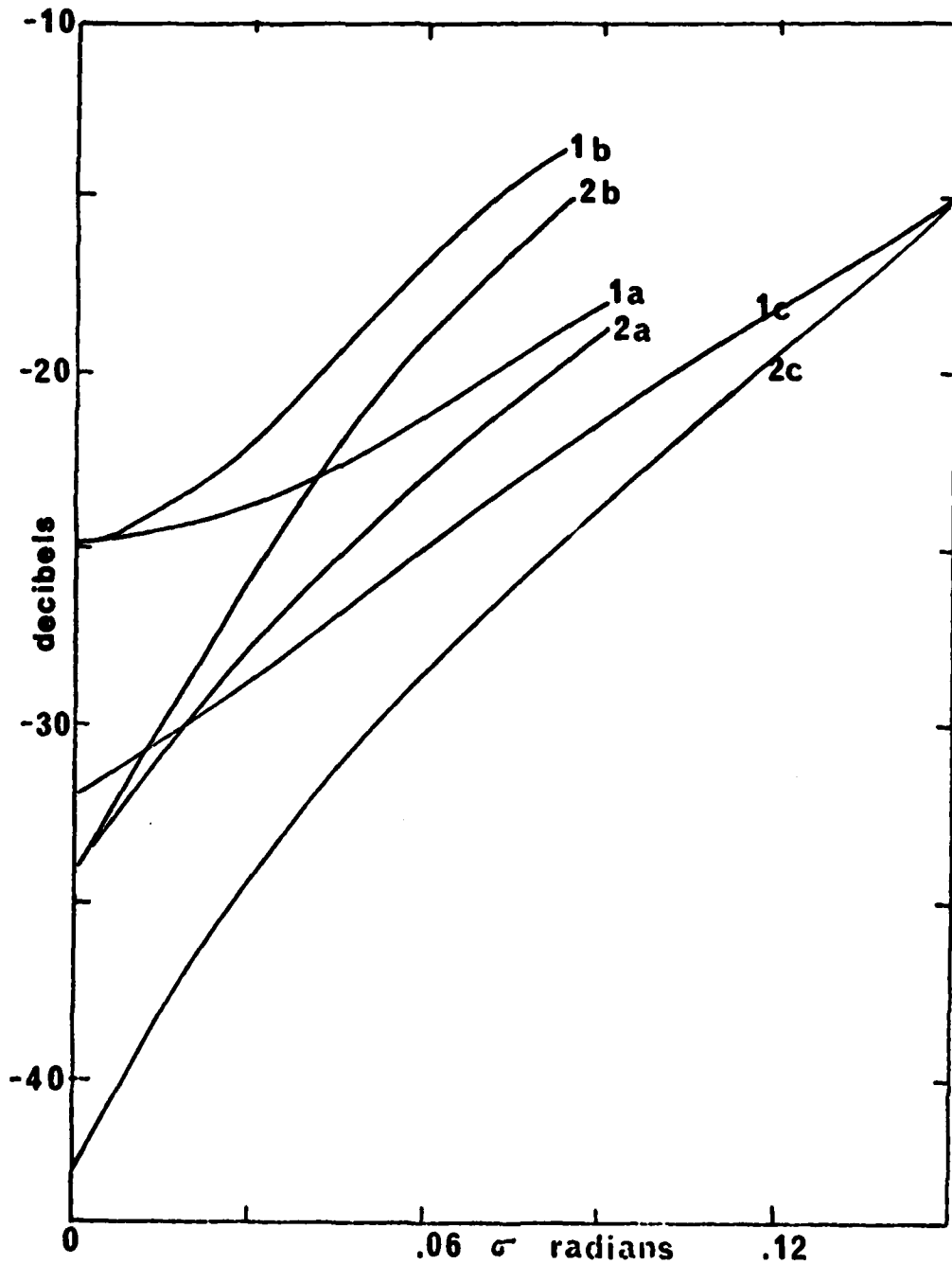


Fig.5.1-21b: Typical variation of first and second sidelobe level (labelled 1 and 2) with rms phase error.

- (a) illumination  $1-(r/a)^2$  C/D = 0.05
- (b) illumination  $1-(r/a)^2$  C/D = 0.1
- (c) Cosine squared illumination C/D = 0.04

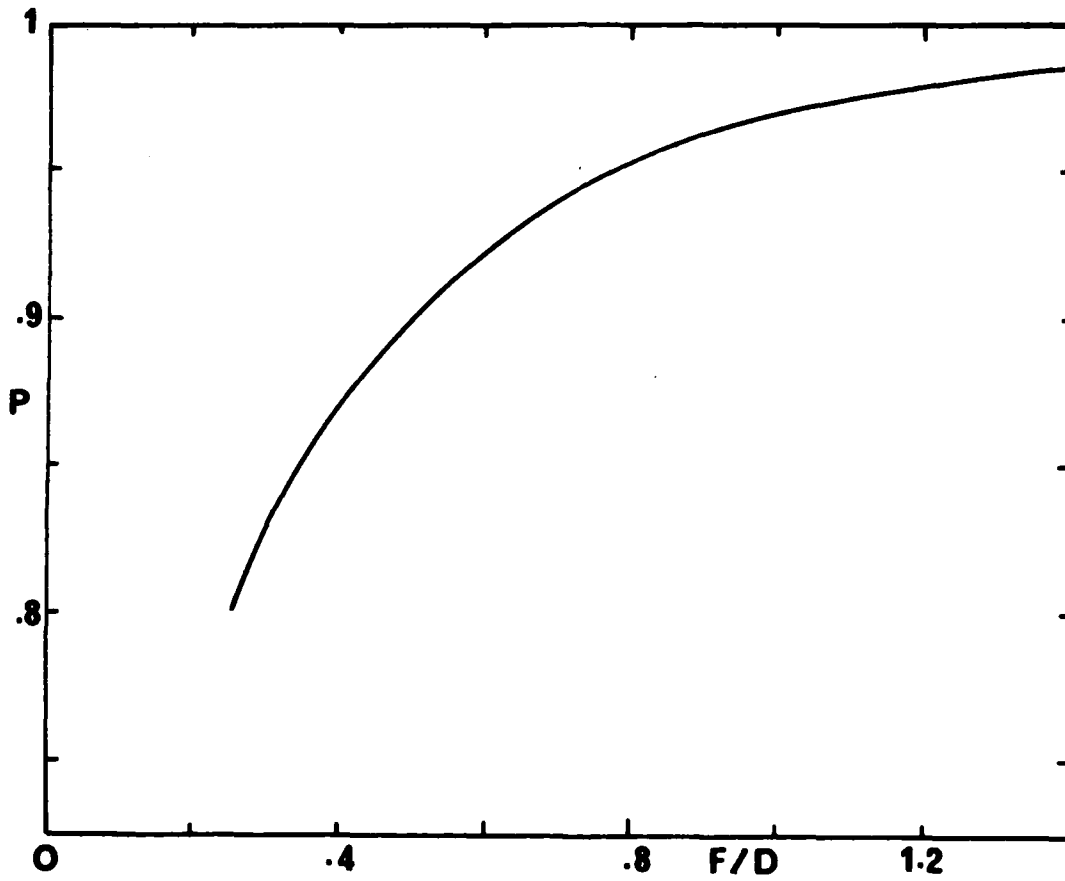


Fig.5.1-21c: The correction factor, P, for deep reflectors.

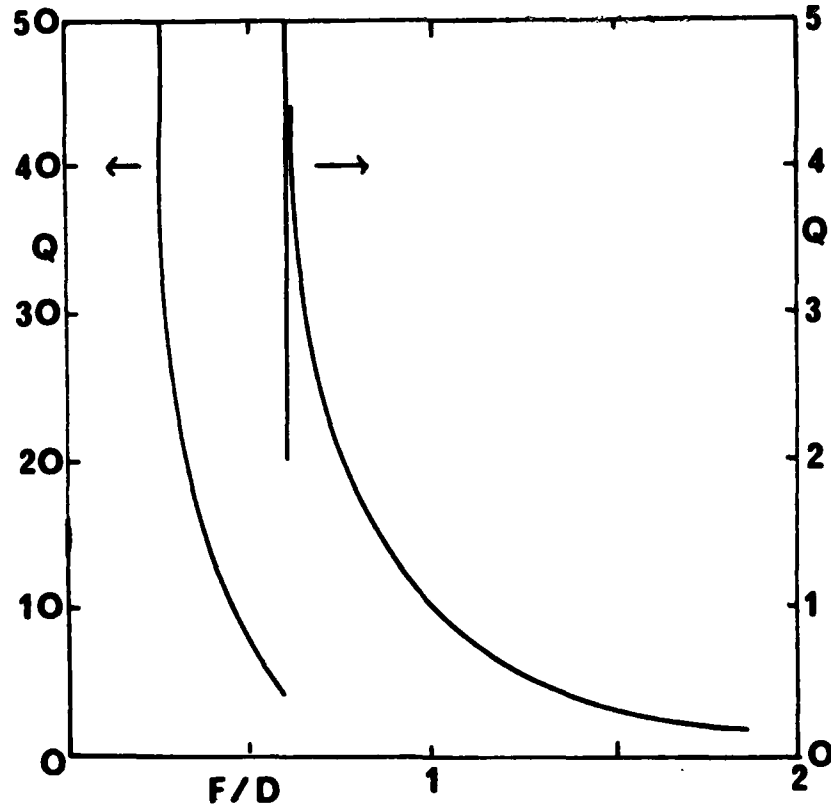


Fig.5.1-22a: Lateral feedshift  
 $Q = (D/F)/((F/D)^2 + 0.02)$  vs F/D.

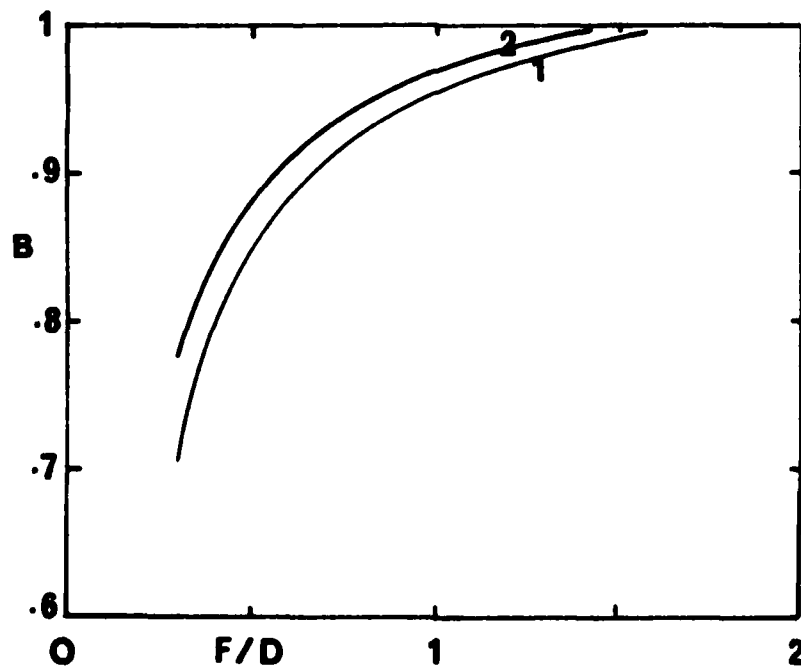


Fig.5.1-22b: Beam deviation factor, B, vs F/D for two aperture

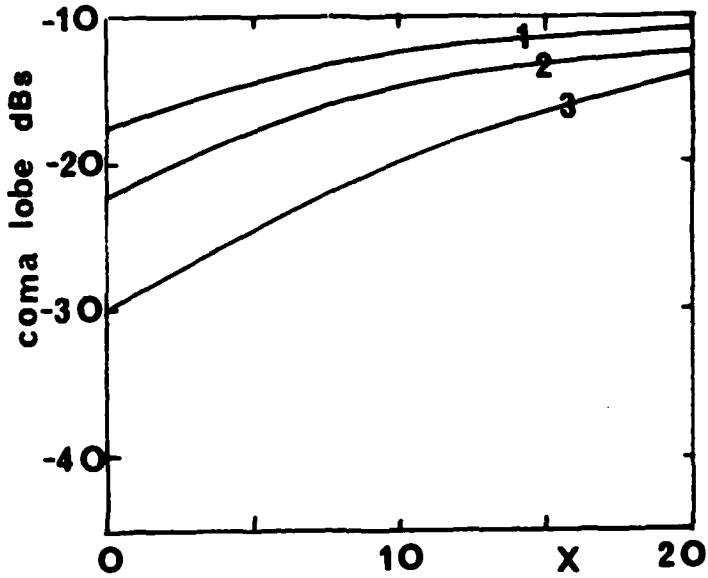


Fig.5.1-22c: Coma lobe (dB) vs X for three aperture illuminations.  
1. Uniform  
2. 10 dB taper  
3.  $(1-(r/a)^2)^2$

Fig.5.1-22d: Gain loss (dB) for two aperture distributions.  
1. Uniform  
2. 10 dB taper

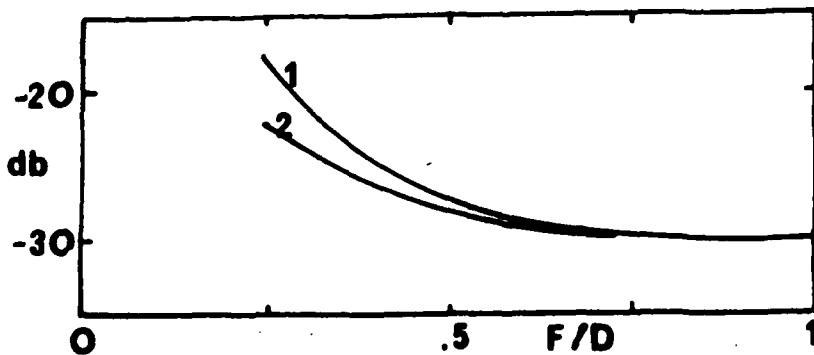
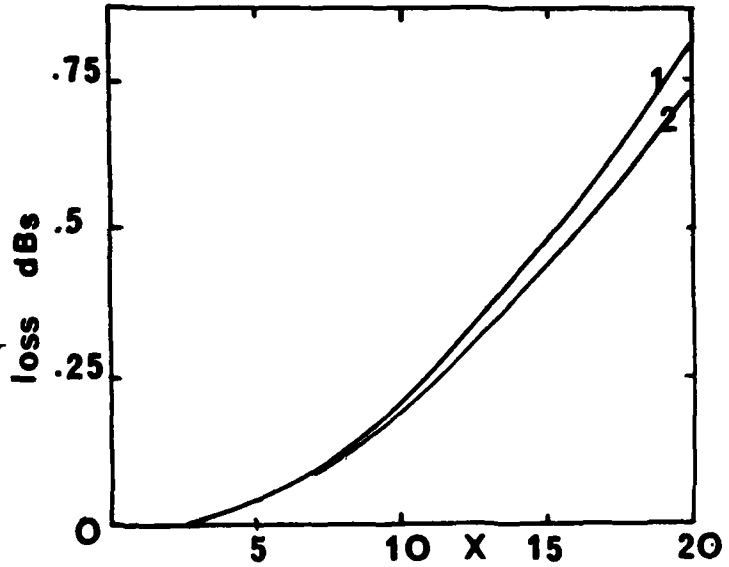


Fig.5.1-22e: Coma lobe (dB) as a function of F/D for lateral shifts of  
(1) 0.5 and  
(2) 0.25 wavelengths.

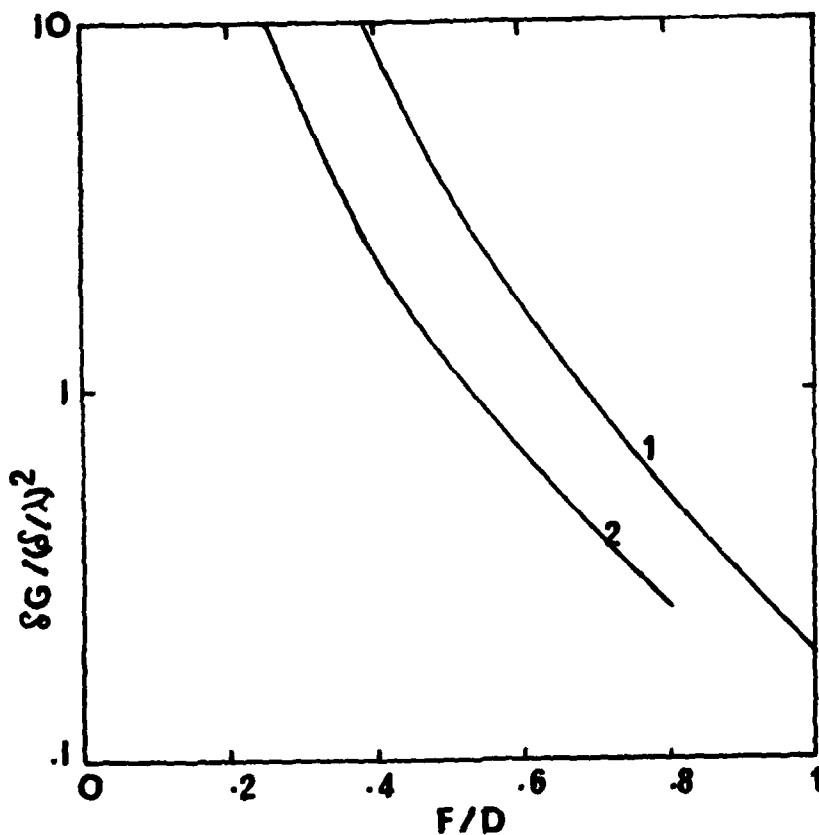


Fig.5.1-23a: Axial feedshift.  $\delta G / (\delta/\lambda)^2$  vs  $F/D$  for two aperture distributions.

- (1) Uniform
- (2)  $(1-(r/a)^2)^2$ ;  $\delta/\lambda$  is the axial feedshift while  $\delta G$  is the gain loss in dB.

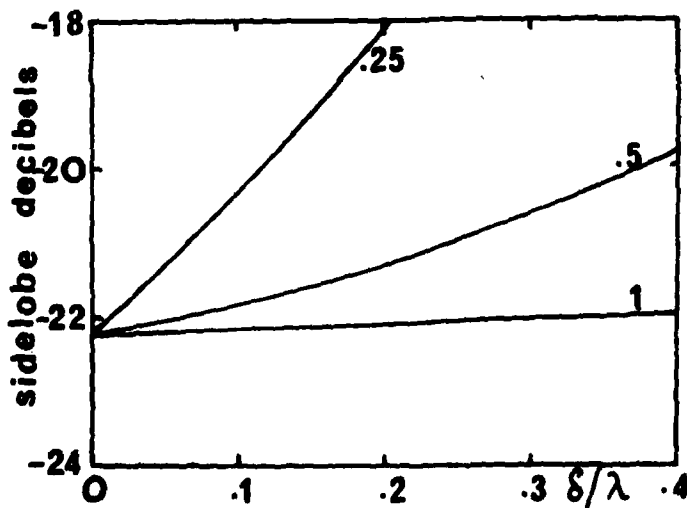


Fig.5.1-23b: Sidelobe level as a function of  $\delta/\lambda$ , the axial feedshift for  $F/D = 0.25, 0.5$  and  $1.0$ . The illumination has a 10 dB edge taper, producing a first sidelobe.

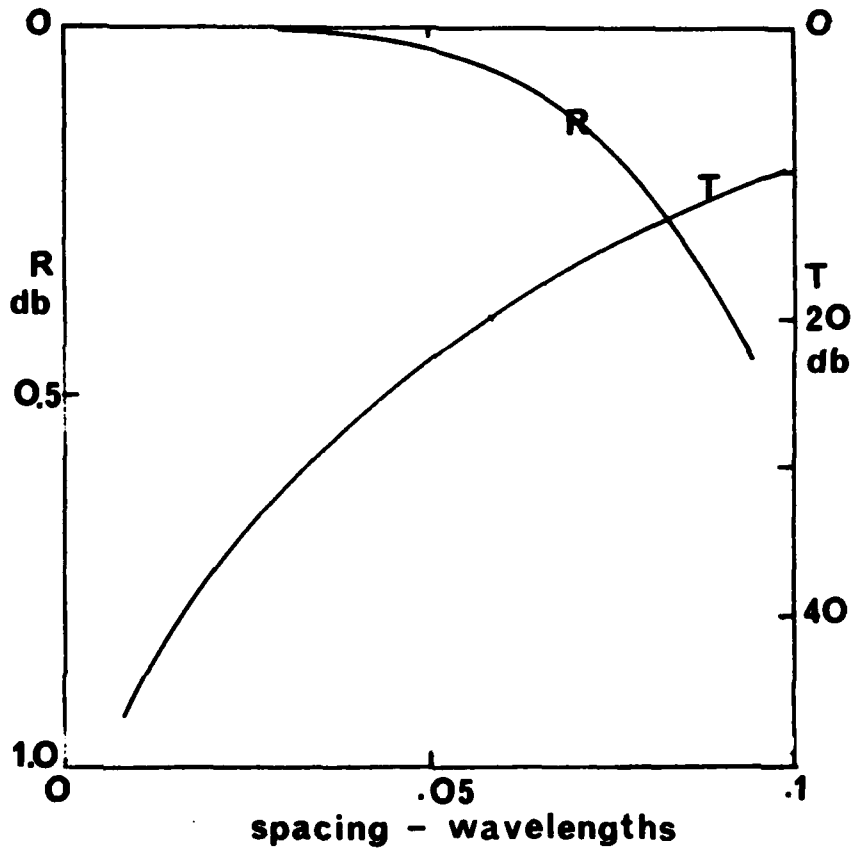


Fig.5.1-24: Mesh losses on transmission, T, and reflection, R, as a function of wire spacing to wavelength. The wire diameter to spacing ratio is 0.1.

## 5.2 Asymmetric (Offset) Parabolic Reflectors

### 5.2.1 Prediction of performance

Although the geometry of an offset reflector (Fig.5.2-1) is less straightforward than that of an axisymmetric reflector and various effects due to the asymmetry must be considered, the removal of all blockage effects brings about major improvements in the antenna sidelobe performance in both the near-in and far-out regions.

The geometry of this offset configuration has been detailed by various authors, notably Cook, Elam and Zucker<sup>1</sup> and Rudge<sup>2</sup> and techniques now exist which permit accurate predictions of the antenna performance<sup>2,18</sup>. The reflector is normally specified in terms of the parameter,  $\theta_o$ , the offset angle,  $F$ , the focal length of the parent paraboloid and  $\theta^*$ , the semi-angle subtended by the reflector rim at the geometric focus. To provide a circular projected aperture of diameter  $d$ , an elliptically contoured reflector is required. The diameter  $d$  is related to the other parameters by:

$$d = \frac{4F \sin \theta^*}{\cos \theta_o + \cos \theta^*} \quad (22)$$

while the reflector itself has dimensions given by:

$$\text{major semi axis} = \frac{2F \sin \theta^* \sqrt{1 + \cos^2 \theta^* + 2 \cos \theta^* \cos \theta_o}}{(\cos \theta^* + \cos \theta_o)^2} \quad (23)$$

$$\text{minor semi axis} = 2F \frac{\sin \theta^*}{\cos \theta^* + \cos \theta_o} \quad (24)$$

Theoretical predictions of the final radiation pattern have so far been limited to the angular zone around boresight and predictions over angles of  $\pm 180^\circ$  do not appear to be available in the literature. Nor are there many published examples of extensive measurements. Good agreement has been obtained over a limited region for sidelobes, gain and cross-polarisation<sup>1,3</sup>. Predictions for a design giving -40 dB sidelobes have been successfully confirmed<sup>4</sup> showing that the removal of blockage does

enable a suitable illumination to be formed across the antenna aperture. Predictions so far as they go are usually accurate within  $\pm 1$  dB at the -20 dB level and both aperture field and current distribution methods can and have been used (see Section 5.1).

The asymmetry of the offset reflector introduces an asymmetric space attenuation effect due to differing distances from the focal point to the two diametrically opposed points on the reflector rim (Fig.5.2-4). The smaller the parametric angles  $\theta_0$  and  $\theta^*$ , the smaller this asymmetry and the less the disturbance caused to the sidelobes. Figure 5.2-5 shows the sidelobe level as a function of offset angle for two values of edge illumination. For the illumination taper-function used, the offset angle requires to be restricted to below  $30^\circ$  for good near-in sidelobe performance in both planes, though even with larger values of  $\theta_0$  excellent performance could be obtained in the plane of asymmetry at the expense of the level in the symmetry plane. Somewhat different sidelobe levels can be obtained using different primary feed illuminations, but the trends remain as shown. Figure 5.2-6 shows the sidelobe level in the asymmetric plane as a function of taper.

A considerable literature on the cross-polarisation levels in the offset reflector has been published (for example, Refs.5 and 6) since the asymmetry of the reflector introduces cross-polarisation. Figure 5.2-7 shows the peak cross-polarisation (for linear polarisation) as a function of the two reflector angles,  $\theta_0$  and  $\theta^*$ . These peaks occur in the plane of asymmetry of the reflector at angles corresponding approximately to the -6 dB levels of the main co-polarised beam. Hence these lobes are contained within the envelope of the main co-polar beam. If the cross-polar performance of the main beam is unimportant, then the effect of the cross-polar radiation in the sidelobe envelope of the antenna will be negligible for most applications.

When circular-polarisation is employed, a beam squint results from the reflector asymmetry. Adatia and Rudge<sup>7</sup> have shown that, to an accuracy of 10% the squint angle,  $\beta_s$ , may be given by:

$$\beta_s = \arcsin \left( \frac{\sin \theta_0}{4\pi F} \right) \quad (25)$$

where  $F$  is the focal length of the parent paraboloid in wavelengths.

In some applications these effects limit the maximum values of  $\theta_o$  and  $\theta^*$  and values below  $35^\circ$  are often adopted for these reasons. (A typical practical configuration might be  $\theta_o = \theta^* + 5^\circ$ ). For cross-polar lobe suppression of 40 dB, the angles must be very small,  $\theta_o < 15^\circ$ ,  $\theta^* < 14^\circ$ , which results in a very long structure. For good sidelobe suppression, however, a shorter structure can be employed although very large values of  $\theta_o$  and  $\theta^*$  imply an asymmetric distribution in the aperture-plane of the antenna, which can raise the levels of the near-in sidelobes.

For offset angles less than about  $50^\circ$  the cross-polarisation can be reduced using a recently developed multi-mode feed<sup>8,9</sup>. This 'matched' feed generates a field with cross-polarisation properties matched to that of the offset reflector. This results from exciting a higher-order mode in the aperture plane of rectangular or conical feed horns. The magnitude of the higher-order mode required to match a given reflector depends upon the angles  $\theta_o$  and  $\theta^*$ . Linearly-polarised feeds have been demonstrated which provide a minimum additional cross-polar suppression of 10 dB over a bandwidth of 5%. Since the modes employed in this matched-feed must remain in a specific relative phase and amplitude relationship, bandwidths of the order of 5-10% are likely to be a practical limitation in the short term, although wider bandwidths are not fundamentally excluded. In principle, the beam-squint, arising from the use of circular polarisation with the asymmetrical reflector, can also be cancelled, although practical devices have yet to be demonstrated.

It is interesting to note that the additional modes employed in the matched-feed devices also lead to compensation of the asymmetric reflector illumination. Hence, in principle, the offset reflector can be designed such that it operates essentially as an unblocked axisymmetric reflector antenna. Attempts to produce more sophisticated aperture illumination distributions in these antennas would be clearly more worthwhile than in the case of their axisymmetric counterparts, in view of the avoidance of blocking.

Dual-offset, or offset Cassegrain reflector systems, although their analysis is more complex, also offer certain advantages. In these systems the sub-reflector can be offset from the main reflector and the primary-feed, to provide a long F/D system, again without blocking.

One variation on the offset Cassegrain principle is termed the 'Open Cassegrain'<sup>1</sup> in which the sub-reflector is offset but the feed is located within the aperture of the main reflector. An example is shown Fig.5.2-2.

Large offset angles result from this configuration and peak cross-polarised levels will be typically of the order of -25 dB.

Adatia<sup>11</sup> has analysed a double-offset Cassegrain (Fig.5.2-3) in which the sub-reflector inclination is adjusted to suppress the cross-polar radiation below -45 dB with linear polarisation. It should be noted that, with linearly-polarised offset parabolic reflectors, the peak cross-polarised radiation generated by the offset reflector occurs in two lobes within the main beam of the antenna. If the cross-polar performance of the main beam is unimportant, then the effect of the cross-polar radiation on the sidelobe envelope of the antenna will be negligible for most applications. When illuminated by a circularly-polarised primary-feed, the offset antenna does not generate cross-polarised radiation but a small beam-squint effect is observed, the direction of which is dependent upon the band of polarisation.

A further notable advantage of the offset reflector, is the reduction in reflector reaction upon the primary-feed<sup>10</sup>. The reflector-feed isolation is typically below -45 dB which must be compared with -20 to -30 dB for an axisymmetric reflector antenna. The high isolation improves the antenna VSWR and reduces cross-coupling between the elements of multiple-beam feeds.

The far-out sidelobes, direct spillover and backlobe radiation from an offset reflector can be estimated approximately using the techniques described for axisymmetric reflectors, in the absence of blocking. Peters<sup>19</sup> has suggested that offset reflectors can offer improved backlobe performance since the more distant edge of the reflector has reduced diffraction and the nearer edge can be castellated. Rim shielding and hoods can also be employed to good advantage.

### 5.2.2 Examples of offset parabolic reflector sidelobe performance

Relatively few examples of the performance of offset reflectors have been published and most have diameters in the range 10-100 wavelengths. Table 5.2.1 contains a tabulation of the data documented and some examples are discussed below.

Example 1 - The Intelsat IVA satellite<sup>17</sup> carries offset antennas, 18 wavelengths square, two for transmit at 4 GHz, the third for receive at 6 GHz. All are circularly polarised. The antennas are fed by an array of horns

with a complex feed network to give shaped coverage over specified land areas and good sidelobe suppression. With  $\theta_o = 35^\circ$  and  $\theta^* = 28^\circ$ , first sidelobe suppression below -27 dB was achieved and inter beam coupling was below this level.

Example 2 - An offset reflector with an offset angle of  $90^\circ$  was fed from a large cylindrical corrugated horn to form a horn-reflector system similar to the hog-horn arrangement<sup>20</sup>. Installing an absorber lined tunnel to reduce spillover energy resulted in suppression of the wide-angle sidelobe (i.e., at angles greater than about  $40^\circ$ ) to below -70 dB. Near-in sidelobes suffered from large offset angle asymmetry and were of the order of -26 dB close to main beam but rapidly falling to -40 dB level. The antenna operated at 37 GHz with a half-power beamwidth of  $1.7^\circ$  and gain of 40 dB. Cross-polar peaks, due to illumination asymmetry caused by the large offset angle, occurred at the -16 dB level, but these were contained within the main co-polar beam. Backlobe radiation was suppressed to below -80 dB.

Example 3 - An offset parabolic reflector with elliptical contour antenna<sup>4</sup> was designed to provide an elliptical beam with half-power beamwidths approximately  $3^\circ$  by  $4^\circ$ . Near-in peak sidelobes in azimuth were specified to be less than -38 dB rapidly falling to the -50 dB level, and in elevation less than -24 dB with a similar rapid fall-off. The illumination taper was -20 dB in both planes. The angular parameters were  $\theta_o = 45^\circ$  and the semi-angles of the two axes,  $\theta_x^*$  and  $\theta_y^*$ , were  $38^\circ$  and  $59^\circ$ . The cross-polarisation was predicted as rather poor at -20 dB but these lobes were contained within the main-beam, and depolarisation of the main-beam was not an important consideration in this design.

The achieved sidelobe levels are shown in Table 5.2.2. Figures provided in brackets refer to predicted values. The performance shown was achieved with some use of absorber to shield the feed supporting structure from stray reflections and to absorb spurious feed radiation. No loss of efficiency is entailed, however, since this activity was concerned only with the spillover radiation (Fig.5.2-8).

Although the data given in Table 5.2.2 is for an elliptical-beam antenna, it does demonstrate the potential of the offset reflector to provide low sidelobe performance. The relatively high level of spillover radiation

Table 5.2.2

Sidelobe performance of an elliptical-aperture offset reflector antenna

Parameter	Level (dB)	
	H plane	E plane
Near-in peak sidelobe peak	-37 (-38)	-24 (-24)
Angular range 10-45°	<-42	<-40
Spillover (past reflector rim)	<-45 (<-50)	-32 (-33)
Backlobe*	<-50 (-34)	<-50 (-34)
Illumination taper	-20	-20
Near-in cross-polarisation peak level (within main beam)	-17 (-18)	<-40 (-∞)
Far-out cross-polar peak level	<-45	<-50

\* This prediction was made for an equivalent axisymmetric reflector and may be pessimistic. Measurements were made with small sheet of absorber behind reflector, hence no firm conclusions regarding offset reflector backlobes can be drawn.

in the E plane is a consequence of the indifferent performance of the simple primary feed employed (i.e., a fundamental-mode rectangular horn). Studies have indicated that an improvement of the order of 7 dB could be realised with an improved feed design. The cross-polarisation peaks are contained within the main-beam envelope and were not of concern in the application for which the antenna was designed. However they could be reduced to the -40 dB level over a 5% band using a 'matched feed' of the type referred to above.

In Fig.5.2-8 some examples are shown of offset-reflector antenna radiation-patterns obtained from an antenna operating in the 26-40 GHz band.

Table 5.2.1

Type	(Degrees)		Frequency (GHz)	D/ $\lambda$	Taper (dB)	First side-lobe (dB)	Sidelobes (dB)		Back-lobe	Cross-polarization (dB)	VSWR	(% Efficiency)	Ref.	Notes
	$\theta_0$	$\theta^*$					10°-45°	70°-120°						
Open Casse-grain	47.5°	7.5	60	203.2	-16	-25	<-45	-37E	-43E	-23		70.4	1	Diameter of sub-reflector = 40 $\lambda$
Off-set	32.25	~30	3.95	36	-	-42						low	12	Cluster of feeds used
Dual off-set		9.6		66		-30	-60	-50	-75	-28		66	13	Dielectric loaded horn
Off-set	15-20	15	28.5	72	-20	-24		-30E	-35E	-38		-	14	Shoulders rather than first side-lobes
Off-set Casse-grain		6	4	400	-15		<-50	-40E	-45E	-45		80	15	Calculated performance of a multiple beam antenna
Off-set	35	30	30	36.2	-12	-25	<-40	-38E	-43E	-24			16	
Off-set	37.5	33	30	70	-4 to -8.5	-20		-37E	-41.5E	-28	<1.2	68	3	This is a multiple feed antenna
Elliptical off-set	45	38	30	14	-20	-24	<-40	-32	<-50	-18		57	4	Elliptical beam antenna with some shielding
Off-set	90	59	37	24	-	-37	<-40	<-50	<-80	-16		-	20	Almost hoghorn configuration. Uses tunnel shroud lined with absorber

E = estimated

### 5.2.3 Conclusions: Asymmetric reflector antennas

The offset parabolic reflector in its single reflector and offset Cassegrainian forms is somewhat more complex to deal with analytically and practically than its axisymmetric counterpart. Nevertheless, techniques have now been developed which allow the design of offset antenna systems to be placed on a firm analytical basis. The advantages of offset systems are very significant when low sidelobe performance is of concern and it appears that the avoidance of blocking and scattering from the feed and its supporting struts is of fundamental importance in these applications. The excellent electrical isolation between primary-feed and offset reflector is another significant advantage in the design of high performance systems.

The disadvantages of the offset systems can be identified as their depolarising properties and the additional mechanical and/or structural problems which arise as a consequence of their asymmetry. However, the point must be made that these disadvantages are open to engineering solutions and that these problems appear considerably more tractable than the fundamental problems represented by blocking effects in axisymmetric systems. The depolarising properties of offset systems have been receiving attention and already methods have been developed by means of which these effects can be compensated. Use of an optimised double-offset reflector system, or a multi-mode feed technique, allows good cross-polar performance to be attained from asymmetric reflector systems without loss of the low-sidelobe capability.

In Table 5.2.3, the projected performance of two low-sidelobe offset reflector antennas is shown. The smaller antenna is a single reflector system, while the larger antenna employs an optimised double-offset configuration. To demonstrate the linearly-polarised performance capabilities of the single reflector offset-antenna, a cross-polar compensating feed has been assumed for this case. For circular polarisation, similar sidelobe and cross-polar performance could be achieved using a more conventional conical feed horn.

For the offset antennas, the reflector profile errors and feed alignment dominate the sidelobe performance. However, for the diameters shown, the tolerances necessary to maintain the sidelobe performance specified are

not too stringent. The spillover and backlobe radiation levels represent the major drawbacks for these small-to-medium large diameter systems. A selective use of shrouds and shielding material could be expected to improve these levels very significantly.

Table 5.2.3

Projected performance of low-sidelobe offset reflectors

Antenna type	Aperture diameter	
	10 $\lambda$	100 $\lambda$
	Single reflector with compensated feed	Dual reflector
$\theta_0$ (degrees)	35	50
$\theta^*$ (degrees)	30	30
Illumination taper (dB)	-18	-18
Aperture efficiency (%) (for the above taper)	60	60
Half-power beamwidth (degrees)	8.1	0.81
Theoretical gain for above efficiency (dB)	25.8	45.8
First sidelobe (dB) in the plane of asymmetry	-42	-40
in the plane of symmetry	-37	-40
Backlobe (dB)	-33	-46
Spillover lobe (dB)	-27	-40
Degradation in first sidelobe level due to (dB)		
(a) a lateral feedshift of 0.25 $\lambda$	-35	No effect
(b) an axial feedshift of 0.25 $\lambda$	-38	No effect
(c) $\lambda/32$ rms surface errors	-34.5	-34.5
(d) $\lambda/64$ rms surface errors	-37.5	-37.5
Estimated final level of the first sidelobe (dB)	<-36	-39
Peak cross-polarisation (dB)	-40	-45

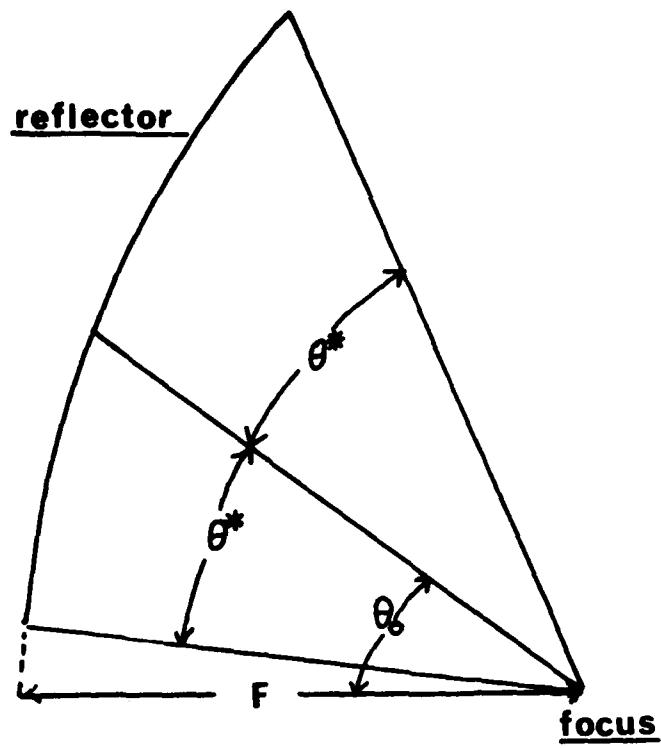


Fig.5.2-1: The offset reflector antenna.

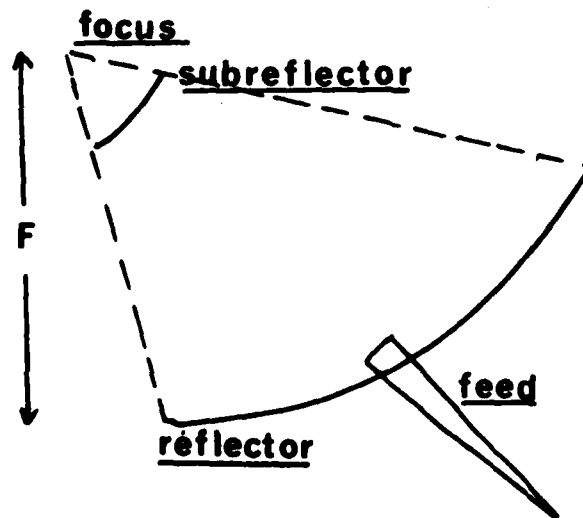


Fig.5.2-2: The Open Cassegrain antenna.

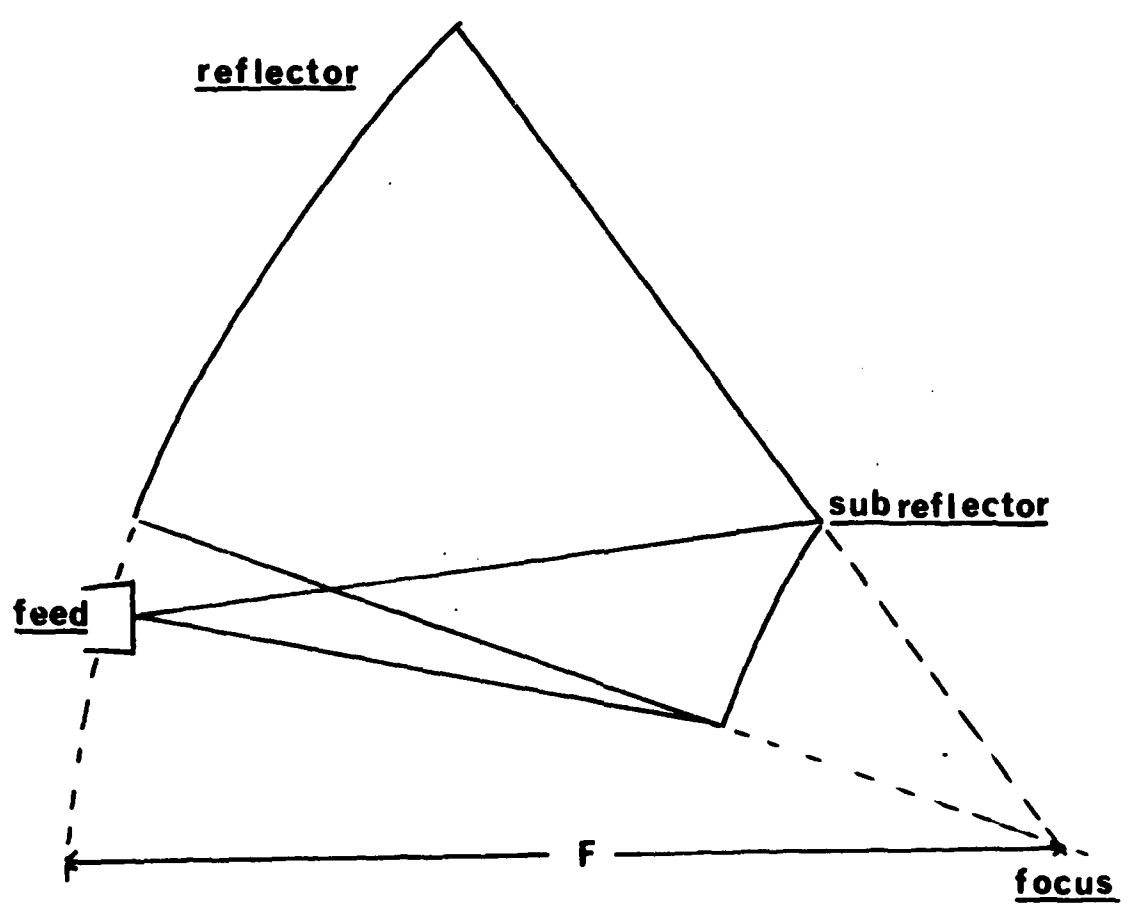


Fig.5.2-3: The doubly offset reflector antenna.

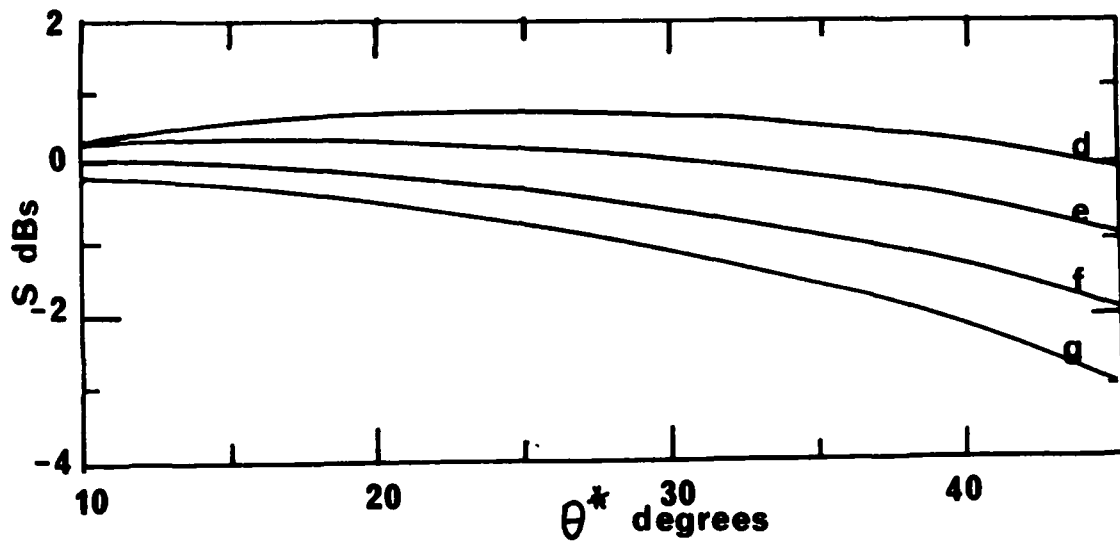


Fig.5.2-4:  $S$ , space attenuation factor for offset reflectors including an additional  $\frac{1}{2}(1 + \cos \theta^*)$  term from the feed expression. For the plane of symmetry (d)  $\theta_0 = 45^\circ$ , (e)  $\theta_0 = 40^\circ$  (f)  $\theta_0 = 35^\circ$ . For the plane of asymmetry curve g holds for any offset angle.

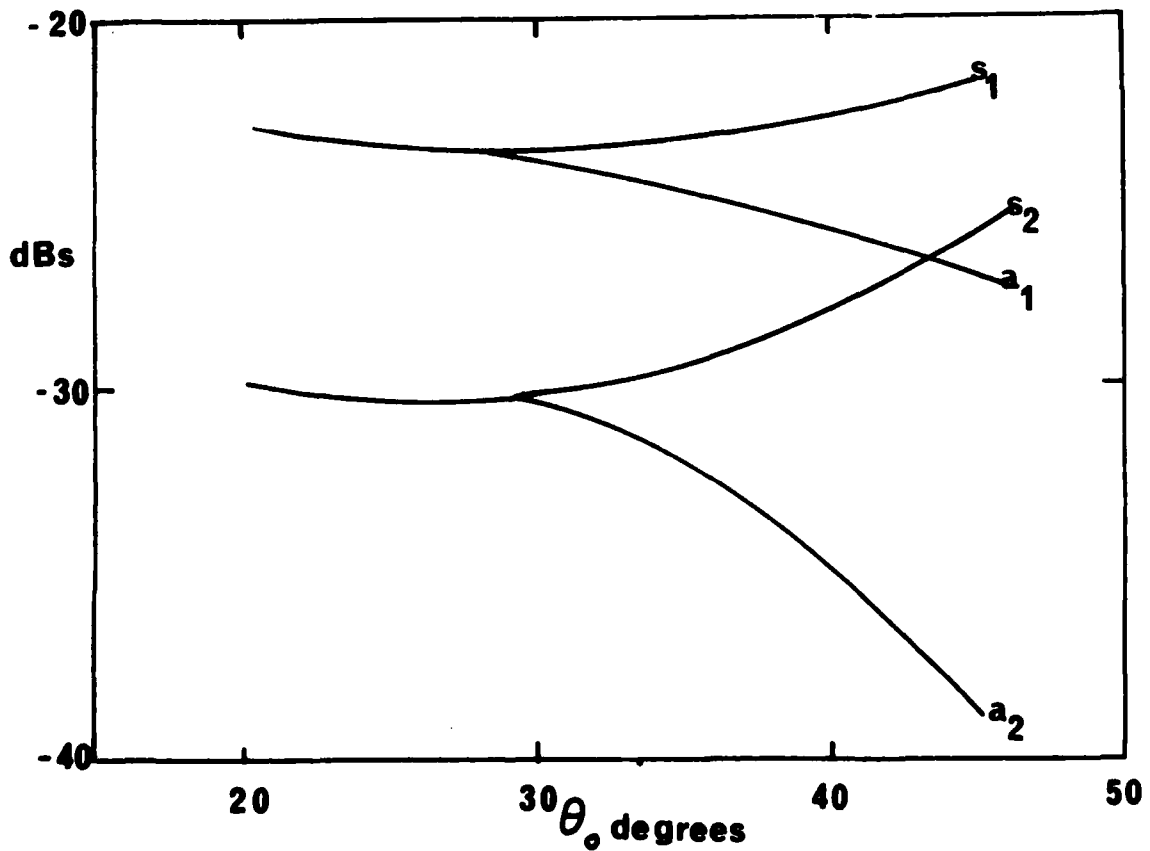


Fig.5.2-5: First sidelobe levels for offset reflectors with  $\theta^* = \theta_0 + 5$  degrees in the plane of symmetry (s) and the plane of

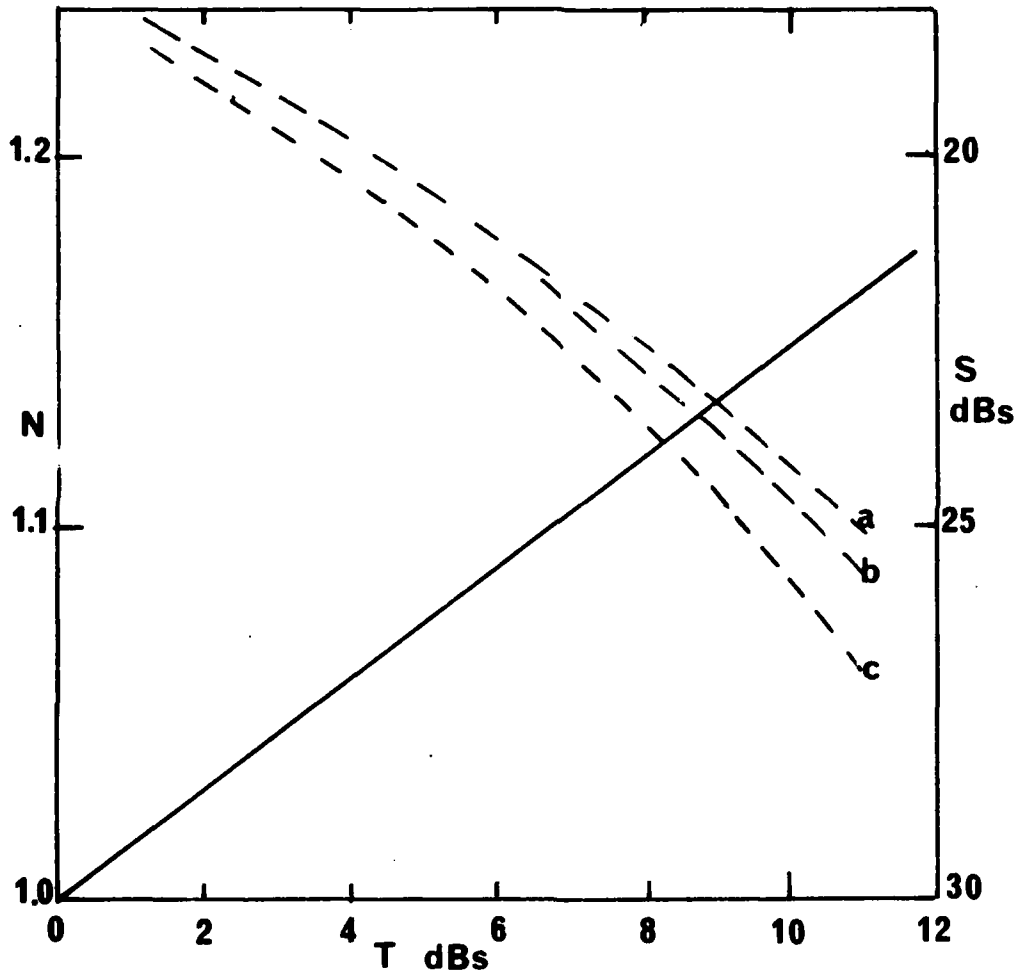


Fig.5.2-6: Beamwidth factor,  $N$ , (solid curve) and first sidelobe level in the asymmetric plane,  $S$  (dashed curve) as a function of taper,  $T$ , across the aperture.  $N$  is defined as  $\sin \psi = N\lambda/d$  where  $\psi$  is the half-power beamwidth,  $d$  is the diameter of the projected aperture. For the sidelobe level curves, a is for  $\theta^* = 10^\circ$ , b for  $\theta^* = 30^\circ$ , c for  $\theta^* = 45^\circ$ .

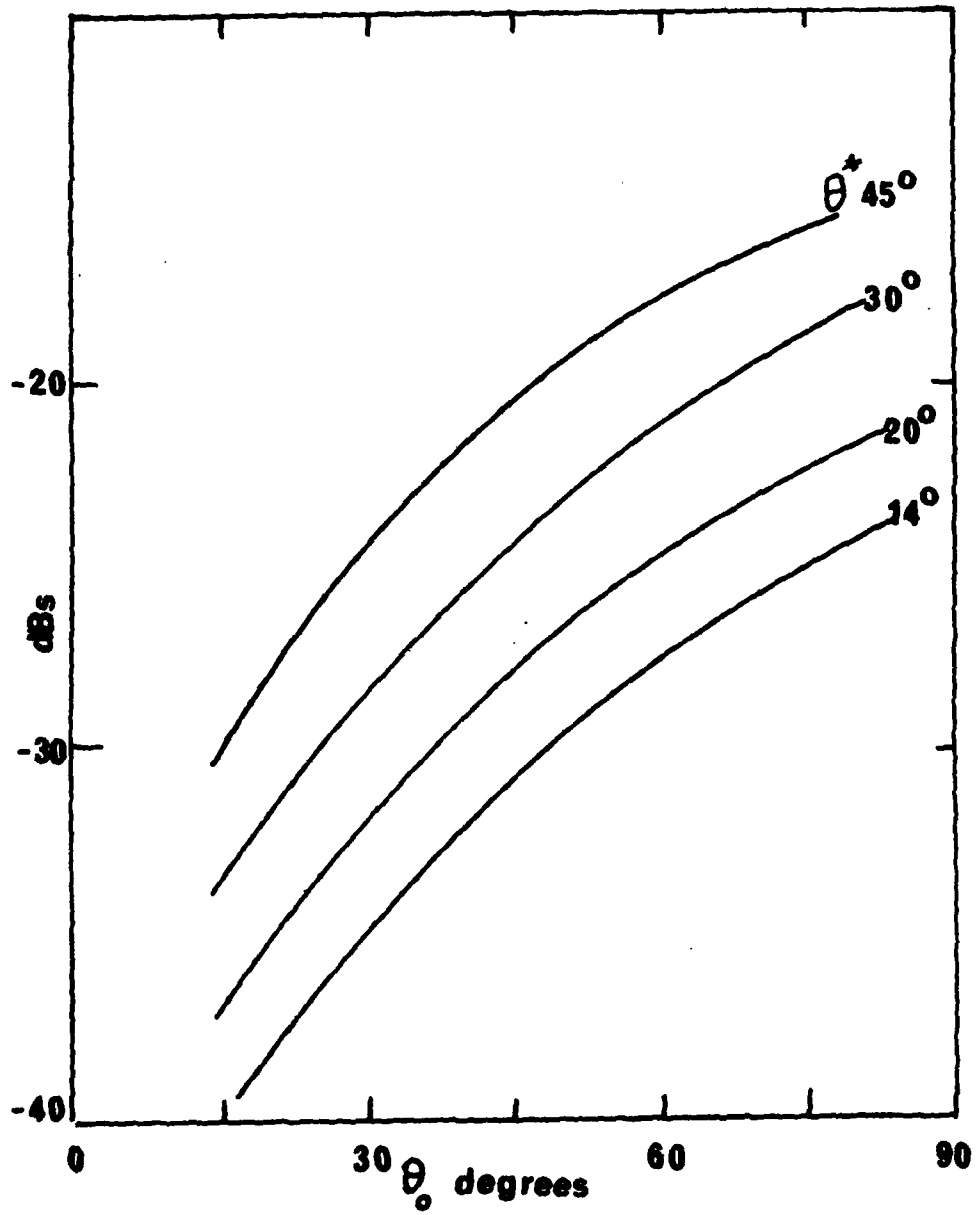


Fig.5.2-7: Peak cross-polarisation relative to the main beam, as a function of the parameters,  $\theta_0$  and  $\theta^*$ , of an offset reflector.

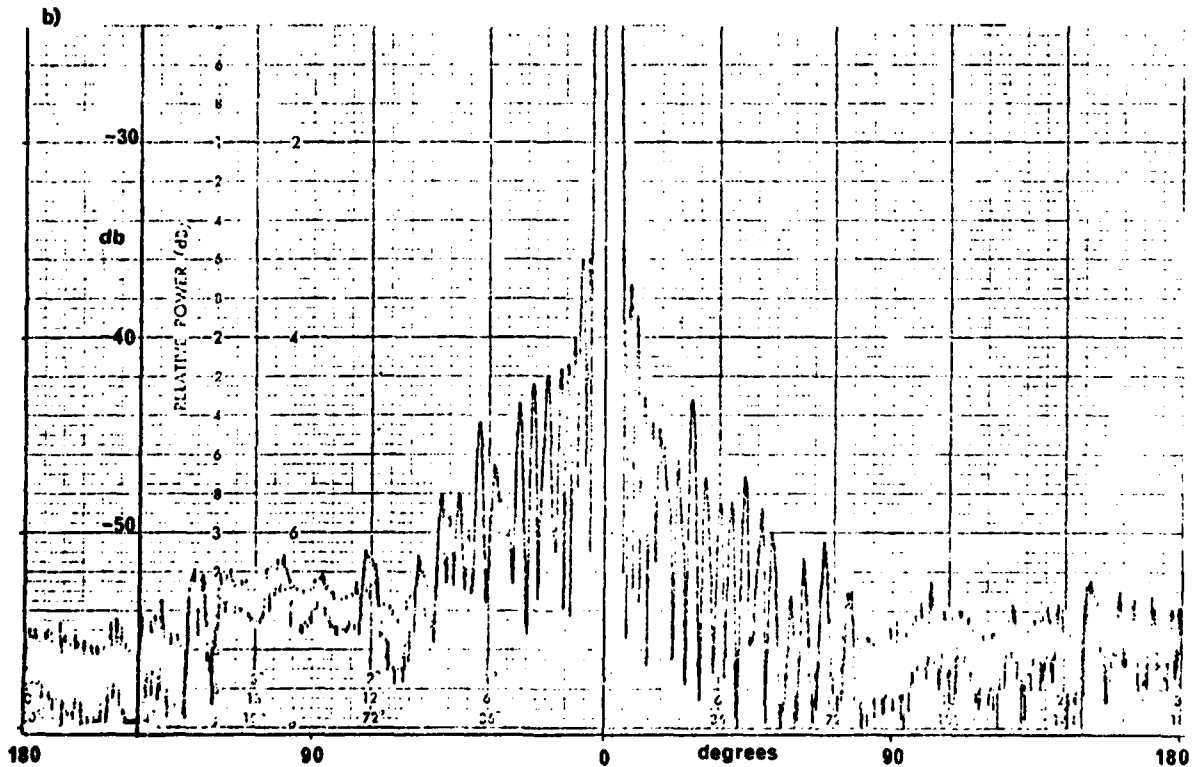
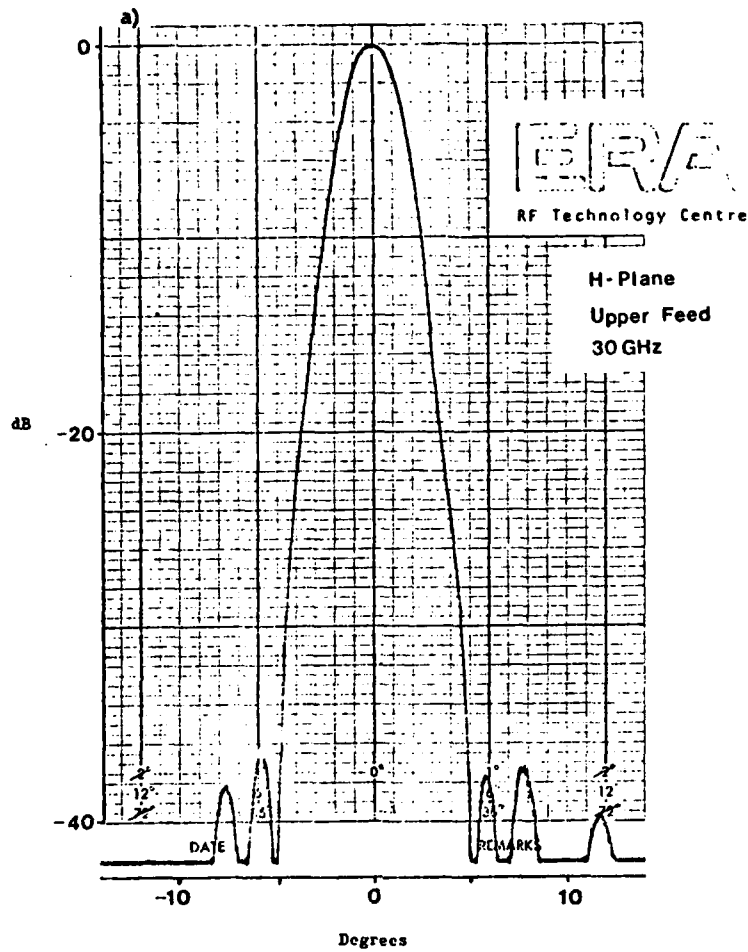


Fig.5.2-8: Radiation pattern of an elliptical offset reflector with half-power beamwidths of  $3^\circ \times 4^\circ$  at 30 GHz

### 5.3 Non-parabolic and Partially Parabolic Reflectors

#### 5.3.1 Spherical reflectors

The principal advantage of a spherical reflector is that it is capable of generating beams over a large angular space without change of beamshape, gain or sidelobe level. The geometry is illustrated in Fig.5.3-1. However, due to spherical aberration, the energy in the reflector focal region is defocused and for F/D ratios less than 0.6, an end-fire line feed must be used. This introduces support problems which increase the blockage. In addition, line feeds of the end-fire type have poor cross-polarisation properties. Simultaneous multiple-beam operation is of poor quality due to mutual coupling, interference and shadowing between adjacent line sources. For F/D ratios greater than 0.6, a horn or similar feed-element can be used at the 'optimum location'. The effective focal length is not R/2 as in an optical system, though the focal length does tend to R/2 as the F/D ratio increases (Fig.5.3-1).

The path length from the feed to the aperture plane by way of the reflecting surface is a function of  $\theta$  which gives rise to a phase error. This error increases slowly with  $\theta$  to a maximum value of  $\Delta_m$  at  $\theta = \theta_m$ ; thereafter the error goes rapidly to large negative values. The 'optimum location' is normally that feed position which will give zero phase error at  $\theta = \theta_A$ , the edge of the aperture.

The maximum phase error  $\Delta_m$  is given by:

$$\Delta_m = R \cos \theta_m \sin^4 \left( \frac{\theta_A}{2} \right) \quad (26)$$

where

$$\sec \theta_m = 1 + \sin^2 \left( \frac{\theta_A}{2} \right) \quad (27)$$

For small values of  $\theta_A$  where  $F/R \gtrsim 0.5$ ,  $\Delta_m$  decreases as  $(F/D)^{-4}$  thus confirming that a point source can be used for high F/D ratios ( $>0.5$ ). There is a limitation on the aperture diameter since the spherical phase error will reduce the directivity gain. The F/D ratio can be specified in terms of a gain loss for a given illuminated aperture diameter D (Fig.5.3-2) if the phase error is to be restricted to less than  $\pm\lambda/16$ ,  $D/\lambda$  must not exceed  $256 (F/D)^3$ . This will keep the forward loss below 0.2 dB. A

symmetric phase error of this type will have a deleterious effect on the sidelobe performance.

For example, a spherical antenna<sup>1</sup> with  $F/D = 0.78$  and a feed taper at the aperture edges of 15 dB, had first sidelobes of -18 dB which are worse than expected with such a taper. The antenna diameter was 150 wavelengths compared with the restriction of 121 wavelengths as given above. Clearly then, the sidelobe performance of a spherical reflector will be inferior to that of a prime-focus parabolic reflector of the same aperture, though the gain and backlobe should be comparable. The degrading factors are:

- the necessity for long  $F/D$  values, which increase the blockage by requiring a larger feed and stronger support structure.
- the inherent phase errors of a spherical reflector though these will be a function of  $F/D$  and  $D$ .

Hyde<sup>2</sup> has studied the focal plane region of a spherical reflector. Unlike a parabolic reflector, when a spherical reflector is illuminated with a plane wave of linear polarisation there is a large amount of power at the focal region in the orthogonal polarisation. Experimental probing of a spherical reflector produces results agreeing well with his predictions and we must conclude that a spherical reflector has a large amount of inherent cross-polarisation. The feed element performance and the presence of support struts will also degrade the cross-polarisation performance which is therefore likely to be inferior to that of a prime focus reflector.

A dual spherical reflector system can also be used<sup>3,4</sup>. For multiple-beam use, a spherical sub-reflector must be used since otherwise the off-axis beams will not be properly reflected. For a single beam, a shaped reflector can be used giving performance similar to a Cassegrain antenna. This spherical dual reflector will suffer from all the defects of a Cassegrain, with the additional defect of stringent relative positioning of sub-reflector vis-a-vis the main reflector since the phase corrections are so much greater. (The spherical aberration can in theory be entirely removed). The performance of such an antenna deteriorates badly off-axis and there is little point in using it in preference to a Cassegrain. Measurements using a Gregorian corrector<sup>5</sup> of 12 wavelengths diameter with a spherical reflector of diameter 94.5 wavelengths ( $F/D = 0.5$ ) gave first sidelobes of -11 to -12 dB at 9.3 GHz. Lower sidelobes

are difficult to achieve with this system as the geometry required to correct for the spherical aberration causes a high inverse illumination taper, in this case +9 dB.

The feed could be replaced by a small array of feed elements which could correct for the phase errors. For a prime focus system the blockage would be unacceptable and for a dual reflector system there appears to be no advantage over a Cassegrain axisymmetric reflector.

Should multiple-beam performance be required, the dual spherical reflector using a spherical sub-reflector will give performance unchanged over the required angular range (which must be less than  $120^\circ$ ). A phased array corrector might have to be larger than the minimum diameter of the sub-reflector, which will enhance the blockage. Also, the area of the antenna must increase with increasing angular range as each beam uses a different portion of the reflecting surface. This may result in off-axis beam degradation due to the aperture illumination being asymmetric for the outer beams.

### 5.3.2 Parabolic-cylinder reflectors

A reflector antenna can take the form of a cylinder which has its semi-circular section replaced by a parabolic one. The parabolic-cylinder reflector can be fed by a line feed, of length  $L$ , which will itself produce a cylindrical wavefront. On reflection, this will become a plane wave, provided that the reflector is in the near-field of the line source. If  $\rho_0$  is the distance between the edge of the reflector and the focal line,  $\rho_0$  must be less than  $\frac{L^2}{\lambda}$  in order for the line feed to give a cylindrical rather than spherical wavefront and so  $L \gg \lambda$  (Ref.1).

Often a relatively small value of  $F/D$  is used to avoid excessive feed blockage which is higher than that encountered in a paraboloid. The use of a small  $F/D$  ratio also avoids the large support structure which becomes necessary with a high  $F/D$  reflector. However, the feed dimensions become relatively large when a large illumination taper is required. The major difficulty with cylindrical reflectors is that the gain of the feed and the reflector are not sufficiently different to reduce spillover sidelobes much below -20 dB in the plane perpendicular to the cylinder. This is particularly true when the electric vector is at right angles to the cylinder axis. If the electric vector is parallel to the cylinder axis,

these sidelobes can be reduced below  $-25$  dB. Aperture efficiencies realisable with parabolic cylinder antennas are high (65%-70%) but backlobes are poor since the feed gain is high.

The effect of blockage has not been discussed but clearly the antenna sidelobe performance will be degraded by blocking and such an antenna is not particularly useful for low sidelobe applications.

The blockage problem can be alleviated by the use of an offset parabolic-cylinder reflector (see Section 5.2). This configuration has been examined by Adata and Rudge<sup>3</sup>. Efficiencies greater than 70% can be realised with this arrangement and sidelobe levels can be kept below  $-20$  dB by using a  $-10$  dB taper across the reflector. A slight widening of the main beam below the  $-20$  dB level can be attributed to the differential taper between the two opposite edges of the reflector. In the orthogonal plane, the line feed may be given a suitable taper to give a low sidelobe level.

*If a cylindrical reflector is fed by a point source the reflected wave is a cylinder with its axis perpendicular to the cylinder's axis. Epis and Watkins<sup>4</sup> used a point feed (a conical horn offset along the focal line) to give a circular beam whose patterns were constant between 16 and 28 GHz. One of the points emphasised by these authors is that the VSWR was less than 1.2 over the whole range whereas a symmetric parabolic cylinder has a rather poor VSWR performance due to radiation reflected back into the feed.*

A further extension of this property is to use the front feed plus cylindrical reflector as a feed for a second reflector<sup>5,6</sup> but in no case were the reported sidelobes better than  $-25$  dB.

The offset parabolic-cylinder antenna is very useful as a beam scanning antenna since the beam maintains its properties and high efficiency<sup>3</sup> over a large scan angle. A phased linear array is a suitable feed for such an antenna. It also has the property that the reflector does not introduce further cross-polarisation and the main design onus for this parameter falls on the performance of the feed array.

The backlobe and spillover lobe will be larger than for a paraboloidal reflector, since the feed again is larger. Tunnel shrouds and absorber might reduce these spurious lobes by as much as 15 dB, but the performance in this respect is still only moderate.

Although the sidelobe levels achieved have not been better than -25 dB (Refs.5,6,7,8), there seems no reason why lower levels of first sidelobe should not be achieved by appropriate tapering<sup>3</sup>. Possibly the high spillover lobe has discouraged designers from aiming at lower sidelobe levels.

### 5.3.3 Parabolic-torus reflector

This reflector is fundamentally a wide-angle scanning antenna where, as in the spherical antenna, the beam is unchanged with scan angle. The parabolic torus is formed by rotating a vertical parabola about a vertical axis positioned a distance  $R$  from the vertex. The geometry is illustrated in Fig.5.3-3. By moving the feed in an arc, radius  $\rho_1$  about the same vertical axis the beam can be scanned over large angles. ( $\rho_1 + F = R$ ).

For low sidelobe applications the offset form of the parabolic torus offers obvious advantages in avoiding aperture blocking effects. The torus is a parabola in any plane section through the vertical rotation axis, and has the appropriate focal length,  $F$ , of the generating curve. In the horizontal plane, the section is a circle which will focus at a distance of half the radius in that plane. The focal length,  $F$ , of the parabola must be chosen to have some suitable compromise value and values of  $F/R$  ranging from 0.45 to 0.5 appear in the literature<sup>2,3,4</sup>. This compromise implies that there are residual phase errors.

The residual phase errors are responsible for the typical triangular shape of a torus radiation-pattern and the widening of the main beam below the -12 dB contour. Sidelobes in the principal planes are less than -20 dB but in the  $45^\circ$  plane are -14 to -15 dB. The actual values of the phase error are proportional to the antenna dimensions so that  $F/D$  must increase as  $D$  increases. There is an upper limit to  $D$  which varies according to the definition of what is acceptable. At 100 wavelengths, the sidelobes have not degraded beyond those levels quoted above.

Various attempts have been made to reduce the effect of the phase errors. Peeler and Archer<sup>5</sup> found that an alternative generating curve of elliptical form could be used which gives zero phase error along planes through the rotation axis and at  $\pm 10^\circ$  to the symmetry axis. The sidelobes in the  $45^\circ$  plane were reduced to below -18.5 dB.

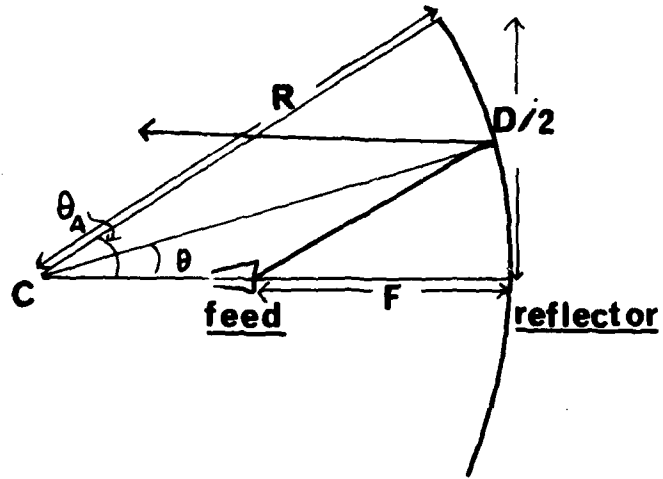


Fig.5.3-1: Geometry of spherical reflector.

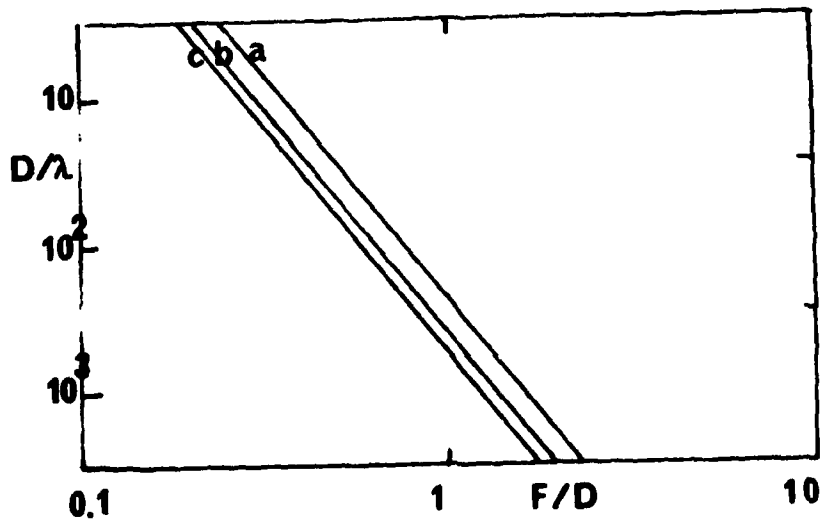


Fig.5.3-2: Limits to spherical reflector aperture,  $D/\lambda$ , set by the  $F/D$  ratio and three values of aperture efficiency loss, (a) 5% (b) 10% (c) 15%.

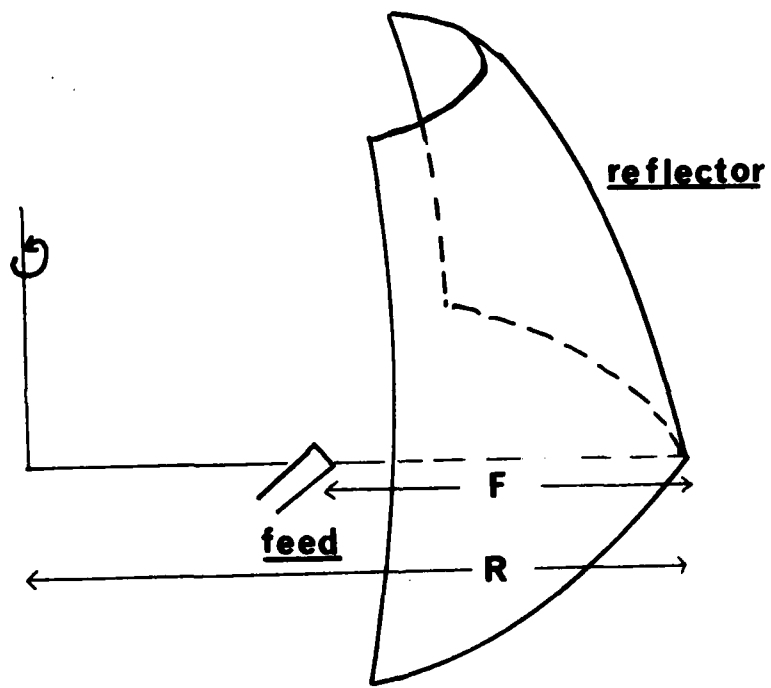


Fig.5.3-3: The Torus reflector.

Another attempt to reduce the phase-error effect<sup>6</sup> was based upon the use of a single large feed-horn flanked by two smaller elements, which were fed through a phasing network. The radiation from this structure was adjusted such that the phase front formed across the reflector by the feed unit cancelled the inherent phase errors of the torus. All sidelobes were reduced to below -22 dB.

The backlobe and spillover lobe of the torus may be estimated in the same way as for a paraboloid reflector and are likely to be of the same order as those for paraboloids of similar focal lengths and diameters.

Clearly this reflector has problems with close-in sidelobes and will never approach levels of -40 dB with reasonable F/D ratios. As an example, for  $F/D = 2.5$  the phase error varies more than  $\pm 2\pi 10^{-3D/\lambda}$  radians over the antenna aperture. At  $F/D = 1.0$ , the phase error variation is 30 times greater (see also Ref.7).

In its favour, however, it must be said that the parabolic torus is an excellent scanning antenna and will scan over  $120^\circ$  without serious degradation in the radiation pattern.

## 5.4 Lens Antennas\*

### 5.4.1 Discussion

A useful discussion of the practical implications of lens theory is given by Silver<sup>1</sup>. Although there is a large amount of more recent literature, most published work has concentrated on the implementation of lens systems and not particularly on advancements in the theory, although a recent dissertation on theory has been given by Brown<sup>2</sup>.

A microwave lens serves the same function as an optical lens in that it collimates the energy and thus modifies the radiated phase front. It is often used in the aperture of a horn to correct a spherical phase-front and can thereby lead to a substantial decrease in the length of the horn. It can be used to produce shaped beams in addition to pencil beams and can perform most of the functions of a reflector with the advantage of no blockage and less stringent surface and positioning tolerances.

If utilised to provide low sidelobe levels, a lens would be fed by a suitable primary-feed, providing a circularly symmetric illumination.

(Fig.5.4-1). The aperture field on the far side of the lens from the feed would then be tapered by the sum of the feed taper and the taper introduced by the curvature of the lens itself.

If  $P(\theta)$  is the power radiated per unit solid angle from the feed horn, at an angle  $\theta$  to the axis then:

$$P(r) r dr = P(\theta) \sin \theta d\theta \quad (28)$$

where  $P(r)$  is the power per unit area in the lens aperture at a distance  $r$  from the axis. This ignores transmission losses through the lens, which for a dielectric are greater on axis than at the periphery, and also losses due to reflection at the refracting surface. The differential  $\frac{d\theta}{dr}$  is a function of lens geometry<sup>1</sup> and can add to, or subtract from, the illumination taper depending on the precise shape of lens chosen.

Summarising, therefore, the plano-hyperbolic lens will increase the edge taper by several decibels; the two-surface lens, with one surface spherically centred on the focus, will decrease the taper, again by several decibels; while the two-surface lens, which gives refraction at both surfaces, may be of either type, and the value of  $\frac{d\theta}{dr}$  may be used to determine the surface equations of the lens.

The first lens type referred to above is much used in conjunction with shortened horns to improve their characteristics. The last type, though it is by far the most difficult to manufacture, is the most popular because it allows most freedom in design. For instance, it is possible to design such a lens with much better scanning properties than an axisymmetric reflector of the same  $F/D$  ratio<sup>4</sup>. A lens with two refracting surfaces has considerable advantages in matching since a lens with one refracting surface will throw back a considerable amount of power into the feed.

Lenses are generally used for scanning or multiple beam systems and therefore  $F/D$  ratios of around unity are used. Gain loss and coma lobe for off-axis positions in a lens optimised for on-axis performance are the same as for an equivalent reflector (i.e., see Section 5.1.4). Axial displacements tend to be less critical with the lens since the large focal-length-to-diameter ratio of a practical lens makes it less sensitive in this respect.

Surface tolerances are also less stringent with a lens, since the rms errors in each surface are likely to be independent and there is also a reduction in effect due to the dielectric constant. If the rms surface error in a reflector is  $\delta$ , then for the same degradation in performance the rms surface tolerances for a lens can be  $\frac{2\delta}{\sqrt{2}|\sqrt{\epsilon_r}-1|}$  where  $\epsilon_r$  is the relative dielectric constant.

There are two types of lens which are of particular interest in antenna work; the solid 'dielectric' type, with relative dielectric constant greater than unity and the 'waveguide', or 'parallel plate' type, where the effective dielectric constant is less than unity. Either class may also include artificial dielectrics<sup>2,3</sup>. The difference in sidelobe performance is not notable and similar problems arise, in that for a large aperture diameter the mass is often high. Also, the insertion loss tends to be high and in some cases, the loss due to mismatch may also be significant.

The mass of the lens may be considerably decreased by 'zoning'<sup>1,2,4</sup>. In this process, rings of material, which are multiples of  $\lambda/|\sqrt{\epsilon_r}-1|$ , are removed from the lens. This procedure has the disadvantage that the steps in the lens surface will scatter radiation at wide-angles from the boresight<sup>5</sup>. An increase in cross-polarised radiation is also likely. Zoning tends to affect off axis scanned beams to a greater extent than the boresight beam. It does also improve the bandwidth to about 10% for a waveguide lens. For a dielectric lens, however, the bandwidth has been quoted as  $\frac{25}{N}$  %, where N is the number of zones. A large F/D ratio will decrease the number of zones since the lens will be less thick, and this will effectively increase the bandwidth. However, for a given F/D, the zoned bandwidth will decrease with aperture size. It should be noted in this context that reflectors do not have this limitation and in the case of a reflector the bandwidth is likely to be set by the primary feed.

The insertion loss of a dielectric lens will depend on the loss tangent of the dielectric itself, and may be as much as 1 dB. The variation in insertion loss, across the aperture of a zoned lens designed for low sidelobe levels, will cause amplitude ripples in the aperture field, which will lead to ill-defined nulls and degraded sidelobes. The effect acts as a form of aperture blockage<sup>5</sup>.

A serious problem is that of matching the lens if one surface is non-refracting. This can be controlled by quarter-wave matching<sup>6,7</sup> though problems arise when two orthogonal linear polarisations are required as the matching will have to be a compromise. If, however, only one linear polarisation is required, the VSWR can be reduced from 1.5 to 1.25<sup>9</sup> over 35-40 GHz though spot values approach 1.05. Several methods are available which all depend on surfacing the lens with a quarter wavelength thickness of a material of dielectric constant  $\sqrt{\epsilon_0 \epsilon_r}$  where  $\epsilon_r$  and  $\epsilon_0$  are respectively the dielectric constants of the lens and the medium it is immersed in. This can be achieved by the use of a surface layer of a second pure dielectric or by cutting grooves one quarter wavelength deep in the surface<sup>6</sup>.

The spillover lobe for a lens antenna is determined exactly as for a reflector though it can be eliminated completely by inserting a conical shroud lined with absorber between the focal point and the lens. The spillover power is thereby absorbed rather than radiated, and no reduction in efficiency need be suffered. An additional loss in a lens, when compared with a reflector, is the insertion loss of the lens itself. This is a function of the dielectric loss tangent, the frequency and the lens thickness. (Values vary and can be up to 2 dB).

Theoretical predictions of lens behaviour are rare and no thorough treatment of far-out radiation appears to have been published. Since the feed radiation is refracted and scattered from the rim of the lens, the backlobe must be considerably lower than that for a reflector, but little relevant practical information has been found in the literature.

#### 5.4.2 Examples of lens performance

Table 5.4.1 gives examples of performance which have appeared in the literature. The information is regrettably sparse though from Mayhan's work<sup>13,14</sup>, lens antennas can give excellent performance.

#### 5.4.3 Conclusions

The major disadvantages of lens antennas are the mass and cost of manufacture. Although the mass may be decreased by zoning techniques, this process degrades the radiation performance and increases the manufacturing difficulties. Small aperture lenses are very useful since their far-out sidelobes are eliminated by the use of a shroud, but the matching

**Table 5.4.1**  
Details of the performance of constructed lens antennas

Lens type	Dielectric plano-convex	Zoned waveguide 2-surface	Artificial dielectric plano-convex	Artificial dielectric plano-convex	Zoned bifocal lens	Dielectric plano-convex**	Dielectric plano-convex**	Dielectric plano-convex
Frequency (GHz)	35	X band	3	4.2	35	61	37	60
Bandwidth (%)		10		12.5				2
Aperture ( $\lambda$ )	25.5	23	3.5	24	50	88	43.5	27
Taper (dB)	-24	-5.2				-18		-20
Predicted near-in sidelobe peak (dB)	-40		-26			-40		
Achieved near-in sidelobe peak (dB)	-41	-20	-26	<-35	<-32	-32	-32	-27
Aperture efficiency (%)	26	32		60	37			
Total losses (dB)				<0.25		0.5		
Surface accuracy (nm)	0.01							
VSWR				1.02				
Far-out sidelobes		-30*	<-30			<-50	<-52	
Dielectric constant ( $\epsilon_r$ )	2.46	0.42	1.8	2.25	2.56	2.53	2.53	2.53
Cross-polarisation (dB)	-29	-26						
F/D	0.41	1(7)		0.83	0.96	0.83	0.83	1.2
Half-power beamwidth (degrees)	2	3.1	21		1.3	1.4	2.8	-4
Reference	10	4,5	11	3	12	13	14	7

\* due to zoning  
\*\* plus shroud; backlobes are <-60 dB

difficulties require that either a lens with two refracting surfaces is used (which is more expensive than a plano-convex lens) or that special matching techniques be employed, which again increase the cost. In any case, the bandwidth is limited by the lens itself and values of more than 10% are rare. The zoning of a lens required for apertures greater than  $15 \lambda$  will have a deleterious effect on the cross-polarisation values as well as the far-out sidelobes.

The major application of large aperture lenses is to the field of multiple beam antennas where the long F/D and total lack of blockage, even when many feeds or even a large phased array feed are employed, become positive advantages. The ability of the lens with two refracting surface to scan over wide angles with less degradation than the equivalent reflector is also a positive advantage.

However, the far-out and backlobe performance of a lens system does not appear to have received much attention in the published literature.

Hence, although a lens avoids aperture blockage effects, and thus, in principle, offers good sidelobe suppression properties, its practical potential is somewhat less attractive. The cross-polar performance of lens antennas also remains largely unknown and historically the lens antenna has found comparatively few applications when compared to the ubiquitous parabolic reflector.

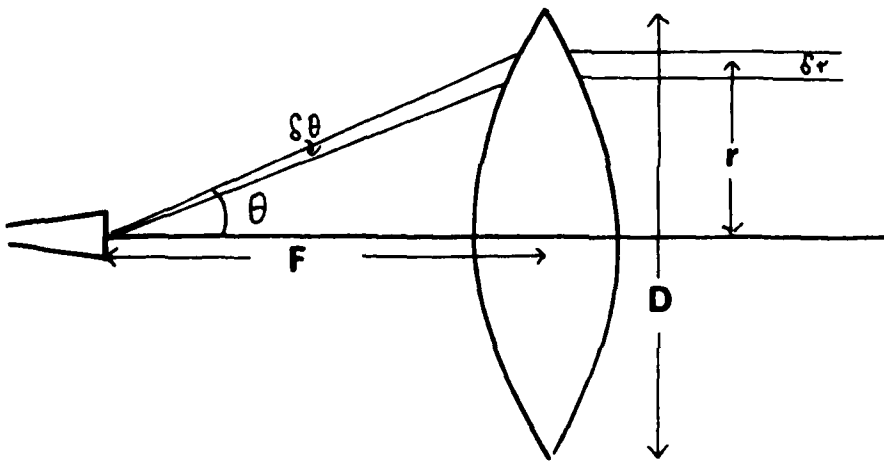


Fig.5.4-1: Lens geometry. A dielectric lens is shown.

## 5.5 Array Antennas

When a number of small radiating elements are combined to produce an overall radiation-field, the resultant antenna is described as an 'array'. The array can take a wide variety of geometries, including planar, cylindrical, spherical or conical and have either one fixed beam or, at the other extreme, a number of beams electrically scanned over a large volume. They have been used for many applications from spaceborne communication antennas to missile search radars<sup>1,2</sup> and have been excluded from many more on the basis of their high cost of implementation.

Because there are many controllable elements present, an array antenna, in principle, gives more freedom to the designer to shape the characteristics of the illumination function and much lower sidelobes should be achievable. In practice, -25 dB is readily (and frequently) achieved while near-in sidelobes of -40 dB are rare. Section 5.5.1 deals with the theoretical drawbacks of producing an array with good sidelobe suppression. This includes the effects of tolerance errors. Subsequent sections deal with examples of specific array types with emphasis on any fundamental bar to achieving low sidelobes.

### 5.5.1 Array theory

#### (i) Choice of illumination distribution

Fundamental theory is covered by texts in Refs.3,4,5. It has already been pointed out (Section 2.3) that cosine-on-a-pedestal distributions for sidelobe levels lower than -40 dB are sensitive to errors in the distribution and that Taylor and Chebyshev distributions are much less sensitive. Unlike a reflector, there is no reason why a non-monotonic distribution with slight illumination enhancement at the array edges should not be used. However, the use of  $N$  individual radiating elements only gives a step wise approximation to the desired illumination function. When  $N$  is very large, the approximation will be good and the step wise error function will be negligible. When  $N$  is small, the error function will dominate and will be worse for any given value of  $N$  as the near-in sidelobe levels are lowered. Therefore a more tapered illumination will be required. For example, Josefsson<sup>6</sup> found that for a circular array of 52 elements (approximately  $7 \times 7$ ) a Chebyshev distribution designed for -35 dB sidelobes could only achieve levels of the order of -30 dB.

An illumination suitable (in theory) for -40 dB sidelobes was found necessary to achieve levels of -35 dB. This procedure obviously results in lower aperture efficiency. On the other hand, a linear array of 49 elements<sup>7</sup> produced a radiation pattern in excellent agreement with the design level of -35 dB.

An alternative method of tapering the illumination across an array is to use an element density taper where elements are removed, allowing the average number of elements per unit area to decrease towards the periphery of the array. This density tapering must be random to avoid additional grating lobe problems. All the remaining elements are then fed uniformly. The beamwidth will be that of a conventional array<sup>11</sup>. The far-out sidelobes do deteriorate and a computed example for a 50 wavelength aperture had peak far-out sidelobes of -32 dB, about 25 dB worse than the theoretical radiation-pattern for a fully-filled, but amplitude tapered, array. An example of density tapering at 12 MHz (Ref.19) which also included some resistive tapering, had sidelobes in the -40 to -50 dB range spread out over much of the forward hemisphere.

Various methods are available to produce a theoretical synthesis of an antenna illumination<sup>4</sup>. James<sup>21</sup> discusses a computer programme which chooses the phases and amplitudes for the elements of an array when two radiation-pattern parameters have been specified. The two parameters are the half-power beamwidth, and the width of the main beam at the level where it equals the peak of the first sidelobe. Other programmes have dealt with the reduction of the number of array-elements<sup>11</sup> or of phase-shifters<sup>22</sup>. All of these techniques resulted in degraded sidelobe performance.

#### (ii) Grating lobes

Though spillover and backlobes are absent from most array types, grating lobes which occur in the near and far-out regions must be avoided for low sidelobe performance. To reduce the grating lobe levels below -40 dB requires that the first grating lobe is either outside the range of real angles, or appears at an angle where the individual radiating-element pattern is down to at least -40 dB. The actual value of the maximum permissible inter-element spacing, which controls the grating lobe angle, depends on whether or not the array is to be used for wide angle-scanning. The larger the scan angle, the closer the spacing. In the limit the

inter-element spacing must be reduced to 0.5 wavelengths. However at wide angles from boresight, the array aperture is foreshortened with a resultant drop in gain and if the maximum scan-angle is restricted to  $\pm 45^\circ$ , the required element spacing will be 0.6 wavelengths<sup>9</sup> (Fig.5.5-3). This spacing assumes a regular rectangular grid of radiating elements. The use of such a small element spacing does have disadvantages. The polarisation purity of an array is determined by the characteristics of the individual array element. Were it feasible, an element of aperture 3-4 wavelengths would offer advantages because such a size would reduce mutual coupling to a low level and, for rectangular waveguide elements, cross-polarisation degradation would also be small. It is known<sup>10</sup> that mutual coupling can have deleterious effects on polarisation performance and for smaller (practical) array elements this can be a problem.

An alternative method of reducing grating lobes while increasing the size and spacing of the array elements involves arranging large elements in a two dimensional lattice with a variable spacing<sup>11</sup>. Figure 5.5-4 shows the permissible element area, as a function of the maximum scan-angle. A rectangular lattice curve would lie below that of the triangular lattice. This figure also shows that the aperiodic circular arrangement is advantageous for small scan angles, but unfortunately it produces vestigial grating lobes within the real range of spatial angles (Fig.5.5-5). Not only is this unsatisfactory but such a two-dimensional array would be difficult to use with a tapered illumination due to the complexities of the feed network.

A method limited in its application but which does remove grating lobes is to add a series of layers of dielectrics to the top of a planar array<sup>23</sup>. This was developed for a limited-scan antenna comprised of large aperture elements, where grating lobes typically arise. However, this results in a narrow band device and is likely to suppress the first grating lobe and leave others unaltered.

### (iii) Mutual coupling

Apart from its degrading effects on the polarisation performance, mutual coupling can be accommodated and allowed for by numerical techniques during the design of the array<sup>7,12,13</sup>. Edge effects can also be avoided

by the use of dummy elements at the array edge<sup>5,13</sup>. A more difficult effect to eradicate is 'reverse coupling'<sup>13</sup> in which power is reflected within the feed and transferred to other feed lines, thence to other feed elements. This results in a significant degradation in sidelobe performance and isolated sidelobes rise above design levels. If the array feed network is constructed in a regular format, this 'reverse coupling' gives errors which are more correlated than random and therefore sharply frequency-dependent. It can be eliminated completely by using a feed network containing directional couplers.

(iv) Amplitude and phase errors

Random errors in amplitude and phase are inherently more likely to occur in an antenna system where large numbers of small units are used and the topic has been studied by many workers.<sup>3,4,13,14</sup> There is a large body of experimental evidence available to supplement this. Rondinelli<sup>14</sup> treats the problem of loss of gain and beam pointing errors, but in the present context these will be neglected in comparison with the effect of errors on the near-in sidelobes. Elliot<sup>3</sup> expresses the mean rise in sidelobe level as:

$$\Delta < 10 \log_{10} \left\{ 1 + 10^{S/10} \left[ k^2 (\sigma_1^2 + 2\sigma_2^2) + 2f^2 \right] \left( \frac{\pi}{D} \right) \right\} \quad (29)$$

where

$\sigma_1$  = rms phase variation due to constructional errors

and

$\sigma_2$  = rms phase variation due to alignment errors

$f$  = normalised rms current variation

$S$  = design sidelobe level in dB (expressed positively)

$k = 2\pi/\lambda$

$D$  = directivity of the array

Inspection of this equation shows that as the array size increases ( $D$  increasing)  $\Delta$  decreases; on the other hand  $\Delta$  increases as the design sidelobe level is lowered (Fig.5.5-6).

Gladman<sup>13</sup> discusses the error sidelobes (Fig.5.5-7) and the fall-off with angle. Again a large array can tolerate a larger error in phase and amplitude.

Mechanical errors generally result in irregular spacings in the array<sup>15</sup> and as such produce phase errors. The effects of displacement errors in a line-fed array, where each element is connected to the generator by a transmission line of unaltered length is shown in Fig.5.5-8. From a knowledge of the mean scattered field, the effects of these errors on the design radiation pattern may be calculated. An optically fed array, i.e., a two-dimensional array irradiated by a source gives a mean scattered field 6 dB lower than a line-fed array, and the reduction in gain is one quarter for the same positional error. To keep the scattered field below -40 dB, the error in spacing  $\frac{\delta\rho}{\lambda}$  must be less than 0.00275 ( $1^\circ$  of phase) and must be less than 0.01 for sidelobes of -30 dB ( $3.6^\circ$  of phase). ap Rhys<sup>16</sup> shows the radiation pattern for a Chebyshev distribution which should have led to sidelobes of -40 dB. Random phase errors having a peak value of  $5^\circ$  degraded the level to -33 dB. A further example, given by Imbriale<sup>17</sup>, is concerned with the degradation in sidelobes as progressively fewer bits are used when a digital phase-shift system is used to scan the beam (Table 5.5.1). The aperture taper remains constant.

Table 5.5.1

Sidelobe level of a 61 element phased array vs number of bits in the phase shifters when the beam is scanned to  $\pm 8.3^\circ$

Number of bits	Sidelobe level	Equivalent phase step (degrees)
Continuous (analogue)	-28.5	0
5 bit (digital)	-25.1	11.25
4 bit (digital)	-18.5	22.5
3 bit (digital)	-12.0	45.0

Another example is the RASSR (reliable advanced solid state radar) array<sup>18</sup> where the illumination was given a Taylor distribution aimed at first sidelobes of -45 dB. Due to the small number of elements (205) the first sidelobe would have been -37 dB but the rms phase and amplitude errors were  $19^\circ$  and 0.8 dB respectively, giving a final level for the near-in sidelobes of -30 dB.

As an example of what can be achieved with good design, Strider's planar array at 56 GHz may be cited<sup>20</sup>. The 10 element array had a Dolph-Chebyshev distribution designed to give first sidelobe level of -25 dB. The agreement between prediction and measurement is within 2 dB over the

first five sidelobes though the measured values are always greater (Fig.5.5-9). Other designs cited by the same author for less stringent sidelobes had better agreement. The positional tolerances were less than  $2^\circ$  rms which fits reasonably well with data from Fig.5.5-8.

(v) Feed networks

An important part of an array is the feed network, which may fall into two basic categories, constrained feeds and optical feeds.

Constrained feeds employ transmission lines between the central input and each element of the array (Fig.5.5-10). Several designs are available<sup>24</sup>. Close control over the amplitude applied to each element is available but care must be taken to avoid multiple mismatches and the use of narrow band components. Directional couplers or similar junctions are essential in low sidelobe design to avoid the effects of 'reverse coupling'. Since the size and complexity of the network increases with the array aperture, the insertion loss also increases. When the aperture and the number of elements becomes large, a space feed<sup>24</sup> may be more economical in mass, cost and insertion loss (Fig.5.5-11). It may be either a reflect-array or of the transmission lens type. The primary-feed is responsible for the array illumination and since this cannot reproduce the non-monotonic illumination tapers required by Taylor or Chebyshev functions, the first sidelobes are at best -40 dB. This may be improved by employing a complex of several feed horns at the primary focus though this requires a treatment of near-field diffraction. Care must be taken not to increase the spillover loss. The spillover lobe is that part of the primary feed radiation which escapes past the array edge and its size may be calculated exactly as in the reflector case. For small apertures, the level is high as is the associated spillover loss. This is likely to make the total loss greater than the insertion loss for a constrained feed. The lower limit in aperture diameter for an optical feed is difficult to specify but is around 15-20 wavelengths. The spillover lobe can be eliminated by the use of an absorber lined cone between focus and array. However, the amplitude distribution may be altered by this. The forward loss due to spillover will be unchanged.

For reflect arrays there is the additional problem of blockage together with all the associated degradation (see Section 5.1).

One other problem arises with space feeds, that of volume occupied since  $F/D$  ratios of unity are generally employed. With a constrained feed, the depth occupied may be as little as 10% of the aperture diameter.

There are hybrid forms of feed network such as the Rotman lens and the R-2R lens which economise a little on occupied volume (see Section 5.5.3).

The final choice of network will depend on application, taking into account not only insertion loss and errors in the array but also mass, power and cost.

For a fixed beam system (which does not require phase shifters), the commonest network has been the constrained feed due to the economy in volume and construction but other types of network can be used (see Section 5.5.3).

If electronic scanning of the beams is required, then a variable phase shifter must be introduced behind each array element in the network (see Section 5.5.2). Each type of network has advantages and disadvantages. Table 5.5.2 lists some of these where low sidelobe performance is of major interest.

Table 5.5.2

Advantages and disadvantages of feed network types for very low sidelobe performance

Advantages	Disadvantages
<p><u>Constrained type</u></p> <p>Aperture illumination can be carefully tailored.</p> <p>Low volume. Suitable wide angle scanning.</p>	<p>Require <math>D &gt; 10 \lambda</math></p> <p>Matching important; Bandwidth important; Transmission losses high and increase with D.</p>
<p><u>Optical type</u></p> <p>Less susceptible to positioning errors than above. Transmission loss low.</p>	<p>Spillover loss 1-2 dB causes far-out sidelobes. Suitable for limited scan.</p> <p>High volume. Require <math>D &gt; 20 \lambda</math>. Reflect-array has blockage.</p> <p>Illumination not so amenable to adjustment.</p>
<p><u>Semi-constrained</u></p> <p>Transmission loss low. Wide angle scanning.</p>	<p>Illumination not so amenable to adjustment. Medium volume. <math>D &gt; 15 \lambda</math>.</p>

5.5.2 Phased arrays

In this sections we shall consider arrays where the beam is scanned by switching of phase-shifters. The problem of phase-shifter choice is beyond this report. insertion losses of 0.7-1.5 dB are common over the frequency range 5-50 GHz, though a recent development termed 'spiraphase' which is incorporated in a reflect array can give insertion losses of less than 0.5 dB at L band. The loss appears to be linear with frequency which is a disadvantage but further work in this element may improve its already good performance<sup>56</sup>.

Phased arrays may incorporate any of the feed network types discussed in Section 5.5.1. The present investigation is limited to linear or planar arrays for the following reasons.

Spherical or cylindrical arrays can scan a beam over  $360^\circ$  without change of electrical characteristics as the aperture is not foreshortened or changed in aspect relative to the radial boresight direction. A special switching network is required to scan the beam and the excitation amplitude on any individual element must also be altered. The amplitude taper across the active region is limited to a taper of -7 to -10 dB (Ref.27,28) in order to avoid the substantial errors in phase and amplitude of excitation which are involved in this switching process. First sidelobes are at best -22 dB for a spherical array. Because of the complex switching network, losses tend to be high at around 10 dB. Examples of such arrays are given by Provencher<sup>28</sup>.

If a cylindrical array of equally spaced elements is considered where half of the cylinder is energised simultaneously, the outer elements in the projected aperture will be more closely spaced<sup>29</sup> than the central elements. The resulting inverse taper has to be compensated. Compared with a planar array of the same aperture and sidelobe level, a cylindrical array will have a reduced efficiency since it will require a steeper taper. A spherical array will be even less efficient and a cylindrical array appears to be capable of slightly better performances than a spherical array. Near-in sidelobe levels of -25 to -30 dB have been achieved<sup>29,30,31</sup>.

Other conformal arrays such as those distributed round a conical surface have the same defects. For instance, an array distributed round a cone and having a taper of -20 dB had first sidelobe levels of -21 dB (Ref.32). The cross-polarisation varied in a complex way with scan angle and frequency. Peak values were approximately -22 dB (see also Ref.33).

An interesting exception is the Dome Antenna<sup>34</sup> where an electronically scanned planar array is combined with an optical type lens in the shape of an hemisphere of passive modules. Each module in the dome consists of a collector, a fixed phase delay and a radiator. It is possible to scan the beam to  $110^\circ$  off the boresight of the planar array. However, the illumination in the models so far constructed results in sidelobe suppression of only 18 to 20 dB. These values do not vary much with scan angle. It is not clear if the illumination could be more tapered to give better sidelobes. The Dome Antenna's great advantage as a wide scan angle device is that no switching network is involved and, therefore, errors

and insertion losses are smaller. It does appear to have a high level of spurious radiation (around -32 dB) over a large angular range,  $\geq 90^\circ$  from boresight. Measured average cross-polarisation was -37 dB.

Table 5.5.2 lists details of some planar arrays constructed with low sidelobes. The most detailed calculations of the losses<sup>37</sup> which are for a lens array breaks down the losses as 1 dB for each phase-shifter, 1 dB for microwave transmission losses and 2.4 dB for the combination of spillover loss, the effects of 3 bit phase shifting errors in amplitude and phase and also element mismatch.

The aperture efficiencies quoted are the antenna efficiency without losses due to phase-shifters or transmission lines. Low sidelobe level does not automatically correspond to low efficiency. On the other hand, system efficiencies are low at less than 50%. The major advantage of such phase-scanning arrays is that at wide angles off boresight, the degradation in performance is small though gain is reduced due to aperture foreshortening.

Any wide angle scanning array employing electronic phase-shifters has limited bandwidth<sup>5</sup> since such phase-shifters have constant value over the band while the amount of phase-shift required between elements for a fixed scan angle is a function of the wavelength. At  $45^\circ$  off boresight, the phase change is  $5.73^\circ$  for a 10% change in bandwidth. For low sidelobe design, this is not supportable; therefore for a sidelobe level of -40 dB and scanning to  $\pm 45^\circ$ , a 5% bandwidth would be the maximum. The use of time delays instead of phase-shifters would be required if the bandwidth were to be larger. These are inconvenient to use in large numbers and have high insertion losses. However a more usual requirement is an operational bandwidth of 10% with an instantaneous bandwidth of perhaps 1% in which case the phase settings can be altered to be suitable for the bandwidth in use.

Table 5.5.2

Details of constructed scanning arrays

Frequency (GHz)	9.5	16.5	-	19.35	9.3
Bandwidth (%)	8.5	6	-	1	
Array network type	Reflect array	Reflect array	Lens array	Waveguide slot	Waveguide slot
Scan angle (degs)	±65	±40	±45	±40	±45
Planar or linear	Planar	Planar	Planar	Linear	Linear
No. of beams	1	1	1(?)	1	1
Aperture (λ)	29	12	41	54	
No. of elements	2400	271	4300	103	
Element arrangement	Triangular	Triangular	Triangular	Linear	
Element spacing (λ)	0.61	0.7	0.676	0.52	
Taper (dB)	-14	-10	Taylor		-22
Predicted side-lobe (dB)	-25	-27	-34		-40
Achieved side-lobe (dB) bore-sight	-26	-27	-34	-25	-42
Achieved sidelobe (dB) at scan extremity	-23	-18	-28	-15	-38
Aperture efficiency (%)	46	40	43.7		51
Total efficiency (%)	37	25	-		25
Insertion loss (dB) total	1	<2	3.6	1.7	3
Phase-shifter (dB)	1	<2	1.2		
Network loss (dB)					
Cross-polarisation (dB)				-25	-25
Accuracy (rms)					
Amp (dB)					
Phase(degrees)		±8	±6		±3
No. of bits	2	Analogue	3		Analogue
VSWR	<1.2	<1.3	<1.3		
Far-out sidelobes	<-36	-33	<-40	>-30	<-50
At angle?(degrees)	>60	>60	>10	0-90	>±90
Half-power beamwidth (degs)	2.5	5.8	1.2	1.4	
Reference	35	36	37	38	12

Table 5.5.2 (Contd.)

Details of constructed scanning arrays

Frequency (GHz)	10(?)	9.2-9.5	55	3
Bandwidth (%)	?	3	10	11
Array network type	Divider network	IF manifold	Parallel plate lens	Lens & 32 element feed
Scan angle (degrees)	±47	±40	±60	
Planar or linear	Planar	Planar	Linear	
No. of beams	1(?)	1	1	
Aperture (λ)	?	24	48	
No. of elements	4000	824	84	
Element arrangement	Triangular	Triangular	Linear	
Element spacing (λ)	0.6	0.745	0.57	
Taper (dB)	Taylor	Taylor	-26.8	Taylor
Predicted sidelobe (dB)	-23	-45	-35 <sup>**</sup>	-36
Achieved sidelobe (dB)	-25	-38	-27	-35
Aperture efficiency (%)		64		70
Total efficiency (%)				
Insertion loss (dB) total				
Phase-shifter (dB)	1.5	<0.9		0.6
Network loss (dB)	0.2	small <sup>*</sup>		3.7
Cross-polarisation (dB)				
Accuracy (rms)				
Amp (dB)		±0.8		
Phase (degrees)	±5	±19		
No. of bits	5	4		5
VSWR	1.35	1.2	1.2	
Far-out sidelobes (dB)	<-50			
At angle? (degrees)	>±50			
Half-power beamwidth (degrees)		2.9	1.6	3.25
Reference	39	18	40	45

\* The network was at IF. The RF front ends had therefore to be stabilised in amplitude and phase.

\*\* All other sidelobe <-35 dB.

### 5.5.3 Fixed-beam arrays

There are some feed networks in which it is possible to produce simultaneous multiple beams with cross-overs at -4 dB. Such a feed network provides a series of uniform aperture distributions which are successively tilted so as to form beams displaced by one beamwidth<sup>41,42</sup>. The Butler matrix<sup>42</sup> requires a large number of directional couplers and phase-shifters and generally gives a uniform illumination across the array. If a tapered distribution is used, the beams are widened and no longer cross-over at 4 dB.

Stein<sup>43</sup> has dealt with the losses incurred in a passive array when several different illuminations are employed. For instance, a function of the form  $\left(1 - \left(\frac{r^2}{a^2}\right)^P\right)^P$ ,  $P = 1, 2$  or  $3$  for a circular aperture of radius  $a$  and radius variable  $r$ , reduces the antenna radiation efficiency by 10-30% depending on the number of beams. This is due entirely to beam coupling factors and the reduction in aperture efficiency due to using such a taper has still to be taken into account.

The transmission line losses increase with aperture size and number of beams as do the effects of any mis-matches and phase errors.

Other forms of passive array include the Luneberg lens which in its three dimensional form is too large and has an inverse illumination which cannot be adjusted, and various geodesic lens types which are a little smaller but have the same problem with illumination<sup>44</sup>. The two dimensional forms are more compact but the beam(s) may only be scanned in one plane.

There are also the Rotman lens and R-2R lens type<sup>45</sup>. Both of these are large in size. The Rotman lens is similar to the 2D Luneberg lens, while the R-2R lens is bulkier because it is a 3D structure. The Rotman lens consists of a parallel plate region fed by coaxial probes along two opposing faces and RF cables connect the output ports to the elements of the antenna array. Archer<sup>45</sup> used printed circuit techniques which reduced the lens size by  $\sqrt{\epsilon_r}$  ( $\epsilon_r$  is the relative dielectric constant of the board). Although there are no comments on the taper employed, side-lobes were about -22 dB and reduced below -34 dB by summing several beams. Beams could be formed over a cone of semiangle  $45^\circ$ .

Similarly an R-2R lens<sup>28</sup> has been quoted with sidelobes less than -30 dB at 3.2 GHz. Insertion losses have not been quoted for any of these designs. Most of the loss will be in the transmission lines rather than in the parallel plate regions. However, the junctions will be lossy and there will be some mutual coupling between probes. Archer<sup>45</sup> claims that, unlike the phased arrays of Section 5.5.2, the sidelobe performance does not fall off with increasing scan angle since there are no phase-shifters involved. The gain is of course still reduced by aperture foreshortening.

#### 5.5.4 Flat plate arrays

In an attempt to reduce the mass and volume of arrays, considerable attention has been given to flat-plate arrays which include stripline and similar types.

Several authors have dealt with the design of the element<sup>46-50</sup>. Many of these are arrayed in designs with poor sidelobes (of the order of -10 dB) but a few examples with sidelobes better than -20 dB are detailed in Table 5.5.3. Good reviews are given by Munson<sup>52</sup> and by Hall and James<sup>58</sup> who emphasise the need to over-design for good sidelobe performance.

A few general conclusions can be drawn from this limited sample:

- large aperture arrays have not been attempted, possibly for mechanical stability reasons.
- small apertures in microstrip can produce good performance equivalent to that generated by other methods.
- losses are not noticeably higher.
- scanning is rare and has been limited to one dimension and phase-shifters have been avoided, presumably because of integration problems.

It is also possible to construct a flat plate array from MILIC (Microwave Image Line for Integrated Circuits). An example will be discussed in the next section on frequency-scanned arrays.

#### 5.5.5 Frequency-scanned arrays

These antennas use a change in frequency to scan the array beam. The most convenient device for this is the use of transmission line in the network to provide a frequency sensitive phase-shift between elements.

Table 5.5.3

Details of constructed flatplate arrays

Frequency (GHz)	X band	L band	13.325
Bandwidth (%)	6	14	
Array network type	Constrained	Constrained	Constrained
Scan angle			None
Planar or linear	Planar	Linear	Planar
No. of beams	1	1(?)	4
Aperture ( $\lambda$ )	5.5		14
No. of elements	52	24	27x9
Element arrangement	Square	Linear	Square
Element spacing ( $\lambda$ )	0.69		0.5
Taper (dB)	Chebyshev		$\cos^2$
Predicted sidelobe (dB)	-40	-29.5	-25
Achieved sidelobe (dB)	-35	-25	-27
Aperture efficiency (%)	70		
Total efficiency (%)	45		50
Insertion loss total (dB)	2	0.65	
Phase-shifter loss (dB)	None	None	None
Network loss (dB)	2		0.75
Cross-polarisation (dB)			
Accuracy (rms)			
Amp (dB)	1		
Phase (degrees)	7		
No. of bits	-		
VSWR	<2.5		<1.2
Far-out sidelobes (dB)		<-30	
At angle?		>72	
Half-power beamwidth (degrees)	-12	3.2	
Reference	6	51	53
Sidelobes at extreme scan	-25*		

\* Mutual coupling is said to be responsible for some of this degradation (1-3 dB.)

Since there are no active phase-shifters, losses are reduced. Hilburn and Prestwood<sup>10</sup> studied a two dimensional array where each element (excited by a slotted line) was itself a slotted waveguide line. This paper contains considerable detail on optimum characteristics for the slots at various sidelobe levels with Chebyshev and Taylor distribution. A 400 element array for 28.5 GHz was designed for a Taylor 30 dB illumination function and achieved these levels while scanning  $17^\circ$  with a frequency range of 3.5 GHz. No cross-polarisation greater than -30 dB was observed.

An array reported by Kinsey and Horvath<sup>53a</sup> at 3.2 GHz had a Taylor excitation to achieve (successfully) -30 dB sidelobes out to a scan angle of  $30^\circ$ . Phase accuracy was held to  $2^\circ$ .

The disadvantage of these waveguide arrays when used for frequency scanning is their bulk and expense since the tolerances in slot positioning are very tight.

A planar array of MILIC rod antennas each coupled to a MILIC transmission line has been tested<sup>54,57</sup> and scans over  $\pm 20^\circ$  for a 10% bandwidth centred on 29.25 GHz. There are problems related to fabrication techniques but the mass and complexity of this array are significantly less than those of the slotted waveguide type.

These frequency scanned arrays have the advantage of dispensing with phase-shifters, thus insertion loss is reduced and phase errors also. The only errors left are amplitude errors and relative positioning errors in the array elements. Serious degradation can occur if the frequency is scanned at too high a speed<sup>55</sup>.

#### 5.5.6 Conclusions: Array antennas

For phased arrays, low sidelobe design, goals can be closely approached at angles near boresight. At wider angles, the phase errors may build up to give poor performance in narrow angular ranges. At extreme angles, the effects of amplitude and phase errors, etc., degrade the levels by several decibels while the gain is reduced by foreshortening. The most serious disadvantage is the reduction in total efficiency due to insertion losses in phase-shifters and feed networks, as well as the gain loss

caused by phase and amplitude errors. Although space feeds may be less lossy for large arrays than constrained feeds, their losses (principally spillover loss) are still high.

Passive networks such as the Rotman lens are bulky but can maintain performance over wide angles.

Frequency-scanning systems can be very effective. The illumination may be carefully shaped and losses are lower than for other arrays because of the absence of phase-shifters.

It is not possible to set up a table of possible parameters for two aperture diameters of 10 and 100 wavelengths since the system needs more careful definition. The following remarks can be made.

For the 10 wavelength array, -40 dB sidelobes can be obtained but the efficiency would be lower than for a well-designed offset reflector due to:

- using an illumination for at least -47 dB since 10 wavelengths is a rather small aperture.
- network losses.

Optical feeds are unsuitable for this size and a constrained feed or a frequency-scanned system must be used.

For the 100 wavelength aperture, better than -40 dB sidelobes could be obtained but the efficiency would again be reduced by network losses which would be greater than those for a  $10 \lambda$  aperture if a constrained network were used. An optical feed could be used for levels down to -40 dB and the insertion loss might be less than the constrained network.

A precise figure cannot be given for the network losses until it is known how many beams at what frequency and what scanning angles are required, but total efficiencies rarely exceed 45%.

For a large aperture, the complexity is enormous and costly though sidelobe levels down to -50 dB should be achievable.

HD-A133 361

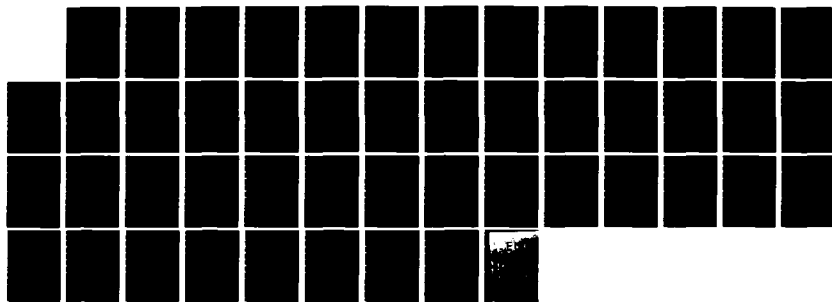
LOW SIDELobe ANTENNA STUDY PART 1 LITERATURE SURVEY AND  
REVIEW(U) ELECTRICAL RESEARCH ASSOCIATION LEATHERHEAD  
(ENGLAND) P R FOSTER ET AL. OCT 77 ERA-RFTC-190476/1  
DRIC-BR-56799

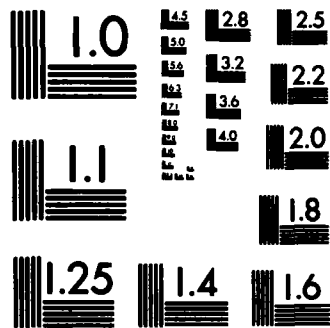
3/3

UNCLASSIFIED

F/G 9/5

NL





MICROCOPY RESOLUTION TEST CHART  
NATIONAL BUREAU OF STANDARDS-1963-A

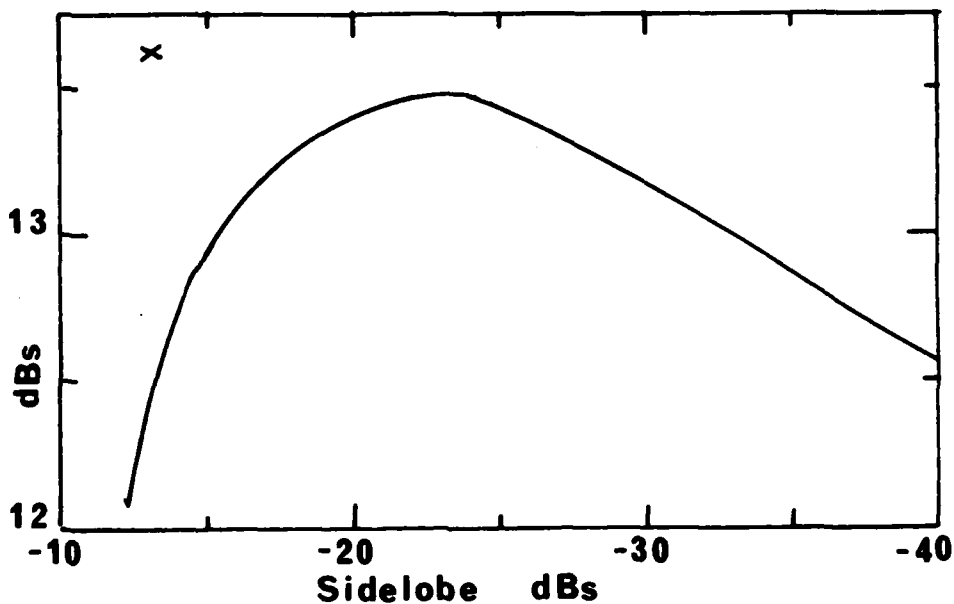


Fig.5.5-1: Directivity (dB) for a linear array of 23 half wavelength spaced elements with Chebyshev distributions of varying sidelobe level. The cross marks the values for a uniform distribution.

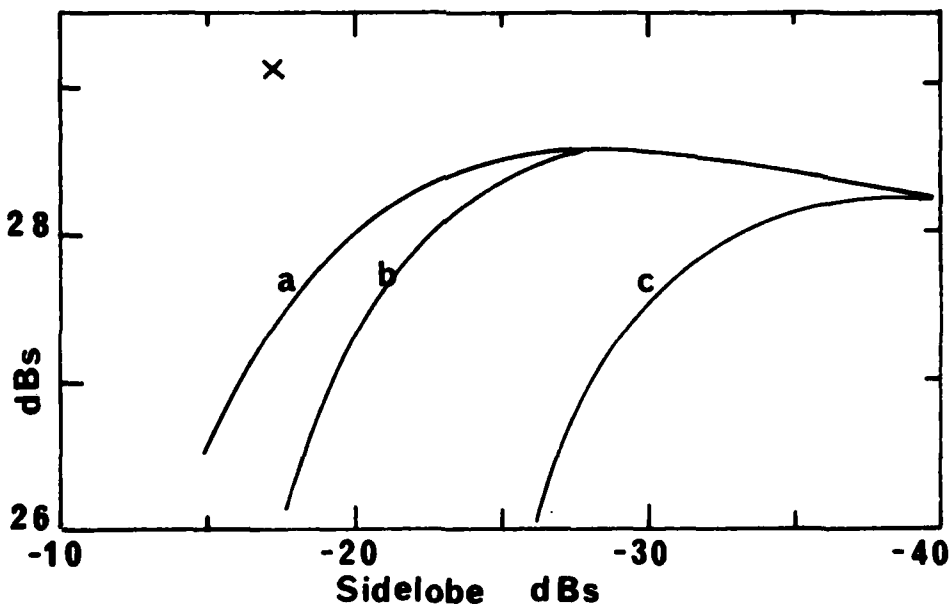


Fig.5.5-2: Directivity (dB) of a hexagonal planar array of 397 isotropic elements at  $0.7 \lambda$  spacing as a function of sidelobe level for various distributions: (a) Taylor  $n = 3$  (b) Taylor  $n = 5$  (c) Chebyshev. The cross marks the values for a uniform distribution.

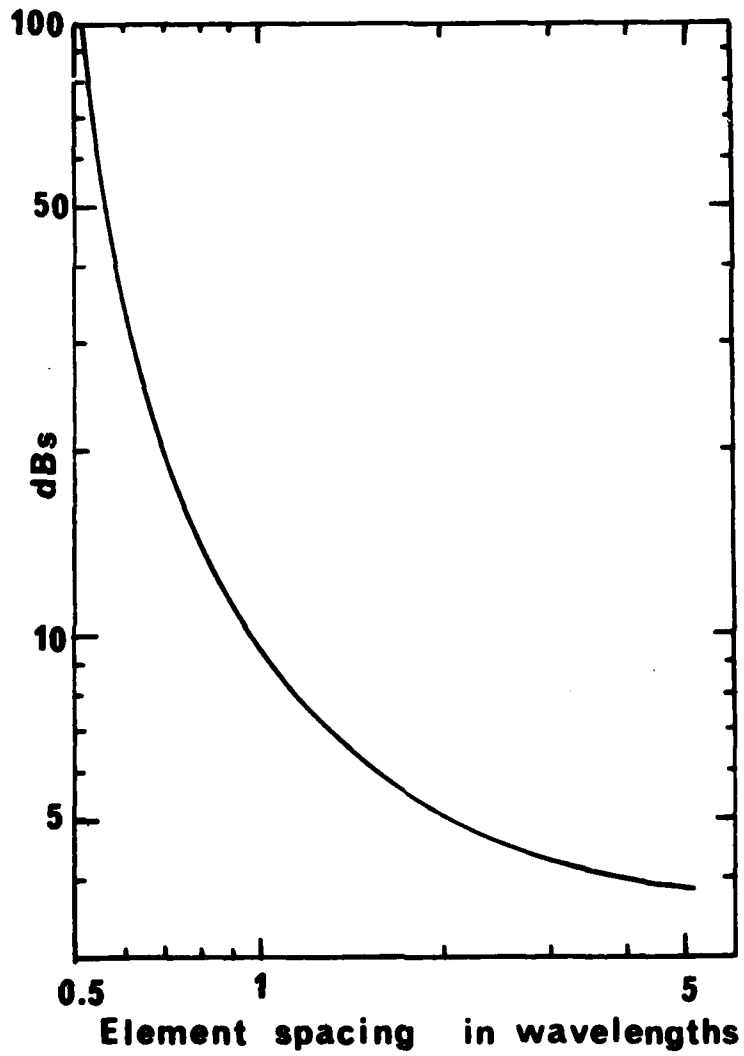


Fig.5.5-3: Grating lobe suppression (dB below main beam) as a function of element spacing (spacing assumed equal to element aperture size). Elements are in a regular rectangular grid.

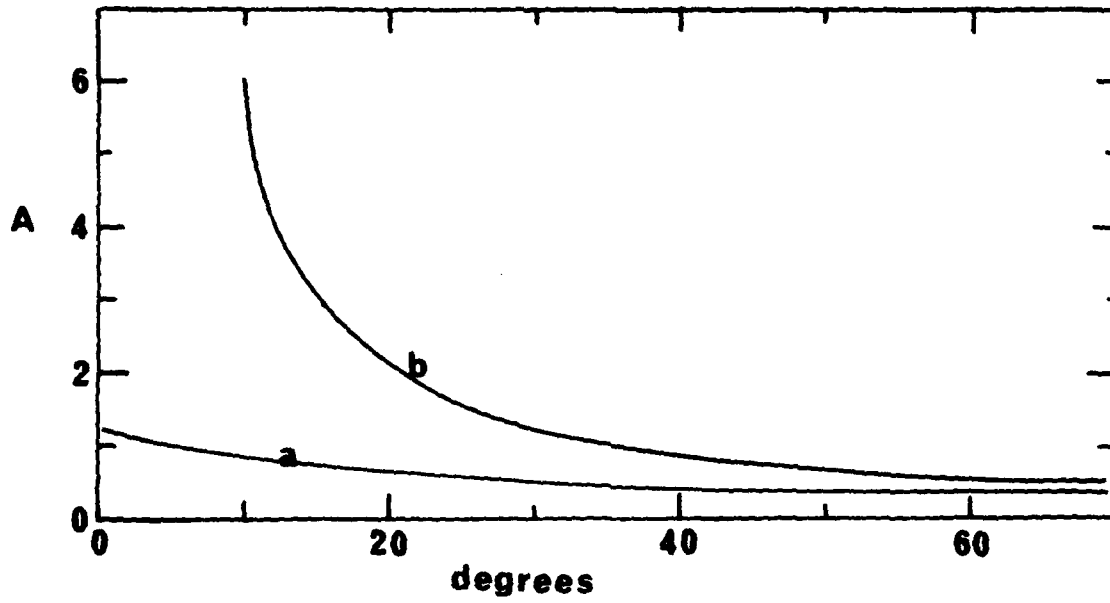


Fig.5.5-4: Maximum element area in terms of wavelengths,  $A$ , as a function of maximum scan angle in degrees for (a) a triangular periodic lattice and (b) an aperiodic circular lattice.

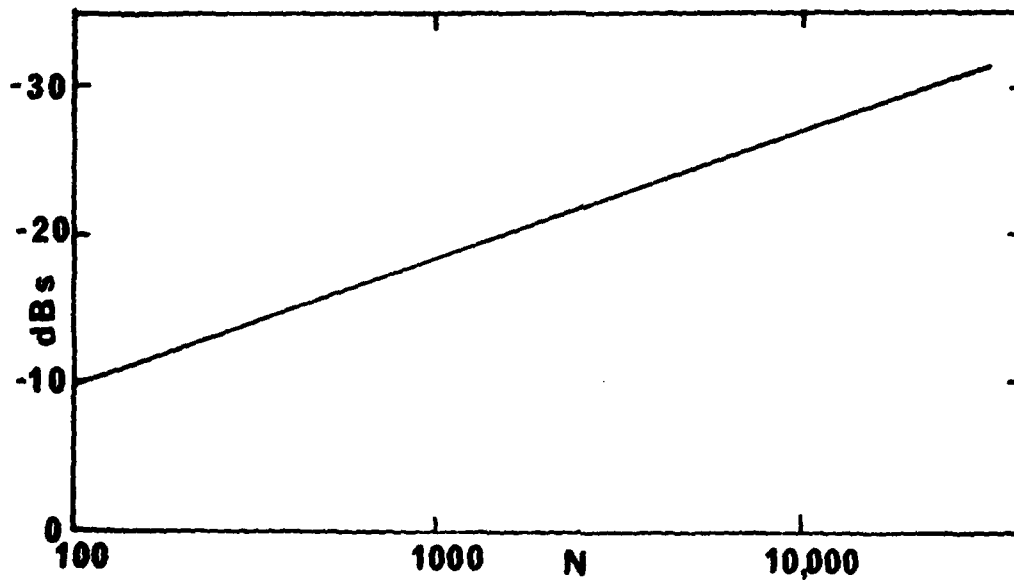


Fig.5.5-5: Peak vestigial grating lobe as a function of the number of elements,  $N$ , in an aperiodic circular lattice. (The mean level is some 10 dB lower).

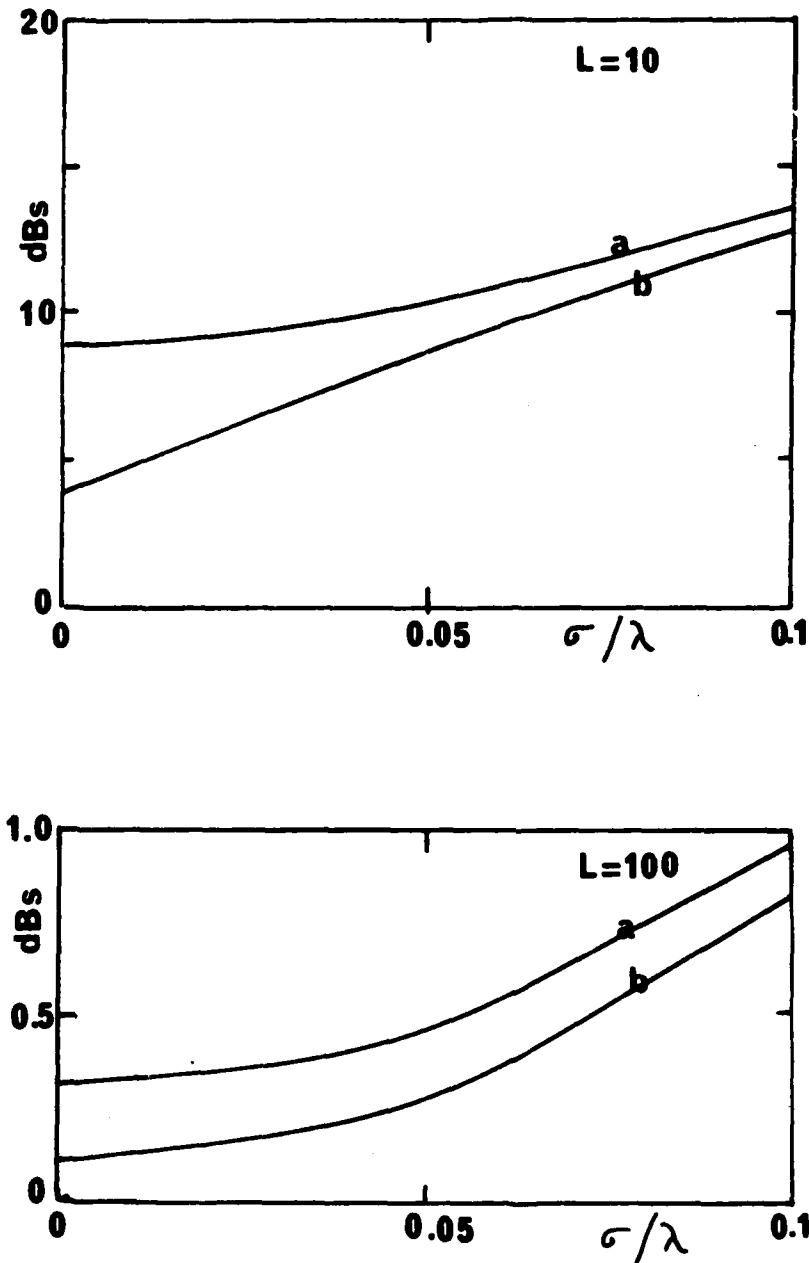


Fig.5.5-6: Sidelobe degradation in dB as a function of the positional error  $\sigma/\lambda$  ( $\sigma_1 = \sigma_2$ ) and two values of  $f$  the rms normalised current error (a)  $f = 0.25$ , (b)  $f = 0.125$ . A square array of side  $L$  wavelengths has been assumed and a design sidelobe level of  $-40$  dB ( $S = +40$ ) (Elliot).

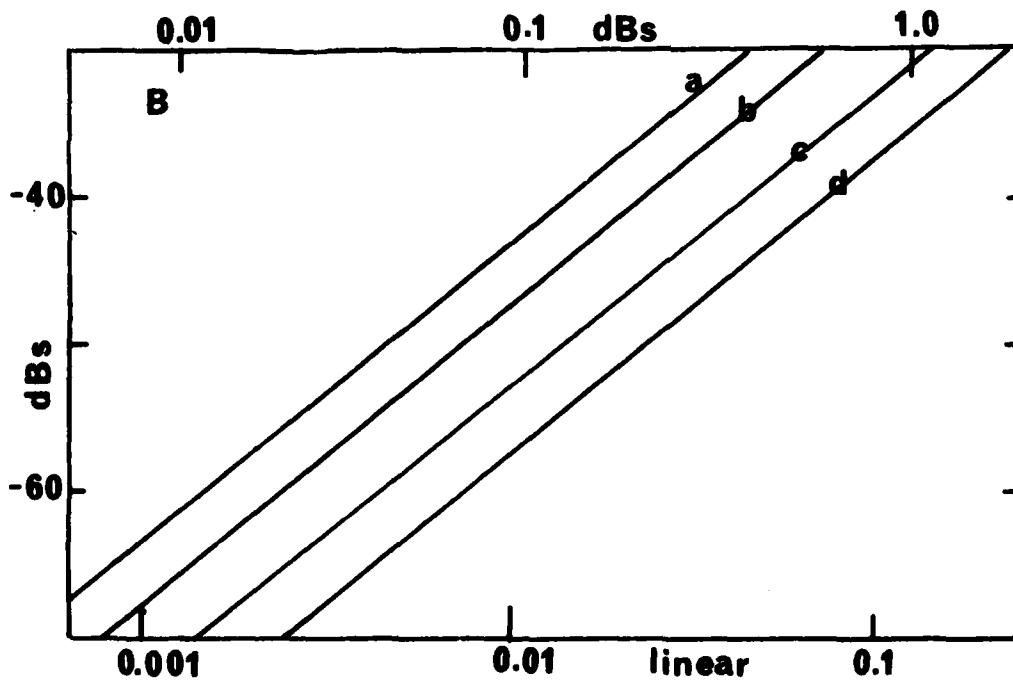
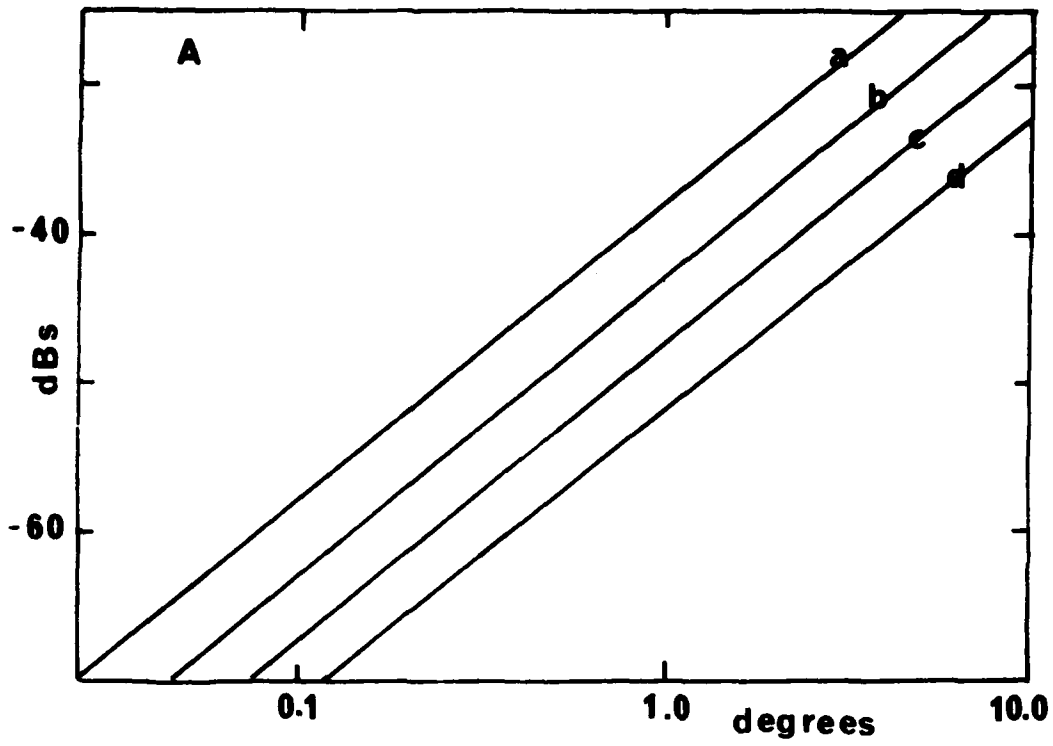


Fig.5.5-7: Sidelobe levels for a linear array as a function of A) rms phase errors, B) rms amplitude errors. (a) is 'correlated', i.e., grating lobe effect, (b) for 10 elements, (c) 30 elements. (d) 40 elements.

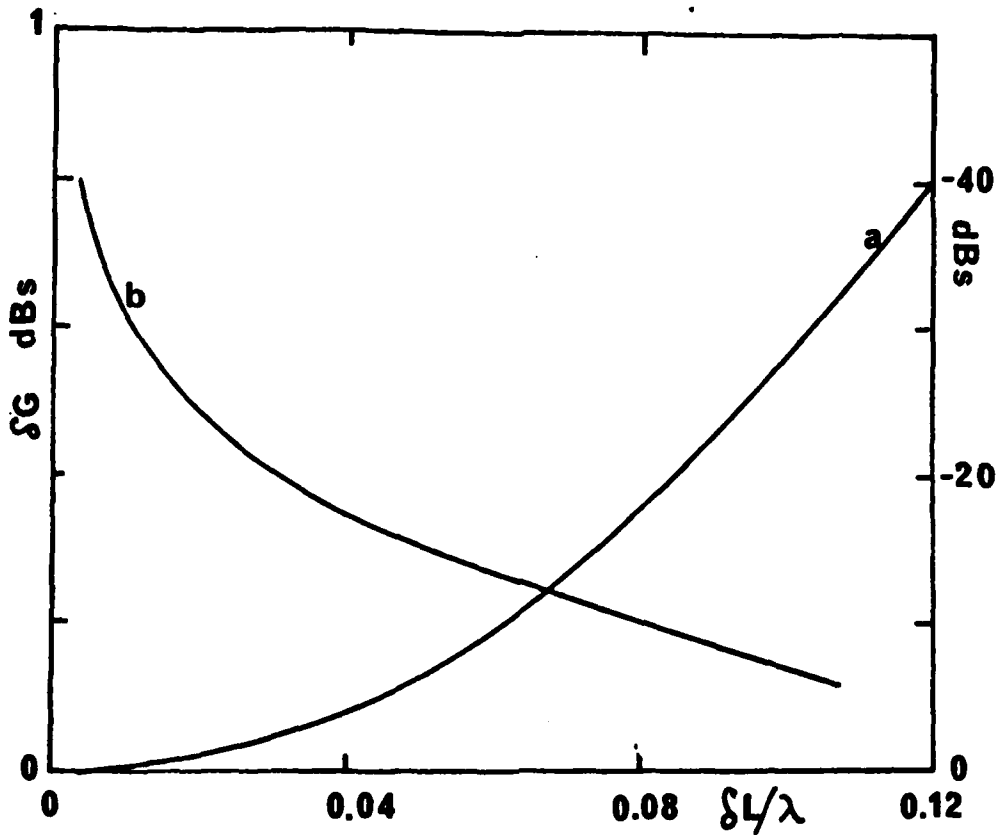


Fig.5.5-8: Degradation in gain  $\delta G$ (curve a) and mean scattered radiation level relative to the mainbeam peak (curve b) with positioning error  $\delta L/\lambda$ . Errors assumed to be uniformly distributed over the range  $\pm\delta L/\lambda$ .

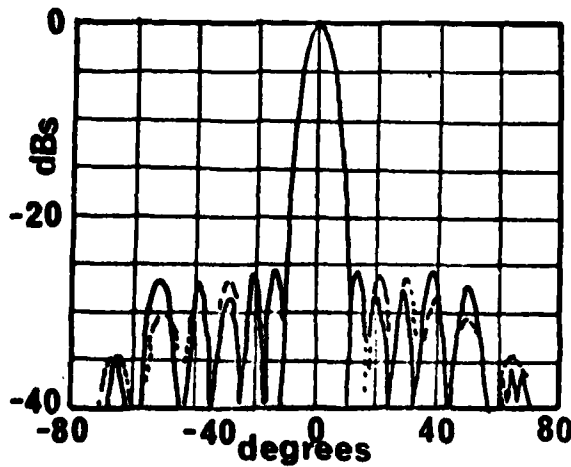


Fig.5.5-9: Predicted (dashed curve) and measured (full curve) radiation pattern for a 56 GHz 10 element array with Chebyshev illumination.

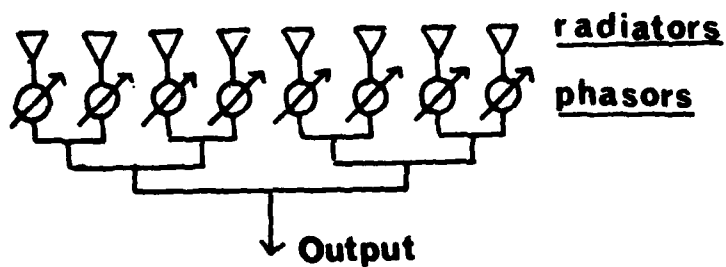


Fig.5.5-10: One type of constrained feed network.

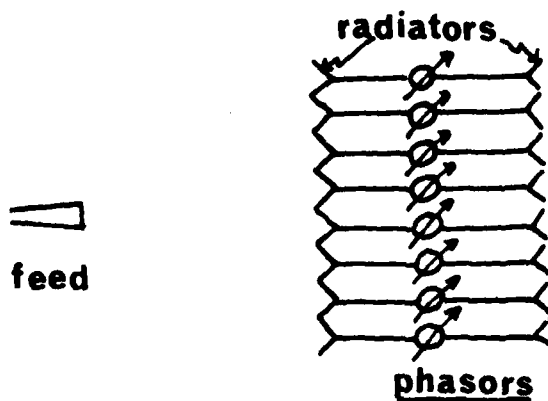


Fig.5.5-11: One type of optical feed network.

## 6 MULTIPLE-BEAM ANTENNAS

The problems involved in beam-scanning or multiple-beam generation with antenna-arrays have been dealt with to a large extent in Section 5.5.3. For reflector or lens antennas the problems in generating multiple-beam coverage are somewhat different. Recently several papers have appeared, mainly directed toward space-communication applications<sup>1,2,3</sup>.

A fundamental difficulty which arises in multiple-beam reflector (or lens) antennas is that of achieving closely spaced beams without excessive spillover. In essence, the cross-over level between beams can be increased (or beam spacing can be reduced) by reducing the spacing between feed elements. However, to achieve a spacing of one half-power beamwidth implies that the radiating aperture of the feed element will be smaller than optimum. Hence the 'too small' feed element lacks gain and much of its radiation becomes spillover. High levels of spillover also imply higher edge illuminations of the main reflector with subsequent higher *near-in sidelobe radiation*<sup>4,5</sup>. We assume here that the multiple-beam antenna is operating on the one feed-element-per-radiated-beam principle.

More sophisticated designs would adopt the hybrid-antenna approach in which the individual primary-feed elements are replaced by an array feed<sup>9,10,11,12</sup>. These techniques are relatively undeveloped at this time and their sidelobe potential has not been clearly established. Levels of the order of -20 dB are indicated in a recent publication but this was not aimed at low sidelobe performance<sup>12</sup>. One penalty which must be paid by the more complex feeds is that of insertion loss, which will certainly be higher than the simple feed approach.

To provide moderately wide angle multiple-beam coverage without excessive coma distortion, the antenna must have a large F/D ratio. For axisymmetric reflectors, the aperture blockage is likely to be high and low sidelobe performance is again difficult to achieve.

Examples of multiple-beam antenna sidelobe performance can be extracted from the literature. A few examples follow:

- (1) An axisymmetric Cassegrain reflector<sup>2</sup> operating at 50 GHz had 7 feed horns arranged linearly. First sidelobes from each beam were at a level of -18 dB, while the cross-over level was -13 dB.

(2) A waveguide lens with an F/D ratio of about unity, was illuminated by a cluster of 19 fundamental-mode conical horns in a triangular matrix<sup>6</sup>. Cross-over levels were approximately -6 dB and peak sidelobes were in the region of -20 dB.

(3) An offset parabolic reflector<sup>4</sup> with three circularly-polarised beams had sidelobe levels of -20 dB and a minimum beam cross-over level of -3.5 dB (i.e., beam spacing of just over one beamwidth). The feed elements were optimum-dimension conical horns and the offset reflector beam-squinting phenomena was utilised to reduce the beam-spacing of the closest pair of beams. Including spillover losses, this antenna realised efficiencies of between 65-68% for each beam.

(4) A 4-beam offset-reflector configuration has been described<sup>7</sup> fed by a set of linearly-polarised rectangular horns, in E plane contact. This antenna produced beam cross-over levels of between -5 and -6 dB with first sidelobe levels suppressed below -20 dB. The peak cross-polar lobes occurred within the main-beams at a level of -26 dB. Reducing the feed dimensions and spacings to produce -3 dB cross-over levels was found to result in increased sidelobe levels (peak -18 dB) while producing little change in the cross-polar levels (peak -25 dB).

(5) A twin main reflector system, employing a pair of offset reflectors has been examined, in which an 'interlaced-beam' technique was employed to provide closely-spaced beams (3 dB cross-overs) with first sidelobes suppressed to -27 dB (Ref.8). In this design alternate beams were generated from one reflector while the interlacing beams were generated from the second.

Very low near-in sidelobe levels will be very difficult to achieve with reflector antennas when closely-spaced beams are specified. Spherical and parabolic-torus reflectors do have the property of scanning beams over wide angles without pattern degradation. However, their inherent phase-error characteristics imply that -40 dB first sidelobe suppression is very unlikely (see Section 5.3).

To conclude, the combination of a low sidelobe specification with a multiple-beam requirement clearly complicates the design procedure. When closely spaced beams are specified this requirement is almost certain to demand some relaxation of the near-in sidelobe specification.

Little data is available on the wide angle sidelobe performance of multiple-beam reflector antennas which are generally designed for coverage of a restricted range of angles. The wide angle performance is certainly unlikely to be better than the single beam case but the degradation may not be severe in many cases, providing offset or unblocked configurations are adopted.

## 7 TRACKING ANTENNAS

The requirements of monopulse tracking in an antenna system designed for low sidelobe levels adds a further set of constraints to the problem and it becomes increasingly difficult to optimise the aperture illuminations for both Sum and Difference Channels. There are three basic methods of tracking:

- conical scan
- multi-mode techniques
- static-split techniques

I. Conical scan is capable of high tracking accuracy. The feed is pointed slightly off-axis and rotated. In a Cassegrain reflector, the sub-reflector may be offset or tilted and rotated. The variation in signal is detected and converted into target displacement angle. This system is applicable to optical systems such as reflectors and lenses though it appears to have been applied only to reflectors. There is no reason why it should not be used in conjunction with a low sidelobe design. The only degradation is in the forward loss, usually about 0.25 dB and the increase in coma lobe due to the beam squint. Such a forward loss corresponds to -30 dB sidelobe degrading to -20 dB. To date, Cassegrain configurations have been designed for near-field illumination<sup>1,2,3</sup>.

The use of such a system complicates the mechanical design of the antenna, particularly if the primary feed system is rotated.

### II. Multi-mode techniques

Another method is to generate an asymmetric illumination across the feed horn of a reflector (or lens) by generating odd waveguide modes as well as even ones in the feed. The odd modes can be extracted to give information on the target displacement angle. Again, high sensitivity can be obtained<sup>4,5,6</sup>. This poses problems for the feed horn when a low sidelobe design is sought because the odd modes must be generated at the same time as the required even modes. Again no such versions have been built for low sidelobes and the design complexity is unknown. The design of the feed horn is critical. However, in view of the fact that multi-mode techniques offer the best compromise between sum and difference illumination of the main antenna aperture, it is likely that these techniques offer the best prospects of achieving low sidelobe performance.

### III. 'Static-split' techniques

Reflectors and Lens: The 4 or 5 horn static-split system has been very popular in the past but examination of Hannan's paper<sup>7</sup> shows that it is difficult to optimise Sum and Difference channel sidelobes and the tracking sensitivity simultaneously. If the Sum channel has sidelobes below -30 dB, the Difference channel is liable to have sidelobes at -10 dB. The 5 horn system, though permitting the Sum channel to take up the optimum illumination function, does lead to poor Difference channel sensitivity and sidelobe performance<sup>8</sup>.

Arrays: Cylindrical and spherical arrays because of their inherent inverse taper have poor sidelobes in both Sum and Difference channels<sup>9</sup>. On the other hand, planar arrays have much more freedom in choosing an aperture illumination and it is possible to obtain good performance in both Sum and Difference channels<sup>10,11,12</sup>. In particular, it is possible to use two separate constrained feed networks which gives the array ideal illuminations with no inter-dependence between the channels. This complicates the feed network but it is possible to obtain -40 dB sidelobes in all channels.

Because of the antisymmetric shape of the illumination function for the Difference channels, the effect of phase front distortions is more marked than for the Sum channel. This topic has been treated by Adatia<sup>8</sup> who considers systematic asymmetric distortions in a reflector. Such distortions have not been considered for an array.

#### Conclusions

The conical scan tracking system will degrade the sidelobe levels while the mode conversion system will not, though it complicates the feed horn design to an unknown extent. The traditional 4 horn static-split feed is not recommended for use with reflectors designed for very low sidelobes. Either the Sum channel sidelobes or the tracking sensitivity are degraded. The difference sidelobes are always poor. The alternative is the 5 horn system which has reduced tracking sensitivity when compared to a mode conversion system. Multi-mode techniques probably offer the best potential for low sidelobe monopulse systems.

Arrays can be arranged to give good monopulse performance but at the price of a considerable increase in complexity.

The cross-polarised radiation of monopulse systems is very dependent upon the specific design of antenna. The change in illumination characteristics between sum and difference modes of operation typically re-distributes the cross-polar radiation fields and can result in undesirable peak lobes being generated. The levels and distributions involved are totally dependent upon the antenna type, dimensions and polarisation.

## 8 RADOMES

References to radomes are usually concerned with their insertion loss. They will act to scatter radiation over wide angles which will affect the far-out sidelobes. Figure 8.1 shows the degradation of a  $160 \lambda$  aperture reflector<sup>1</sup> due to a fibreglass radome with pseudo-random struts. The reduction in forward gain was 1 dB.

A study of losses incurred when using a radome of various constructions is given by Kay<sup>2</sup>. Although sidelobes are not treated specifically, some patterns show the appearance of single far-out lobes at -30 dB. If the energy lost due to the radome is assumed to be rescattered isotropically, then the far-out sidelobes will be a few decibels below isotropic or (say)  $-G_0 - 5$  dB for a forward loss of 1 dB.

Measurements on a 44 cm lens at 61 GHz (Ref.3) which was used inside a hemispherical radome of Pyrex (no metal struts) showed a general deterioration in sidelobe level. The illumination on the lens was aimed at a -40 dB Taylor distribution with a fall off after the first two sidelobes (Figure 8.2).

A further example<sup>4</sup> at 37 GHz showed a similar degradation to -30 dB over  $\pm 24^\circ$  (half-power beamwidth of  $2^\circ$ ). The sidelobes did not decrease below -50 dB until angles of  $\pm 72^\circ$  off boresight were reached. (Gain of lens = 38 dB).

Radomes are likely to degrade the performance of an antenna in the far-out regions to somewhere around isotropic. Close in sidelobes are not individually affected though high value isolated grating lobes can occur at the -30 dB level.

Detailed information on the design of radomes<sup>5</sup> is available though it concerns only the forward loss. As has been pointed out, a knowledge of the forward loss will give some indication of the effects on the far-out sidelobes.

The question of radome performance, when good sidelobe suppression is mandatory, becomes increasingly important. Relatively little information appears to be available on the optimisation of radomes with regard to sidelobe performance, and this is clearly an area which will require further attention in the future.

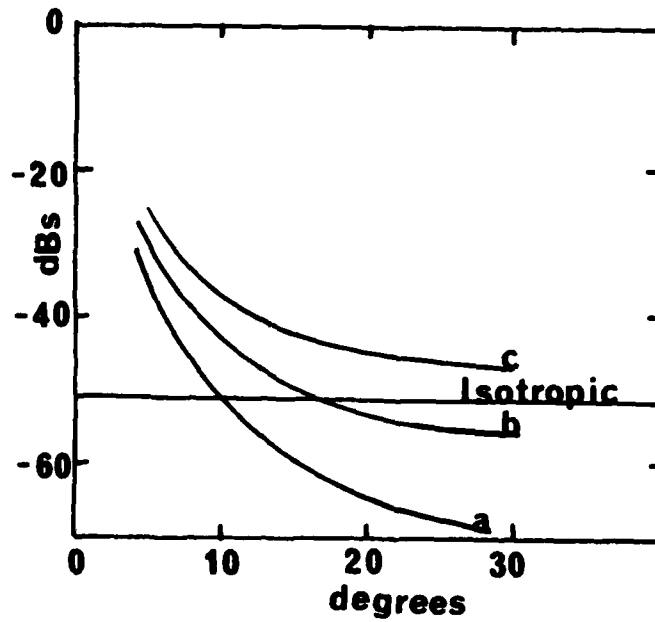


Fig.8.1: Sidelobe envelope of an axisymmetric reflector of  $160 \lambda$  aperture:  
(a) reflector alone  
(b) reflector plus struts  
(c) reflector plus struts plus radome

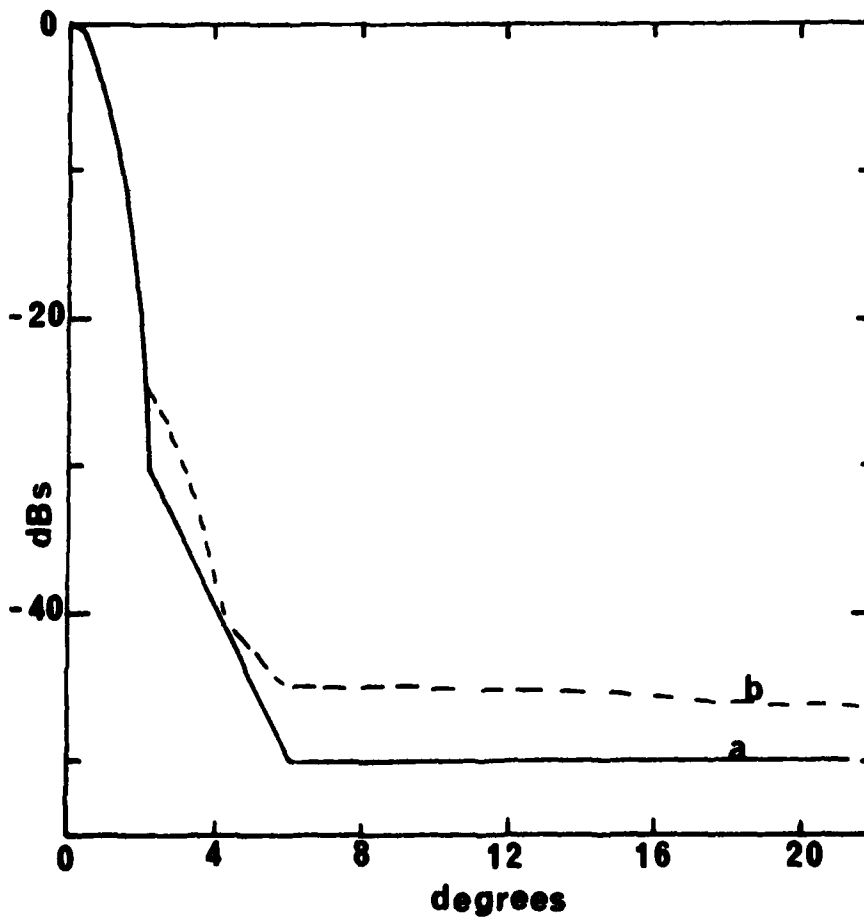


Fig.8.2: Sidelobe envelope of (a) a lens, (b) the same lens plus radome.

## 9 BRIEF COMMENTS ON ANTENNA TEST RANGES

Problems arise when measuring antenna radiation patterns in that the inaccuracy provided by the site must be much less than the level at which sidelobes are sought<sup>6</sup>. If it is a requirement that all sidelobes, spillover etc., be below -40 dB, then the test range must be 'clean' over a wide angle to about 20 dB below this level<sup>1</sup>.

In addition, there is the problem of the antenna-transmitter distance. The usual distance is taken to be  $R > 2D^2/\lambda$  (Fig.9.1). The actual ground area to be freed from spurious reflection therefore becomes very large.

The problem can be avoided by using near-field probe techniques but the accuracy required to establish precise sidelobes over wide angles is very stringent, and the method is more suited to determination of the far-field pattern around boresight. Grimm<sup>5</sup> considers the effects of errors on the near-field measurements as they degrade the computed far-field pattern. The traverse time is of the order of 1 to 2 hours to collect the data for one measurement. It is not suited to small antennas because of probe interaction<sup>2</sup>.

Sometimes a reflector may be defocused in order to focus the beam at a particular distance. For shaped beams this is not allowed<sup>2</sup>. It has been suggested that celestial radio sources would make useful test objects for large aperture antennas. Unfortunately, sidelobe levels above -23 dB and cross-polarisation above -30 dB are all that can be hoped for<sup>3</sup>.

It is noticeable that publications dealing with large earth-stations do not often include sidelobes more than a few degrees from boresight. However, a  $1000 \lambda$  reflector has been measured around the main lobe region<sup>4</sup>.

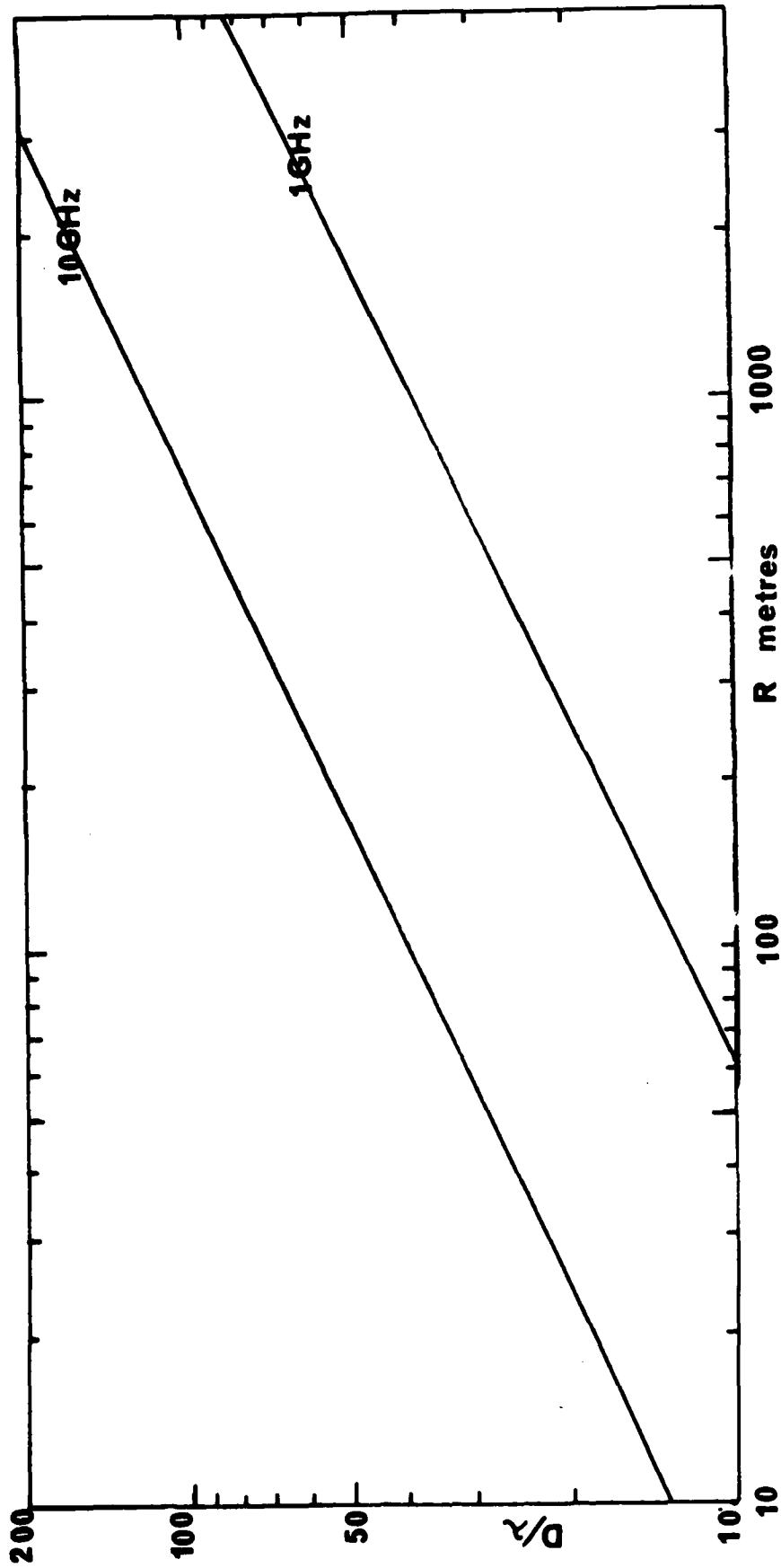


Fig. 9.1:  $R = 20^2/\lambda$  in metres as a function of  $D/\lambda$ , the antenna aperture in wavelengths, for 2 frequencies.

## 10 CONCLUSIONS

At least in theory, it is feasible to achieve low sidelobe performance, at the expense of aperture efficiency, by suitably tapering the illumination characteristics of the radiating 'aperture' (or 'effective aperture') of an antenna. In practice, there can be a variety of constraints which make such aperture-illumination tapering non-realizable, or introduce secondary effects which degrade the sidelobe performance.

For low-gain antennas the concept of a well-defined radiating aperture is not always either clear-cut or, in some cases, even useful. As the gain of antennas decrease, then to an increasing extent any conducting surface in the immediate vicinity of the antenna must be considered as a part of the overall radiating structure. The most drastic cases of this phenomenon are usually associated with quasi-directional antennas in which sidelobe radiation is of no great concern. However, it must be borne in mind that for any low-gain antenna there is an increased possibility that coupling effects between the radiator and its surrounding structure will significantly modify the free-space radiation characteristics of the antenna.

The sensitivity of a low gain antenna to its immediate environment can generally be minimised by use of antenna types which provide a well-defined radiating aperture, with illumination tapers which reduce the fields to low levels at the aperture periphery. Such antennas are also desirable with regard to good backlobe and sidelobe suppression. To provide practical examples of antennas exhibiting these characteristics, the Potter dual-mode horn, or the corrugated hybrid-mode horn, are two types of conical waveguide horn which meet these requirements. These antennas can be dual polarised with either linear or circular polarisations and can be operated over bandwidths of 4% (Potter horn) and 40% (corrugated horn).

For medium- and high-gain antennas, the increased dimensions of the radiating aperture (in terms of wavelengths) provide generally better potential for sidelobe suppression by aperture-illumination tapering techniques. For antenna types which offer the antenna designer reasonable control over the aperture-illumination characteristics (i.e., reflector-antennas, lens antennas and arrays), the principal sources of sidelobe radiation arise from secondary effects other than diffraction from the main aperture.

In the case of axisymmetric reflector antennas, aperture blockage effects are a major contributor to the sidelobe radiation. With these antennas, peak sidelobe levels of the order of -25 dB are typical even for relatively well-designed antennas. Backlobe radiation can be reduced to very low levels by use of shrouds or castellations, but the blockage effects arising from the primary-feed (or sub-reflector) and the associated support structure represent a serious limitation upon the use of these antennas in low sidelobe applications.

Offset reflector antennas can overcome these inherent limitations of the axisymmetric designs, by ensuring that the primary-feed hardware does not protrude into the radiating aperture of the reflector. Well-designed offset antenna systems can reduce the peak sidelobe levels to below -40 dB in the near-in region, with sidelobe suppressions to -50 dB or -60 dB or below at wider angles. The electrical isolation between primary-feed and reflector is also exceptionally good with offset reflector configurations, thus allowing good VSWRs to be achieved more readily. Some additional complications are apparent in the design of offset antennas but these can be accommodated with modern design practice. The depolarising effects which are inherent with asymmetrical reflector structures can be overcome, either by use of new primary-feed technology, or by employing the optimised double-offset Cassegrainian geometry. In general terms, offset reflector systems offer very significant advantages when low sidelobe performance is mandatory.

Lens antennas also offer a means of avoiding aperture blockage, although the isolation between feed and lens is less good than the offset configuration. The lens must be shrouded to avoid spillover radiation in the forward half-plane. These antennas could provide good sidelobe suppression for some applications, although they tend to become bulky and lossy when large apertures are required. The bandwidth of lens antennas is also more restricted than a comparable reflector. The electrical performance of the lens antenna can be improved in some respects by zoning but the effect of this on the wide-angle sidelobe performance appears to be an unknown.

Antenna arrays can offer good potential for low sidelobe applications. Providing a sufficiently large number of elements are available (e.g., not less than 15 in one dimension) it should be possible to achieve

very low sidelobe levels. However, strongly tapered apertures also imply lower efficiencies, and in addition to the aperture efficiency sacrificed for improved sidelobe suppression, there may be substantial losses due to the array feeding network. These additional losses can amount to several decibels, resulting in an overall antenna efficiency of the order of 25-30% or less.

It is also worth noting that a planar array requires close to 10,000 elements to produce a  $1^\circ$  half-power beamwidth. This number can be reduced by array-thinning techniques but the price for such thinning must be paid in both gain and, more particularly, in degradation of the sidelobe suppression. In view of these factors, it would appear that planar array techniques are more appropriate to medium-gain applications, when good sidelobe suppression is required. Linear arrays are likely to find more applications in this respect, particularly when combined with reflector systems which collimate the beam in the orthogonal plane.

The mechanical and structural aspects of a stringent sidelobe specification will be extremely important. It is difficult to be categorical in terms of the required mechanical tolerances unless the antenna configuration is well defined. In many applications the required tolerances do not appear to be excessive. The nature of the tolerance error and, in some cases, its spatial distribution can be very important. For example, in the case of a reflector or lens antenna profile, a small spatially-periodic error can produce a significant increase in the peak sidelobe levels of the antenna, while a randomly distributed error of the same magnitude would be much less significant. Data has been collected in the body of this report to provide guidance in this respect, and it must be emphasised that adequate attention to this aspect of low sidelobe performance should be given at the design stage.

In many practical applications it is necessary to locate a 'low sidelobe' antenna within a radome cover. The possibility of sidelobe degradation introduced by the radome itself must be accepted as being a very real one. It appears that this aspect of low sidelobe antenna performance has not received the attention it merits. In view of the enhanced jamming threat, it is recommended that attention be directed toward the sidelobe degradation introduced by the radome and the implications of low sidelobe specifications upon the radome design.

In conclusion, this survey and review of low sidelobe antennas has indicated that sidelobe suppression to lower levels than those commonly achieved with existing antennas is, in the majority of cases, both theoretically and practically feasible. The rather indifferent sidelobe performance of many existing designs appears to be more a result of insufficient emphasis being placed upon this aspect of the system performance, and general acceptance of levels of sidelobe radiation which in view of the present jamming threat, are now totally unrealistic. It is suggested that, with an application of good design practice, significant improvements can be made in the sidelobe performance of a wide range of radiating systems.

11 LIST OF REFERENCES

The references are listed according to the chapter or section of this report in which they appear.

References for Chapter 1

1. Dax P: Noise jamming of long range search radars. *Microwaves*, 14, September 1975, p.52.
2. Jones, S R and Kelleher, K S: A new low-noise high gain antenna  
IEEE International Convention Record, part 1 - 1963, p.11.
3. Hansen, R C: Low noise antennas. *Microwave J* 2, June 1959, p.19

References for Chapter 2

Section 2

1. Elliot, R S: Microwave Scanning Antennas, Vol.11, Chapter 1, Academic Press, New York, 1966.

Sections 2.1 and 2.2

1. Hansen, R C: (ed) Microwave scanning antennas. Vol.1 Academic Press, New York, 1967, p.47.
2. White, W D: Pattern limitations in multiple-beam antennas, Trans IEEE on Ant. and Prop. AP-10 July 1962, p.403.
3. Bickmore, R W and Spellmire, R J: A two-parameter family of line sources, Hughes Aircraft Co. TM 595, 1956.
4. Taylor, T T: Design of line-source antennas for narrow beamwidth and low sidelobes. Trans IEEE on Ant. and Prop. AP-3, January 1955, p.16.
5. Elliott, R S: Design of line source antennas for narrow beamwidth and asymmetric low sidelobes, Trans IEEE on Ant. and Prop. AP-23, January 1975, p.100.
6. Elliott, R S: Antenna patterns with arbitrary sidelobe topography, European Microwave Conference, Rome 1976, p.283.

Section 2.3

1. Hansen R C: (ed) Microwave scanning antennas, Vol.1, Chapter 1, Academic Press, New York, 1966.
2. Nash, R T: Beam efficiency limitations of large antennas, Trans IEEE on Ant. and Prop. AP-12, 1964, p.918.
3. Sciambi, A F: The effect of the aperture illumination on the circular aperture antenna pattern characteristics. Microwave J.,8, August 1965, p.79.
4. Taylor, T T: Design of circular aperture for narrow beamwidth and low sidelobes. Trans IEEE on Ant. and Prop. AP-8, January 1960, p.17.
5. Hansen, R C: Tables of Taylor Distributions for circular aperture antennas. Trans IEEE on Ant. and Prop. AP-8, January 1960, p.23.
6. Hansen, R C: A one-parameter circular aperture distribution with narrow beamwidth and low sidelobes. Trans IEEE on Ant. and Prop. AP-24, July 1976, p.477.
7. Elliot, R S: Design of circular apertures for narrow beamwidth and asymmetric low sidelobes. Trans IEEE on Ant. and Prop. AP-23, July 1975, p.523.
8. Peters, L: Side and backlobe structure of directive antennas. IEEE Conference on Communications, 1972, p.41-1.

9. Burns, O P; Ecker, H A and Hoy, E B: Shaping antenna and amplitude distribution for low sidelobes, AFCRL - 71-0180, February 1971.
10. Ruze, J: Antenna tolerance theory - a review Proc. IEEE, 54, 1966, p.633.
11. Vu, T B: Influence of correlation interval and illumination taper in antenna tolerance theory. Proc IEE, 116, 1969, p.195.
12. Dragone, C and Hogg, D C: Wide-angle radiation due to rough phase fronts. BSTJ, 42, September 1963, p.2285.

References for Chapter 3

Section 3.1.1

1. Silver, S: (ed) Microwave antenna theory and design, McGraw - Hill, 1949, Chapter 10.
2. Yu, J S; Rudduck, R C and Peters, L: Comprehensive analysis for E plane of horn antennas by Edge diffraction theory. Trans IEEE on Ant. and Prop. AP-14, March 1966, p.138.
3. Lawrie, R E and Peters, L: Modifications of horn antennas for low sidelobe levels. Trans IEEE on Ant. and Prop. AP-14, September 1966, p.605.
4. Thourel, L: The antenna, Chapman and Hall, London, 1960.
5. Collin, R E and Zucker, F S: (ed) Antenna theory, Chapter 15, Vol.1, McGraw - Hill, 1969.
6. Rudge, A W and Shirazi, M: Investigation of reflector-antenna radiation. Final report of ESRO/ESTEC Contract No.SC/11/73/HQ. University of Birmingham, UK. June 1974.
7. Baldwin, R and MacInnes, P A: Radiation patterns of dielectric loaded horns. Trans IEEE on Ant. and Prop. AP-21, May 1973, p.576.
8. Ashton, R and Baldwin, R: Rectangular horn with dielectric slab insert. Electronics Letters, 9, January 1973, p.26.
9. King, A P: The radiation characteristics of conical horn antennas. Proc IRE 38, March 1950, p.249.
10. Hartsuiker, A P; Baars, J W M; Dreuth, S and Gelato-Volders, L: Interferometric measurements at 1415 MHz of radiation patterns of paraboloidal antennas at Dwingeloo Radio Observatory. Trans IEEE on Ant. and Prop. AP-20, March 1972. p.166.
11. Burns, O P; Ecker, H A and Hoy, E B: Shaping antenna and amplitude distribution for low sidelobes, AFCRL-71-0180. February 1971.
12. Cowan, J: Dual-band reflector feed element for frequency re-use applications. Electronics Letters, 9, 1973, p.596.
13. Wohlleben, R; Mattes, H and Lochner, O: Simple small primary feed for large opening angles and high aperture efficiency. Electronic Letters 8, September 1972, p.476.
14. Gruner, R W: A 4 and 6 GHz prime focus CP feed with circular pattern symmetry. Int. Sym. Digest on Ant. and Prop. 1974. p.72.
15. Epis, J J: Compensated electromagnetic horns. Microwave J 4, May 1961, p.84.
16. Rudge, A W et al: Study of performance and limitations of multiple beam antennas. ESTEC Contract No.2277/74 HP, ERA-IITRI RF Technology Centre, Cleeve Road, Leatherhead, UK. September 1975.

17. Rudge, A W; Pratt, T and Fer, A: Cross-polarised radiation from satellite antennas. Proc. AGARD. Conference on Antennas for Avionics, Munich 1973, Paper 16, pp.1-8.
18. Adatia, N A and Rudge, A W: High performance offset-reflector spacecraft antenna development study. Final report on ESA Contract No.2654/76/NLSW. ERA RF Technology Centre, Leatherhead, UK. November 1976.

### Section 3.1.2

1. Love, A W: The diagonal horn antenna. Microwave J., 5, March 1962, p.117.
2. Potter, P D: A new horn antenna with suppressed sidelobes and equal beamwidths. Microwave J, 6, June 1963, p.71.
3. Shirazi, M: Design of a Q-band antenna pt.II, Dual-mode feed design. MOD Contract No.AT 2027/080RL, October 1974.
4. Bailey, M C: The development of an L-band radiometer dual-mode horn. Trans IEEE in Ant. and Prop. AP-23, May 1975, p.439.
5. Han, C C and Wickert, A N: A new multimode rectangular horn antenna generating a circularly polarised elliptical beam. Trans IEEE on Ant. and Prop. AP-22, 1976, p.746.
6. Cohn, S B: Flare-angle changes in a horn as a means of pattern control. Microwave J. 13, October 1970, p.41.
7. Sciambi, A F and Goudey, K R: High power monopulse tracking feed. Int. Microwave Symposium, Cherry Hill, New Jersey. 1976, p.145.
8. Satoh, T: Cross-polarisation characteristics of a dielectric loaded horn antenna. Electronics and communications in Japan, 57-B No.10, 1974, p.81.
9. Ajioka, J A and Harry, H E: Shaped beam antenna for earth coverage from a stabilised satellite. Trans IEEE on Ant. and Prop. AP-18, May 1970, p.323.

### Section 3.1.3

1. Simmons, A J and Kay, A F: The scalar feed - A high-performance feed for large paraboloid reflectors IEE Conf. Pub. 21, 1966, p.213.
2. Clarricoats, P J B and Saha, P K: Propagation and radiation behaviour of corrugated feeds. Proc. IEE, 118, 1971, p.1167.
3. Clarricoats, P J B and Saha, P K: Radiation pattern of a lens-corrected conical scalar horn. Electronics Letters, 5, 1969. p.592.
4. Cahill, T C; Gill, G and Syrogos, H: Modular design of millimetre antennas. Microwave J, 16, November 1973, p.53.

5. Smith, C M: Low sidelobe antennas for millimetre-wave applications Paper B7. Millimeter Wave Techniques Conference, San Diego, 1974.
6. Jansen, J K M; Jeuken, M E J and Lambrechtse, C W: The scalar feed, Arch. Elek., Ubertragung 26, January 1972, p.22.
7. Love, A W: (ed) Electro-magnetic horn antennas, IEEE Press 1976.
8. Frank, Z: Very wide-band corrugated horns. Electronics Letters 11, 20 March 1975, p.131.
9. Mentzer, C A and Peters, L: Properties of cutoff corrugated surfaces for corrugated horn design. Trans IEEE on Ant. and Prop. AP-22, March 1974, p.191.
10. Narashimhan, M S: Corrugated conical horn as a space-feed for a phased array illumination. Trans IEEE on Ant. and Prop. AP-22, September 1974, p.720.
11. Coleman, H P; Brown, R M and Wright, B D: Paraboloid reflector offset fed with a corrugated conical horn. Trans IEEE on Ant. and Prop. AP-23, November 1975. p.817.
12. Baldwin, R and McInnes, P A: A rectangular corrugated feed-horn. Trans IEEE on Ant. and Prop. AP-23, November 1975. p.814.
13. Bahret, W and Peters, L: Small aperture, small flare angle corrugated horns. Trans IEEE, on Ant. and Prop. AP-16, July 1968, p.494.

### Section 3.2

1. Chandler, C H: An investigation of dielectric rod as waveguide. J. Applied Physics 20, 1949, p.1188.
2. Felsen, L B: Radiation from a tapered surface wave antenna. Trans IEEE on Ant. and Prop. AP-8, 1960, p.577.
3. Marcuse, D: Radiation losses of the dominant mode on round dielectric waveguide. BS TJ, 49, 1970, p.1665.
4. Collins, R E and Zucker, F J: (ed) Antenna theory Vol.II Chapter 21. McGraw - Hill 1969.
5. Smits, V C: Rear gain control of a dielectric rod antennas. Microwave J. 11, December 1968, p.65.
6. Dombek, K P: Dielectric feeds for reflector antennas. European Microwave Conference 1974. p.51.
7. Lantz, P A and Thibodeau, G R: NASA space-directed antennas, NASA X-525-67-430. September 1967.
8. Levin, B J and Kietzer, J E: Hybrid millimetre wave integrated circuits ECOM-74-0577-F, October 1975.
9. Crosswell, W F; Chatterjee, J S; Mason, V B and Tai, C T: Aperture excited dielectric antennas, NASA Report TN D-7342, May 1974.

10. Lighthart, L P and den Hollander, C J: Theory and design of medium gain dielectric antennas, European Microwave Conference, Rome 1976, p.174.
11. James, J R: *Engineering approach to the design of tapered dielectric-rod and horn antennas*. Radio and electron. Eng. 42, June 1972, p.251.
12. Clarricoats, P J B and Salema, C E R C: Antennas employing conical dielectric horns, Pt.I. Proc. IEE, 120, July 1973, p.741.
13. Ibid Pt.II, p.750.
14. Bartlett, H E and Moseley, R E: Dielectric guides - highly efficient low noise antenna feeds. Microwave Journal, 9, December 1966, p.53.

#### Section 3.3.1

1. Kraus, J D: Antennas. McGraw - Hill, New York 1950. p.211.
2. Lantz, P A and Thibodeau, G R: NASA space-directed antennas NASA X-525-67-430 September 1967, p.216.
3. Cowles, P R and Parker, E A: Helical feeds at millimetre wavelengths, Electronics Letters, 7, 1971, p.513.
4. Adams, A T; Greenhough, R K; Wallenberg, R F; Meidelovicz, A and Lumjiak, C: The quadrifilar helix antenna. Trans IEEE on Ant. and Prop. AP-22, March 1974, p.173.

#### Section 3.3.2

1. Jordan, C E et al: Developments in broad band antennas. IEE Spectrum. April 1965, p.58.

#### Section 3.3.3

1. Hansen, R C (ed): Microwave scanning antennas, Vol.II, Chapter 2, Academic Press, 1966, p.117.
2. Bawer, R and Wolfe, J J: Printed circuit balun for use with spiral antennas. Trans. IEEE on microwave theory and techniques, MTT-8, May 1960, p.319.

#### Section 3.3.4

1. Smith, C E: Log-periodic antenna design handbook, Smith Inc. 1960.

#### Section 3.3.5

1. King, F; Erbach, D R and Yee, J S: A broad-band quadruple-ridged waveguide radiator, January 1974. Army Missile Research Dev. and Eng. Lab. RE-74-7.
2. Kerr, J L: Short axial length broad-band horns, October 1970. E COM 3344.

## References for Chapter 4

### Section 4.1

1. Wilson, A C and Cottony, H V: Radiation patterns of finite-size corner-reflector antennas. Trans IEEE on Ant. and Prop. AP-8, March 1960, p.144.
2. Cottony, H V and Wilson, A C: Gain of finite-size corner reflectors. Trans IEEE on Ant. and Prop. AP-6, October 1958, p.366.

### Section 4.2

1. Ehrenspeck, H W: The short-backfire antenna. Proc. IEEE, 52, August 1965, p.1138.
2. Wong, J L and King, H E: A cavity backed dipole with wide bandwidth characteristics. Trans IEEE on Ant. and Prop. AP-21, September 1973, p.725.
3. Ehrenspeck, H W: A new class of medium-size high efficiency reflector antennas. Trans IEEE on Ant. and Prop. AP-22, March 1974. p.329.
4. Hartmann, G K and Engelhardt, W: Dispersion measurements of one-element short backfire (SBF) antennas. Trans IEEE on Ant. and Prop. AP-23, March, 1975, p.289.
5. Large, A C: Short backfire antennas with waveguide and linear feeds. Microwave J. 19, August 1976, p.49.
6. Hristov, H D and Kumar, A: X-band waveguide-fed long backfire antenna with dielectric surface wave structure, Electrical Eng. Dept. Departmental Report, Queen Mary College (London) 1976.

### Section 4.3

1. Pippard, A B: The hoghorn, an electromagnetic horn radiator of medium-sized aperture J IEE, 93 Pt.3A, 1946, p.1536.
2. Coleman, H P; Brown R M and Wright, B D: Paraboloid reflector offset fed with a corrugated conical horn, Trans IEEE on Ant. and Prop. AP-23, November 1975, p.817.
3. Crawford, A B; Hogg, D C and Hunt, L E: A horn-reflector antenna for space communications, BSTJ, 40, 1961, p.1095.
4. Grady, R R: Sidelobe control in the horn-reflector antenna, National Electronic Conference, 1970, p.360.
5. Thomas, D T: Analysis and design of elementary blinders for large horn-reflector antennas. BSTJ, 50, November 1971, p.2979.
6. Siller, C A Jr: Design of multiple edge blinders for pyramidal horn-reflector antennas. Trans IEEE on Ant. and Prop. AP-23, September 1975, p.695.

7. Afifi, M S: Minimisation of scattered radiation from microwave antennas, IEE Conference Pub. No.39, 1968, p.8.
8. Jones, S R and Kelleher, K S: A new low-noise high-gain antenna. IEEE International Convention Record Pt.1, 1963, p.11.
9. James, G L: Electro-magnetic effect of edges, Chapter 3, PhD. Thesis, University of Canterbury, New Zealand, 1973.
10. Rudge, A W and Adata, N A: New class of primary-feed antennas for use with offset parabolic-reflector antennas. IEE Electronics Letters, 11, 1975. p.597.

References for Chapter 5

Section 5.1

1. Lantz, P A and Thibodeau, G R: NASA space-directed antennas. Goddard Space Flight Centre X-525-67-430. September 1967.
2. Rudge, A W and Withers, M J: New techniques for beam steering with fixed parabolic reflectors. Proc IEEE, 118, 1971. p.859.
3. Koch, G F: Coaxial feeds for high aperture efficiency and low spillover of paraboloidal reflector antennas. Trans IEEE on Ant. and Prop. AP-21, March 1973, p.164.
4. Hansen, R C: Design trade-off study for reflector antenna systems for shuttle imaging microwave systems. JPL. N75-14940. August 1974.
5. Wood, P J: Reflector profiles for the pencil beam Cassegrain antenna. The Marconi Review, 35, No.185 1972, p.121.
6. Silver, S: Microwave antenna theory and design McGraw - Hill, New York, 1949.
7. James, G L: Electro-magnetic effect of edges. PhD. Thesis, University of Canterbury, New Zealand, 1973.
8. Ufimtsev, P. Ya: The method of fringe waves in the physical theory of diffraction. Sovyetskoye Radio Moscow, 1962.
9. Keller, J B: Geometrical theory of diffraction, J. Opt. Soc. Am, 52, 1962, p.116.
10. James, G L and Kerdemeledis, V: Reflector antenna radiation pattern analysis by equivalent currents. Trans IEEE on Ant. and Prop. AP-21, January 1973, p.19.
11. Ratnasiri, P A J; Kouyoumijian, R G and Pathak, P H: The wide angle sidelobes of reflector antennas. Electro-science Laboratory, AFCRL-69-0413, March 1970.
12. Afifi, M S: Minimization of scattered radiation from microwave antennas, IEE Con. Pub. 39, 1968, p.8. London. Interference problems associated with the operation of microwave communication systems.
13. Knop, C M: On the front to back ratio of a parabolic dish antenna. Trans IEEE on Ant. and Prop. AP-24, January 1976, p.109.
14. Mentzer, C A and Peters, L: GTD Analysis on Cassegrain antennas. IEEE Trans on Ant. and Prop. AP-23. September 1975, p.702.
15. Maanders, E J: Some aspects of ground station antennas for satellite communication PhD Thesis, Eindhoven University of Technology, August 1975.
16. Cornbleet, S: Progress in microwave communication antennas in the UK. Microwave J, 10, December 1967, p.18.
17. Lewin, L: Main-reflector-rim diffraction in the back direction. Proc.IEE, 119, August 1972, p.1100.

18. Blacksmith, P A: Method for reducing far-out sidelobes AFCRL-TR-57-115, July 1957.
19. Collins, R E and Zucker, F J: (ed) Antenna theory Vol.11, McGraw - Hill 1969, p.49.
20. Han, C C; Albernaz, J and Lusignan, B B: Reduction of ground antenna near-in sidelobes in the direction of geo-stationary orbit. Int. Sym. Digest on Antennas and Propagation, 1973, p.310.
21. Corona, P; d'Ambrosio, G and Franschetti, G: Reflector antennas with very high front-to-back ratio. Theory and experiments on models. Paper B5/1, Vol.1, European Microwave Conf. Stockholm, 1971.
22. Rusch, W V T and Sorensen, O: Aperture blocking of a focused paraboloid, Technical University of Denmark, ESTEC No.2170/74JS. July 1974.
23. Hartsuiker, A P; Baars, J W M; Dreuth, Suiker and Gelato-Volders, L: Interferometric measurements at 1415 MHz of radiation patterns of paraboloid antennas at Dwingeloo Radio Observatory, Trans IEEE on Ant. and Prop. AP-20, March 1972, p.166.
24. Kreutel, R W: Wide-angle sidelobe envelope of a Cassegrain antenna. Comsat Tech. Rev. 6, Spring 1976, p.71.
25. Kay, A F: Electrical design of metal space frame radomes, Trans IEEE on Ant. and Prop. AP-13, March 1965, p.188.
26. Sheftman, F I: Experimental study of sub-reflector support structures in a Cassegrainian antenna. Lincoln Lab. Tech. Report 416, September 1966.
27. Rusch, W V T: Phase error and associated cross-polarisation effects on Cassegrainian-fed microwave antennas. Trans IEEE on Ant. and Prop. AP-14, May 1966, p.266.
28. Microwave components and techniques; aerial tolerances. Ministry of Technology, August 1970.
29. Ruze, J: Lateral-feed displacement in a paraboloid. Trans IEEE on Ant. and Prop. AP-13, September 1965, p.660.
30. Rudge, A W; Pratt, T and Fer, A: Cross-polarised radiation from satellite antennas AGARD Con. Antennas for avionics, Munich, March 1973, p.1.
31. Rudge, A W and Shirazi, M: Investigation of reflector antenna radiation ESTEC SC/11/73/HQ Final Report. University of Birmingham. June 1974.
32. Wood, P J: Depolarisation with Cassegrainian and front-fed reflectors, IEE Electronics Letters, 9, 1973, p.597.
33. Koffman, I: Feed polarisation for parallel currents in reflectors generated by conic sections. Trans IEEE on Ant. and Prop. AP-14, January 1966, p.37.

34. Levy, D J and Momyer, W R: Metallic meshes for deployable spacecraft antennas. SAMPE Journal, May 1973, p.4.
35. Fitzgerald, W D; Lunn, V L and Keeping, K J: Experimental Evaluation of a 1000  $\lambda$  antenna. Lincoln Lab. Report 46G-4 1963.
36. Ravenscroft, I A and Knox, D M: Control and reduction of interference in front-fed aerial systems. IEE Conf. Pub. 39.
37. Dahlsjo, O: A low sidelobe Cassegrain antenna, IEE Conf. Proc. Radar, Present and future, London 1973.
38. Lockett, N: The electrical performance of the Marconi 90 ft space communications aerial. Marconi Review, 34, 1971, p.50.
39. Tolbert, C W; Straiton, A W and Krause, L C: A 16 ft diameter millimetre wavelength antenna system. Trans IEEE on Ant. and Prop. AP-13, March 1965, p.225.
40. Morikawa, H; Ogata, M and Kawakami, H: A newly developed Intelsat earth station. IEEE Communications Conference. Vol.1, pp.8-30.
41. Pratt, T and Claydon, B: The prediction of polar diagrams of large Cassegrain antennas, Marconi Review 34, p.1, 1971.
42. Vu, The Bao: Influence of correlation interval and illumination taper in antenna tolerance theory. Proc. IEE, 116, 1969, p.195.
43. Claydon, B: Microwave reflector antennas with multiple and scanned beams. PhD thesis Queen Mary College, October 1974.
44. Yokoi, H and Fukumuro, H: Low-sidelobe paraboloidal antenna with microwave absorber. Electronics and comm. in Japan. 54-B, No.11, 1971. p.34.
45. Peters, L: Side and backlobe structure of directive antennas. IEEE International Communications Conference. 1972. p.41.1.
46. Foldes, P: A new earth station antenna for domestic satellite communications RCA Review, 33, December 1972, p.695.
47. Adata, N A et al: A study of limitations in RF sensing signals due to distortions of large spacecraft antennas. ESTEC Contract No.2330/74AK, ERA-IITRI, RF Technology Centre, September 1975.
48. Imbriale, W A et al: Large lateral feed displacements in a parabolic reflector. Trans IEEE on Ant. and Prop. AP-22. November 1974, p.742.

## Section 5.2

1. Cook, J S; Elam, E M and Zucker, H: The open Cassegrain antenna. BSTJ, 44, September 1965. p.1255.
2. Rudge, A W: Offset parabolic reflector antennas. Lecture notes for 'Reflector antenna theory and computation'. University of Southern California. 1976.

3. Rudge, A W; Foster, P R; Williams, N and Adata, N: Study of the performance and limitations of multiple beam antennas. Final Report. ESTEC Contract No.2277/74 HP ERA-IITRI, RF Technology Centre, Leatherhead, UK, September 1975.
4. Rudge, A W and Adata, N: Study of an offset parabolic reflector antenna, MOD Contract Final Report, ERA-IITRI, RF Technology Centre. Leatherhead, UK, April 1976.
5. Chu, T and Turrin, R H: Depolarisation properties of offset reflector antennas. Trans IEEE on Ant. and Prop. AP-20, 1973, p.339.
6. Dijk, J et al: The polarisation losses of offset paraboloid antennas. Trans IEEE on Ant. and Prop. AP-21, July 1974, p.513.
7. Adata, N and Rudge, A W: Beam-squint in circularly polarised offset-reflector antennas. Electronics Letters 11, October 1975, p.513.
8. Rudge, A W and Adata, N A: A new class of primary-feed antennas for use with offset parabolic-reflector antennas. Electronics Letters, 11, November 1975, p.597.
9. Rudge, A W and Adata, N A: Matched-feeds for offset parabolic reflector antennas. European Microwave Conference, Rome, 1976, p.143.
10. Dragone, C and Hogg, D C: The radiation pattern and impedance of offset and symmetrical near-field Cassegrainian and Gregorian antennas. Trans IEEE on Ant. and Prop. AP-22, 1974, p.472.
11. Adata, N A: Cross-polarisation of reflector antennas. PhD. Thesis EE Dept. University of Surrey, December 1974.
12. Duncan, J W: Multiple beam antennas for communications satellite, EASCON, 1975, p.24.
13. Mizugutch, Y; Akagawa, M and Yokoi, H: Offset dual reflector antenna. Int. Sym. on Ant. and Prop. Amherst, 1976, p.2.
14. Gans, M J and Semplak, R A: Some far-field studies of an offset launcher. BSTJ, 54, September 1975, p.1319.
15. Ohm, E A: A proposed multiple beam microwave antenna for earth stations and satellites. BSTJ. 53, 1974, p.1657.
16. Rudge, A W and Shirazi: Multiple beam antennas: offset reflectors with offset feeds. Final Report. ESTEC Contract No.1725/72PP. University of Birmingham. UK, July 1973.
17. Taormina, F; McCarty, D K; Crail, T and Nakatani, D: Intelsat IVA Communications antenna-frequency re-use through spatial isolation. IEEE Communications Conference 1976, pp.4-10.
18. Rudge, A W: Multiple-beam antennas: offset reflectors with offset feeds. IEEE Trans Ant. and Prop. AP-23, May 1975, p.317.
19. Peters, L: Side and backlobe structure of directive antennas. IEEE Conference on Communications, 1972, p.41-1.
20. Coleman, H P et al: Paraboloidal reflector offset fed with a corru-

### Section 5.3.1

1. Turrin, R H: A multibeam spherical reflector satellite antenna for the 20 and 30 GHz bands. Bell STJ, 54, 1975, p.1011.
2. Hyde, G: Studies of the focal region of a spherical reflector: stationary phase evaluation. Trans IEEE on Ant. and Prop. AP-16, November 1968, p.646.
3. Bresler, A D: Multiple-beam spherical-reflector antenna systems for satellite communications. IEEE Comm. Conf. 1973. p.17-10.
4. Stein, E and Erdmann, M O: Implementation of a fixed multiple beam spherical antenna system and measured test results. IEEE Comm. Conf. 1973, p.17-16.
5. Holt, F S and Bouche, E L: A Gregorian corrector for spherical reflectors. Trans IEEE on Ant. and Prop. AP-12, January 1964, p.44.

### Section 5.3.2

1. Silver, S: Microwave antenna theory and design. McGraw - Hill, 1949.
2. Wolfe, E A: Antenna analysis. John Wilry and Sons Inc. 1966.
3. Adatia, N A and Rudge, A W: Study of an offset parabolic cylinder reflector antenna. Final Report. MOD Contract. ERA-11TRI RF Technology Centre, Leatherhead, UK, November 1975.
4. Epis, J E and Watkins, S N: Broadband beam antennas for EHF. Microwave J. 18, August 1975, p.45.
5. Spenser, R C; Holt, F S; Johnanson, H M and Sampson, J: Double parabolic cylindrical pencil beam antenna. Trans IEEE on Ant. and Prop. AP-3, January 1955, p.4.
6. Dragone, C: An improved antenna for microwave radio systems. BSTJ. 53, September 1974, p.1351.
7. Wilkinson, E J: A dual-polarised cylindrical-reflector antenna for communications satellites. Microwave J. 12, December 1973, p.27.
8. Kiely, D G: Parabolic cylinder aerials. Wireless Engineer. March 1951, p.73.

### Section 5.3.3

1. Wolfe, E A: Antenna analysis. John Wiley and Sons Inc. 1966.
2. Kelleher, H S: A new microwave reflector IRE Convention Record, Pt.11, Vol.1, 1953, p.56.
3. Hyde, G; Kreutel, R W and Smith, L V: The unattended earth terminal multiple beam torus antenna. Comsat Tech. Review 4, 1974, p.231.

4. Jackson, J A C and Goodall, E G A: A 360° scanning microwave reflector, Marconi Review, 21, 1st Quarter, 1958, p.30.
5. Peeler, G D and Archer, D H: A toroidal microwave reflector. IRE Convention Record, 1956, p.242.
6. Mavroides, W G and Provencher, J H: Off-axis sidelobe in elliptic torus reflectors. AFCRC-TR-58-199. December 1958.
7. Meier, R and Thomas, R K: Multifrequency microwave scanning radio-meter antenna. Int. Sym. Digest in Antennas and Propagation. Boulder 1973, p.295.

#### Section 5.4

1. Silver, S: Microwave antenna theory and design, McGraw - Hill, 1949.
2. Brown, J: Chapter 18, Vol.11, Antenna Theory (ed. Collin and Zucker) McGraw - Hill, 1969.
3. Kock, W E: Metallic delay lenses. Bell system T J, 27, 1948, p.58.
4. Dion, A R and Ricardi, L J: A variable coverage satellite antenna system. Proc. IEEE, 59, 1971, p.252.
5. Lu, H S: On the computation of the radiation pattern of a zoned waveguide lens. Trans IEEE on Ant. and Prop. AP-22, 1974, p.483.
6. Cohn, S B and Morila, T: Microwave lens matching by simulated quarter wave transformer. Trans IEEE on Ant. and Prop. AP-4, January 1956, p.33.
7. Green, K A and Gill, G J: Lens antennas for millimetre wavelengths, Proc. of submillimetre waves symposium, New York, 1970.
8. Compton, R T and Collin, R E: Antenna theory (ed Collin and Zucker) McGraw - Hill, Chapter 15, Vol.1, 1969.
9. Smith, C M: Low sidelobe antennas for millimetre wave applications, Paper B7, Millimetre wave techniques Conference, San Diego, 1974.
10. Jones, E M T: Paraboloid reflector and hyperboloid lens antennas. Trans IEEE on Ant. and Prop. AP-2, 1952, p.119.
11. Manwarren, T E and Farrar, A: An artificial dielectric lens suitable for high power application. Conference on High Reliability Electronics Components, Paris. 1972, p.561.
12. Kales, M L and Brown, R M: Design considerations for two-dimensional symmetric bootlace lens. AP-13, July 1965, p.521.
13. Mayhan, J T: A low sidelobe Ku-band antenna-radome study. Trans IEEE on Ant. and Prop. AP-23, July 1975, p.569.
14. Mayhan, J T: Effect of random phase errors at Ka Band resulting from a composite material radome. Trans IEEE on Ant. and Prop. AP-24, May 1976, p.356.

Section 5.5

1. Durrani, S H: Maritime communications via satellites employing phased arrays. Trans IEEE on aerospace elect. systems. AES-9, July 1973, p.504.
2. Johnson, C M: Ballistic missile defense radars. IEEE Spectrum, 7, March 1970, p.32.
3. Elliot, R S: Microwave scanning antennas (ed. Hansen) Chapter 1, Vol.11 Academic Press, 1966.
4. Collin, R E and Zucker, F J: (ed) Antenna theory, Chapters 5 and 6, McGraw - Hill, 1969.
5. Stark, L: Microwave theory of phased arrays, Proc IEEE, 62, December 1974, p.1661.
6. Josefsson, K; Moeschlin, L and Svensen, T: A stripline flat-plate antenna with low sidelobes. Int. Sym. on Ant. and Prop. 1974. p.282.
7. Louapre, M E and Fujioka, J K: A high-efficiency electrically scanned phased array for space-borne radiometric applications. Proc. IEEE, 56, November 1968, p.2011.
8. Goto, N: A synthesis of array antennas for high directivity and low sidelobes. Trans IEEE on Ant. and Prop. AP-20, 1972, p.425.
9. Rudge, A W et al: Study, design, construction and evaluation of a multiple beam antenna. ESTEC Contract No.2277/74 HP, ERA-IITRI RF Technology Centre, Leatherhead, UK, September 1975.
10. Hilburn, J L and Prestwood, F H:K-band frequency-scanned waveguide array. Trans IEEE on Ant. and Prop. AP-22, March 1974, p.340.
11. Patton, W T: Limited scan arrays. Phased array antennas. Artech House, 1972, p.332.
12. Alexander, D K and Sichelstein, B A: A dual beam antenna - A unique waveguide phased array with independently steered beams. Phased array antennas. Artech House, 1972, p.357.
13. Gladman, B R: A theoretical study of low sidelobe antenna arrays. PhD Thesis. University of London, September 1975.
14. Rondinelli, L A: Effects of random errors on the performance of antenna arrays of many elements. IRE National Conv. Record. Pt.1, 1959, p.174.
15. Aerial tolerances, Chapter 2. Ministry of Technology. August 1970.
16. ap Rhys, T L: Large airborne radar antennas, IEE Conference on Antennas for Aircraft and Spacecraft, London, June 1975, p.1.
17. Imbriale, W A: Adaptive and phased arrays. Lecture Notes. University of California, March 1976.

18. Collins, J and Hartwell, T: The RASSR phased array, Naecon 1972 Record, p.174.
19. Wynne, D; Chute, F S and James, C R: Sidelobe levels of a large radio telescope employing a combination of physical and resistive tapering. Trans IEEE on Ant. and Prop. AP-23, March 1975, p.278.
20. Strider, C A: Millimetre wave planar arrays, Paper B6, 1974, Millimetre Waves Techniques Conference, San Diego.
21. James, P W: Optimisation of planar arrays for lowest sidelobe level. Proc. IEE, 120, October 1973, p.1193.
22. Goto, N and Cheng, D K: Phase-shifter thinning and sidelobe reduction for large phased arrays. Trans IEEE on Ant. and Prop. AP-24, March 1976, p.139.
23. Mailloux, R J: Synthesis of spatial filters with Chebyshev characteristics. Trans IEEE on Ant. and Prop. AP-24, March 1976. p.175.
24. Turner, E M: Antennas in perspective. Microwave J. 11, December 1968, p.32.
25. Ince, W J: Recent advances in diode and ferrite phaser technology for phased-array radars. Microwave J. Pt.1 September 1972, p.36. Pt.11, October 1972, p.31.
26. Mailloux, R J and Blacksmith, P: Array and reflector techniques for airport precision approach radars Microwave J, October 1974, p.35.
27. Schrank, H E: Theoretical aspects of spherical phased arrays, Phased array antennas, Artech House Inc. 1972, p.323.
28. Provencher, J H: A survey of circular symmetric arrays. loc. cit. p.292.
29. Nelson, E A and Britt, P P: Cylindrical phased arrays. Beam scanning and sidelobe control. NAECON 72 Record. p.189.
30. Giannini, R J; Gutman, J H. and Hannan, P W: A cylindrical phased array for ATC interrogation. Microwave J. 16, October 1973. p.46.
31. Holley, A E; Du Fort, E C and Dell-Imagine, R A: An electronically scanned beacon antenna. Trans IEEE on Ant. and Prop. AP-22, January 1974, p.3.
32. Munger, A D; Vaughn, G; Provencher, J H and Gladman, B R: Conical array studies. Trans IEEE on Ant. and Prop. AP-22, January 1974, p.35.
33. Hsiao, J K and Chu, A G: Patterns and polarisations of simultaneously excited planar arrays on a conformal surface. Trans IEEE on Ant. and Prop. AP-22, January 1974, p.81.
34. Schwatzman, L and Stangel, J: The dome antenna. Microwave J. 18, October 1975, p.31.
35. Tang, R; Burns, R W and Wong, N S: Phased array antenna for airborne application. Microwave J. 14, January 1971, p.31.

36. Gautier, F: Study of a reflect array in KU band. IEE Conf. Publication No.77, 'Aerospace Antennas', London 1971, p.279.
37. Kahrilas, P J: HAPDAR - An operational phased array. Proc. IEEE, 56, November 1958, p.1967.
38. Wilheit, T: The electronically scanning microwave radiometer (ESMR) experiment. Nimbus 5 Users' Guide.
39. Scudder, R M and Sheppard, W H: AN/SPY-1 phased array antenna. Microwave J. 17, May 1974, p.51.
40. Green, K A and Gill, G J: Feasibility study for a radiator and power divider for 50-60 GHz phased array. NASA CR-111949. August 1971.
41. Butler, J E: Digital, matrix and intermediate-frequency scanning in Microwave scanning antennas. Chapter 3, Vol.III (ed.Hansen) Academic Press, 1966.
42. Hering, K H: The design of hybrid multiple beam forming networks, Phased array antennas. Artech House Inc. 1972, p.240.
43. Stein, S: On cross-coupling on multiple-beam antennas. Trans IEEE in Ant. and Prop. AP-10, September 1962, p.548.
44. Johnson, R C: Optical scanners in microwave scanning antennas, Vol.1, Chapter 3, (ed. Hansen) Academic Press. 1972.
45. Archer, D: Lens-fed multiple beam arrays. Microwave J.18, October 1975, p.37.
46. Dubost, G; Nicholas, M and Havot, H: Theory and applications of broadband microstrip antennas. European Microwave Conference, Rome, 1976, p.275.
47. James, J R and Wilson, G F: New design for microstrip antenna arrays. European Microwave Conference, Hamburg. 1975, p.103.
48. Howell, J Q: Microstrip antennas. IEEE Int. Symposium on Ant. and Prop. 1972. Williamsburg, p.177.
49. Lewis, L R; Fassett, M and Hunt, J: A broadband stripline array element. IEEE Int. Symposium on Ant. and Prop. 1974, Illinois. p.335.
50. Derneryd, A G: Microstrip array antenna. European Microwave Conference, Rome, 1976, p.339.
51. Kinsey, R R: The AN/TPS-59. Antenna row-board design. IEEE Int. Microwave Symposium. 1974 Atlanta. p.57.
52. Munson, R E: Conformal microstrip antennas and microstrip phased arrays. Trans IEEE on Ant. and Prop. AP-22, January 1974, p.74.
53. Bazire, T W; Croydon, R and Cary, R H J: A printed antenna/radome (Radant) for airborne doppler navigational radar. IEE Conference on Antennas for Aircraft and Spacecraft. June 1975, London, p.35.

- 53a Kinsey, R R and Horvath, A L: Transient response of centre-series fed array. Phased array antennas. Artech House Inc. 1972, p.261.
54. Williams, N and Rudge, A W: Development of a dielectric frequency-scanned array: technology evaluation. Final Report. MOD Contract ERA-IITRI, RF Technology Centre, Leatherhead, UK, June 1976.
55. Patel, M R and Arora, R K: Radiation distortions in fast-frequency-scanned antenna arrays. Trans IEEE on Ant. and Prop. AP-24, July 1976, p.536.
56. Phelan, H R: L-band spiraphase reflectarray. Microwave J. 20, January 1977, p.47.
57. Williams, N; Rudge, A W and Gibbs, S E: Millimetre-wave insular guide frequency-scanned array. IEE Int. Microwave Conference, San Diego, 1977.
58. Hall, P S and James, J R: A survey of flat profile microwave antenna. Technical Note RT 103 Royal Military College of Science, Shrivenham, UK. April 1977.

References for Chapter 6

1. Graham, E A: Space vehicle multibeam antenna system design. IEEE Conference on Communications, 1969, p.49-1.
2. Kumazawa, H and Kairkomi, M: Multiple-beam antenna for domestic communication satellite. Trans IEEE on Ant. and Prop. AP-21, November 1973. p.876.
3. Scott, W G; Luh, H S and Matthews, E W: Design trade-offs for multiple-beam antennas in communication satellites. IEEE Communications Conference 1976, p.4-1.
4. Rudge, A W et al: Study of the performance and limitations of multiple-beam antennas. ESTEC Contract No.2277/74 HP RFTC Report, September 1975.
5. White, W D: Pattern limitations in multiple beam antennas. Trans IEEE on Ant. and Prop. AP-10, July 1962, p.430.
6. Dion, A R and Ricardi, L J: A variable coverage satellite antenna system. Proc. IEEE, 59, 1971, p.252.
7. Rudge, A W: Multiple-beam antennas: offset reflectors with offset feeds. Trans IEEE on Ant. and Prop. AP-23, May 1975, 3, p.317.
8. Rudge, A W: Multiple-beam offset reflector antenna for spacecraft. Proc. IEE Int. Conf. Antennas for aircraft and spacecraft, London, June 1975, p.136.
9. Rudge, A W and Withers, M J: New technique for beam-steering with fixed parabolic reflectors. Proc. IEE. 118, 7, July 1971, p.857.
10. Mailloux, R J and Blacksmith, P: Array and reflector techniques for airport precision radars, Microwave J. October 1974, p.35 (and AGARD Conf. Munich 1973).
11. Tang, R: Survey of time-delay beam-steering techniques. Proc. of the 1970 phased-array Ant. Symp. Airtech House, 1972, p.254.
12. Borgiotti, G V: An antenna for limited scan in one plane: Design antenna and numerical simulation. IEEE Trans Ant. and Prop. AP-25, March 1977, p.232.

References for Chapter 7

1. Gronlund, M P S et al: Nutating sub-reflector in a Cassegrainian antenna system, p.102. IEE Symposium on The design and construction of large steerable aeriels. No.21.
2. Viskanta, V S and Rose, R E: Conical scanning system for Pioneer Jupiter spacecraft. Trans IEEE on aerospace electronics systems. AES-8, 1972, p.236.
3. Lockett, N: The electrical performance of the Marconi 90 ft space communications aeriels. Marconi Review, 34, 1971. p.50.
4. Sato, Y et al: Development of satellite communications earth station antenna. NEC Research and Development, October 1970, p.15.
5. Morikawa, H et al: Satellite communications earth station for the Malaysian Government. Mitsubishi Denki Engineer, 31.
6. Morikawa, H; Ogati, M and Kawakani, A: A newly developed Intelsat earth station. International Communications Conference 1973. Conference Record, pp.8-30.
7. Hannan, P W: Optimum feeds for all three modes of a monopulse antenna. I:Theory. IEEE Trans on Ant. and Prop. AP-9, 1961. p.444.
8. Adatia, A et al: A study of limitations in RF sensing due to distortions of large spacecraft antennas. ESTEC Contract No.2330/74 AK, RF Technology Centre, Leatherhead, UK, September 1975.
9. Nelson, E A and Britt, P P: Cylindrical phased arrays. Beam scanning and sidelobe control. NAECON 72 Record, p.189.
10. Kinsey, R R: The AN/TPS-59 antenna row-board design. IEEE Int. Microwave Symposium. Atlanta. 1974.
11. ap Rhys, T L: Large airborne radar antennas. IEE Conference on Antennas for Aircraft and Spacecraft, London, June 1975. p.1.
12. Wong, N S; Tang, R and Barber, E E: Multi-element high power monopulse feed with low sidelobes and high aperture efficiency. Trans IEEE on Ant. and Prop. AP-22, May 1974, p.403.

References for Chapter 8

1. Meeks, M L and Ruze, J: *Evaluation of the Haystack antenna and radome.* IEEE Trans on Ant. and Prop. AP-19, November 1971, p.723.
2. Kay, A F: *Electrical design of metal space frame radomes.* IEEE Trans on Ant. and Prop. AP-13, March 1965, p.188.
3. Mayhan, J T: *A low sidelobe Ku-band antenna-radome study.* IEEE Trans on Ant. and Prop. AP-23, July 1975, p.569.
4. Mayhan, J T: *Effect of random phase errors at Ka-band resulting from a composite material radome.* IEEE Trans on Ant. and Prop. AP-24, May 1976, p.356.
5. Jasik, H: (ed) *Antenna Engineering Handbook, Chapter 32.* McGraw - Hill, 1961.

References for Chapter 9

1. Doro, G and Saitto, A: Dual polarisation antennas for OTS. IEE Conference on Antennas for Aircraft and Spacecraft, London, 1975. p.76.
2. Wood, P J and Lockett, N J: A new type of test range for satellite polar diagram measurements. IEE Conference on Antennas for Aircraft and Spacecraft, London, 1975. p.186.
3. Baars, J W N and Hughes, C D: Antenna measurement techniques at 11 GHz. IEEE Conference on Satellite Communication System Technology, London, 1975, p.253.
4. Fitzgerald, W D; Lynn, U L and Keeping, K J: Experimental evaluation of  $\sim 1000$  wavelength antenna. Lincoln Lab. Report. May 1963.
5. Grimm, K R: Antenna analysis by near-field measurements. Microwave J. 19, April 1976, p.43.
6. Jasik, H: (Ed) Antenna engineering handbook. Chapter 34, McGraw-Hill, 1961.

12 GLOSSARY

Half-power beamwidth (HPBW):

The width of the antenna radiation patterns at the point where the gain is 3 dB below the peak forward gain.

Beam efficiency:

The percentage of the total power in the antenna radiation pattern which is included between the pattern's first nulls.

Aperture efficiency:

The forward gain of an antenna compared with the forward gain of an identical aperture when uniformly illuminated. The quantity can be expressed as a decimal fraction or more usually as a percentage.

Figure of Merit G/T:

A term used in ground station antennas to specify the antenna performance, where G is the antenna forward gain and T is the input system noise temperature. G/T is usually expressed in decibels.

Directivity:

The maximum power per unit solid angle radiated by the antenna to the power per unit solid angle obtained from an isotropic radiator, radiating the same total power.

Correlation interval:

Distance on average where rms phase errors across an illuminated aperture become independent.

GLOSSARY (Contd.)

Current frequency designation		Previous frequency designation	
Band	GHz	Band	GHz
A	<0.25	VHF	<0.3
B	0.25-0.5	UHF	0.35-1.0
C	0.5- 1.0		
D	1-2	L	1-2
E	2-3	S	2-4
F	3-4		
G	4-6	C	4-8
H	6-8		
I	8-10	X	8-12.5
J	10-20	K <sub>U</sub>	12.5-17.5
K	20-40	K	17.5-26
L	40-60	K <sub>a</sub> (Q)	26-40
M	60-100	V	40-60
		O	60-90

DOCUMENT CONTROL SHEET  
(Notes on completion overleaf)

Overall security classification of sheet ..... **UNCLASSIFIED** .....

(As far as possible this sheet should contain only unclassified information. If it is necessary to enter classified information, the box concerned must be marked to indicate the classification eg (R),(C) or (S)).

1. DRIC Reference (if known) <b>BR56799</b>	2. Originator's Reference	3. Agency Reference <b>D/DRLS/4/19/5</b>	4. Report Security Classification <b>UNCLASSIFIED</b>
5. Originator's Code (if known)	6. Originator (Corporate Author) Name and Location <b>Electrical Research Association Leatherhead, Surrey, KT22 7SA.</b>		
5a. Sponsoring Agency's Code (if known)	6a. Sponsoring Agency (Contract Authority) Name and Location <b>Directorate of Research Electronic Systems (DRLS) The Adelphi, London, WC2N 6BB.</b>		
7. Title <b>LOW SIDELobe ANTENNA STUDY FINAL REPORT PART I LITERATURE SURVEY AND REVIEW</b>			
7a. Title in Foreign Language (in the case of translations)			
7b. Presented at (for conference papers). Title, place and date of conference			
8. Author 1. Surname, initials <b>FOSTER PR</b>	9a. Author 2 <b>RUDGE A W</b>	9b. Authors 3, 4...	10. Date pp ref
11. Contract Number <b>K/LR21b/1120</b>	12. Period	13. Project	14. Other References
15. Distribution statement <b>UNLIMITED</b>			
Descriptors (or keywords) <b>MICROWAVE ANTENNAS, LOW GAIN, HIGH GAIN, BROADBAND, ANTENNA RADIATION PATTERNS, EFFICIENCY, POLARISATION.</b>			
Abstract <b>This report has considered the level of sidelobe suppression which can be achieved with antennas in a broad range of types and has attempted to identify the principal parameters governing the sidelobe performance for any given antenna type.</b>			

## NOTES ON COMPLETION OF DOCUMENT CONTROL SHEET

This Document Process Sheet is designed specifically for MOD reports and reports produced by Contractors.

Boxes marked\* below need be completed only if the information is readily available.

- \*1. DRIC reference: Enter DRIC reference (BR number) if one has been assigned.
2. Originator's Reference: Enter the report number by which the document is identified by the originator of the report, in the form in which it appears on the cover.
3. Agency reference: Enter reference number allocated by sponsoring agency (contract authority) in the case of contract reports.
4. Report Security Classification: Enter security classification or marking which limits the circulation of the report, or enter UNLIMITED when this applies.
- \*5. Originator's Code: Code number for the DRIC-standardised form of the entry appearing in Box 6.
- \*5a. Sponsoring Agency's Code: Code number for the DRIC-standardised form of the entry appearing in Box 6a.
6. Originator (corporate author): Enter name and location of the organisation preparing the report.
- 6a. Sponsoring Agency (Contract Authority): Enter the name of the monitoring MOD Branch or Establishment in the case of Contractor's reports. If an MOD report covers work funded by an outside agency, enter the name of that agency.
7. Title: Enter the complete report title in capital letters but omitting initial definite or indefinite articles. If the report covers a specific period, enter this after the title, eg (1.1.1972-31.3.1972).
- 7a. Title in Foreign Language: In the case of translations, enter the foreign language title (transliterated if necessary) and the translated English title in Box. 7.
- 7b. Conference Papers: If 7 is the title of a paper presented at a Conference, or a Conference proceedings, enter the Conference Title, where it was held and the date.
8. Author 1: Enter the name of the first author, followed by his initials.
- 9a. Author 2: Enter the name of the second author, followed by his initials.
- 9b. Authors 3,4...: Enter third and following authors' names.
10. Date: Enter the month (in figures) and the year of the report (Dec., 1969 is written 12.1969). If the report is undated but a period covered by the report is indicated, enter the date at the end of the period. pp.ref. Enter the inclusive number of pages in the report containing information, i.e. including appendices, tables and illustrations, and the total number of references cited.
11. Contract Number: Enter the number of the contract or grant under which the report was written.
12. Period: (always associated with the Contract Number). Only to be used for reports covering a specific period, e.g. quarterly, annual or final reports. Enter QR-1, AR, FR, as appropriate.
13. Project: Enter project name or number.
14. Other Reference: Enter any reference, other than those in Boxes 2 or 3, by which the report may be identified.
15. Distribution statement. Enter any limitations on the distribution of the document. If distribution is limited to particular groups eg MOD, MOD and its Contractors, etc. it should be stated. If the distribution is the responsibility of another authority eg a HQ Directorate (Technical Policy Authority) enter "Distribution controlled by MOD Technical Policy Authority". Enter "via DRIC" after "Authority" where appropriate and name the Technical Policy Authority if possible.

**Descriptors:** Any number of descriptors (or key-words) can be entered. If selected from a published thesaurus, eg The Thesaurus of Engineering and Scientific Terms (TRST), this should be indicated.

**Abstract:** The abstract should preferably not exceed 150 words, i.e. it can be considerably shorter than the Abstract to be provided on the Title Page of the Report. Information available in the report title need not be included in the abstract.

END

FILMED

10-83

DTIC